Investigating the potential interactions between glutamatergic signalling and Alix (ALG-2 interacting protein X)

Sharifah S. Asysyura Syed Salim

Research thesis submitted for the degree of Doctor of Philosophy at Royal Holloway University of London in August 2016

Declaration of Authorship

I, Sharifah S. Asysyura Syed Salim, hereby declare that the work presented in this thesis is my own unless otherwise indicated, and that all published work has been acknowledged. Furthermore, I affirm that I have neither fabricated nor falsified the results reported herein.

Signed: 

Date 06 August 2016

Abstract

Previous work has identified a novel dopamine receptor interacting protein, Alix (ALG-2 (apoptosis-linked gene 2-interacting protein X), using D1 receptor C-terminal domain or D3 receptor third cytoplasmic loop as 'baits' in separate yeast two-hybrid screens. Alix is thought to be important for the stability and trafficking of dopamine receptors and is an ubiquitous adaptor protein that was first described for its capacity to bind to the calcium-binding protein, ALG-2. It is known to be involved in apoptosis, regulation of cell adhesion, protein sorting, adaptation to stress conditions, endosomal trafficking and neuronal cell death. However, the exact cellular role for this protein in neuronal signalling remains poorly understood.

There is strong evidence to support the existence of direct interactions between dopamine receptors and NMDA receptors and dopamine receptor interacting proteins such as Alix may facilitate intracellular ‘cross talk’ between both neurotransmitter signalling pathways. Furthermore, Alix has been recently found within the human postsynaptic density (PSD) and since NMDA receptors are central components of the PSD, we hypothesized that Alix may be able to influence NMDA receptor function.

We have evaluated the effects of recombinant wildtype and truncated Alix proteins in NMDA receptor function using an NMDA receptor cell death assay in transiently transfected human embryonic kidney-293 cells (HEK293). We found that coexpression of Alix had a significant effect on NMDA receptor triggered cell death and we have examined Alix expression and colocalisation with NMDAR in HEK293 cells as well as endogenous Alix expression within cultured primary cortical and hippocampal neurons. Our results suggest that Alix can influence the NMDA receptor induced cell death pathway and suggests a previously unreported role for Alix as a potential modulator of NMDA receptor function.

Contents **page**

1. Introduction 1-20

1.1 Dopamine receptors 1

1.2 Dopamine receptor interacting proteins (DRIPs) 3

1.3 Glutamate receptors 5

1.4 Post Synaptic Density 9

1.5 Potential crosstalk pathways between dopamine and glutamate receptors and their implications 10

1.6 ALG-2 interacting protein X (Alix) 13

1.7 Cellular mechanism of Alix in apoptosis 18

1.8 Alix in the PSD and role in neuronal function 20

Aims and Objectives 21

2.1 Materials 22-24

2.1 General chemicals 22

2.1.1 Reagents purchased from Sigma-Aldrich Co. Ltd. (Poole, Dorset, England) 22

2.1.2 Reagents purchased from other suppliers 22

2.1.3 Molecular weight standards 23

2.1.4 Antibodies 23

2.1.5 Kits 24

2.1.6 Equipment 24

2.2 Methods 25-44

2.2.1 Plasmid cDNAs 25

2.2.2 Transformation of plasmid DNA 31

2.2.3 Miniprep of plasmid DNA 31

2.2.4 Maxiprep of plasmid DNA 32

2.2.5 Qiagen Maxiprep protocol 32

2.2.6 Restriction Enzyme Digestion 33

2.2.7 Starting HEK 293 cell cultures from frozen 34

2.2.8 Preparing frozen cultures of HEK 293 cells 34

2.2.9 Cell culture and transfection of HEK 293 cells 35

2.2.10 Trypan blue exclusion assay 36

2.2.11 Hippocampus and Cortex Dissection 37

2.2.12 Coverslip preparation 37

2.2.13 Dissection of the cortex and hippocampus coverslip preparation 37

2.2.14 Immunocytochemistry 38

2.2.15 Western Blotting 39

2.2.16 Fraction preparation 41

2.2.17 Colocalization Analysis 43

2.3 Antibody Dilution 44

3. Investigating the potential modulation of NMDA by Alix in Cell Death Assay 45-84

3.0 Introduction 45

3.1 Cell Death Assay 47

3.1.1 Transfection efficiency 47

3.2 Alix modulate NMDA-induced cell death 49

3.2.2 Coexpression of Alix with GluN1 or GluN2A alone 56

3.2.3 An NMDAR antagonist, AP5 abolishes cell death in the absence or presence of Alix 61

3.2.4 The effect of different NMDA concentrations on cell death in 65

the absence and presence of human Alix

3.2.5 Modulation of NMDA cell death by mouse Alix WT 68

3.2.6 Modulation of NMDA cell death by mouse Alix CT 76

3.2.7 Modulation of NMDA cell death by mouse Alix NT 85

3.2.8 Modulation of NMDA cell death by mouse Alix DPRD 92

3.2.9 Modulation of NMDA cell death by mouse Alix NT + CT coexpression 100

3.3 Summary 108

4. Investigating the protein expression of recombinant Alix and GluN1 in cotransfected HEK293 cells and brain lysates/neuronal fractions 110-124

4.1 Introduction 110

4.2 Western Blotting Analysis Alix Modification of NMDA 111

4.3 Western Blotting Analysis of GluN1 subunit expression in Alix cotransfected cells 114

4.4 Western Blotting Analysis of Alix in Neuronal Fraction 117

4.5 Western Blotting Analysis of GluN1 in Neuronal Fraction 120

4.6 Summary 124

5. Investigating Alix localization in cotransfected HEK293 cells 126-152

5.1 Introduction 126

5.2 Localisation of Alix in HEK293 cells 127

5.2.1 Expression of Alix within the cytoplasm 127

5.2.2 Alix distribution and cellular endosome marker localisation 132

5.2.3 Alix distribution and the cytoskeleton 137

5.3 Localisation of Alix in NMDAR activated HEK293 cells 142

5.3.1 Activated NMDARs and Alix localization 142

5.3.2 Nonactivated NMDAR and Alix localization 147

5.4 Summary 152

6.1 Localisation of Alix in primary cortical and hippocampal neurons 153-183

6.1.1 Expression of Alix within the cytoplasm of cortical neurons and hippocampal neurons 153

6.2.1 Endogenous Alix distribution in cortical and hippocampal neurons and the localization of the cellular endosome marker, EEA1 158

6.2.2 Endogenous Alix distribution and the cytoskeleton within cortical neurons 163

6.2.3 Endogenous Alix expression with NMDA receptors in cortical and hippocampal neurons 168

6.2.4 Endogenous Alix with PSD 95 in cortical neurons 173

6.2.5 Endogenous Alix localisation with synaptophysin in cortical neurons 177

6.3 Summary 183

7. Discussion 185-175

7.1 Discussion of modulation of NMDA receptor function by Alix in Cell Death Assay 185

7.2 Discussion of western blot analysis of NMDA/Alix coexpression within HEK293 cells 196

7.3 Discussion of Alix localization in cotransfected HEK293 cells, primary cortical and hippocampal cultures 201

7.4 General summary 208

7.5 Future studies 210

References 211-223

List of Tables and Figures

Figure 1.1 - D1-like receptors and D2-like receptors 2

Table 1.1 - The 11 DRIPs from a human adult brain 4

Figure 1.2 - The NMDA receptor cascade 7

Figure 1.3 - Schematic illustration of the apoptotic pathways 8

Figure 1.4 - Schematic diagram of the network of proteins in the postsynaptic density 10

Figure 1.5 - Diagram of glutamate and dopamine receptors intracellular 'crosstalk' pathways 12

Figure 1.6 - Domain architecture of Alix 13

Figure 1.6.1 : BLAST sequence analysis between human Alix (Homo sapiens) and mouse Alix (Mus musculus) 15

Figure 1.7 - The endosomal ESCRT pathway 17

Figure 1.8 - Schematic illustration of programmed cell death (PCD) 18

Figure 2.1- cDNA plasmid Alix GFP tagged in pCMVTag2C 26

Figure 2.2 - cDNA plasmid Alix wild type in pCI Flag tagged plasmid 27

Figure 2.3 - cDNA plasmid Alix NT in pCI Flag tagged plasmid 28

Figure 2.4 - cDNA plasmid Alix CT corresponds in pCI Flag tagged plasmid 29

Figure 2.5 cDNA plasmid Alix Alix DPRD in pCI Flag tagged plasmid 30

Figure 3.1.1 a: Transfection efficiency by eGFP and Alix plasmid 47

Table 3.1.1 b: Percentage of eGFP following transfection of plasmid 48

Figure 3.1 a - Modulation of NMDA cell death by Alix activated 49

Table 3.1 a - Percentage cell death after 6 hours treatment 50

Figure 3.1 b - Modulation of NMDA cell death by Alix not activated 51

Table 3.1 b - Percentage cell death after 6 hours treatment 52

Table 3.1 c - Anova Analysis of NMDA cell death by Alix GFP 53

Figure 3.2 a - Coexpression of Alix with GluN1 or GluN2A alone activated 57

Table 3.2 a - Percentage cell death after 6 hours treatment 58

Figure 3.2 b - Coexpression of Alix with GluN1 or GluN2A alone not activated 59

Table 3.2 b - Percentage cell death after 6 hours treatment 59

Figure 3.3 a - The effects of 100 µM AP5 on Alix coexpression activated 61

Table 3.3 a - Percentage cell death after 6 hours treatment 62

Figure 3.3 b - The effects of 100 µM AP5 on Alix coexpression not activated 63

Table 3.3 b - Percentage cell death after 6 hours treatment 64

Figure 3.4 - The effect of different NMDA concentrations in the absence and presence of human Alix 65

Table 3.4 - Percentage cell death after 6 hours treatment 66

Figure 3.5 - Schematic representation of Alix deletion mutants 68

Figure 3.6 a - Modulation of NMDA cell death by mouse Alix WT activated 69

Table 3.6 a - Percentage cell death after 6 hours treatment 70

Figure 3.6 b - Modulation of NMDA cell death by mouse Alix WT not activated 71

Table 3.6 b - Percentage cell death after 6 hours treatment 72

Table 3.6 c - Anova Analysis of NMDA cell death by Alix WT 74

Figure 3.7 a - Modulation of NMDA cell death by mouse Alix CT activated 77

Table 3.7 a - Percentage cell death after 6 hours treatment 78

Figure 3.7 b - Modulation of NMDA cell death by Alix CT not activated 79

Table 3.7 b - Percentage cell death after 6 hours treatment 80

Table 3.7 c - Anova Analysis of NMDA cell death by Alix CT 82

Figure 3.8 a - Modulation of NMDA cell death by mouse Alix NT activated 85

Table 3.8 a - Percentage cell death after 6 hours treatment 86

Figure 3.8 b - Modulation of NMDA cell death by Alix NT not activated 87

Table 3.8 b - Percentage cell death after 6 hours treatment 88

Table 3.8 c: Anova Analysis of NMDA cell death by Alix NT 89

Figure 3.9 a - Modulation of NMDA cell death by mouse Alix DPRD activated 92

Table 3.9 a - Percentage cell death after 6 hours treatment 93

Figure 3.9 b - Modulation of NMDA cell death by Alix DPRD not activated 94

Table 3.9 b - Percentage cell death after 6 hours treatment 95

Table 3.9 c: Anova Analysis of NMDA cell death by Alix DPRD 97

Figure 3.10 a - Modulation of NMDA cell death by mouse Alix NT + CT activated 100

Table 3.10 a - Percentage cell death after 6 hours treatment 101

Figure 3.10 b - Modulation of NMDA cell death by mouse Alix NT + CT not activated 102

Table 3.10 b - Percentage cell death after 6 hours treatment 103

Table 3.10 c: Anova Analysis of NMDA cell death by Alix CTNT 105

Figure 4.1 - Protein expression of Alix protein in Alix/NMDAR cotransfected cells 112

Figure 4.1a - Normalised levels of activated Alix protein expression 112

Figure 4.1b - Normalised levels of not activated Alix protein expression 113

Table 4.1 - Alix expression levels from Figures 4.1 a and b 113

Figure 4.2 - Western Analysis of GluN1 expression when cotransfected with Alix 115

Figure 4.2a - Normalised levels of protein expression in activated GluN1 116

Figure 4.2b - Normalised protein expression of non activated GluN1 116

Table 4.2 - Normalised protein levels of GluN1 from Figures 4.2a and b 117

Figure 4.3 - Protein expression of Alix in whole rat adult and embryo brain lysates 119

and neuronal fractions

Figure 4.3a - Normalised levels of protein expression of Alix in whole rat adult and embryo brain lysates and neuronal fractions 120

Table 4.3 - Protein expression of Alix from brain lysates and neuronal fractions in Figure 4.3a 120

Figure 4.4 - Protein expression of GluN1 in whole rat adult and embryo brain lysates and some of the neuronal fractions 122

Figure 4.4a - Normalised levels of protein expression of GluN1 in whole rat adult and embryo brain lysates and some of the neuronal fractions 123

Table 4.4 - Protein expression levels from Figure 4.4a 123

Figure 5.1 - Intracellular distribution of Alix in the presence of Hoechst dye in HEK293 cells 128

Figure 5.2 - Colocalisation analysis from images shown in Figure 5.1 129

Figure 5.3 - Intracellular distribution of Alix in a larger cluster in the presence of Hoechst dye in HEK293 cells 130

Figure 5.4 - Colocalisation analysis from images shown in Figure 5.3 131

Figure 5.5 - Intracellular distribution of Alix with cellular endosome marker EEA1 in HEK293 cells 133

Figure 5.6 - Colocalisation analysis from images shown in Figure 5.5 134

Figure 5.7 - Intracellular distribution of Alix with cellular endosome marker EEA1 in HEK293 cells 135

Figure 5.8 - Colocalisation analysis from images shown in Figure 5.7 136

Figure 5.9 - Intracellular distribution of Alix with phalloidin in HEK293 cells 138

Figure 5.10 - Colocalisation analysis from images shown in Figure 5.9 139

Figure 5.11- Intracellular distribution of Alix with phalloidin in HEK293 cells 140

Figure 5.12 - Colocalisation analysis from images shown in Figure 5.11 141

Figure 5.13 - Intracellular distribution of Alix in NMDAR activated HEK293 cells 143

Figure 5.14- Colocalisation analysis from images shown in Figure 5.13 144

Figure 5.15- Intracellular distribution of Alix in NMDAR activated HEK293 cells 145

Figure 5.16- Colocalisation analysis from images shown in Figure 5.15 146

Figure 5.17- Intracellular distribution of Alix in NMDAR non activated HEK293 cells 148

Figure 5.18- Colocalisation analysis from images shown in Figure 5.17 149

Figure 5.19- Intracellular distribution of Alix in NMDAR non activated HEK293 cells 150

Figure 5.20- Colocalisation analysis from images shown in Figure 5.19 151

Figure 6.1- Alix in primary cortical neuronal cultures stained with Hoechst 154

Figure 6.2- Colocalisation analysis from images shown in Figure 6.1 155

Figure 6.3- Alix in primary hippocampal neuronal cultures stained with Hoechst 156

Figure 6.4- Colocalisation analysis from images shown in Figure 6.3 157

Figure 6.5- Alix in cortical neurons against EEA1 159

Figure 6.6- Colocalisation analysis from cortical images shown in Figure 6.5 160

Figure 6.7- Alix in hippocampal neurons against EEA1 161

Figure 6.8- Colocalisation analysis from hippocampal images shown in Figure 6.7 162

Figure 6.9- Alix in cortical neurons against phalloidin 164

Figure 6.10- Colocalisation analysis of cortical neurons from images shown in Figure 6.9 165

Figure 6.11- Alix in hippocampal neurons against phalloidin 166

Figure 6.12-Colocalisation analysis of hippocampal neurons from images shown in Figure 6.11 167

Figure 6.13- Alix and GluN2A/2B in primary cortical neurons 169

Figure 6.14 -Colocalisation analysis of cortical neurons images 170
shown in Figure 6.13

Figure 6.15- Alix and GluN2A/2B in primary hippocampal neurons 171

Figure 6.16- Colocalisation analysis of hippocampal neurons images 172
shown in Figure 6.15

Figure 6.17- Alix and PSD95 in primary cortical neurons 174

Figure 6.18- Colocalisation analysis of cortical neurons images 175
shown in Figure 6.17

Figure 6.19- Alix and PSD95 in primary hippocampal neurons 176

Figure 6.20- Colocalisation analysis of cortical neurons images 177
shown in Figure 6.19

Figure 6.21- Alix and synaptophysin in primary cortical neurons 179

Figure 6.22- Colocalisation analysis images shown in Figure 6.21 180

Figure 6.23- Alix and synaptophysin in primary cortical neurons 181

Figure 6.24- Colocalisation analysis images shown in Figure 6.23 182

Figure 7.1- NMDA cell death by Alix in activated and non activated cells 186

Figure 7.2- NMDA cell death by Alix WT in activated and non activated cells 192

Figure 7.3- NMDA cell death by Alix CT in activated and non activated cells 193

Figure 7.4- NMDA cell death by Alix DPRD in activated and non activated cells 194

Figure 7.5- NMDA cell death by Alix NT in activated and non activated cells 195

Abbreviations

AIF	apoptosis-inducing factor
ALG-2	apoptosis-linked gene 2
Alix	ALG-2 Interacting Protein 1
AMPA	α-amino-3-hydroxyl-5-methyl-4-isoxazole-propionate
AMPARs	α -amino-3-hydroxy-5-methyl-4-isoxazole propionic acid receptors
AP5	2*R*-amino-5-phosphonopentanoate
$CaCl_2$	Calcium Chloride Chloride
CaMKIV	Calcium/calmodulin-dependent protein kinase IV
cAMP	cyclic adenosine monophosphate
cDNA	Complementary DNA
CHMPs	charged multi vesicular body proteins
CLLs	chronic lymphocytic leukemias
D	Dopamine
DARPP-32	Dopamine- and cAMP-regulated phosphoprotein, Mr 32 kDa
DMEM	2-Propanol, α- Minimum Essential Medium
DMSO	Dimethyl Sulfoxide
DRIP	Dopamine Receptor Interaction Protein
DTT	Dithiotreitol
EEA1	early endosome antigen 1
EDTA	Ethylenediaminetetraacetic acid
EGFP	Enhanced Green Fluorescent Protein
EPSC	excitatory postsynaptic current
ERK	extracellular signal-regulated protein kinase
ESCRT	endosomal sorting complex required for transport

GFP	Green Fluorescent Protein
GNB2LI	guanine nucleotide binding protein, β-peptide 2-like I
GPCRs	G-protein Coupled Receptors
HEPES	4-(2-hydroxyethyl)-1-piperazineethanesulfonic acid
IGFIR	insulin-like growth factor 1 receptor
IL4	interleukin-4
KCl	Potassium chloride
L1/NgCAM	neuron-glia cell adhesion molecule
LBPA	lysobisphosphatidic acid
LTP	long term potentiation
LTD	long term depression
MAPK	mitogen-activated protein kinase
MAPK	p38 mitogen-activated protein kinase p38
MVBs	multivesicular bodies
NaH_2PO_4	Sodium Dihydrogen Phosphate
$NaHCO_3$	Sodium Bicarbonate
NMDA	N-Methyl-D-Aspartate
NMDARs	*N*-methyl-D-aspartate receptors
NO	nitric oxide
NOS	Nitric Acid Synthase
NP40	Nonidet P 40
$ONOO^-$	toxic peroxynitrite
PB	peripheral blood
PBS	Phosphate Buffered Saline
PCD	Programmed cell death

PCP	phencyclidine
PFA	Paraformaldehyde
PKA	cAMP-dependent protein kinase
PKC	Protein Kinase C
PLC	Phospholipase C
PSD	post synaptic density
PSD95	post synaptic density protein 95
PSS	physiological salt solution
ROS	reactive oxygen species
SDS	Sodium dodecyl sulphate
SDS-PAGE	Sodium dodecyl sulphate Polyacrylamide Gel Electrophoresis
SNARE	SNAP (Soluble NSF Attachment Protein) Receptor
SOC	Super Optimal *broth*
TB	Terrific broth
TBS-T	Tris-Buffered Saline Tween 20
VPS4	vacuolar protein sorting associated protein 4

Acknowledgements

Firstly I would like to thank my supervisor at Royal Holloway, Dr Philip Chen, for all his guidance and support throughout my PhD. He has helped me, guided me and has been invaluable to the progress of my PhD. I would also like to thank my second supervisor at St Georges, Dr Jamal Nasir, since without his preliminary work in identifying the novel human DRIPs, my project would not have been possible. I am also appreciative to my advisor at Royal Holloway, Dr Pavlos Alifragis, for all his invaluable advice and help. Also, I would like to thank all the member of level 3 lab for their countless help (Kayvan, Helena, Anila, Paul, Francia, Andrea, Katrin, JJ, Arnold and many more), support and discussions over the years, without you guys I may not have made it this far.

This project would not have been possible without funding from the South West London Acedemic Network (SWan). I would also like to extend a thank you to Dr. Jamal Nasir for providing the cDNA plasmids for Alix (GFP tagged in pCMVTag2C), Dr. Remy Sadoul for providing the cDNA plasmids Alix (Flag tagged in pCi) and Dr. Philip Chen for providing the cDNA plasmids GluN1 in pRK7 and GluN2A in pRK7.

I would also like to thank all my parents, in laws, friends and family for all their help, encouragement, love and support throughout my PhD. Especially to my beloved husband who has been there through the ups and down and provided me with endless encouragement, advice and support that I have needed throughout the years. I am also thankful of my two beautiful children for whom this PhD is made worthwhile.

Thank you again to each and every one of you who has shaped my PhD to an enjoyable and enriching experience.

1. Introduction

1.1 Dopamine receptors

Dopamine receptors are a class of metabotropic G protein-coupled receptors (Zhan et al., 2008). They are composed of mainly seven homomeric transmembrane α helices that are prominent in the mammalian brain (Missale et al., 1998). The neurotransmitter dopamine is the primary catecholamine endogenous ligand for dopamine receptors (Missale et al., 1998). There are mainly five subtypes of dopamine receptors, D_1, D_2, D_3, D_4, and D_5 (Missale et al., 1998; LaHoste et al., 2000).The D_1 and D_5 receptors are members of the D_1-like family of dopamine receptors, and the D_2, D_3 and D_4 receptors are members of the D_2-like family (Missale et al., 1998, LaHoste et al., 2000). The activation of the D_1-like family of dopamine receptors is coupled to the G protein Gs, which subsequently activates adenylyl cyclase increasing the intracellular concentration of the second messenger cyclic adenosine monophosphate (cAMP) thereby activating a cAMP-dependent protein kinase (PKA) and mediating the phosphorylation of dopamine (Figure 1.1) (Missale et al., 1998; Gould and Manji, 2005; Girault and Greengard, 2004). Whereas, the activation of the D_2-like family of receptors is coupled to the G protein G_i, which directly inhibits the formation of cAMP by inhibiting the enzyme adenylate cyclase Figure 1.1) (Gould and Manji, 2005; Missale et al., 1998; Girault and Greengard, 2004).

.

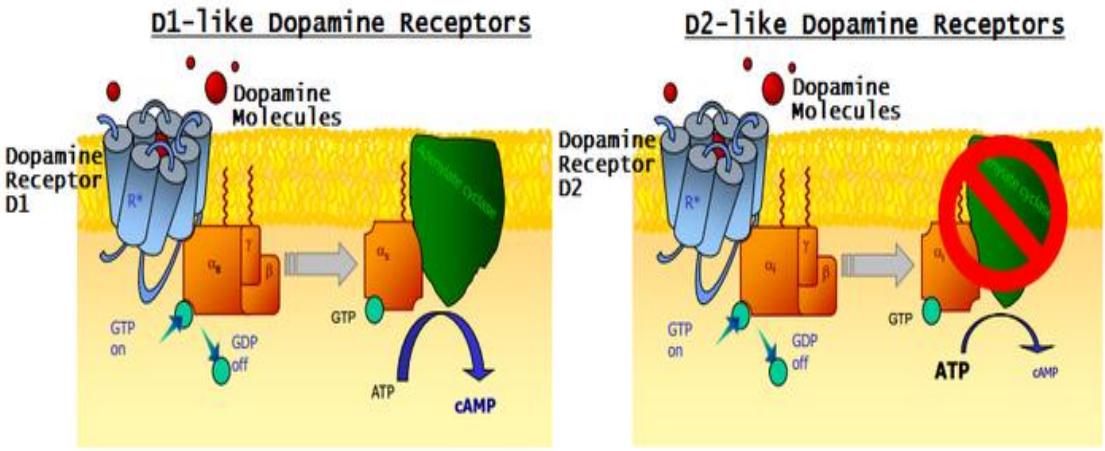

Figure 1.1 D1-like receptors couple with G proteins and activate adenylyl cyclase which catalyses the conversion of ATP to cAMP and pyrophosphate, which in turn serve as a regulatory signal to activate various other molecules. D2-like receptors which includes dopamine receptors D2, D3 and D4, also couple with G proteins but act in inhibiting adenylyl cyclase (Finch, 2013).

1.2 Dopamine receptor interacting proteins (DRIPs)

Dopaminergic neurons are mainly found in substantia nigra and ventral tegmental area and are thought to be involved in the control of movements, the signalling of error in prediction of reward, motivation, and cognition (Carrion and Poppel, 2007). There is abundant evidence that the dopamine system is involved in schizophrenia especially from the observation that a large number of antipsychotics such clozapine and chlorpromazine have dopamine-receptor antagonistic effects on D2 receptors (Greengard, 2001), Tenn et al., 2003, Peleg-Raibstein et al., 2008). Eleven dopamine receptor interacting proteins (DRIPs) were identified from a human adult brain cDNA library (Table 1.1) (Zhan et al., 2011). In this study they found that all the DRIPs might play an important role in dopamine signalling and are mapped to regions of the genome implicated in schizophrenia (Zhan et al., 2011). Amongst the identified dopamine receptor interacting protein include DOCK10 which is an interleukin-4 (IL4)-inducible gene in chronic lymphocytic leukemias (CLLs) mainly expressed in peripheral blood (PB) leukocytes (Yelo et al., 2008), guanine nucleotide binding protein, β-peptide 2-like I (GNB2LI) which is a housekeeping gene and a novel dopamine receptor interacting protein, Alix (ALG-2 interacting protein 1). Alix is a calcium-binding protein necessary for caspase-dependent and –independent cell death under the control of ALG-2 (Trioulier et al., 2004). Zhan and colleagues proposed that Alix may be important for the stability and trafficking of dopamine receptors at the membrane surface and found that it was able to up-regulates D1 and D3 receptor expression (Zhan et al., 2008).

Table 1.1 Dopamine receptor interacting proteins (DRIPs)

Receptor	DRIP	Gene	Protein Name	Chromosome	Function
D1	DRIP-4	*PDCD6IP*	AIP1, Alix, HP95	3p23	Cell death
	DRIP-7	*GNB2LI*	Unknown	5q35	G-protein signalling
	DRIP-1	*CI4ORF28*	Unknown	14q21	Unknown
	DRIP-2	*DOCK10*	Nbla10300, ZIZ3	2q36	G-protein signalling
	DRIP-6	*LM02YRDC*	Unknown	11p13	Neuronal development
	DRIP-3	*TERF2IP*	RAP1	1p34	Translation
D2	DRIP-5	*MLLT3*	AF9, YEATS3	16q23	Telomeric repeat maintenance
	DRIP-8	*PDCD6IP*	AIP1, Alix, HP95	9p21	Development
D3	DRIP-4	*P4HAI*	Unknown	3p23	Cell death
D4	DRIP-10	*KIFIA*	ATSV, C2orf20, HSN2C, MRD9, SPG30, UNC104	10q22	Enzyme
	DRIP-11	*PIM2*	PIM2	2q37	Molecular motor
D5	DRIP-9		Unknown	Xp11	Cell death

Table 1.1: The 11 DRIPs that were identified from a human adult brain cDNA library (Zhan et al., 2011).

1.3 Glutamate receptors

Glutamate receptors are a family of ionotropic or metabotropic glutamate receptors (Kristiansen et al., 2007) that are responsible for the glutamate-mediated post-synaptic excitation of neuronal cells, and play vital roles in neural communication, memory formation and learning (Debanne et al., 2003; Liu et al., 2006, Kantrowitz and Javitt, 2010).

The ionotropic glutamate receptors are split into three main families, AMPA receptor (α-amino-3-hydroxyl-5-methyl-4-isoxazole-propionate), NMDA receptor (N-Methyl-D-Aspartate) and Kainate receptor. Each receptor family is composed of a number of specific subunits, GluA1–GluA4 (AMPA receptors), GluK1–GluK5 (kainate receptors), GluN1, GluN2A–GluN2D, GluN3A, and GluN3B (NMDA receptors)(Traynelis et al., 2010). All ionotropic glutamate receptors are tetrameric assemblies and although AMPAR and kainate can be heteromeric or homomeric, NMDARs are only functional as heteromeric complexes of GluN1 and GluN2 subunits (Traynelis et al., 2010). The metabotropic glutamate receptors are G-protein coupled receptors (GPCRs) that have been subdivided into three groups. Group I mGlu receptors (mGlu1 and mGlu5) are coupled to PLC and intracellular calcium signalling, while group II (mGlu2 and mGlu3) and group III receptors (mGlu4**,**mGlu6**,** mGlu7 and mGlu8) are negatively coupled to adenylyl cyclase (Endoh, 2004).

All ionotropic glutamate receptors are ligand-gated nonselective cation channels which allow the flow of K^+ out, Na^+ and sometimes Ca^{2+} in to the cell following glutamate binding whereas metabotropic receptors indirectly modulate ion-channels on the plasma membrane through G protein dependent signalling cascade (Kantrowitz and Javitt, 2010). Upon glutamate binding, an agonist will trigger a series of conformational changes in the multisubunit receptor complex which results in the opening of the central ion channel of

the receptor and allows cation flow and a subsequent change in membrane excitability. This change in membrane excitability results in the generation of an excitatory postsynaptic current (EPSC) (Nicoll and Malenka, 1999)(Figure 1.2). This will then cause current depolarization, and, if enough glutamate receptors are activated may trigger an action potential in the postsynaptic neuron that then produce excitatory postsynaptic potential which results in an increase of Ca^{2+} concentration triggering a cascade of molecular events in the postsynaptic cells (Karakas et al., 2015). The duration of EPSP would depend on the agonist binding rate and the opening rate of the postsynaptic receptors (Hammond C. 2008). At resting membrane potentials, NMDA receptors are functionally 'silent' due to an internal binding site within the ion pore for an Mg^{2+} ion, and are subject to voltage-dependent Mg^{2+}blockThis blockade is removed by membrane depolarisation (Johnson and Ascher, 1990). Therefore for NMDA receptors to open, they rely on the coincident depolarisation produced by AMPA receptor opening. Furthermore NMDA receptors are permeable to Ca^{2+} which is an important intracellular signalling molecule in the nervous system (Pearlstein et al., 2015). Through transducing signaling cascades and regulating gene expression, the flow of Ca^{2+} through NMDA receptors is thought to cause both long term potentiation (LTP) and long term depression (LTD) (Lau et al., 2009).

The NMDA receptor is of considerable interest as it is thought to play a critical role in synaptic plasticity through calcium flux, a cellular mechanism for learning and memory (Paoletti et al., 2013). The NMDA receptor which is clustered at the synapse by components of the post synaptic density (PSD) is distinctive as it is both ligand-gated and voltage-dependent and it requires coactivation by two ligands, glutamate and either D-serine or glycine (Anson et al., 1998). The NMDA receptor forms a heterotetramer of two GluN1 and two GluN2 subunits. There are several receptor isoforms with distinct brain distributions and functional properties derived by alternate splicing of the GluN1

transcripts and differential expression of the GluN2 subunits (GluN2A, GluN2B, GluN2C and GluN2D) with both the GluN2A and GluN2B isoforms dominating expression in the adult brain (Kantrowitz and Javitt, 2010).

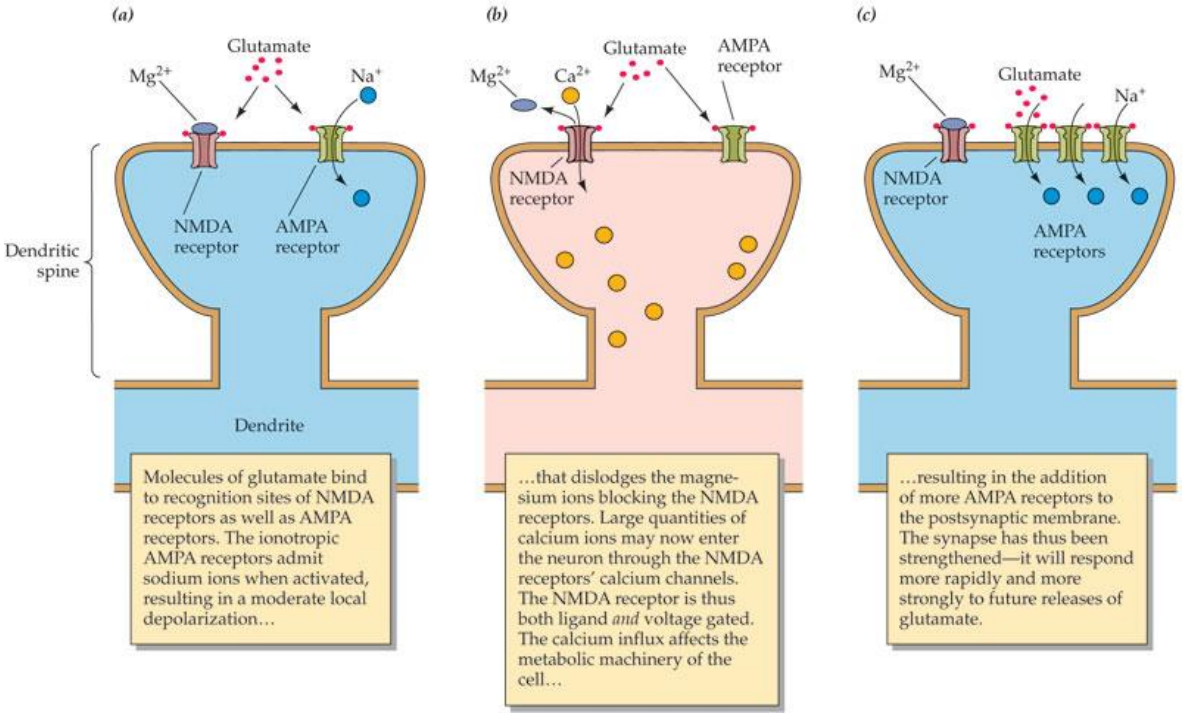

Figure 1.2 The NMDA receptor is different from most receptor molecules because it is both ligand-gated and voltage-sensitive. When the NMDA receptor is activated, Ca^{2+} ions flow through its channel into the neuron. The reason for the low Ca^{2+} conductance at these membrane potentials is that magnesium ions (Mg^{2+}) block the NMDA receptor's central Ca^{2+} channel. AMPA receptor activation allows Na^+ ions to flow into the neuron, so sufficient activation of AMPA receptors can partially depolarize the membrane that removes the Mg^{2+} block. The NMDA receptor now responds strongly and admits large amounts of Ca^{2+} through the channel which starts a cascade of effects (Breedlove, S. Marc., Watson, Neil. V., 2013).

Among the glutamate receptor channels, NMDA receptors are generally the most permeable to Ca^{2+} (Lipton, 2004). Excessive activation of the NMDA receptor leads to production of damaging free radicals and other enzymatic processes that contributes to cell death (Figure 1.3) (Budd et al., 2000; Lipton and Nicotera, 1998; Lipton, 2004). The activation of NMDA receptors allows Ca^{2+} (and other cations) to enter the cell (Lipton and Nicotera, 1998). In synaptic transmission under normal conditions the NMDA receptor

channel is blocked by Mg^{2+} and only activated for brief periods of time (Lipton, 2004). Over activation of the NMDA receptor causes an excessive amount of Ca^{2+} influx into the nerve cell which then triggers a variety of processes that can lead to necrosis or apoptosis (Tenneti et al., 1998)(Figure 1.3). They include processes such as Ca^{2+} overload of mitochondria, resulting in oxygen free radical formation and activation of caspases, Ca^{2+}-dependent activation of neuronal NOS, leading to increase NO production and the formation of toxic peroxynitrite ($ONOO^{-}$), and stimulation of mitogen-activated protein kinase p38 (MAPK p38), which activates transcription factors that can go into the nucleus and influence neuronal injury and apoptosis (Dawson et al., 1991; Lipton and Nicotera, 1998; Lipton, 2004).

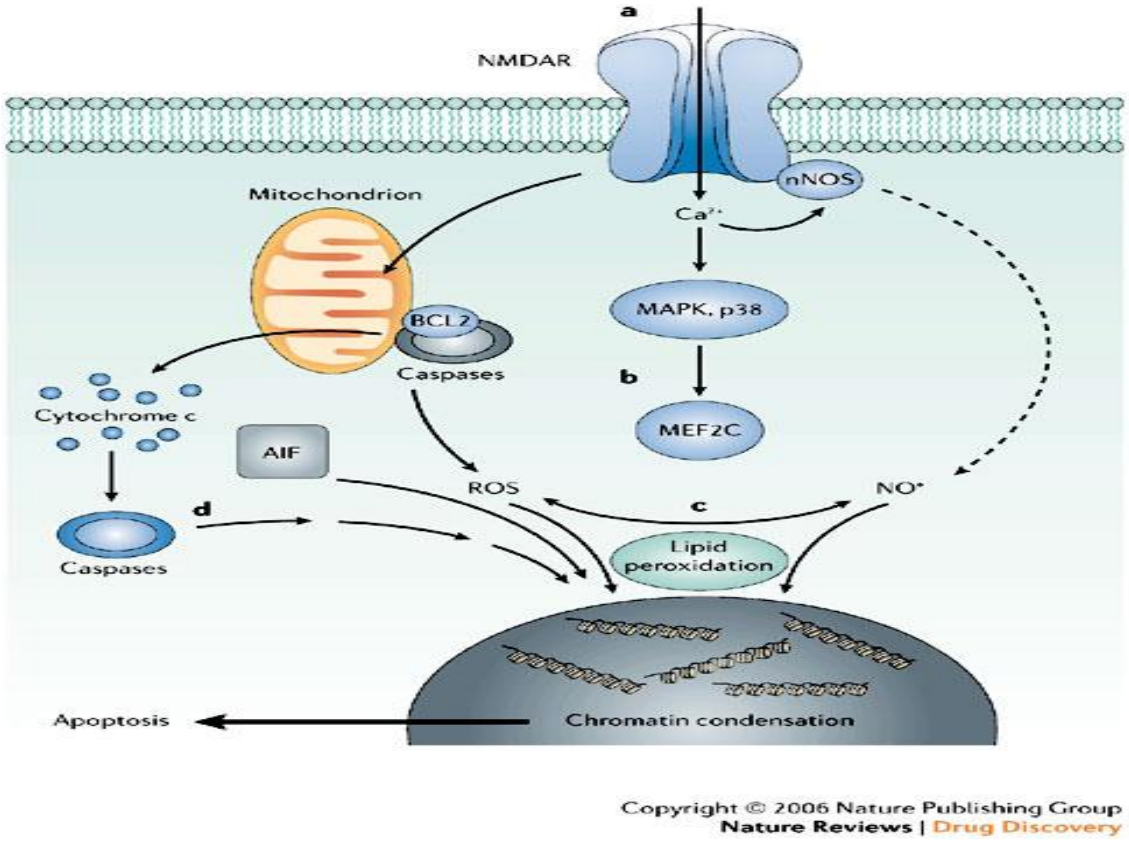

Figure 1.3: Schematic illustration of the apoptotic pathways triggered by excessive NMDA receptor activity. The cascade includes NMDAR overexpression, activation of the p38 mitogen-activated kinase (MAPK)–MEF2C (transcription factor) pathway (MEF2 is then cut by caspases to form an endogenous dominant-

interfering form that contributes to neuronal cell death, toxic effects of free radicals such as nitric oxide (NO) and reactive oxygen species (ROS) and activation of apoptosis-inducing enzymes including caspases and apoptosis-inducing factor (Lipton, 2006).

1.4 Post Synaptic Density

The post synaptic density is a structure located beneath the postsynaptic membrane and is comprised of membrane receptors, ion channels, scaffold and adaptor proteins, signalling proteins, cell adhesion molecules and components of the cytoskeleton (Kennedy, 1997) (Figure 1.4). Several functions have been proposed for this structure including regulation of adhesion, control of receptor clustering, and regulation of receptor function (Siekevitz, 1985). Glutamate receptors, such as NMDARs (*N*-methyl-D-aspartate receptors) are located more to the centre of the membrane and AMPARs (α-amino-3-hydroxy-5-methyl-4-isoxazole propionic acid receptors), are located more at the peripheral of the postsynaptic membrane (Feng and Zhang, 2009). On stimulation, the excitatory glutamatergic synapses such as glutamate is released from the presynaptic terminal and acts on the glutamate receptor channels NMDA and AMPA on the postsynaptic side to allow the influx of specific ions that depolarize postsynaptic membranes and thus, neuronal signals are received, decoded and further propagated by the PSD (Feng and Zhang, 2009).

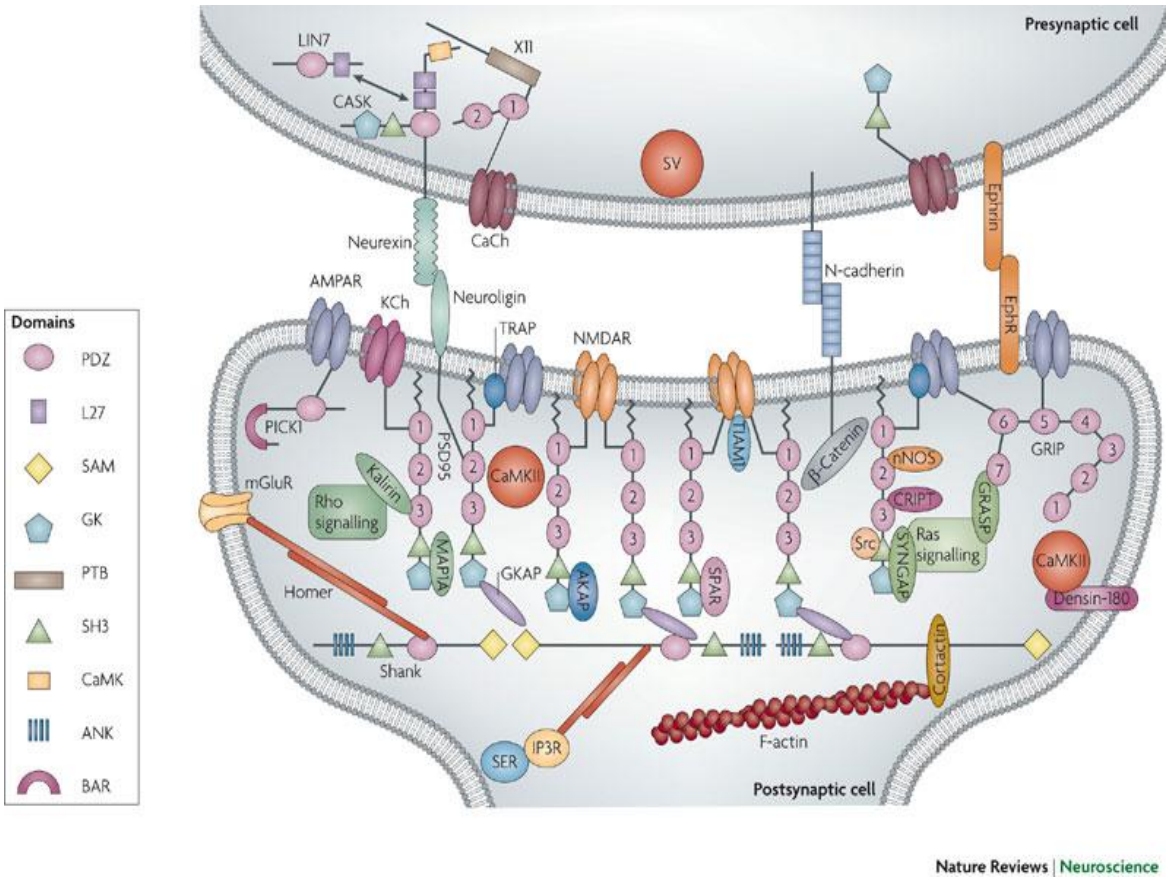

Figure 1.4: Schematic diagram of the network of proteins in the postsynaptic density. Only major pathways and certain classes of PSD are shown (Feng and Zhang, 2009). The post synaptic density comprises of membrane receptors, ion channels, adaptor proteins, signalling proteins, cell adhesion molecules and components of the cytoskeleton.

1.5 Potential crosstalk pathways between dopamine and glutamate receptors and their implications

There have been many studies that support the idea of a functional interaction between dopamine receptors and glutamate receptors (Greengard, 2001, Lee et al., 2002, Liu et al., 2006). One of these is the interaction of D1 receptor carboxyl tail that directly couples to NMDA receptor subunit GluN1-1a and GluN2A (Lee et al., 2002) and enhances D1 receptor cAMP accumulation (Pei et al., 2004). However, it is still not known how the other potential interactions further downstream of the receptors might take affect at the molecular level such as downstream targets DARPP-32 (Figure 1.5). Alix and other

DRIPs known to interact with dopamine receptors identified by Zhan et al., 2011 may also play a role in glutamate receptor signalling and potentially make an important contribution to in the interactionsbetween dopaminergic and glutamatergic signalling pathways.

Alix is a calcium-binding protein necessary for caspase-dependent and –independent cell death under the control of ALG-2 which is a protein with sequence homology to calmodulin that is implicated in regulating DARPP-32 (Figure 1.5) (Trioulier et al., 2004,(Sadoul, 2006). Calcium/calmodulin-dependent protein kinase IV (CaMKIV) is the most important Ca^{2+}-activated CREB kinase along with NR2B and CaMKIV are considered to be memory related genes and synaptic plasticity genes (Li et al., 2011).

NMDA receptors are of considerable interest in schizophrenia as evidenced by the ability of NMDAR antagonists such as phencyclidine (PCP) and ketamine to induce many symptoms and deficits that are associated with schizophrenia (Hirsch et al., 1997, Scott and Aperia, 2009, Kantrowitz and Javitt, 2010). There is also evidence that glutamate receptor deficiencies occur in some cases of schizophrenia where a restricted deletion of the essential GluN1 subunit of the NMDA receptor was selectively eliminated in 40–50% of cortical and hippocampal in early postnatal corticolimbic interneurons as well as another study that generated a mouse model expressing only 5% of the GluN1 subunit that triggers behavioural and pathophysiological symptoms that resemble schizophrenia (Hirsch et al., 1997).

The excitatory postsynaptic potential (EPSP) produced by the activation of NMDA receptor increases the concentration of Ca^{2+} in the cell which can in turn function as a second messenger in various signalling pathways such as the extracellular signal regulated kinase (ERK) pathway and reverse cyclic AMP-stimulated phosphorylation through activation of calcineurin that affects DARPP-32 (Figure 1.5) (Gould and Manji,

2005; Hirsch et al., 1997). DARPP-32 has a central role in dopaminergic and glutamatergic signaling in integrating the activity of these two pathways (Gould and Manji, 2005). DARPP-32 mediates the drug-related changes in the activity of the ERK pathway (Gould and Manji, 2005). Activation of the ERK cascade depends on both dopamine and glutamate receptor activation and is known to be important for long-term synaptic plasticity (Gould and Manji, 2005).

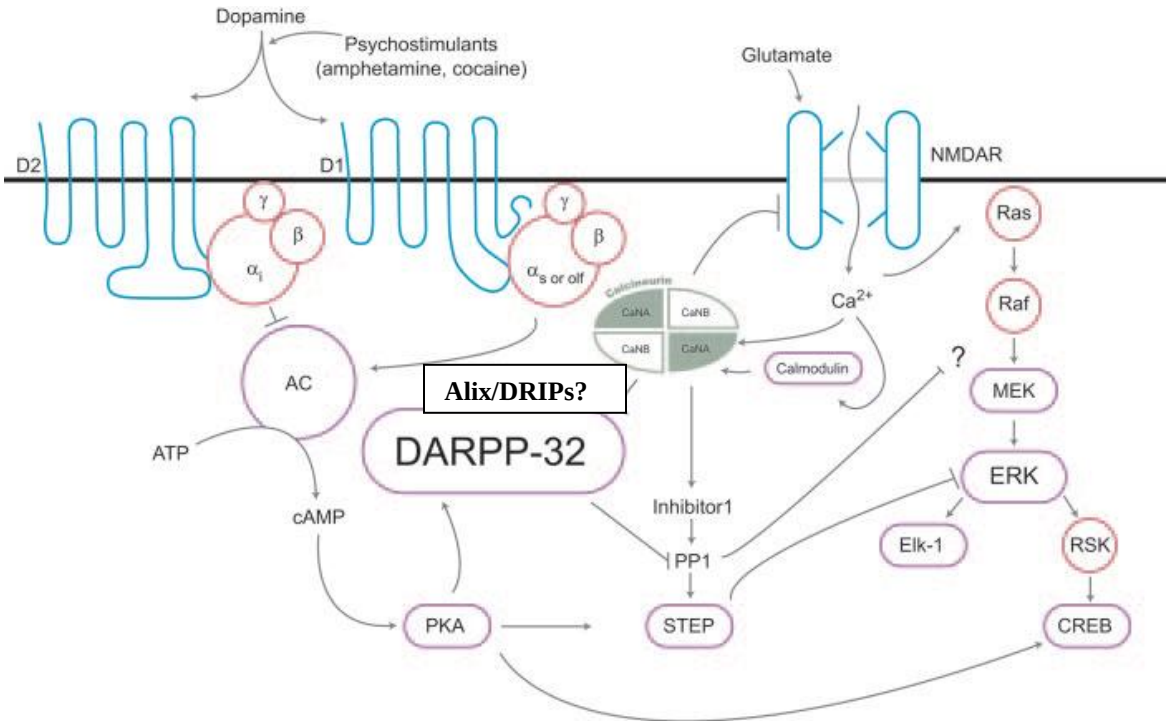

Figure 1.5: Diagram of the downstream signalling pathways for glutamate and dopamine receptors and potential intracellular 'crosstalk' pathways (Gould and Manji, 2005)

1.6 ALG-2 interacting protein X (Alix)

Alix is a cytoplasmic adaptor protein that is 95 kDa in size, contains a proline rich C terminal region and is widely conserved in eukaryotes (Subramanian et al., 2004). It was first characterized as an interactor of ALG-2 (apoptosis-linked gene 2) and is involved in apoptosis, regulation of cell adhesion, protein sorting, adaptation to stress conditions, ESCRT (endosomal sorting complex required for transport)-mediated membrane invagination, abscission in cytokinesis and budding of human immunodeficiency virus (HIV) (Trioulier et al., 2004; Ohkouchi et al., 2004).

ALG-2 is a calmodulin type calcium binding protein that is required for apoptotic induction while the down regulation of ALG-2 enhances cell survival by interfering with Ca^{2+} mediated apoptotic signals (Wu et al., 2002; Subramanian et al., 2004). The ability of Alix to participate in a spectrum of activities stems from its domain architecture (Figure 1.6). BLAST analysis of Alix amino acid sequences shows that Alix has a 97% sequence homology between human and mouse (Figure 1.6.1). Therefore there is a high degree of amino acid sequence conservation within the Alix protein sequence and within the functional domains (Bro1 and SH2) between these species.

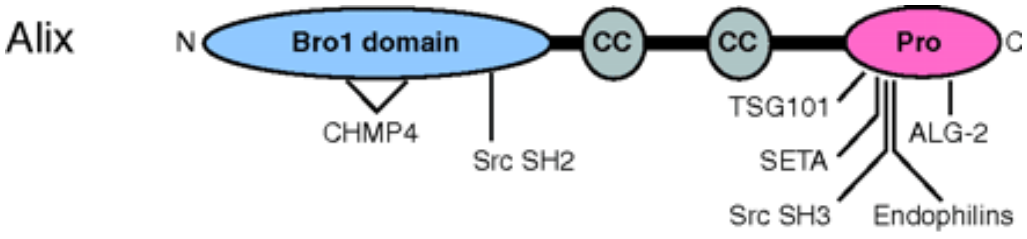

Figure 1.6: Domain architecture of Alix. The N-terminal of Bro1 domain mediates localization to endosomes, an important functional site for Alix. The C-terminal region interacts with the majority of proteins that connect Alix to cellular processes. The Bro1 domain and C-terminal region are linked by a relatively uncharacterized sequence containing two coiled-coil domains (Odorizzi, 2006).

```
Homo sapiens  1    MATFISVQLKKTSEVDLAKPLVKFIQQTYPSGGEEQAQYCRAAEELSKLRRAAVGRPLDK  60
Mus musculus  1    MASFIWVQLKKTSEVDLAKPLVKFIQQTYPSGGEEQAQYCRAAEELSKLRRSALGRPLDK  60
```

<<<----------

```
Homo sapiens  61   HEGALETLLRYYDQICSIEPKFPFSENQICLTFTWKDAFDKGSLFGGSVKLALASLGYEK  120
Mus musculus  61   HEGALETLLRYYDQICSIEPKFPFSENQICLTFTWKDAFDKGSLFGGSVKLALASLGYEK  120
```

```
Homo sapiens  121  SCVLFNCAALASQIAAEQNLDNDEGLKIAAKHYQFASGAFLHIKETVLSALSREPTVDIS  180
Mus musculus  121  SCVLFNCAALASQIAAEQNLDNDEGLKTAAKQYQFASGAFLHIKDTVLSALSREPTVDIS  180
```

```
Homo sapiens  181  PDTVGTLSLIMLAQAQEVFFLKATRDKMKDAIIAKLANQAADYFGDAFKQCQYKDTLPKY  240
Mus musculus  181  PDTVGTLSLIMLAQAQEVFFLKATRDKMKDAIIAKLANQAADYFGDAFKQCQYKDTLPKY  240
```

```
Homo sapiens  241  FYFQEVFPVLAAKHCIMQANAEYHQSILAKQQKKFGEEIARLQHAAELIKTVASRYDEYV  300
Mus musculus  241  FYFQEVFPTLAAKQCIMQANAEYHQSILAKQQKKFGEEIARLQHAAELIKNVASRYDEYV  300
```

```
Homo sapiens  301  NVKDFSDKINRALAAAKKDNDFIYHDRVPDLKDLDPIGKATLVKSTPVNVPISQKFTDLF  360
Mus musculus  301  NVKDFSDKINRALTAAKKDNDFIYHDRVPDLKDLDPIGKATLVKPTPVNVPVSQKFTDLF  360
```

```
Homo sapiens  361  EKMVPVSVQQSLAAYNQRKADLVNRSIAQMREATTLANGVLASLNLPAAIEDVSGDTVPQ  420
Mus musculus  361  EKMVPVSVQQSLAVFSQRKADLVNRSIAQMREATTLANGVLASLNLPAAIEDVSGDTVPQ  420
```

```
Homo sapiens  421  SILTKSRSVIEQGGIQTVDQLIKELPELLQRNREILDESLRLLDEEEATDNDLRAKFKER  480
Mus musculus  421  SILTKSTSVVEQGGIQTVDQLIKELPELLQRNREILEESLRLLDEEEATDNDLRAKFKDR  480
```

-N Terminal-<<---------->>-C terminal----------

```
Homo sapiens  481  WQRTPSNELYKPLRAEGTNFRTVLDKAVQADGQVKECYQSHRDTIVLLCKPEPELNAAIP  540
Mus musculus  481  WQRTPSNDLYKPLRAEGAKFRAVLDKAVQADGQVKERYQSHRDTIALLCKPEPELNAAIP  540
```

```
Homo sapiens  541  SANPAKTMQGSEVVNVLKSLLSNLDEVKKEREGLENDLKSVNFDMTSKFLTALAQDGVIN  600
Mus musculus  541  SANPAKTMQGSEVVSVLKSLLSNLDEIKKERESLENDLKSVNFDMTSKFLTALAQDGVIN  600
```

```
Homo sapiens  601  EEALSVTELDRVYGGLTTKVQESLKKQEGLLKNIQVSHQEFSKMKQSNNEANLREEVLKN  660
Mus musculus  601  EEALSVTELDRIYGGLTSKVQESLKKQEGLLKNIQVSHQEFSKMKQSNNEANLREEVLKN  660
```

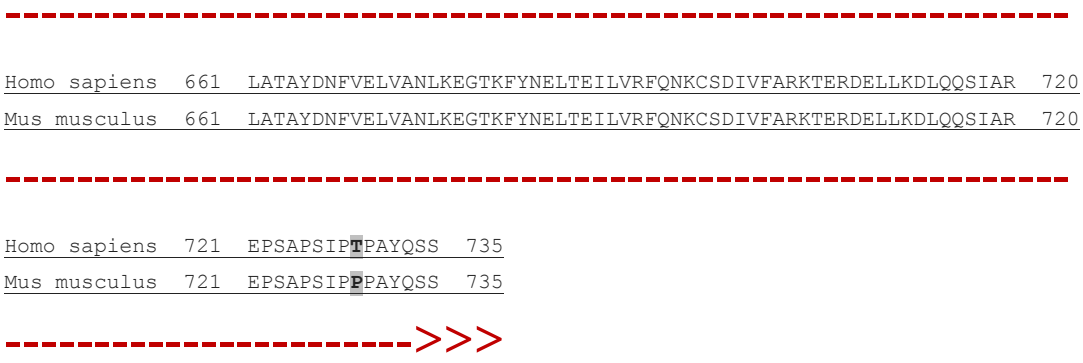

Figure 1.6.1 : BLAST sequence analysis between human Alix (Homo sapiens) and mouse Alix (Mus musculus). N terminal indicated with green spaced lines underneath include the Bro domain and Src homology domain (Src SH2). C terminal indicated with red spaced lines underneath include the proline rich region, the ALG-2 interacting domain and Src homology domain (Src SH3). The grey marked background indicates sequences that differ between human Alix (Homo sapiens) and mouse Alix (Mus musculus). We noticed that there is little difference between the sequences and most changes were homologous and spread out throughout the protein sequence.

A common factor in many apoptotic proceses is the cytosolic Ca^{2+} release from ER stores which induce caspase 9 activation and regulated by ALG-2 (Strappazzon et al., 2010). The interaction between Alix and ALG-2 through its C-terminal proline-rich region is shown to be Ca^{2+} dependent, where Ca^{2+} binding to ALG-2 induces a conformational change which allows it to interact with Alix (Katoh et al., 2003; Strappazzon et al., 2010). It is suggested that interaction of Alix with ALG-2 in a Ca^{2+}-dependent manner implies that there is a relationship between Alix and Ca^{2+} signalling (Ohkouchi et al., 2004). Strappazzon et al., 2010 theorise that ALG-2 and Alix cooperate in transducing the Ca^{2+} regulated signal during cell death considering ALG-2 needs to bind to Ca^{2+} in order to interact with Alix. They also found that Alix is required for the caspase 9 activation that is induced by calcium elevation which suggest that Alix and ALG-2 act upstream of caspase 9.

The endosomal system is a series of intracellular compartments of endocytosed trafficked molecules where most endocytosed protein are returned to the membrane and some degraded proteins are trapped in vesicles budding from the membrane to the lumen of the endosomes (Mahul-Mellier et al., 2009). This leads to the formation of multivesicular bodies (MVBs) that will be hydrolysed after fusion with lysosomes which trigger the sequential building of the ESCRTs on to the endosomal membrane (Gruenberg and Stenmark, 2004). Endosomal membrane vesiculation is triggered by CHMPs (charged multi vesicular body proteins) and Alix which binds to both ESCRT-I and ESCRT-III, as well as to LBPA (lysobisphosphatidic acid) to form a lattice entrapping transmembrane proteins facilitating the budding of vesicles inside MVBs (Sadoul, 2006). (Mahul-Mellier et al., 2009) suggest that endosomal function is central to neurodegenerative pathologies and adaptor protein Alix seems to mediate interaction within endosomes control the initiation of a neuronal death programme.

The ESCRT machinery can be recruited to many different biological membranes to help mediate membrane fission events and most of the ESCRT pathway proteins involve 5 complexes which are ESCRT-0,-I,-II,-III and VPS4 (vacuolar protein sorting associated protein 4), whilst Alix would function as a discrete protein in the ESCRT pathway (Wollert and Hurley, 2010). Early acting factors such as ESCRT-I, ESCRT-II and Alix would interact with upstream recruiting factors and deform membranes, recruit ESCRT-III subunit and form filaments within the necks of membrane tubules and mediate membrane fission (Wollert and Hurley, 2010). Endosomal ESCRT-III is thought to be very transient and (Chassefeyre et al., 2015) hypothesize that ESCRT-III assemblies comprising of Alix, Chmp4, and Chmp2 can reshape the plasma membrane during cytokinesis and membrane repair and that the endosome has been shown to play an important role in postsynaptic plasticity.

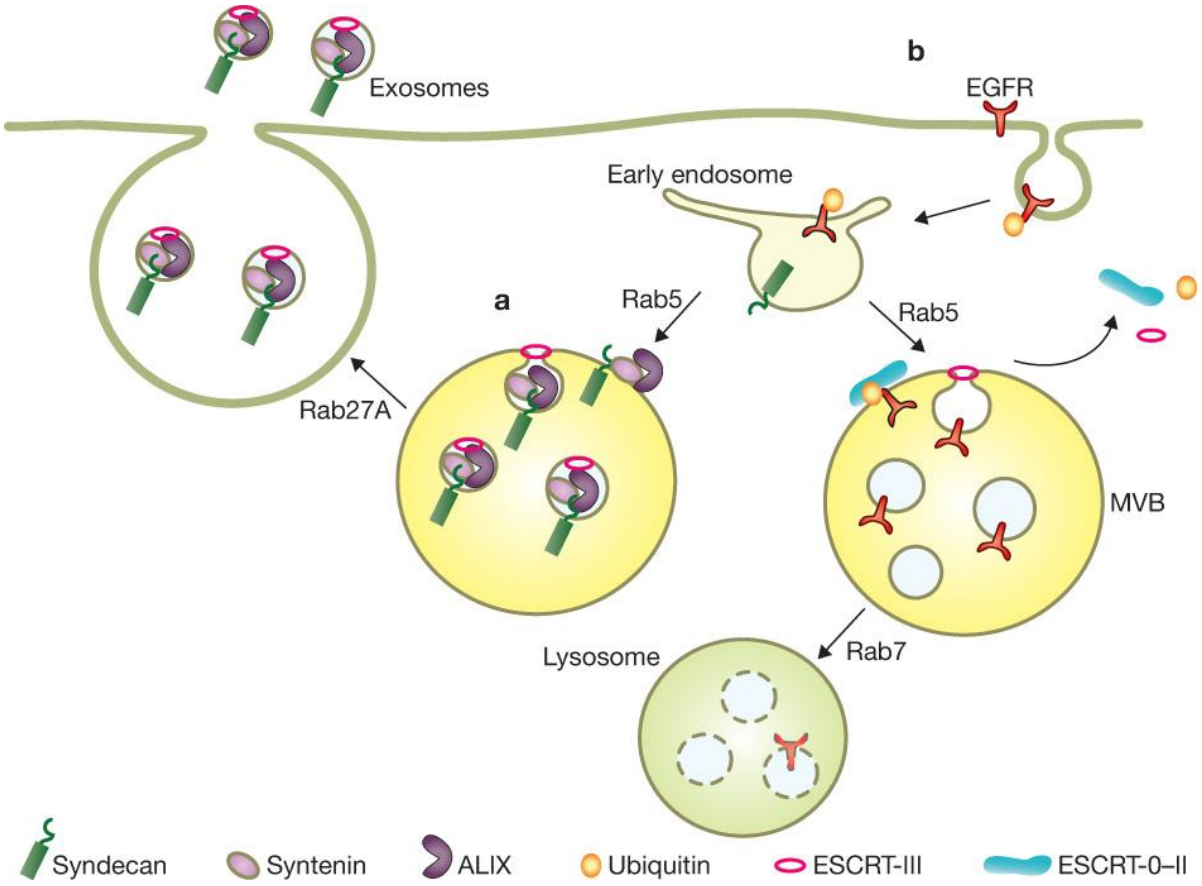

Figure 1.7 The endosomal ESCRT pathway. The MVB pathway appears to require the sequential function of the ESCRT complexes and recruitement of Alix mediated by Chmp4 to the Bro1 domain of Alix for apoptotic signalling (Hurley and Odorizzi, 2012).

1.7 Cellular mechanism of Alix in apoptosis

Programmed cell death (PCD) has been divided into two general types: PCD, in which the cell plays an active role; and passive cell death such as necrotic cell death. The PCD development has been classified morphologically into three main types, type 1, apoptotic, type 2, autophagic, and type 3, cytoplasmic (Clarke, 1990). The best characterized PCD is apoptosis where cells display membrane blebbing, loss of the asymmetry, nuclear fragmentation, and activation of caspases which is family of cell-suicide cysteine proteases (Thornberry and Lazebnik, 1998; Sperandio et al., 2004).

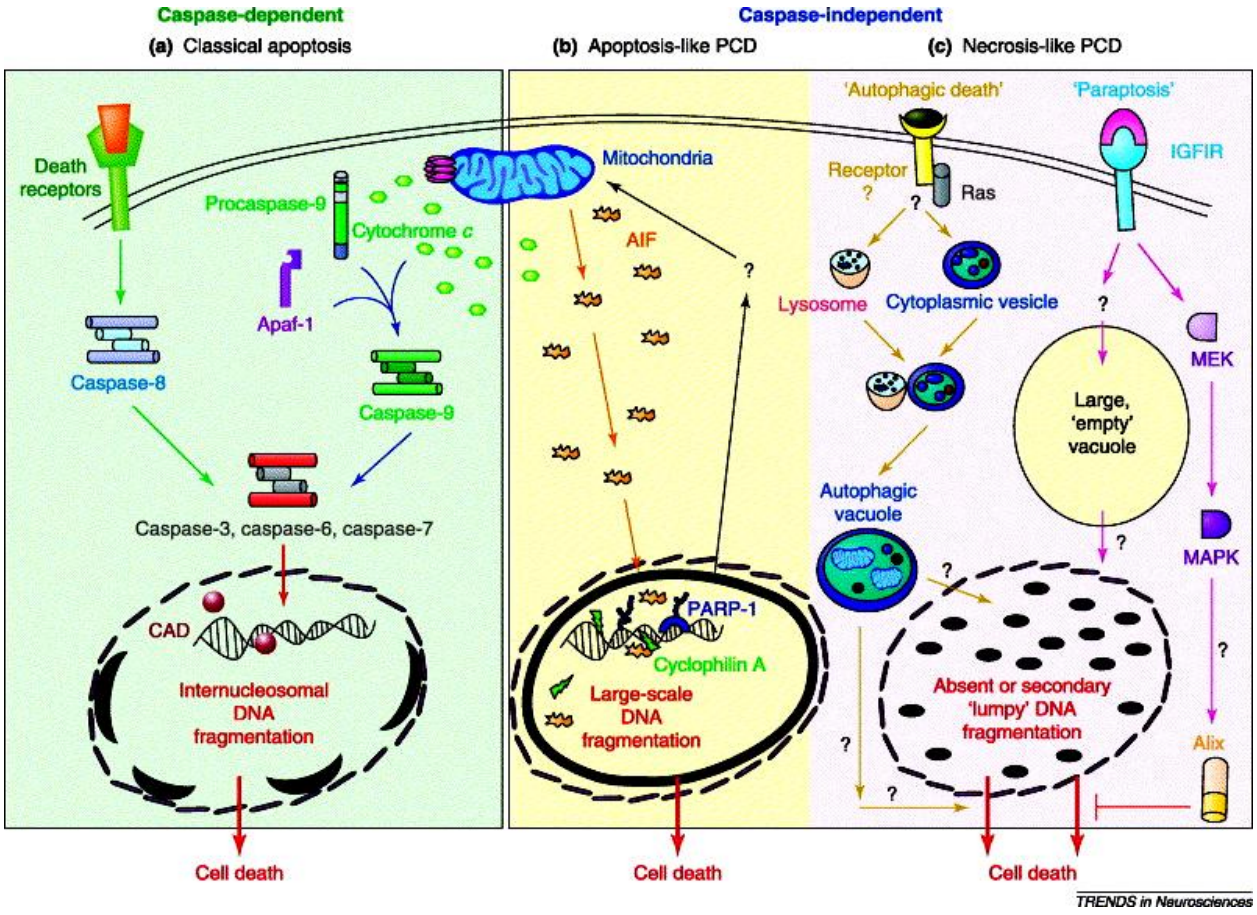

Figure 1.8: Schematic illustration of PCD. PCD can be divided to three types: **(a)** classical apoptosis (featuring 'crescent-like' chromatin condensation), **(b)** apoptosis-like PCD (featuring partial and peripheral chromatin condensation) and **(c)** necrosis-like PCD (featuring no primary chromatin condensation) (Krantic et al., 2005).

Apoptosis is activated through two major pathways (Figure 1.8). The first is the intrinsic pathway, which is initiated by the mitochondrial release of cytochrome *c*, and activation of caspase-9 and the second is the extrinsic pathway, initiated by the activation of cell surface death receptors such as Fas, and resulting in the activation of caspase-8 or -10 (Salvesen and Dixit, 1997). Cytochrome *c* associates with procaspase-9 to form a complex called the apoptosome after being released in the cytosol due to permeabilization of the outer mitochondrial membrane. (b) Apoptosis-like PCD is mediated by effectors such as apoptosis-inducing factor (AIF). Nuclear DNA damage leads to AIF release and its translocation to the nucleus, which is then associated with chromatin condensation and large-scale DNA fragmentation. (c) Necrosis-like PCD is not as well known. However, the existence of at least two forms of such PCD has been proposed with both forms displaying cytoplasmic vacuoles. The first is paraptosis, is triggered by the activation of the insulin-like growth factor 1 receptor (IGFIR) via the mitogen-activated protein kinase (MAPK) pathway. The activation of paraptosis is accompanied by the formation of large empty vacuoles and can be selectively inhibited by Alix (Sperandio et al., 2004). The second form is ‘autophagic degeneration’ and is mediated by the activation of mutated Ras. This death is associated with the formation of lysosome derived vacuoles with a double-membrane appearance (Sperandio et al., 2004; Krantic et al., 2005). It is found that cells that lack Alix, exhibits minor mitotic defects and abscission failure which results in termination of the midbody and coalescence into single cells with multiple nuclei (Morita et al., 2010).

1.8 Alix in the PSD and role in neuronal function

Alix was recently found in the human post synaptic density (hPSD) which is an important structure for nervous system disease and behaviour (Bayes et al., 2011). Using rat forebrain extracts, Alix was coeluted with Chmp2b and PSD-95 and at the synapse Chmp4b and Alix were found to form a stable polymer representing the ESCRT-III complex that associates with synaptic structures (Chassefeyre et al 2015). Further analysis of the immunoprecipitated ESCRT-III complex using mass spectrometry, revealed Alix within the ESCRT-III complex as well as Chmp 2b and GluN2B suggesting that the lysates contain a detectable amount of NMDA receptor subunit. These data indicate that Chmp2b and Alix exist within stable ESCRT-III and are attached to the spinos skeleton, around the PSD, at the spine shell and may play an unsuspected role in the regulation of long-term synaptic plasticity.

Calcium is important for regulating a variety of cellular responses especially in neurons and it is now well established that alterations in intracellular Ca^{2+} is a common factor of many apoptotic processes (Strappazzon et al., 2010). Overexpression of Alix *in vivo* correlates with calcium induced cell death in degenerating neurons of rat hippocampus undergoing epileptic seizures and in cultured neurons overexpression was sufficient to activate caspases and thereby apoptosis (Strappazzon et al., 2010). However, Alix apoptotic functions were dependent on their capacity to bind to ALG-2 where the expression of Alix lacking its ALG-2 binding site could block naturally occurring death of motor neurons during development of the chick embryo (Strappazzon et al., 2010; Mahul-Mellier et al., 2008). It was recently found that exosomes are secreted by neurons, and cortical neurons in culture have been found to release exosomes that contain Alix and AMPA receptors and the cell adhesion molecule L1/NgCAM, which, in the central nervous system is expressed only by neurons (Chivet et al., 2012).

Aims and Objectives:

1. Assess the role of the dopamine receptor interacting protein (DRIP), Alix in NMDA receptor function by examining its effect on recombinant NMDA receptor activity in mammalian cell lines such as HEK293 cells.

2. Analyse the co-expression of recombinant Alix and recombinant glutamate receptors using immunocytochemistry in mammalian cell lines and investigate endogenous expression of Alix in cultured primary neurons.

2.1 Materials

2.1 General chemicals

2.1.1 Reagents purchased from Sigma-Aldrich Co. Ltd. (Poole, Dorset, England)

2-Propanol, α- Minimum Essential Medium (DMEM), Beta-Mercaptoethanol, Dithiotreitol (DTT), Calcium Chloride Chloride ($CaCl_2$), Glucose, Horse Serum, HEPES, Laminin, Magnesium Chloride, Nonidet p-40 (NP40), Phosphate Buffered Saline (PBS), Poly-D-Lysine Hydrobromide, Potassium Chloride, Sodium Dodecyl Sulfate (SDS), Terrific broth (TB) tablets, TWEEN20, Sodium Bicarbonate ($NaHCO_3$), Sodium Chloride, Sodium Dihydrogen Phosphate (NaH_2PO_4), TritonX-100.

2.1.2 Reagents purchased from other suppliers

Agarose, (Bioline, London England)

Amino-5-Phosphonovaleric Acid (D-AP5) (Ascent Scientific, Cambridge, Cambridgeshire, UK)

Bradford dye (Bio Rad, Hemel Hempstead, Hertfordshire, UK)

Ethidium bromide (Bio-Rad Laboratories, Hemel Hempstead, Hertfordshire England)

Ethanol, Dimethyl Sulfoxide (DMSO), Methanol, Paraformaldehyde (PFA), Phenol: Chloroform: Iso-Amyl Alcohol (VWR International Ltd., Lutterworth, Leicestershire, England).

B-27 Supplement (50x), Fetal Bovine Serum (FBS), Gentamycin, Glycine, Lipofectamine 2000, L-Glutamine 200mM, Neurobasal Medium, NuPage MOPS buffer, NuPage transfer buffer, NuPage SDS-polyacrylamide gel, Penicilin Streptomycin, TrypLE Express, Ultra Pure Tris, ProLong Gold reagent (Life Technologies, Paisley, UK)

Magnetofection - NeuroMag (Oz Biosciences, Marseille, France)

N-methyl-D-aspartate (NMDA) (Abcam, Cambridge, Cambridgeshire, UK)

Protease Inhibitor, EDTA Free (Roche, Mannheim, Germany)

NEB 5-alpha *E.coli.* competent cells (New England Biolabs, Hitchin, UK)

Restriction enzymes (New England Biolabs, Hitchin, UK or Roche, Mannheim, Germany)

2.1.3 Molecular weight standards

BLUE Wide Range Prestained Protein Ladder (Geneflow, Swift Valley, Rugby, UK)

2.1.4 Antibodies

Anti-Alix mouse antibody (Abcam, Cambridge, Cambridgeshire, UK)

Anti-FLAG rabbit antibody (Sigma Aldrich, Poole, Dorset, UK)

Anti-NMDAR1 mouse antibody (BD Biosciences, San Jose, California, USA)

Anti-EEA1 mouse antibody (BD Biosciences, San Jose, California, USA)

Anti-LAMP1 mouse antibody (Enzo Life Sciences, Matford Court, Exeter, UK)

Anti-PSD95 mouse antibody (Abcam, Cambridge, Cambridgeshire, UK)

Anti-NR2A/2B rabbit antibody (Millipore UK)

Anti-PSD95 rabbit antibody (Abcam, Cambridge, Cambridgeshire, UK)

Anti-EEA1 rabbit antibody (Abcam, Cambridge, Cambridgeshire, UK)

Alexa Fluor 568 Goat Anti-Mouse (Life Technologies, Paisley, UK)

Alexa Fluor 488 Donkey Anti-Rabbit (Life Technologies, Paisley, UK)

Alexa Fluor 488 Goat Anti-Mouse (Life Technologies, Paisley, UK)

IRDye 800 Goat Anti-Mouse (Licor bioscience Ltd, Nebraska, USA)

2.1.5 Kits

Qiagen EndoFree Plasmid Maxi Kit (Qiagen Ltd, Crawley, West Sussex, UK)

2.1.6 Equipment

Bio-Rad gel casting system, Bio-Rad wide mini-sub cell electrophoresis system, Gel Doc XR system, PowerPac 300 power supply, GenePulser Xcell electroporator (Bio-Rad Laboratories, Hemel Hempstead, Hertfordshire England)

Nanodrop spectrophotometer (Thermo Scientific, Wilmington, USA)

Odyssey Infrared Imagining System (Li-cor Biosciences, Nebraska, USA).

Olympus spinning disc confocal system (CARV from Digital Imaging Solutions) with an EM-CCD camera (Rolera/QI Cam 3500) mounted on an Olympus X71 microscope, using a 100x fluoplan objective.

2.2 Methods

2.2.1 Plasmid cDNAs

In order to assess the effects of Alix co-expression on NMDA receptor triggered cell death in HEK293 mammalian cells we obtained cDNAs of various recombinant proteins from a number of sources. cDNA plasmids for Alix (GFP tagged in pCMVTag2C) were kindly donated by Dr. Jamal Nasir (Zhan et. al. 2008), Alix (Flag tagged in pCi) donated by Dr. Remy Sadoul (Chatellard-Causse et al., 2002a) GluN1 in pRK7 and GluN2A in pRK7 (Schorge and Colquhoun, 2003) kindly donated by Dr. Philip Chen.Variants of the Alix plasmids are represented in the figures below created using SNAPGENE. Alix human corresponds to human Alix cDNA subcloned into GFP tagged in pCMVTag2C. Alix wild type coresponds to mouse Alix cDNA subcloned into pCI Flag. Alix CT corresponds to a fragment expanding from amino acid 468 to 869 of Alix and Alix NT corresponds to amino acids 1-434. Alix DPRD lacks a fragment encompassing a proline rich region from amino acids 717 to 867 of Alix.

Alix Human in pcDNA3.1 His A

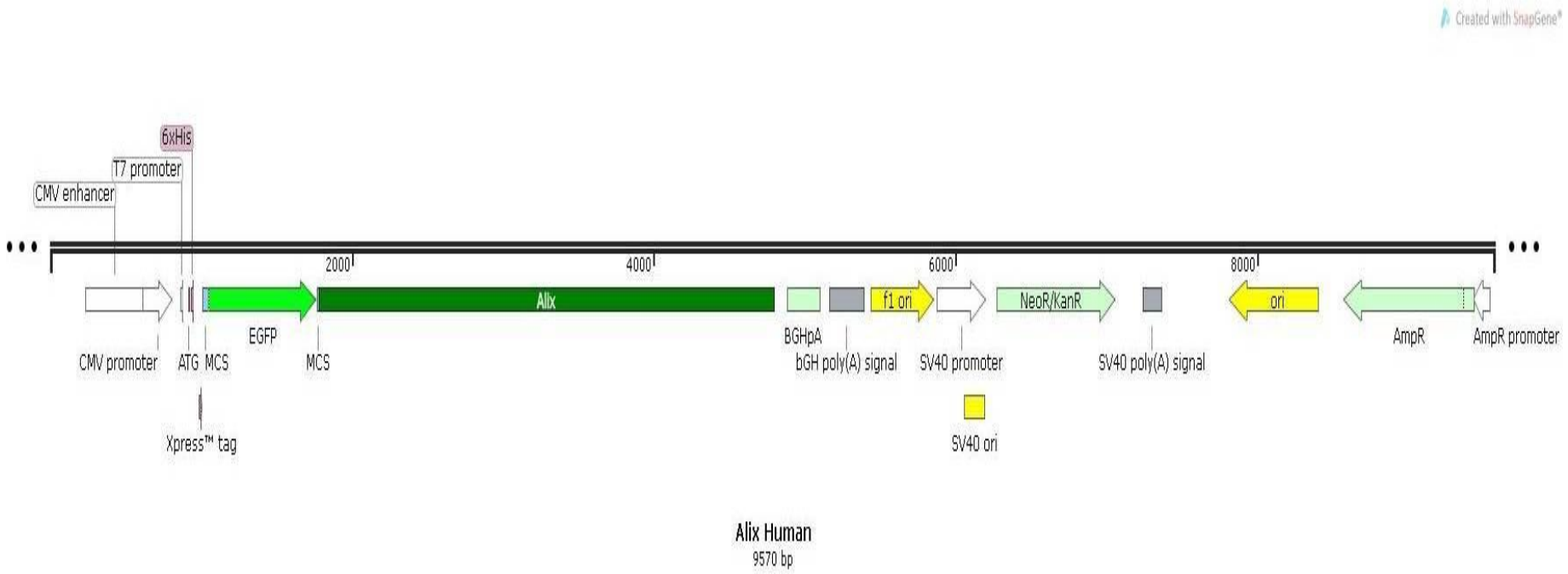

Figure 2.1 The figure represents the cDNA plasmid Alix GFP tagged in pCMVTag2C with full human Alix cDNA subcloned into GFP tagged in pCMVTag2C.

Alix WT Mouse in pCI Neo

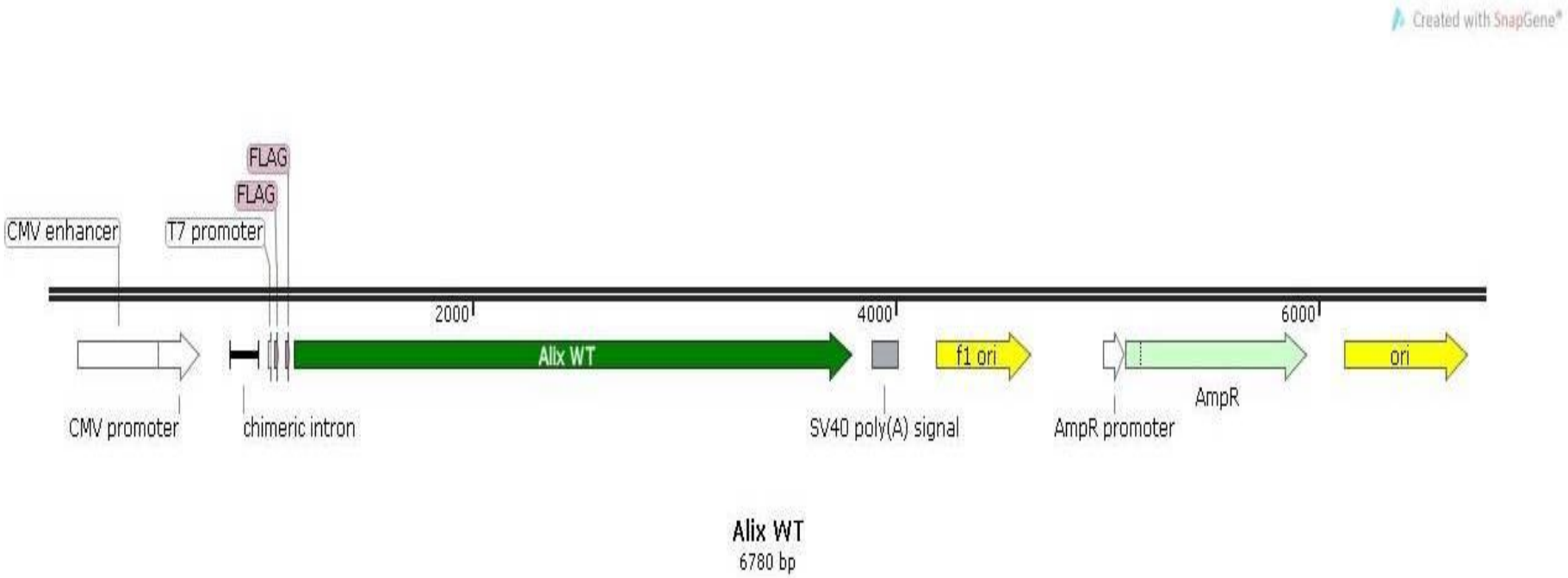

Figure 2.2 The figure represents the cDNA plasmid Alix wild type which coresponds to full mouse Alix cDNA subcloned into pCI Flag tagged plasmid.

Alix NT Mouse in pCI Neo

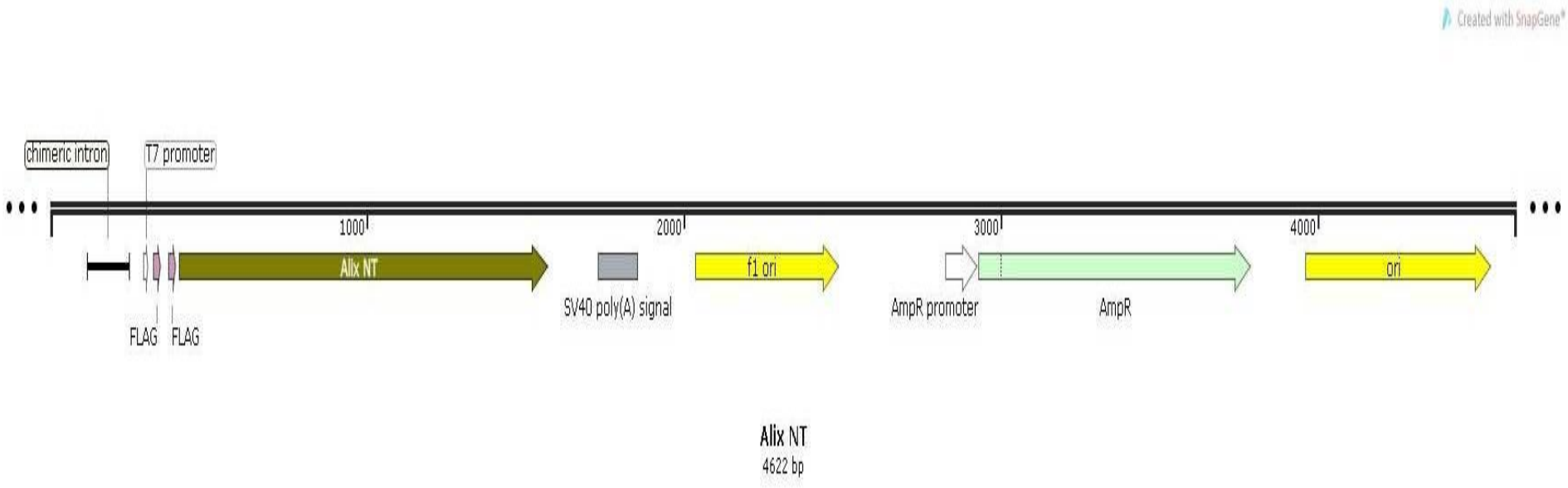

Figure 2.3 The figure represents the cDNA plasmid Alix NT corresponds to a fragment containing amino acids 1 to 434 of Alix subcloned into pCI Flag tagged plasmid.

Alix CT Mouse in pCI Neo

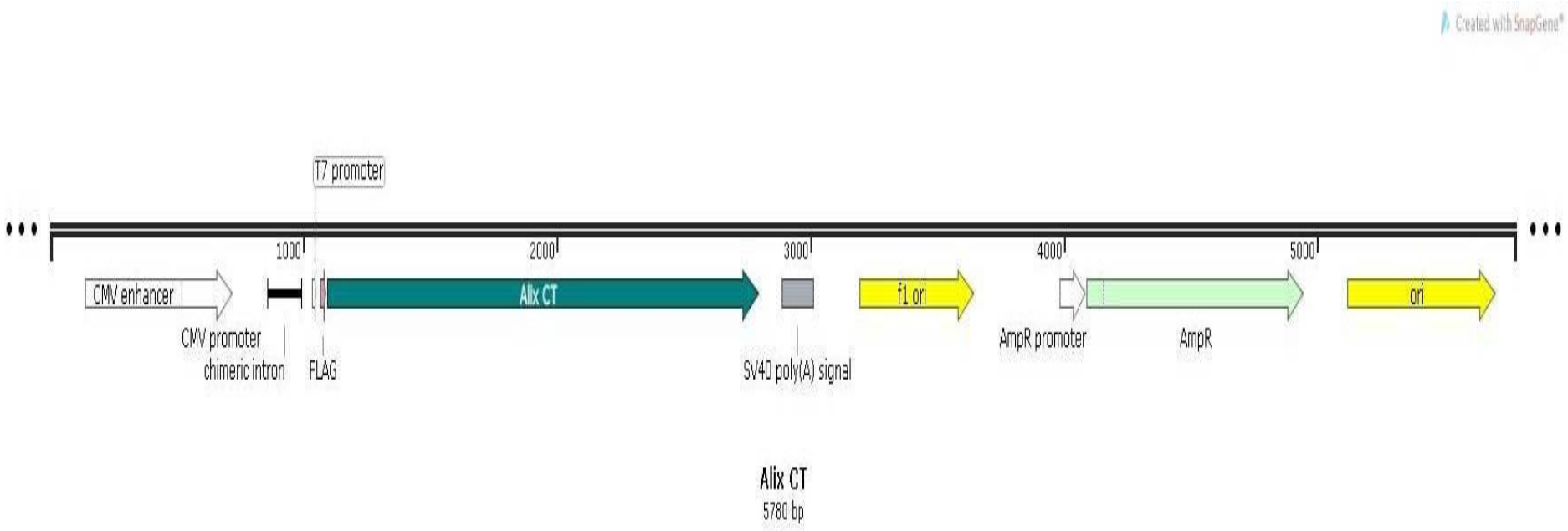

Figure 2.4 The figure represents the cDNA plasmid Alix CT corresponds to a fragment containing amino acids 468 to 869 of Alix subcloned into pCI Flag tagged plasmid.

Alix DPRD Mouse in pCI Neo

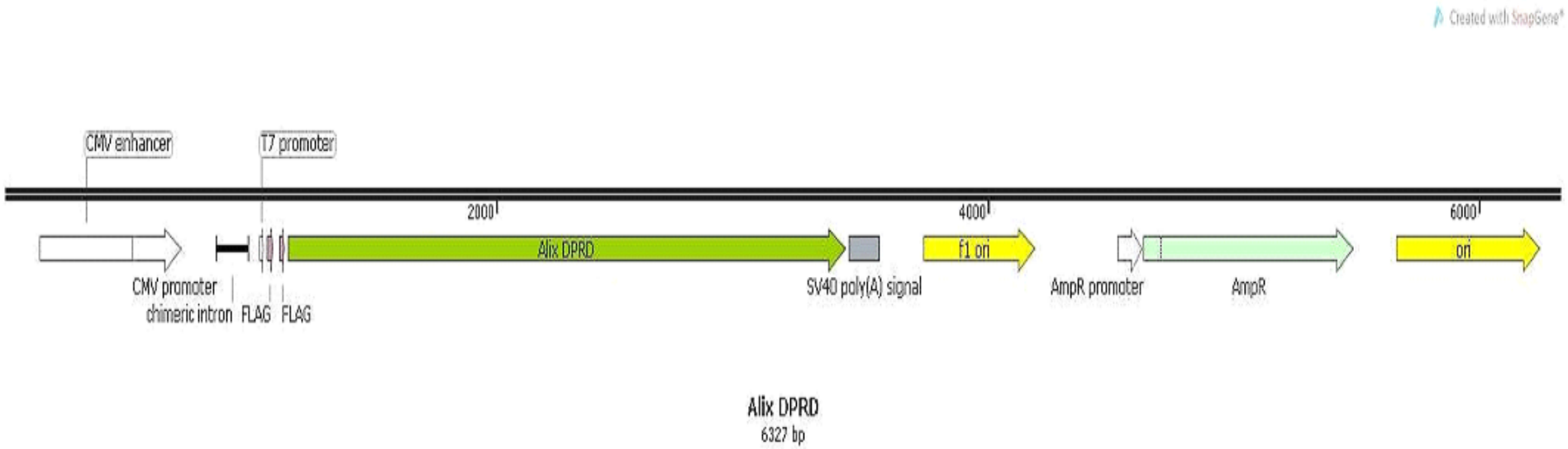

Figure 2.5 The figure represents the cDNA plasmid Alix Alix DPRD lacks a fragment encompassing a proline rich region from amino acids 717 to 867 of Alix subcloned into pCI Flag tagged plasmid.

2.2.2 Transformation of plasmid DNA

Transformations were done using frozen bacterial stocks of NEB 5α competent cells (New England Biolabs). We used a ratio of 50 µl of the competent cells to 0.5-1 µg/µl of plasmids. The mixture was mixed by gentle flicking and left on ice for 30 minutes. It was then put in a 42 ºC water bath for 30 seconds for heat shock. This was then placed on ice for 5 minutes without prior mixing. A prewarmed SOC media was added to the mix with a ratio of 950 µl per each 50 µl of competent cell and plasmid mixture. This was then placed in a prewarmed 37 ºC shaker for 60 minutes at 250 rpm. Each sample was mixed properly by gentle flicking before streaked on to a Luria Bertani (LB) agar selection plate (with the appropriate antibiotic of 100 µg/ml ampillicin or kanamycin) and incubated overnight at 37 ºC. A single, well isolated colony was grown overnight in 1 ml of Terrific Broth (TB) medium (with the appropriate antibiotic of 100 µg/ml ampillicin or kanamycin) as a small scale culture at 37 ºC. This was used to start a large-scale culture using 5 ml of sample in 50 ml of TB medium (with the appropriate antibiotic of 100 µg/ml ampillicin or kanamycin) grown overnight in a shaker at 37 ºC. Cells were then centrifuged at +4 ºC for 15 minutes at 4,000g and the medium aspirated. Cells were plated on an LB-agar plate supplemented with 100 µg/ml ampillicin or kanamycin.

2.2.3 Miniprep of plasmid DNA

Bacterial colonies were grown overnight in TB medium with the respective antibiotics of kanamycin (Alix plasmid) and ampicilin (GluN1 plasmid and GluN2A plasmid). 1.5 ml volume of bacterial culture was taken and spun down at 8000 rpm for 3 min. The supernatant was aspirated. 150 µl Solution 1 (50 mM glucose, 25 mM Tris-Cl (pH 8.0), 10 mM EDTA (pH8.0)) was added and pellet resuspended using pipette tip. 300 µl fresh Solution 2 (0.2 N NaOH, 1% SDS) was added and mixed by inverting rapidly and

vigorously. 200 µl of Solution 3 (3 M potassium acetate, 11.5% acetic acid) was immediately added and mixture vortexed and shaken for a few seconds and incubated on ice for 5 minutes. The mixture was then centrifuged at maximum speed for 5 min and transfered to a new tube. 3 µl RNase A added (10 mg/ml), mixed and incubated at 37 ºC for 30 min. 400 µl Phenol : Chloroform : Isoamylalcohol was added and vortex for 15 seconds and centrifuged for 2 minutes at maximum speed and aqueous layer transferred to a new tube. 850 µl 99% Ethanol was added and centrifuged at maximum speed for 5 minutes. The DNA pellet was washed with 1x 500 µl of 70 % ethanol and dried at room temperature and resuspended in 50 µl 1x TE buffer (10mM Tris-Cl, 1mM EDTA, pH 8.0).

2.2.4 Maxiprep of plasmid DNA

2.2.5 Qiagen Maxiprep protocol

Large scale preparation of the plasmid (Maxiprep) (Qiagen) was done following the manufacturers protocol. We diverged slightly from the protocol at the final DNA precipitation step by centrifuging the final isopropanol DNA elution for 60 min at 5000 rpm, 4 ºC, transferring the DNA pellet to a 1.5 ml microcentrifuge tube, washing the DNA pellet in 70 % ethanol centrifuging in a benchtop microfuge for 5 minutes at 13000 rpm to spindown the DNA pellet before resuspending in 200 µl 1 x TE buffer. Restriction digests with the appropriate restriction enzymes were performeds and digested plasmids were run on a 1 % agarose gel in 1 x TAE buffer. All plasmids were sequenced for verification before the tissue culture experiments.

2.2.6 Restriction Enzyme Digestion

A typical analytical digestion reaction was made of the following components:

10x restriction enzyme buffer	1.0 µl
Miniprep/maxiprep DNA	1.0 µl (approx. 0.5 µg)
(10xBovine Serum Albumin)	1.0 µl (if required)
Restriction enzyme	0.5 µl (approx. 5U)
(2nd restriction enzyme)	0.5 µl (if required)
Deionised water	made up to a final volume of 10 µl

Preparative digestion reactions of DNA contained 1x restriction enzyme buffer (NewEnglandBiolabs), 1-5 µl DNA, 0.5 µl restriction enzyme at a concentration of 5 U/ µl (NewEnglandBiolabs) and deionised water (Purite, Thane, UK) making the final volume to 10 µl. Reactions were carried out at 37 ºC for 1 hour.

Plasmid fragments were separated by gel electrophoresis in a 1 % agarose (Sigma) gel made in 1x TAE buffer (40 mM Trisacetate, 1 mM EDTA (pH 8.0)) for 30 minutes at 100V. To visualize DNA under UV light (wavelength = 302 nm) 3 µl 10 mg/ml ethidium bromide was added while 100ml of agarose was in liquid form. To estimate the molecular size of the DNA bands, 1.0 µg λ–bacteriophage digested with Sty I (size 19329, 7743, 6223, 4254, 3472, 2690, 1882, 1489, 925 bp) was added in an adjacent well. This was done in electrophoresis tanks filled with 1x TAE buffer. The bands are visualised using a UV transilluminator and the yield of the DNA was determined by spectrophotometry using the Nanodrop spectrophotometer.

2.2.7 Starting HEK 293 cell cultures from frozen

HEK293 cells were cultured from frozen and thawed by briefly immersing the vial in a 37 ºC water bath or thawed by hand for a few minutes. Upon thawing, the outside of the vial was immediately wiped with 70 % Ethanol, cells were then centrifuged at 6000 rpm for 10 min. The supernatant was aspirated and later the pellet resuspended. The contents of the vial were added to a 25 cm² flask. 9 ml of DMEM medium (Minimum Essential Medium, α Modification [α-MEM]) supplemented with 100 units/ml penicillin G sodium, 100 µg/ml streptomycin, 4 mM L-glutamine, and 10 % fetal bovine serum) was added to the flask. The flask was gently rocked to distribute cells evenly over the growth surface and incubated in a 37 ºC, 5 % CO_2, humidified incubator. The cells were examined under a microscope the next day and the medium aspirated and replaced with fresh, prewarmed growth medium. The culture was expanded to an estimated 70-80 % confluency confirmed visually under an inverted microscope. The cells were expanded by aspirating the medium and washed twice with prewarmed sterile PBS. 1-2 ml of TrypLE Express (Invitrogen) was added and the cells were treated for 1-2 minutes or until the cells detached. 10 ml of growth medium was added to stop trypsinization and the cells were resuspended gently. The cells were counted using a haemocytometer and then the desired numbers of cells were added to a new flask with and an appropriate volume of growth medium (1×10^6 in 10 ml DMEM in a 25 cm² flask, 3×10^6 in 30 ml DMEM in a 75 cm² flask and 7×10^6 in 50 ml DMEM in a 175 cm² flask). The plate was gently rocked to evenly distribute the cells before incubation in a 37 ºC, 5 % CO_2 humidified incubator.

2.2.8 Preparing frozen cultures of HEK 293 cells

To prepare frozen cultures the cells were trypsinised after washing with PBS twice. The

cells were pooled together and centrifuged at 6000 rpm for 10 min. The supernatant was aspirated and the pellet resuspended in freezing medium (20 %,α-MEM/ DMEM, 70 % FBS, and 10 % DMSO)(1 ml for every 1 x 10^6 cells) 1 ml aliquots were dispensed into sterile cryovials and frozen slowly by placing the vials in a thick-walled styrofoam container at -80 ºC overnight. Vials were removed from styrofoam and placed in liquid nitrogen (-196 ºC) for long term storage.

2.2.9 Cell culture and transfection of HEK 293 cells

HEK-293 cells were cultured as described previously in DMEM medium (Minimum Essential Medium, α Modification [α-MEM]) supplemented with 50 mg/ml Gentamycin, 4 mM L-glutamine, and 10 % fetal bovine serum). Cells were plated at a density of 2×10^5 cells/1 ml DMEM medium onto each well of a 24 well tissue culture plate and incubated in a 5% CO_2 incubator at 37 °C for 24 h.

Cells were transiently transfected using lipofectamine 2000 (Invitrogen). The DNA plasmids in 100 µl of DMEM medium (without FBS, L-glutamine and antibiotics) were added to each well of a 24 well plate with 1 ml of medium that contained attached cells at approximately 50-85% confluency. In experiments that used two, three or four different plasmids, equal concentrations of the plasmids were added. Transient transfections was performed with 10 µl lipofectamine/well. Cells were left for 18- 20 h at 37 °C in a 5% CO_2 incubator.

Cells were exposed to various treatments 18-20 h after the start of the transfection. Control cells were incubated in a physiological salt solution (PSS; 140 mM, NaCl; 1.4 mM $CaCl_2$; 5.4 mM KCl; 1.2 mM NaH_2PO_4; 21 mM glucose; 26 mM $NaHCO_3$; pH 7.4) for 10 min in a 5% CO_2 incubator at 37 °C. Activation of NMDARs was performed by incubating the cells

in PSS containing NMDA (1 mM) and glycine (50 µM) for 10 min. After the 10-min treatments at 5% CO_2, and 37 °C, cells were placed in fresh media for 6 h before assessment of cell death. 100 µM AP5 was added to each well to block any NMDAR activation by low levels of glutamate or glycine in the culture media before the PSS treatment. The transfection was terminated by replacing the medium. To determine transfection efficiency, transfection was performed with GFP using a varying DNA: lipofectamine ratios at varying confluency of cells and hours of transfection. The cells were then fixed with 2 % Paraformaldehyde (PFA) for 10 min and washed twice with PBS. Transfection efficiency was later determined by the percentage of cells that emitted fluorescence intensity of cells positive for EGFP under a spinning disc confocal system (CARV from Digital Imaging Solutions) with an EM-CCD camera (Rolera/QI Cam 3500) mounted on an Olympus X71 microscope. We diverged slightly from the protocol (in result 3.2.3) when AP5 was added to each well in all stages of before transfection, during transfection and during treatment to block any NMDAR activation by low levels of glutamate or glycine in the culture media before the PSS treatment.

2.2.10 Trypan blue exclusion assay

Cell death was determined by trypan blue exclusion (Wagey et al., 2001a). Six hours following treatment, cell death was assessed both in attached cells after trypsinisation and floating cells in the medium and PSS by trypan blue exclusion. The percentage of the combined attached and floating cells in the PSS and media was determined by removing the PSS and media from each well and adding trypan blue (1:1 ratio). Cell counts were performed on a haemocytometer in 5 counting grids of $1mm^2$ (each grid corresponding to 1×10^{-4}) and the average number of live and dead cells was calculated as a percentage of cell death. All data points correspond to the mean ± SE of values performed from at least

three separate transfections. Statistical comparisons of cell death between groups were performed using a paired *t*-test to determine which groups were statistically different from each other.

2.2.11 Hippocampus and Cortex Dissection

2.2.12 Coverslip preparation

Glass coverslips (13mm) (VWR, Lutterworth, Leicestershire, UK) were washed with 70 % ethanol and a final wash with PBS before being coated with poly-D-lysine (100 µg/ml in PBS) in a 24 well plate. These were then left overnight and washed with PBS twice before coated with Laminin (100 µg/ml in PBS) overnight. These were then washed with PBS twice just before plating.

2.2.13 Dissection of the cortex and hippocampus coverslip preparation

The pregnant female rat was killed through humane schedule 1 methods and the uterus removed. The embryonic yolk sac was opened up by careful slicing, taking care to avoid damaging the embryo. The embryo (E18) was exposed and harvested by pulling away the embryonic yolk sac. The head of the embryo was severed and the top of the skull was peeled off to reveal the brain which was then carefully removed from the skull. To culture cortical neurons the brain was placed dorsal side up and an incision was made between the two hemispheres to separate them. Each hemisphere was placed cortex side down and any noncortical forebrain tissue was removed. Meningeal tissue was removed while holding the hemisphere down. To culture hippocampal neurons, further cuts were peformed along the longitudinal fissure of the cerebrum cutting off the posterior to lambda region (midbrain, hindbrain and cerebellum). The exposed hippocampus was carefully removed using forceps

along the hippocampal fissure. The dissection was done in cold PBS and hippocampi were left in ice cold PBS until ready for dissociation.

Dissociation was done by chopping cortex or hippocampus into small pieces and transferred to a 15 ml tube containing 1 ml 25 % trypLE/PBS solution and incubated for 20 minutes at 37 °C. The trypLE was aspirated and 1 ml of warmed DMEM (as described previously) and titrated with a fine bore 1000 µl blue tip until all the pieces were dissociated. The mixture was topped up to 10 ml of DMEM and spun at 1500 rpm for 3 minutes. The DMEM was then aspirated and 1 ml of Neurobasal Media (Neurobasal Medium supplemented with 2 % B27 serum free supplement 50x, 1 % Penicilin Streptomycin, Glutamine 300 µM final concentration and β-mercaptoethanol 25 µM final concentration) was added to the pellet and again titrated with a fine bore 1000 µl blue tip. The cells were then counted using a haemocytometer and approximately 2 x 10^5 cells were plated in each coated well of a 24 well plate. The neurons are maintained in culture for 14 days before use and fresh media was added to the wells every 3-5 days.

2.2.14 Immunocytochemistry

HEK 293 were cultured as described previously in 2.2.3.2 or 2.2.4.2 section with the exception that the 24 well plates were coated with poly-D-lysine on glass cover slips at a density of 1.75 × 10^5 cells/1 ml DMEM incubated in a 5% CO_2 incubator at 37 °C for 24 h. HEK 293 cells were transiently transfected and treated as described previously in 2.2.3.2 section. HEK 293 cells or primary neurons (cultured as described previously in 2.2.4.2 section) were then fixed with 4 % Paraformaldehyde (PFA) for 10 min and washed three times with PBS on ice. Cells were blocked in PBS containing 5% horse serum and 0.1% Tween-20 for 45 minutes at room temperature prior to incubation with the appropriate primary and secondary antibody (varying concentrations, see table in section 2.2.7).

Coverslips were incubated with different combinations of primary (1 hour incubation) and secondary (1 hour incubation) antibodies and then embedded using the ProLong Gold reagent (Invitrogen). The cells were visualised on a spinning disc confocal system (CARV from Digital Imaging Solutions) with an EM-CCD camera (Rolera/QI Cam 3500) mounted on an Olympus X71 microscope, using a 100 x fluoplan objective. The microscope confocal system was supported by Image Pro 6.0 software. To avoid potential digital overlap, the images in this report are single section images.

2.2.15 Western Blotting

HEK-293 cells were cultured as described previously in 2.2.3.2 section with the exception that cells were expended to grow in a T25 flask at a density of 1.2×10^6 cells in 10 ml of DMEM incubated in a 5% CO_2 incubator at 37 °C for 24 h. Cells were transiently transfected and treated as described previously in 2.2.3.2 section. After the 10 minutes treatment with activated or non activated PSS, the cells were then lysed for protein extraction on ice. Proteins from a T25 flask were collected by trypsinisation, spun down and washed twice with PBS. The pellet was then left in 2 ml 1/2x protease inhibitor (Roche) on ice for 1 hour until viscous. This was then homogenised with a fine bore 1000 µl blue tip until dissolved and spun down at 16,000 rpm for 15 minutes. The pellet was washed twice with 500 µl of 1/2x protease inhibitor and spun down at 10,000 rpm for 15 minutes. The supernatant was discarded and the pellet solubilized with buffer Px to a 1:1 ratio (0.2 M sodium phosphate pH 7.5, 1 % Triton X-100 and supplemented with protease inhibitors) on ice for 1 hour. It was then spun down at 16,000 rpm for 2 minutes and the supernatant collected.

The protein concentration of the protein extract was determined by Bradford's Protein Assay. The Bio Rad dye was diluted 1:4 ratio of dye to water and 1 ml of diluted reagent

was added to 4µl of the sample to be assayed in a 1ml cuvette. The samples were mixed, and the colour left to develop for 5 minutes. Known protein concentrations of BSA were run alongside to produce a standard curve. Absorbance readings at 595 nm were obtained once the colour had developed, and used to calculate the protein concentration based on the BSA standard curve.

Equal concentrations of protein were prepared by diluting 1:4 with 4 x NuPage sample buffer and denatured at 90 °C for 5 minutes. Protein samples were loaded on a 4-12 % pre-cast NuPage gel in XCell Sure Lock mini gel system (Invitrogen). Electrophoresis was performed at 100 V for 1 hour in 1 x MOPS running buffer (Invitrogen). The separated polypeptides were transferred to 0.45 µm nitrocellulose by electroblotting in 1 x transfer buffer (NuPage 20x transfer buffer Invitrogen) using the Bio Rad mini system at 140V for 1 hours and 30 minutes. The nitrocellulose paper was then blocked with a solution of 0.5 % blocking buffer (1X TBS, 0.1 % Tween-20 with 5 % milk) and aspirated immediately with SNAP i.d. (Merck Milipore) and washed three times with TBS-T (50 mM Tris Base, 150 mM NaCl, 0.1 % Tween 20). Once blocked the blot was incubated with the necessary primary antibody overnight and secondary antibodies for 10 minutes (refer table in section 2.2.7) and washed 3 times with TBS-T immediately after. The bound antibodies were visualized with Odyssey Licor Imaging system by placing the membrane in some buffer and sliding it into the machine and selecting the specific Alexa Fluor channel (700 or 800) depending on the antibodies used. The membrane is then scanned with a manufacturer standard intensity and saved. Analysis of the western was done using Image studio Lite (Licor) by exporting the image into the software. The western bands are then quantified by selecting the auto add rectangle around the bands of interest which then produced a table of fluorescent intensity readings.

2.2.16 Fraction preparation

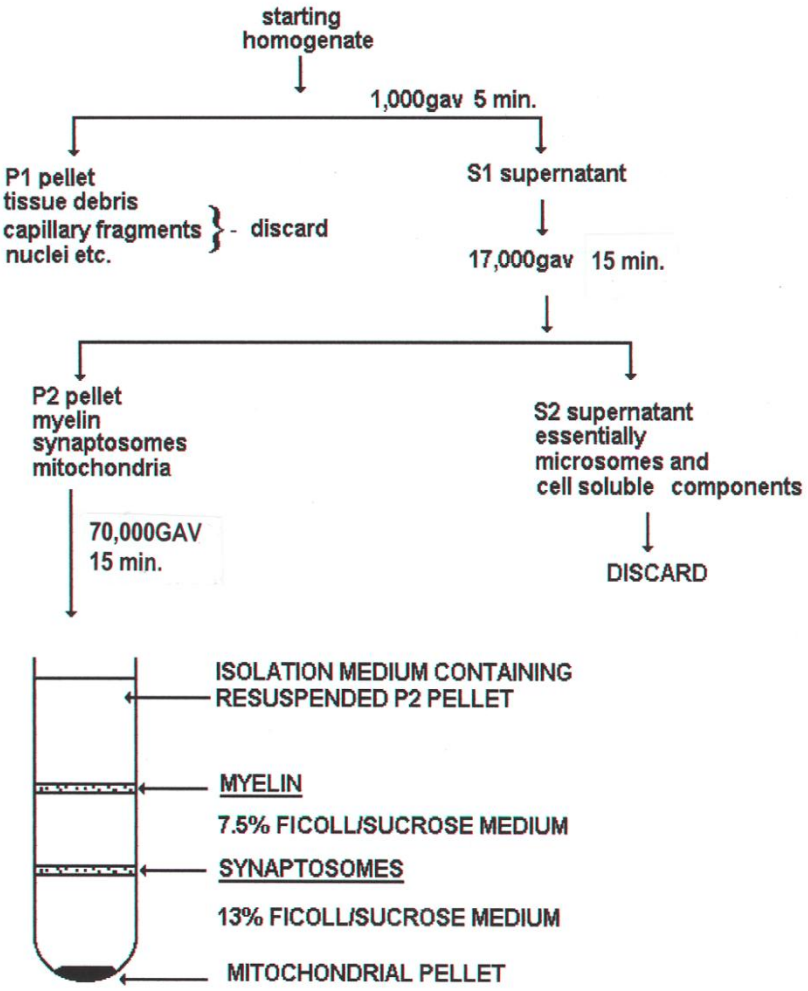

Rats were killed by decapitation and the forebrain of the animal was swiftly removed. The forebrains were dropped into ice-cold isolation medium (0.32M-sucrose/l mM-sodium-EDTA/l0 mM-Tris/ HCI, pH7.4) and chopped into small blocks with a scalpel. The blood and other debris were washed off the brain tissue by adding up more isolation medium and decanting the supernatant from the top of the minced tissue. This washing procedure was repeated. The chopped tissue was then homogenized in a motor driven glass Teflon homogeniser (clearance 0.1mm) by 6 up down strokes with a motor speed of 600 r.p.m./min. (Citenco motor-speed 6). This homogenate was diluted with isolation medium

and spun at 2000rpm in a Sorval RC-5B for 5 min 4°C. The supernatant from this spin was centrifuged at 12,000rpm for 15 min using the Sorval RC-5B, producing the crude mitochondrial/synaptosomal pellet. This pellet was resuspended in 3 ml of isolation medium using syringe fitted with wide bore needle, diluted with 12% Ficoll/sucrose medium (12% (w/w) Ficoll, 0.32M-sucrose, 1mM sodium-EDTA, pH7.4) and gently homogenized by hand in a Potter-type homogenizer (clearance 0.375mm). The crude mitochondrial suspension was introduced into a centrifuge tube and above this 5ml of 7.5% Ficoll/sucrose medium [7.5% (w/w) Ficoll, 0.32M-sucrose, 1 mM sodium-EDTA, pH7.4] was carefully layered. Finally, on top of this 10ml of isolation medium was layered. This will form the top layer of a three step gradient. Successive layers were added under the homogenate using a wide bore needle and syringe. The tubes were centrifuged at 26,000rpm for 45min in a 3 x 23ml in the SW28 rotor using the Beckman L7 centrifuges. Myelin and synaptosomes banded at the first and second interphases respectively, with the free mitochondria being pelleted at the bottom. The myelin layer was carefully removed and the synaptosomes were gently sucked off from the interphase and transfered to a polyethylene tube for the 12 x 50ml SS34 angle rotor for the Sorval RC-5B. The two fractions were pelleted at 20,000rpm for 20 min using the Sorval centrifuge. In addition to harvesting the myelin and synaptosomal fractions the remaining gradient medium was poured off. The mitochondrial pellet was resuspend in 3 ml isolation medium and the myelin in 2 ml of isolation medium. The synaptosome layer was carefully resuspended in 7ml sodium resuspension medium (2.5mM Hepes, 8mMKC1, 110mM NaCl, 2.6mM $CaCl_2$, 10mM glucose pH 7.4). The resuspended mitochondrial pellet might contain some synaptosomal contamination. This was removed by layering the resuspended material over 1.3M (15 ml) sucrose and pelleting the mitochondria fraction through this layer.

2.2.17 Colocalization Analysis

The slides are prepared with the relevant cells or tissue and fluorophores as described in 2.2.14. Measurements of the degree of colocalization were determined by observing if the fluorophores are in the same place (co-occurrence) and if there is a relationship between their intensities (correlation). The fluorescent images that were taken from each slide were converted from an RGB coloured format to 8 bit image using ImageJ. The background was substracted from each image and a threshold was set. A colocalization analysis plugin available from ImageJ was chosen and this generated various colocalisation coefficients for two 8 bit images or stacks. The generated coefficients were plotted as a scattergram that generates a colour scatter pixel plot that represents the actual colour in the image showing the relationship of the intensities between a pair of displayed images. A Pearson correlation coefficient was used to analyse degree of colocalisation or overlap between the pixel intensities of each set of fluorophore pairs within a region of interest (ROI). We then calculated the mean from at least three pairs of images and obtained a mean Pearson correlation coefficient.

2.3 Antibody Dilution

Antibody	Host	Company	Dilution
Anti-Alix	mouse	Abcam	1:100
Anti-FLAG	rabbit	Sigma Aldrich	1:1000
Anti-NMDAR1	mouse	BD Biosciences	1:1000
Anti-EEA1	mouse	BD Biosciences	1:1000
Anti-LAMP1	mouse	Enzo Life Sciences	1:1000
Anti-PSD95	mouse	Abcam	1:500
Anti-NR2A/2B	rabbit	Millipore	1:250
Anti-PSD95	rabbit	Abcam	1:500
Anti-EEA1	rabbit	Abcam	1:500
Alexa Fluor 568	Goat Anti-Mouse	Life Technologies	1:1000
Alexa Fluor 488	Donkey Anti-Rabbit	Life Technologies	1:1000
Alexa Fluor 488	Goat Anti-Mouse	Life Technologies	1:1000
IRDye 800	Goat Anti-Mouse	Licor bioscience	1:10,000

3. Investigating the potential modulation of NMDA by Alix in Cell Death Assay:

3.0 Introduction:

Previous work has identified a novel dopamine receptor interacting protein, Alix (ALG-2 (apoptosis-linked gene 2-interacting protein X), using D1 receptor C-terminal domain or D3 receptor third cytoplasmic loop as 'baits' in separate yeast two-hybrid screens (Zhan et al., 2008). Alix is thought to be important for the stability and trafficking of dopamine receptors and is a ubiquitous adaptor protein that was first described for its capacity to bind to the calcium-binding protein, ALG-2. It is known to be involved in apoptosis, regulation of cell adhesion, protein sorting, adaptation to stress conditions, ESCRT (endosomal sorting complex required for transport) and neuronal cell death. Alix has been recently found within the human postsynaptic density (PSD) (Bayes et al. 2011) and Alix may be able to facilitate intracellular ‘cross talk’ between both dopamine and glutamate signalling pathways. Given that NMDARs are a central component of the PSD and have the capacity to trigger neuronal cell death, we hypothesized that Alix may be able to influence NMDA triggered cell death. Little is known about how these proteins interact with the NMDA receptor and their cellular functioning and further study is thus needed to understand this.

It is found that a proportion of HEK cells transfected with NMDAR subunits die following exposure to NMDAR agonists, depending on the NMDAR subunit composition (Wagey et al., 2001b). To establish if the activation of Alix, is involved in NMDA induced cell death we evaluated the cell death percentage in HEK293 cells transfected with NMDAR subunits. Activation of NMDARs was performed by incubating the cells in PSS containing NMDA and glycine. The cell death percentage was later calculated by trypan blue exclusion six hours following activation.

In this chapter, approaches to quantify NMDAR-induced cell death were used to analyse the effect of Alix on NMDA receptor function. We decided to start with an assessment of Alix on the NMDA cell death assay in HEK293 mammalian cell line as they are easy to maintain and transfect. To attain this goal we did a small and large scale preparation of the transformed human EGFP tagged Alix, GluN1, GluN2A, mouse FLAG tagged Alix WT, mouse Alix NT (N-terminal regions covering amino acids (1 to 434), mouse Alix CT (C-terminal regions covering amino acids (468 to 869) and mouse Alix DPRD (deletion of a proline rich domain in the C-terminal region of Alix). The clones were confirmed positive by restriction enzyme digestion and sequencing.

3.1 Cell Death Assay:

3.1.1 Transfection efficiency

Transfection efficiency was determined by the percentage of cells that emitted green fluorescence under Fluorescence/Confocal Microscope with a range of 100-200 cells per transfection condition. eGFP gene expression was performed using either pEGFP-N1 or Alix (GFP tagged in pCMVTag2C) and was analysed by direct fluorescence using a confocal microscope with a 20x objective. Varying ratios of cDNA and lipofectamine were used and the highest percentage transfection (as judged from eGFP fluorescence) was found from a ratio of 1:5 DNA to lipofectamine.

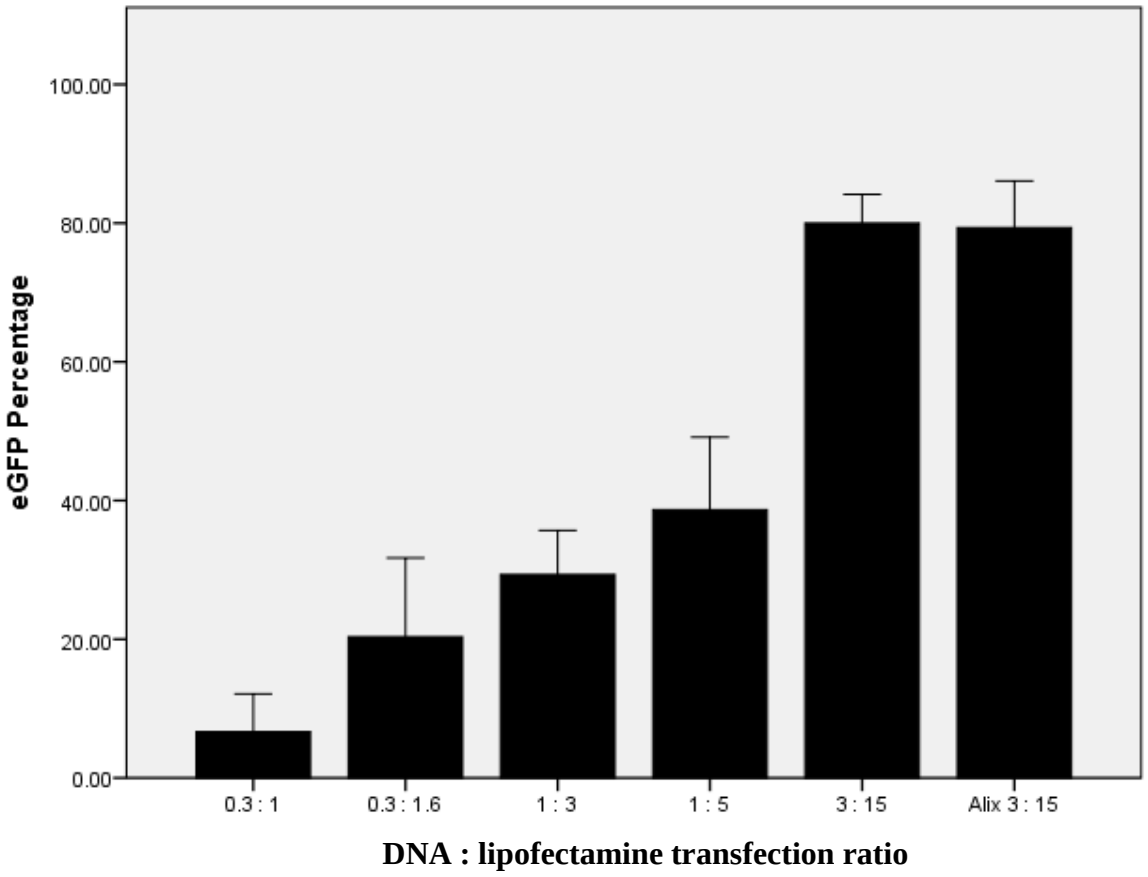

Figure 3.1.1 a: Transfection efficiency by eGFP and Alix plasmid. All data points correspond to the mean ±SE of values.

Column	Transfection	Percentage cell death ± SEM (%)	Sample size (n)
1	**eGFP 0.3 ug/ul + 1 ul Lipofectamine**	**7% ± 3%**	**3**
2	**eGFP 0.3 ug/ul + 1.6 ul Lipofectamine**	**20% ± 6%**	**3**
3	**eGFP 1 ug/ul + 3 ul Lipofectamine**	**29% ± 3%**	**3**
4	**eGFP 1 ug/ul + 5 ul Lipofectamine**	**39% ± 5%**	**3**
5	**eGFP 3 ug/ul + 15 ul Lipofectamine**	**80% ± 2%**	**3**
6	**Alix 3 ug/ul + 15 ul Lipofectamine**	**79% ± 3%**	**3**

Table 3.1.1 b: Percentage of eGFP after 24 hours following transfection of plasmid with lipofectamine.

3.2 Alix modulate NMDA-induced cell death

To quantify NMDAR-induced cell death transfection efficiency was determined at a 1:5 ratio of DNA:lipofectamine for a 24 hours transfection duration between 50-85% confluency. The effects of Alix on NMDA cell death assay was determined by following the protocol by Wagey et al., 2001, where the Hek293 cells were transiently transfected using lipofectamine with the plasmids that was previously prepared in different combination.

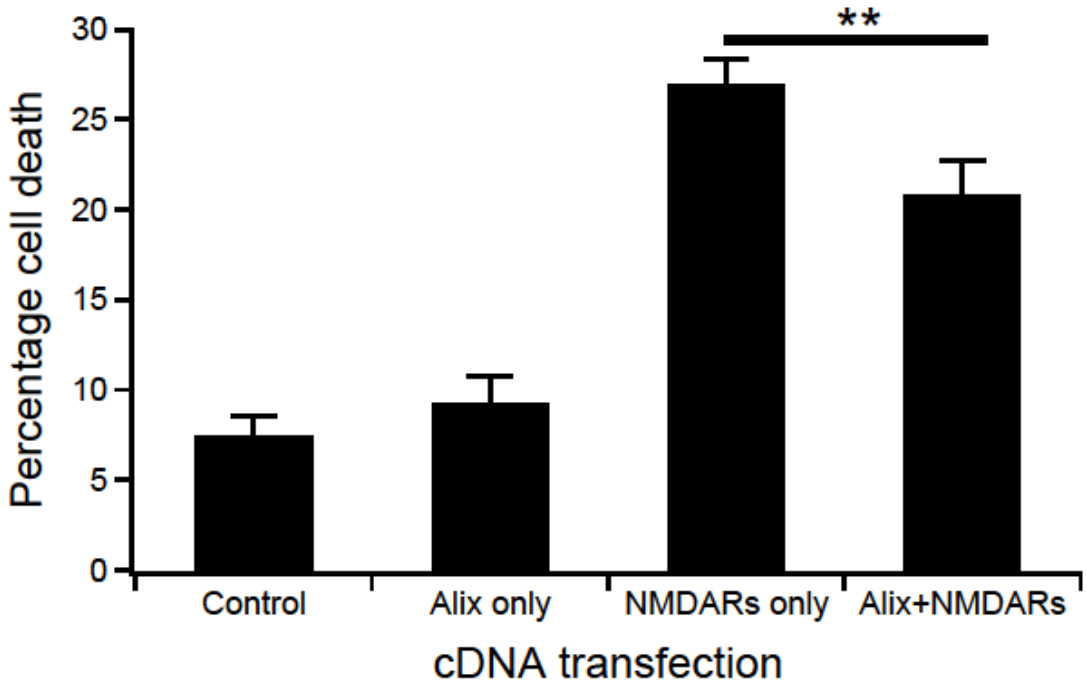

Figure 3.1 a: Modulation of NMDA cell death by Alix. The cells were activated with physiological salt solution (PSS) with 1 mM NMDA and 50 µM Glycine. All data points correspond to the mean ± SE of values and statistical comparisons of cell death between groups were performed using a paired *t*-test to determine which groups were statistically different from each other. The bar marked with ** denotes that it is statistically very significant with a P value of less than 0.05.

Table 3.1 a: Percentage cell death after 6 hours following treatment with 1 mM NMDA/ 50 µM Glycine.

Column	Transfection	Percentage cell death ± SEM (%)	Sample size (n)
1	**Lipofectamine only**	**9.6 ± 0.9**	**11**
2	**Alix/EGFP only**	**10.1 ± 1.5**	**7**
3	**GluN1/GluN2A/EGFP**	**27.4 ± 1.4**	**12**
4	**GluN1/GluN2A/Alix**	**21.6 ± 1.9**	**9**

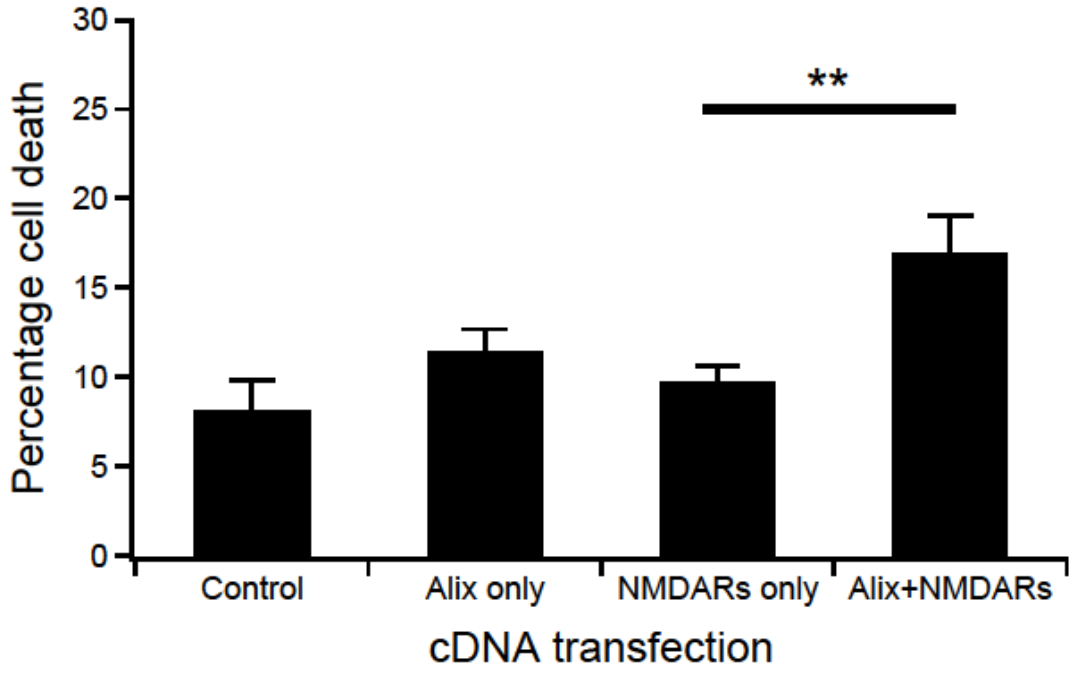

Figure 3.1 b: Modulation of NMDA cell death by Alix. The cells were treated with physiological salt solution (PSS) only. All data points correspond to the mean ± SE of values and statistical comparisons of cell death between groups were performed using a paired *t*-test to determine which groups were statistically different from each other. The bar marked with ** denotes that it is statistically very significant with a P value of less than 0.05.

Table 3.1 b: Percentage cell death after 6 hours following treatment with physiological salt solution (PSS) only.

Column	Transfection	Percentage cell death ± SEM (%)	Sample size (n)
1	**Lipofectamine only**	**11.9 ± 0.7**	**7**
2	**Alix/EGFP only**	**12.4 ± 0.8**	**7**
3	**GluN1/GluN2A/EGFP**	**11.6 ± 0.7**	**14**
4	**GluN1/GluN2A/Alix**	**17.3 ± 1.0**	**11**

Transfection comparison		Mean Difference	Significance
Control Activated	Control Activated	-17.4426%*	P<0.001
	NMDA+ Alix GFP Activated	-11.7297%*	P<0.001
	NMDA+ Alix GFP Not Activated	-7.4576%*	P<0.001
Alix GFP Activated	NMDAR only Activated	-16.4842%*	P<0.001
	NMDA+ Alix GFP Activated	-10.7713%*	P<0.001
	NMDA+ Alix GFP Not Activated	-6.4993%*	P = 0.001
NMDAR only Activated	Control Activated	17.4426%*	P<0.001
	Alix GFP Activated	16.4842%*	P<0.001
	NMDA+ Alix GFP Activated	5.7129%*	P = 0.002
	Control Not Activated	16.0221%*	P<0.001
	Alix GFP Not Activated	14.8968%*	P<0.001
	NMDAR only Not Activated	15.7512%*	P<0.001
	NMDA+ Alix GFP Not Activated	9.9850%*	P<0.001
NMDA+ Alix GFP Activated	Control Activated	11.7297%*	P<0.001
	Alix GFP Activated	10.7713%*	P<0.001
	NMDAR only Activated	-5.7129%*	P = 0.002
	Control Not Activated	10.3092%*	P<0.001
	Alix GFP Not Activated	9.1839%*	P<0.001
	NMDAR only Not Activated	10.0383%*	P<0.001
Control Not Activated	NMDAR only Activated	-16.0221%*	P<0.001
	NMDA+ Alix GFP Activated	-10.3092%*	P<0.001
	NMDA+ Alix GFP Not Activated	-6.0371%*	P = 0.003
Alix WT Not Activated	NMDAR only Activated 3	-14.8968%*	P<0.001
	NMDA+ Alix GFP Activated	-9.1839%*	P<0.001
	NMDA+ Alix GFP Not Activated	-4.9118%*	P = 0.030

NMDAR only Not Activated	NMDAR only Activated	-15.7512%*	P<0.001
	NMDA+ Alix GFP Activated	-10.0383%*	P<0.001
	NMDA+ Alix GFP Not Activated	-5.7663%*	P<0.001
NMDA+ Alix GFP Not Activated	Control Activated	7.4576%*	P<0.001
	Alix GFP Activated	6.4993%*	P = 0.001
	NMDAR only Activated	-9.9850%*	P<0.001
	Control Not Activated	6.0371%*	P = 0.003
	Alix GFP Not Activated	4.9118%*	P = 0.030
	NMDAR only Not Activated	5.7663%*	P<0.001

Table 3.1 c: Anova Analysis table of statistically significant NMDA cell death by Alix GFP. All data points correspond to the mean difference of values and statistical significance of cell death between groups. Anova analysis was performed using Tukey post-hoc analysis to determine which groups were statistically different from each other. Only statistically significant pairwise comparison is displayed and the values marked with * denotes that it is statistically significant at the level 0.05.

To assess cell death in HEK-293 cells, a trypan blue exclusion assay was performed 6 hours following various treatments. A T-test and an ANOVA analysis using SPSS was performed to determine the statistical significance of the various treatments. The negative control culture transfected without any DNA and maintained in PSS only had a mean of 11.9 ±0.7% cell death at 6 hours (Figure 3.1b). The negative control with lipofectamine only that was activated with NMDA (1 mM) and glycine (50 µM) had a mean of 9.6 ±0.9% cell death at 6 hours (Figure 3.1a). Paired t-test and ANOVA analysis (Table 3.1c) shows that the difference between the activated and non-activated negative control is considered to be not statistically significant.

In cultures that were transfected with human EGFP-Alix cDNA alone and maintained in PSS, cell death at 6 hours was 12.4 ± 0.8% (Figure 3.1b). In cultures that were transfected with human EGFP-Alix cDNA activated in PSS with NMDA (1 mM) and glycine (50 µM)had a mean of 10.1 ±1.5% cell death at 6 h (Figure 3.1a). Paired t-test and ANOVA analysis (Table 3.1c) shows that the difference between activated and non-activated cells expressing human EGFP-Alix cDNA alone is considered to be not statistically significant. There was also no statistical significance between the cell death measured between activated or non activated cells expressing human EGFP-Alix cDNA alone and the negative control (without DNA).

As a positive control, cells were transfected with GluN1/GluN2A subunits and those cells maintained in PSS displayed a mean of 11.6 ±0.7% cell death at 6 h (Figure 3.1b). Whereas, cells transfected with GluN1/GluN2A subunits that were activated with PSS with NMDA (1 mM) and glycine (50 µM)had a mean of 27.4 ±1.4% cell death at 6 h (Figure 3.1a). Treatment with NMDA and glycine significantly enhanced cell death. Paired t-test shows that the difference between the activated and non activated positive control is considered to be extremely statistically significant with a P value of less than 0.0001. While the ANOVA analysis gave a significance value of $P<0.001$ (Table 3.1c).

To determine if Alix has any cytotoxic effect on GluN1/GluN2A subunits transfected HEK cells, Alix was transfected with GluN1/GluN2A subunits and treated with PSS alone or with PSS and NMDA plus glycine and cell death was assessed 6 hours following the treatments. As shown in Figure 3.1a, transfecting Alix with GluN1/GluN2A significantly reduced the percentage of dead cells compared with cells expressing GluN1/GluN2A subunits and activated with NMDA. The culture transfected with Alix, GluN1/GluN2A subunits and activated with PSS and NMDA with glycine had a mean of 21.6 ±1.9% cell death at 6 hours (Figure 3.1a). Paired t-test shows that the difference

between the activated positive control and activated cells containing Alix, GluN1, GluN2A is considered to be statistically significant with a P value of 0.0081 which correlate with the ANOVA analysis significance value of .002 (Table 3.1c).

Non activated cells transfected with Alix and GluN1/GluN2A subunits yielded a mean of 17.3 ±1.0% cell death at 6 hours (Figure 3.1b). It is a higher percentage of cell death compared to GluN1/GluN2A subunits that were not activated. Paired t-test shows that the difference between the non-activated positive control and non-activated Alix, GluN1, GluN2A is considered to be extremely statistically significant with a P value of 0.0002 which correlates with the ANOVA analysis significance value of $P<0.001$ (Table 3.1c).There was however no statistical significance in cell death between activated and non-activated cells expressing Alix, GluN1, GluN2A (P value of 0.0511) (Figure 3.1a and b) (Table 3.1c).

3.2.2 Coexpression of Alix with GluN1 or GluN2A alone

To confirm that Alix is not causing a high amount of cell death without the overexpression of NMDAR (Since GluN2 subunits are not transported to the cell surface unless they associate with GluN1 subunits, (McIlhinney et al., 2003) we did a control experiment where we repeated the cell death assay with Alix and GluN1 or Alix with GluN2A alone to test if there is any significant cell death compared to the negative control (Figure 3.2).

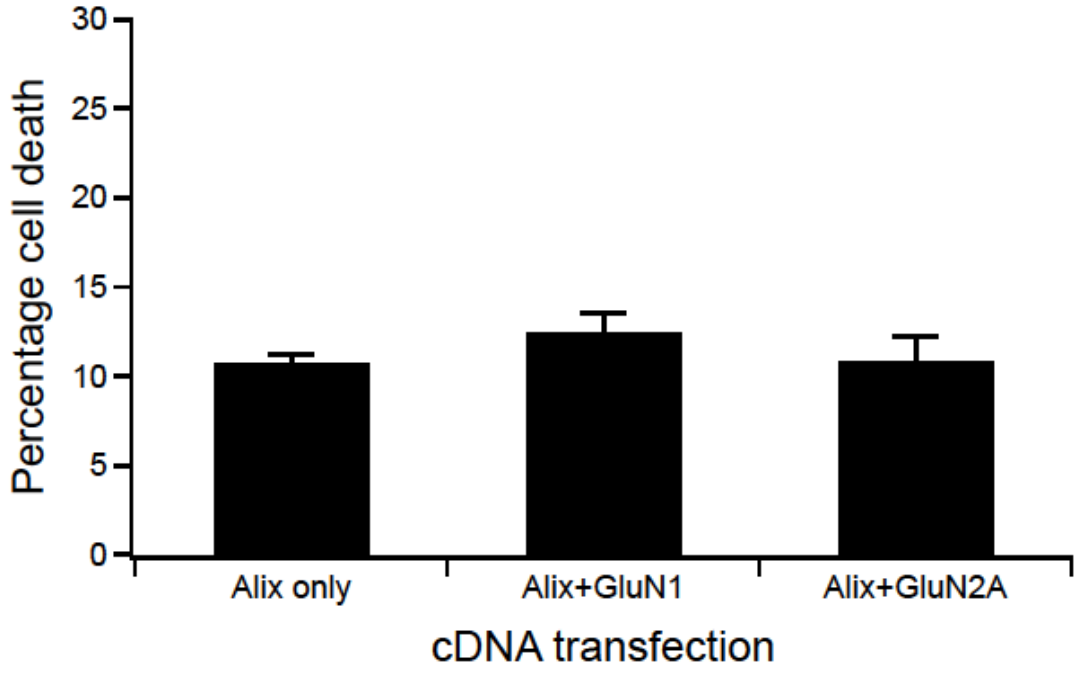

Figure 3.2 a: Modulation of NMDA cell death by Alix. The cells were activated with physiological salt solution (PSS) with 1 mM NMDA and 50 µM Glycine. All data points correspond to the mean ± SE of values and statistical comparisons of cell death between groups were performed using a paired *t*-test to determine which groups were statistically different from each other.

Table 3.2 a: Percentage cell death after 6 hours following treatment with 1 mM NMDA/ 50 µM Glycine.

Column	Transfection	Percentage cell death ± SEM (%)	Sample size (n)
1	**Alix/EGFP only**	**6.9 ± 1.0**	**3**
2	**Alix/GluN1/ EGFP**	**8.5 ± 0.9**	**3**
3	**Alix/GluN2A/ EGFP**	**7.1 ± 0.7**	**3**

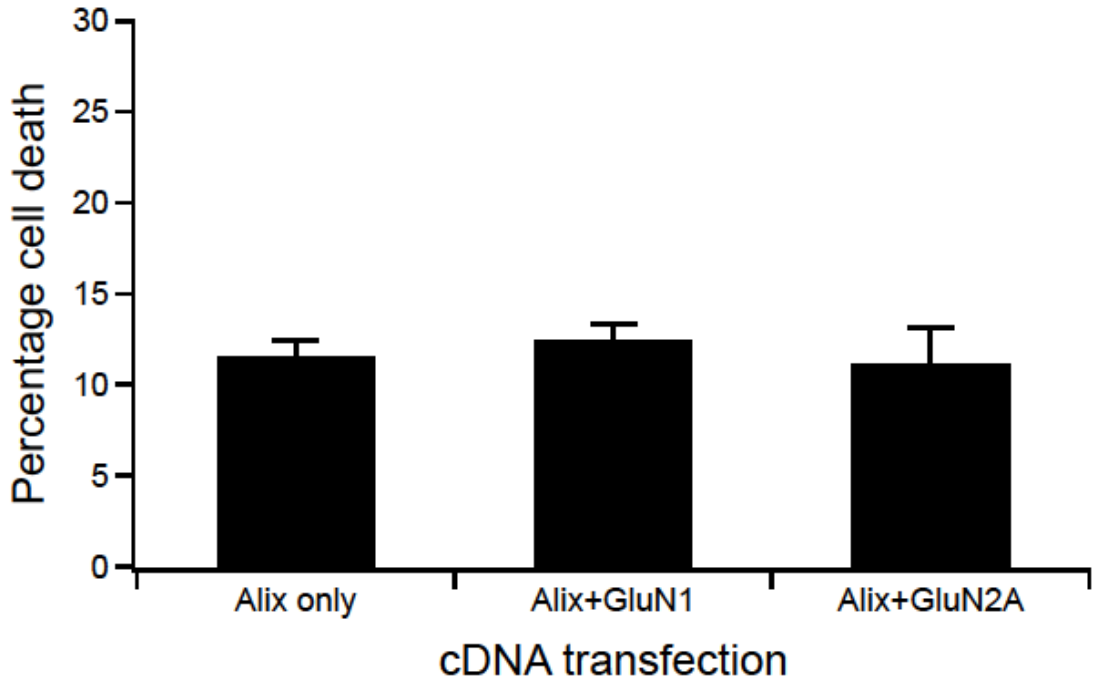

Figure 3.2 b: Modulation of NMDA cell death by Alix. The cells were treated with physiological salt solution (PSS) only. All data points correspond to the mean ± SE of values and statistical comparisons of cell death between groups were performed using a paired *t*-test to determine which groups were statistically different from each other.

Table 3.2 b: Percentage cell death after 6 hours following treatment with physiological salt solution (PSS) only.

Column	Transfection	Percentage cell death ± SEM (%)	Sample size (n)
1	**Alix/EGFP only**	**7.3 ± 1.4**	**3**
2	**Alix/GluN1/ EGFP**	**9.3 ± 1.5**	**3**
3	**Alix/GluN2A/ EGFP**	**7.7 ± 1.5**	**3**

As expected we found that by transfecting Alix with GluN1 alone and Alix with GluN2A alone (both activated and without activation) we did not find an increase of cell death (all transfections yielded an average of around 10% cell death) compared to negative control (Figure 3.2 a and b). This differs from the observations in Figure 3.1, where Alix expression increased NMDAR triggered cell death in the absence of 1mM NMDA in the PSS.

3.2.3 An NMDAR antagonist, AP5 abolishes cell death in the absence or presence of Alix

Next we examined if NMDAR activation is behind the increased cell death caused by Alix (in PSS only). Therefore, we repeated the NMDA cell death assay with AP5 to block NMDA triggered calcium influx to see if the increased cell death in the presence of Alix is caused by NMDAR activation (Figure 3.3).

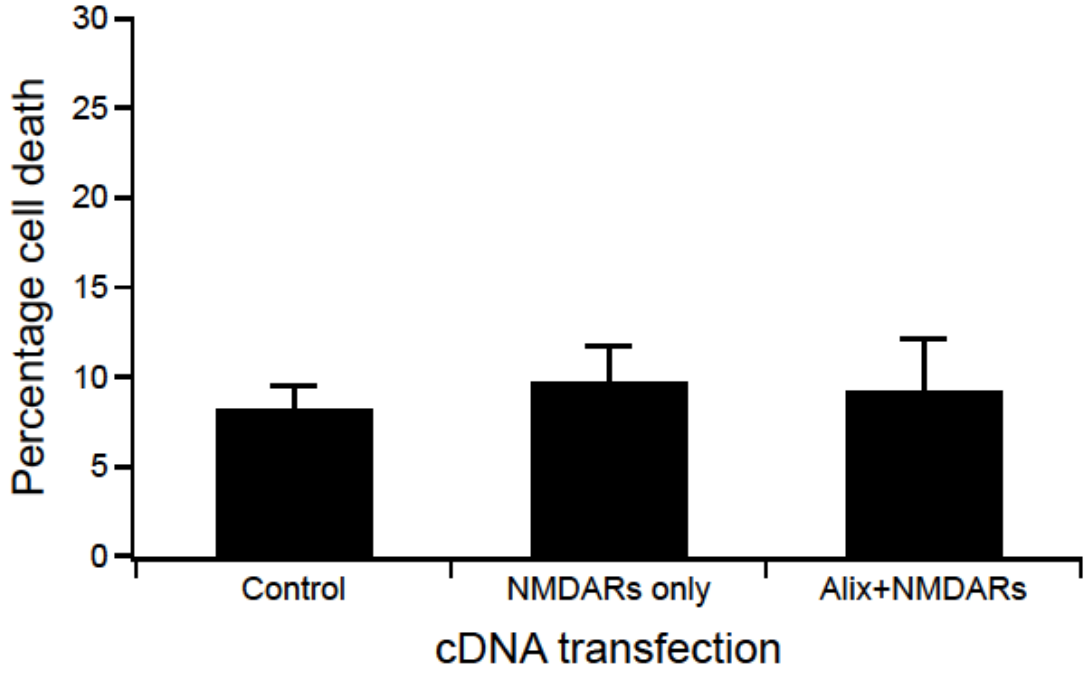

Figure 3.3 a: The effects of 100 µM AP5 on Alix coexpression. The cells were activated with physiological salt solution (PSS) with 1 mM NMDA and 50 µM Glycine. All data points correspond to the mean ±SE of values and statistical comparisons of cell death between groups were performed using a paired *t*-test to determine which groups were statistically different from each other.

Table 3.3 a: Percentage cell death after 6 hours following treatment with 1 mM NMDA/ 50 µM Glycine.

Column	Transfection	Percentage cell death ± SEM (%)	Sample size (n)
1	**Lipofectamine only**	**8.3 ± 1.3**	**3**
2	**GluN1/GluN2A/EGFP**	**8.5 ± 0.9**	**3**
3	**GluN1/GluN2A/Alix**	**7.1 ± 0.7**	**3**

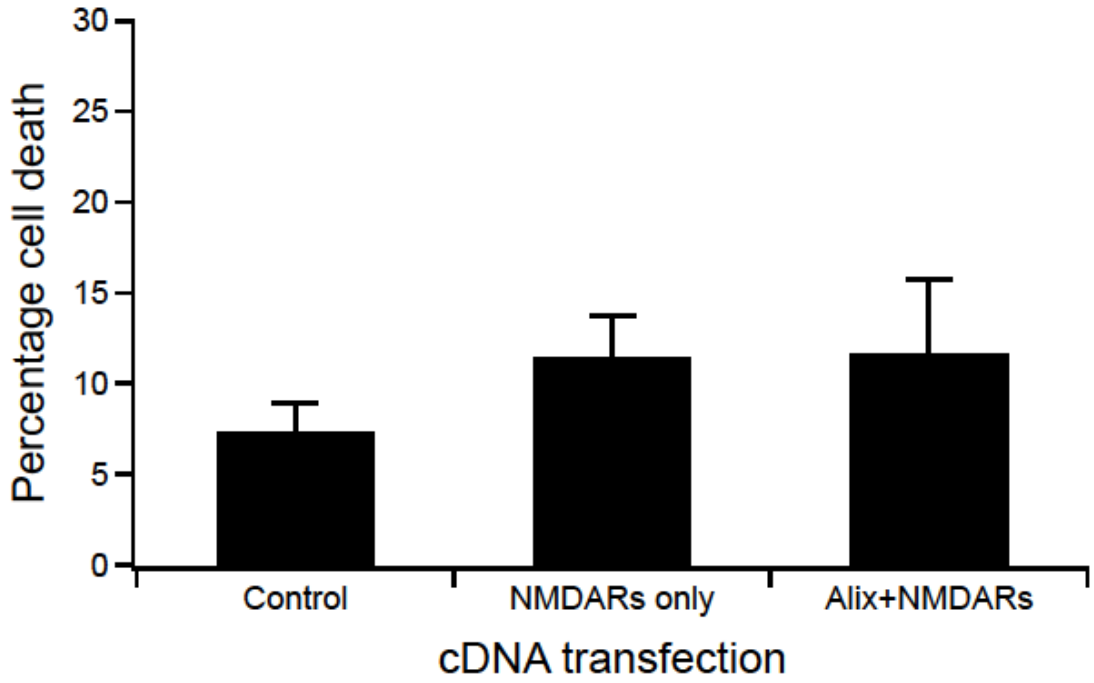

Figure 3.3 b: The effects of 100 µM AP5 on Alix coexpression. The cells were treated with physiological salt solution (PSS) only. All data points correspond to the mean ± SE of values and statistical comparisons of cell death between groups were performed using a paired *t*-test to determine which groups were statistically different from each other.

Table 3.3 b: Percentage cell death after 6 hours following treatment with physiological salt solution (PSS) only.

Column	Transfection	Percentage cell death ± SEM (%)	Sample size (n)
1	**Lipofectamine only**	**7.3 ± 1.4**	**3**
2	**GluN1/GluN2A/EGFP**	**9.3 ± 1.5**	**3**
3	**GluN1/GluN2A/Alix**	**7.7 ± 1.5**	**3**

We found that by adding AP5 to the medium before, during and after treatment (activated or without activation) that we were able to abolish the higher percentage of cell death caused by Alix and NMDAR as previously seen in Figure 3.1. Therefore, the increased cell death seen in the cells cotransfected with Alix requires NMDAR activation.

3.2.4 The effect of different NMDA concentrations on cell death in the absence and presence of human Alix

After seeing the result of AP5 treatment we examined whether this was due to an increased sensitivity NMDARs to NMDA when coexpressed with Alix. We modulated the concentration of NMDA in the PSS buffer in activated assay to see if this affected the cell death caused by Alix (Figure 3.4).

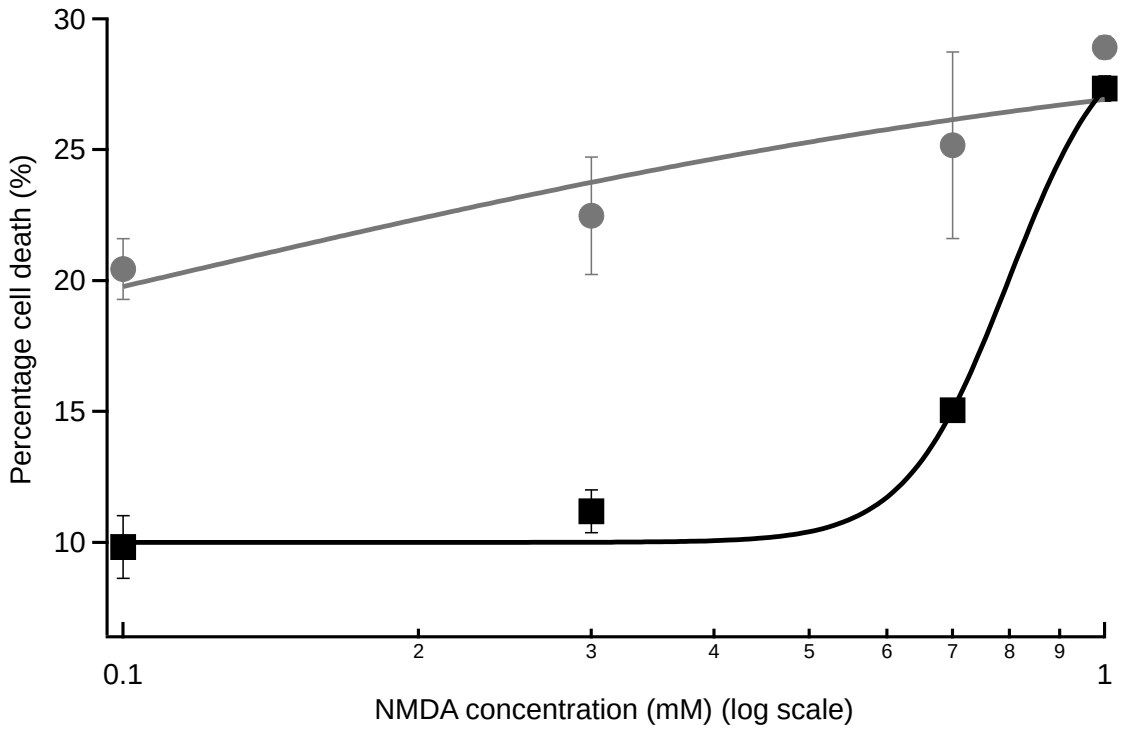

Figure 3.4: The effect of different NMDA concentrations on cell death in the absence (black filled squares) and presence of human Alix (filled grey circles). The cells were activated with physiological salt solution (PSS) with varying NMDA concentration and 50 µM Glycine. Partial dose-response curves were fit to the data using the Hill equation under conditions where the maximum and minimium were fixed at 30 and 10 % respectively.

Table 3.4: Percentage cell death after 6 hours following treatment with 1 mM NMDA/ 50 µM Glycine.

Column	Transfection	Percentage cell death ± SEM (%)	Sample size (n)
1	**GluN1/GluN2A/Alix 0.01mM NMDA**	**18.7 ± 1.9**	**3**
2	**GluN1/GluN2A/EGFP 0.01mM NMDA**	**9.8 ± 1.2**	**3**
3	**GluN1/GluN2A/Alix 0.1mM NMDA**	**21.9 ± 2.0**	**3**
4	**GluN1/GluN2A/EGFP 0.1mM NMDA**	**11.2 ± 0.8**	**3**
5	**GluN1/GluN2A/Alix 0.3mM NMDA**	**22.5 ± 1.5**	**3**
6	**GluN1/GluN2A/EGFP 0.3mM NMDA**	**15.0 ± 0.4**	**3**
7	**GluN1/GluN2A/Alix 0.7mM NMDA**	**28.5 ± 0.7**	**3**
8	**GluN1/GluN2A/EGFP 0.7mM NMDA**	**27.3 ± 0.5**	**3**

We found that by gradually increasing the NMDA concentration we also increased cell death caused by expression of NMDAR in the HEK293 cells (Figure 3.4 black squares). The same gradual increase was found by coexpression of Alix with NMDAR but a higher cell death percentage was observed compared to levels seen with NMDARs expressed alone (Figure 3.4grey circles). The addition of Alix to NMDAR caused a high

percentage of cell death (18.7 %) even in the presence of a low concentration of NMDA (10 μM) compared to the levels of cell death observed at the same concentration in cells expressing NMDARs alone (9.8 %). Therefore the relatively high cell death observed in cells expressing both Alix and NMDARs in the presence of PSS could be caused by low concentrations of glutamate/glycine in the culture media. Further analysis of the data was performed by fitting the Hill equation to the partial dose-response curves and showed that in the presence of Alix the NMDA EC50 for triggering NMDAR cell death decreased to 0.11 ± 0.04 mM compared to 0.80 ± 0.02 mM for NMDAR only cells. Therefore the presence of Alix decreased the NMDA concentration required to trigger cell death when coexpressed with NMDARs.

3.2.5 Modulation of NMDA cell death by mouse Alix WT

Our findings have shown that Alix is able to influence NMDAR activity in our cell death assay and suggest some form of functional interaction between these molecules may occur. We decided examine other variants of Alix in this assay. We used a mouse form of Alix and a number of deletion variants of the Alix mouse protein were used. Alix N-T and Alix C-T, which correspond to the N-terminal half and C-terminal half of the protein, respectively and Alix DPRD is Alix lacking the proline-rich domain.

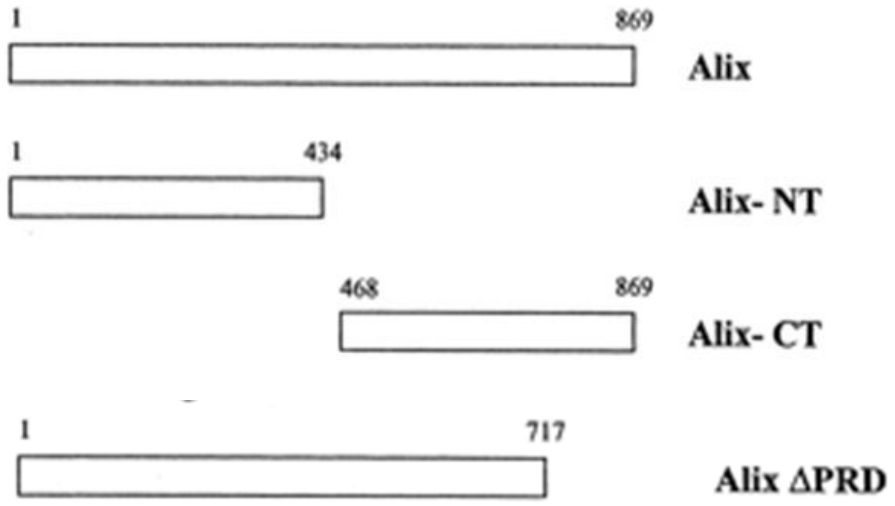

Figure 3.5: Schematic representation of Alix deletion mutants (Chatellard-Causse et al., 2002).

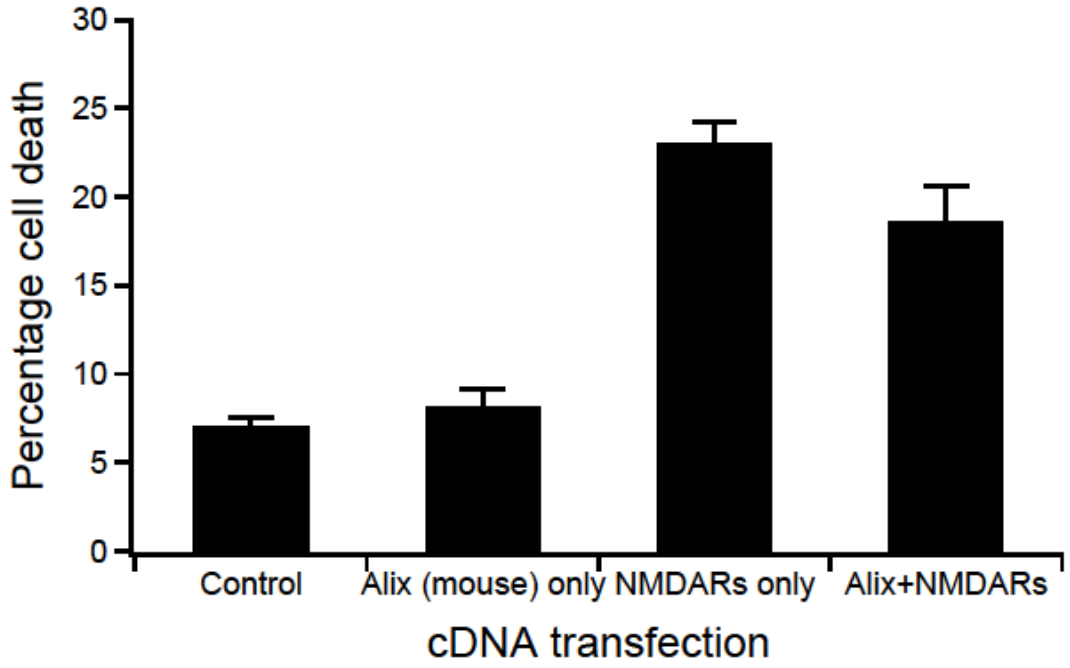

Figure 3.6 a: Modulation of NMDA cell death by mouse Alix WT. The cells were activated with physiological salt solution (PSS) with 1 mM NMDA and 50 µM Glycine. All data points correspond to the mean ±SE of values and statistical comparisons of cell death between groups were performed using a paired *t*-test to determine which groups were statistically different from each other.

Table 3.6 a: Percentage cell death after 6 hours following treatment with 1 mM NMDA/ 50 µM Glycine.

Column	Transfection	Percentage cell death ± SEM (%)	Sample size (n)
1	**Lipofectamine only**	**7.1 ± 0.5**	**3**
2	**Alix WT/EGFP**	**8.2 ± 1.0**	**3**
3	**GluN1/GluN2A/EGFP**	**23.1 ± 1.1**	**3**
4	**GluN1/GluN2A/Alix WT**	**18.6 ± 1.9**	**3**

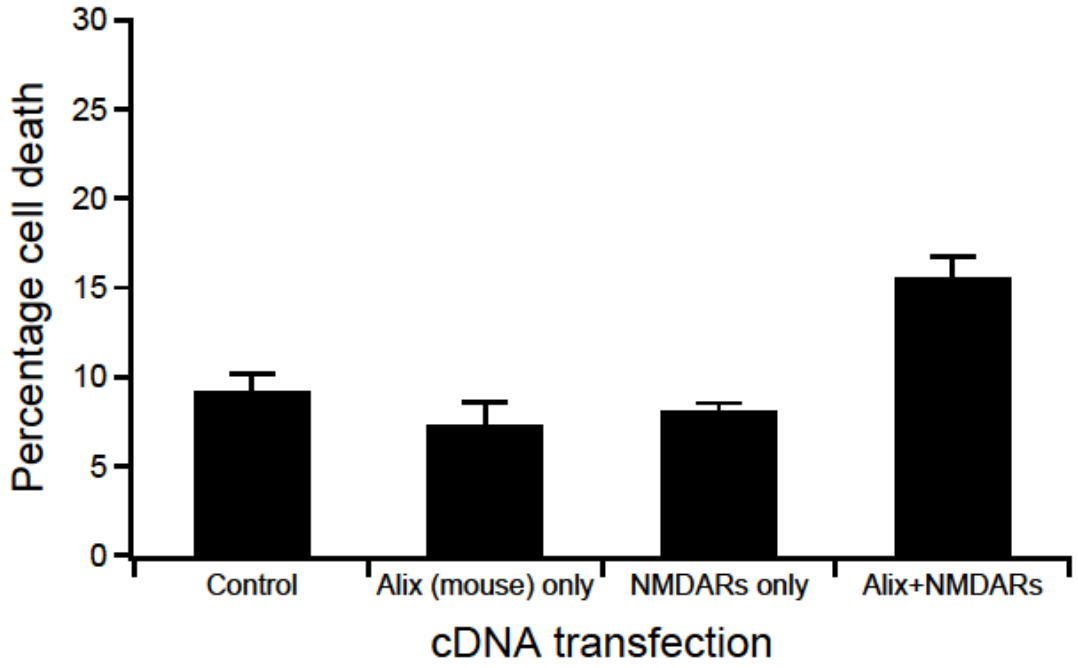

Figure 3.6 b: Modulation of NMDA cell death by mouse Alix WT. The cells were treated with physiological salt solution (PSS) only. All data points correspond to the mean ± SE of values and statistical comparisons of cell death between groups were performed using a paired *t*-test to determine which groups were statistically different from each other.

Table 3.6 b: Percentage cell death after 6 hours following treatment with physiological salt solution (PSS) only.

Column	Transfection	Percentage cell death ± SEM (%)	Sample size (n)
1	**Lipofectamine only**	**9.3 ± 0.9**	**3**
2	**Alix WT/EGFP**	**7.4 ± 1.2**	**3**
3	**GluN1/GluN2A/EGFP**	**8.2 ± 0.4**	**3**
4	**GluN1/GluN2A/Alix WT**	**15.6 ± 1.1**	**3**

Transfection comparison		Mean Difference	Significance
Control Activated	NMDAR only Activated	-16.02376%*	P<0.001
	NMDA+ Alix WT Activated	-11.53522%*	P<0.001
	NMDA+ Alix WT Not Activated	-8.52800%*	P = 0.001
Alix WT Activated	NMDAR only Activated	-14.92207%*	P<0.001
	NMDA+ Alix WT Activated	-10.43353%*	P<0.001
	NMDA+ Alix WT Not Activated	-7.42631%*	P = 0.004
NMDAR only Activated	Control Activated	16.02376%*	P<0.001
	Alix WT Activated	14.92207%*	P<0.001
	Control Not Activated	13.82659%*	P<0.001
	Alix WT Not Activated	15.72405%*	P<0.001
	NMDAR only Not Activated	14.94409%*	P<0.001
	NMDA+ Alix WT Not Activated	7.49576%*	P = 0.004
NMDA+ Alix WT Activated	Control Activated	11.53522%*	P<0.001
	Alix WT Activated	10.43353%*	P<0.001
	Control Not Activated	9.33804%*	P<0.001
	Alix WT Not Activated	11.23551%*	P<0.001
	NMDAR only Not Activated	10.45554%*	P<0.001
Control Not Activated	NMDAR only Activated	-13.82659%*	P<0.001
	NMDA+ Alix WT Activated	-9.33804%*	P<0.001
	NMDA+ Alix WT Not Activated	-6.33083%*	P = 0.017
Alix WT Not Activated	NMDAR only Activated	-15.72405%*	P<0.001
	NMDA+ Alix WT Activated	-11.23551%*	P<0.001
	NMDA+ Alix WT Not Activated	-8.22829%*	P = 0.002
NMDAR only Not	NMDAR only Activated	-14.94409%*	P<0.001
	NMDA+ Alix WT	-10.45554%*	P<0.001

Activated	Activated		
	NMDA+ Alix WT Not Activated	-7.44832%*	P = 0.004
NMDA+ Alix WT Not Activated	Control Activated	8.52800%*	P = 0.001
	Alix WT Activated	7.42631%*	P = 0.004
	NMDAR only Activated	-7.49576%*	P = 0.004
	Control Not Activated	6.33083%*	P = 0.017
	Alix WT Not Activated	8.22829%*	P = 0.002
	NMDAR only Not Activated	7.44832%*	P = 0.004

Table 3.6 c: Anova Analysis of table of statistically significant NMDA cell death by Alix WT. All data points correspond to the mean difference of values and statistical significance of cell death between groups. Anova analysis was performed using Tukey post-hoc analysis to determine which groups were statistically different from each other. Only statistically significant pairwise comparison is displayed and the values marked with * denotes that it is statistically significant at the level 0.05.

As a negative control, cells transfected without any DNA and maintained in PSS only had a mean of 9.3 ±0.9% cell death at 6 hours (Figure 3.6 b). The negative control without any DNA that was activated with PSS with NMDA (1 mM) and glycine (50 µM) had a mean of 7.1 ± 0.5% cell death at 6 hours (Figure 3.6 a). Paired t-test and ANOVA analysis (Table 3.6c) shows that the difference between the negative control activated and not activated is considered to be not statistically significant.

In cultures that were transfected with mouse AlixWT subunits alone and maintained in PSS, cell death at 6 hours was 7.4 ± 1.2% (Figure 3.6 b). In cultures that were transfected with AlixWT subunit alone activated in PSS with NMDA (1 mM) and glycine (50 µM)had a mean of 8.2 ±1.0% cell death at 6hours (Figure 3.6 a). Paired t-test and ANOVA analysis (Table 3.6c) shows that the difference between Alix alone activated and not activated is

considered to be not statistically significant. There was also no statistical significance in cell death between activated or non activated cells expressing Alix alone and the activated or non activated negative control (without DNA).

The positive control culture transfected with GluN1/GluN2A subunits and maintained in PSS only had a mean of 8.2 ± 0.4% cell death at 6 hours (Figure 3.6 b). Whereas, the positive control expressing GluN1/GluN2A subunits that was activated with PSS with NMDA (1 mM) and glycine (50 µM) had a mean of 23.1 ± 1.1% cell death at 6 hours (Figure 3.6 a). Treatment with NMDA and glycine significantly enhanced cell death. Paired t-test shows that the difference between the activated and non-activated positive control is considered to be extremely statistically significant with a P value of less than 0.0001 which correlates with the ANOVA analysis significance value of $P<0.001$ (Table 3.6c).

To determine if mouse Alix has any cytotoxic effect on GluN1/GluN2A subunit transfected HEK cells, Alix was transfected with GluN1/GluN2A subunits and treated with PSS alone or with PSS and NMDA plus glycine and cell death was assessed 6 hours following the treatments. As shown in Figure 3.6 a, transfecting Alix with GluN1/GluN2A significantly reduced the percentage of dead cells compared with positive control GluN1/GluN2A subunits. The culture transfected with Alix, GluN1/GluN2A subunits and activated with PSS and NMDA with glycine had a mean of 18.6 ± 1.9% cell death at 6 hours (Figure 3.6 a). Paired t-test and ANOVA analysis shows that the difference between the activated positive control and activated cells expressing mouse Alix, GluN1, GluN2A is considered to be not statistically significant.

Alix transfected with GluN1/GluN2A subunits and not activated (PSS alone) also yielded a surprising result with a mean of 15.6 ± 1.1% cell death at 6 hours (Figure 3.6 b). It is a higher percent of cell death compared to cells expressing GluN1/GluN2A subunits

that were not activated. Paired t-test shows that the difference in cell death between the non activated positive control and non activated cells expressing Alix, GluN1 and GluN2A together is considered to be extremely statistically significant which correlate with the ANOVA analysis significance value of $P<0.001$ (Table 3.6c). There was however no statistical significance in cell death in activated or non-activated cells expressing Alix, GluN1, GluN2A (P value of 0.2361). These results are similar to those observed for the EGFP tagged human Alix used in earlier cell death experiments (Figure 3.1a and b).

3.2.6 Modulation of NMDA cell death by mouse Alix CT

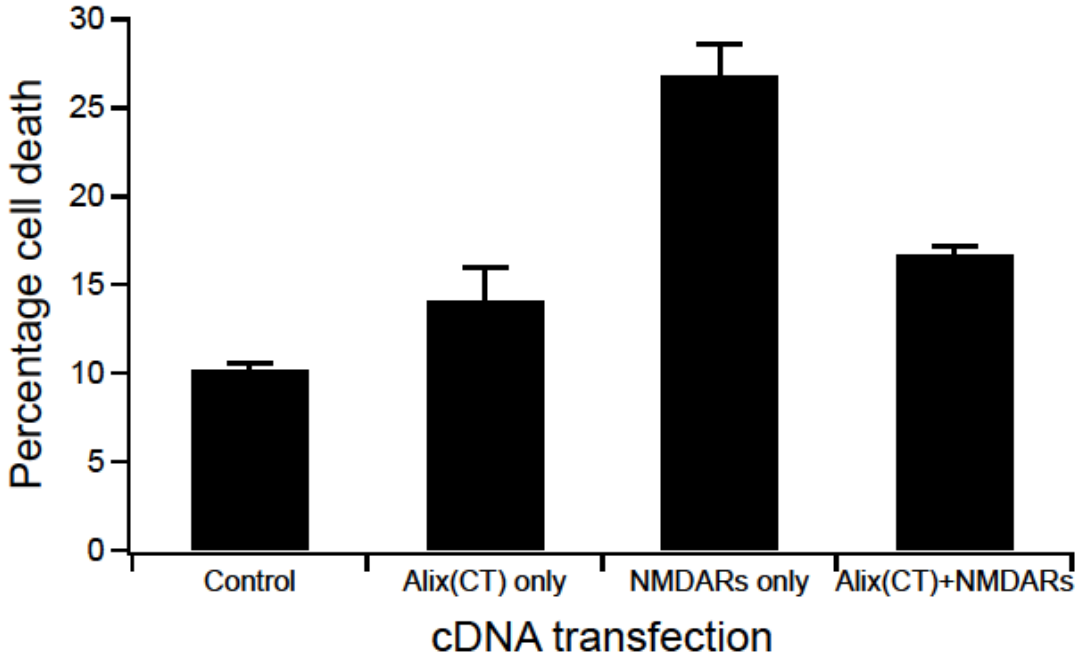

Figure 3.7 a: Modulation of NMDA cell death by mouse Alix CT. The cells were activated with physiological salt solution (PSS) with 1 mM NMDA and 50 µM Glycine. All data points correspond to the mean ± SE of values and statistical comparisons of cell death between groups were performed using a paired *t*-test to determine which groups were statistically different from each other.

Table 3.7 a: Percentage cell death after 6 hours following treatment with 1 mM NMDA/ 50 µM Glycine.

Column	Transfection	Percentage cell death ± SEM (%)	Sample size (n)
1	**Lipofectamine only**	**10.2 ± 0.3**	**3**
2	**Alix CT/EGFP**	**14.2 ± 1.9**	**3**
3	**GluN1/GluN2A/EGFP**	**26.8 ± 1.7**	**3**
4	**GluN1/GluN2A/Alix CT**	**16.7 ± 0.5**	**3**

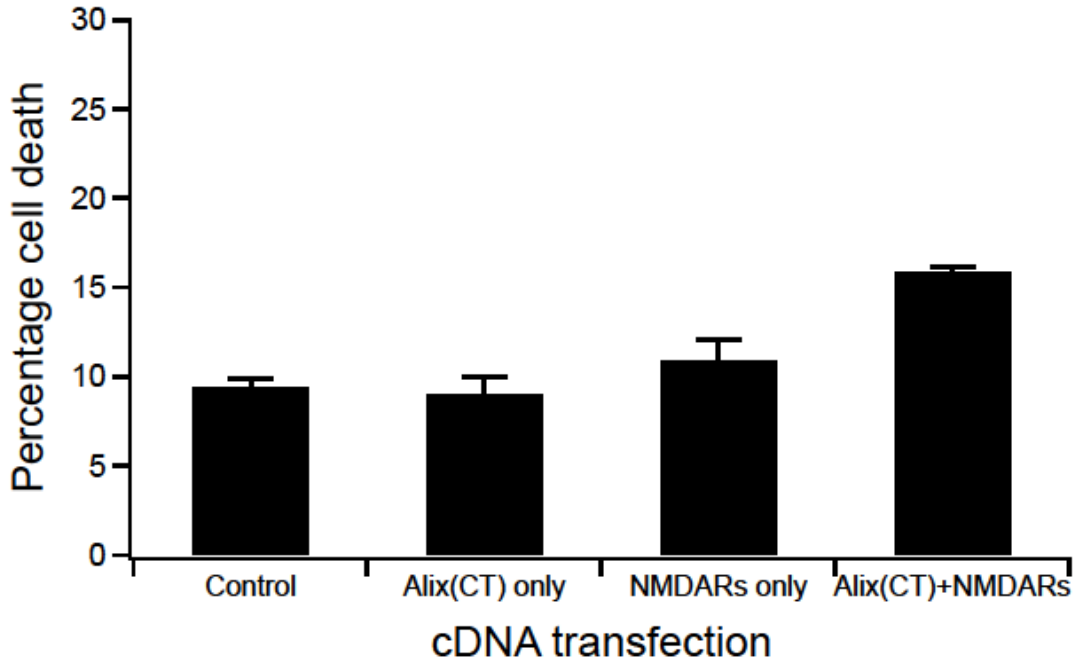

Figure 3.7 b: Modulation of NMDA cell death by Alix CT. The cells were treated with physiological salt solution (PSS) only. All data points correspond to the mean ± SE of values and statistical comparisons of cell death between groups were performed using a paired *t*-test to determine which groups were statistically different from each other.

Table 3.7 b: Percentage cell death after 6 hours following treatment with physiological salt solution (PSS) only.

Column	Transfection	Percentage cell death ± SEM (%)	Sample size (n)
1	**Lipofectamine only**	**9.5 ± 0.4**	**3**
2	**Alix CT/EGFP**	**9.1 ± 0.9**	**3**
3	**GluN1/GluN2A/EGFP**	**11.0 ± 1.1**	**3**
4	**GluN1/GluN2A/Alix CT**	**15.9 ± 0.3**	**3**

Transfection comparison		Mean Difference	Significance
Control Activated	NMDAR only Activated	-16.56591%*	P<0.001
	NMDA+ Alix CT Activated	-6.44449%*	P = 0.002
	NMDA+ Alix CT Not Activated	-5.65768%*	P = 0.006
Alix CT Activated	NMDAR only Activated	-14.52863%*	P<0.001
	NMDA+ Alix CT Activated	-4.40721%*	P = 0.040
NMDAR only Activated	Control Activated	16.56591%*	P<0.001
	Alix CT Activated	14.52863%*	P<0.001
	NMDA+ Alix CT Activated	10.12142%*	P<0.001
	Control Not Activated	17.32639%*	P<0.001
	Alix CT Not Activated	17.70731%*	P<0.001
	NMDAR only Not Activated	15.81505%*	P<0.001
	NMDA+ Alix CT Not Activated	10.90823%*	P<0.001
NMDA+ Alix CT Activated	Control Activated	6.44449%*	P = 0.002
	Alix CT Activated	4.40721%*	P = 0.040
	NMDAR only Activated	-10.12142%*	P<0.001
	Control Not Activated	7.20497%*	P = 0.001
	Alix CT Not Activated	7.58589%*	P<0.001
	NMDAR only Not Activated	5.69363%*	P = 0.005
Control Not Activated	NMDAR only Activated	-17.32639%*	P<0.001
	NMDA+ Alix CT Activated	-7.20497%*	P = 0.001
	NMDA+ Alix CT Not Activated	-6.41816%*	P = 0.002
Alix CT Not Activated	NMDAR only Activated	-17.70731%*	P<0.001
	NMDA+ Alix CT Activated	-7.58589%*	P<0.001
	NMDA+ Alix CT Not Activated	-6.79908%*	P = 0.001
	NMDAR only	-15.81505%*	P<0.001

NMDAR only Not Activated	Activated 3		
	NMDA+ Alix CT Activated	-5.69363%*	P = 0.005
	NMDA+ Alix CT Not Activated	-4.90682%*	P = 0.018
NMDA+ Alix CT Not Activated	Control Activated	5.65768%*	P = 0.006
	NMDAR only Activated	-10.90823%*	P<0.001
	Control Not Activated	6.41816%*	P = 0.002
	Alix CT Not Activated	6.79908%*	P = 0.001
	NMDAR only Not Activated	4.90682%*	P = 0.018

Table 3.7 c: Anova Analysis of table of statistically significant NMDA cell death by Alix CT. All data points correspond to the mean difference of values and statistical significance of cell death between groups. Anova analysis was performed using Tukey post-hoc analysis to determine which groups were statistically different from each other. Only statistically significant pairwise comparison is displayed and the values marked with * denotes that it is statistically significant at the level 0.05.

The negative control culture transfected without any DNA and maintained in PSS only had a mean of 9.5 ± 0.4% cell death at 6 hours (Figure 3.7 b). The negative control without any DNA that was activated with PSS with NMDA (1 mM) and glycine (50 µM) had a mean of 10.2 ± 0.3% cell death at 6 hours (Figure 3.7 a). Paired t-test and ANOVA analysis shows that the difference between the negative control activated and not activated is considered to be not statistically significant.

In cultures that were transfected with Alix CT subunits alone and maintained in PSS, cell death at 6 hours was 9.1 ± 0.9% (Figure 3.7 b). In cultures that were transfected with Alix CT subunit alone activated in PSS with NMDA (1 mM) and glycine (50 µM) had a mean of 14.2 ± 1.9% cell death at 6 hours (Figure 3.7 a).

The positive control culture transfected with GluN1/GluN2A subunits and maintained in PSS only had a mean of 11.0 ± 1.1% cell death at 6 hours (Figure 3.7 b). Whereas, the positive control GluN1/GluN2A subunits that was activated with PSS with NMDA (1 mM) and glycine (50 μM) had a mean of 26.8 ± 1.7% cell death at 6 hours (Figure 3.7 a). Treatment with NMDA and glycine significantly enhanced cell death. Paired t-test shows that the difference between the activated and non-activated positive control is considered to be extremely statistically significant with a P value of less than 0.0001 which correlates with the ANOVA analysis significance value of $P<0.001$ (Table 3.7c).

Transfecting Alix CT with GluN1/GluN2A significantly reduced the percentage of dead cells compared with positive control GluN1/GluN2A subunits. The culture transfected with Alix CT, GluN1/GluN2A subunits and activated with PSS and NMDA with glycine had a mean of 16.7 ± 0.5% cell death at 6 hours (Figure 3.7 a). Paired t-test shows that the difference between the activated positive control and activated cells expressing Alix CT, GluN1 and GluN2A is considered to be statistically significant with a P value of 0.0432 which correlates with the ANOVA analysis significance value of $P<0.001$ (Table 3.7c).

Non activated Alix CT transfected with GluN1/GluN2A subunits (PSS alone) yielded a mean cell death of 15.9 ± 0.3% cell death at 6 hours (Figure 3.7 b). It is a higher percent of cell death compared to GluN1/GluN2A subunits that were not activated. Paired t-test shows that the difference between the non activated positive control and non activated cells expressing mouse Alix CT, GluN1, GluN2A is considered to be statistically significant with a P value of 0.0277 which correlate with the ANOVA analysis sig value of .018 (Table 3.7c).There was however a statistical significance in the T-test in cell death between activated and non-activated cells expressing Alix CT, GluN1, GluN2A (P value of 0.0471) but no statistical significance in the ANOVA analysis. Thus the Alix-CT mutant containing only the C-terminal region of Alix is able to replicate the enhanced cell death

seen with the full length human (Figure 3.1) and mouse Alix variants (Figure 3.6) in the absence of NMDA/glycine.

3.2.7 Modulation of NMDA cell death by mouse Alix NT

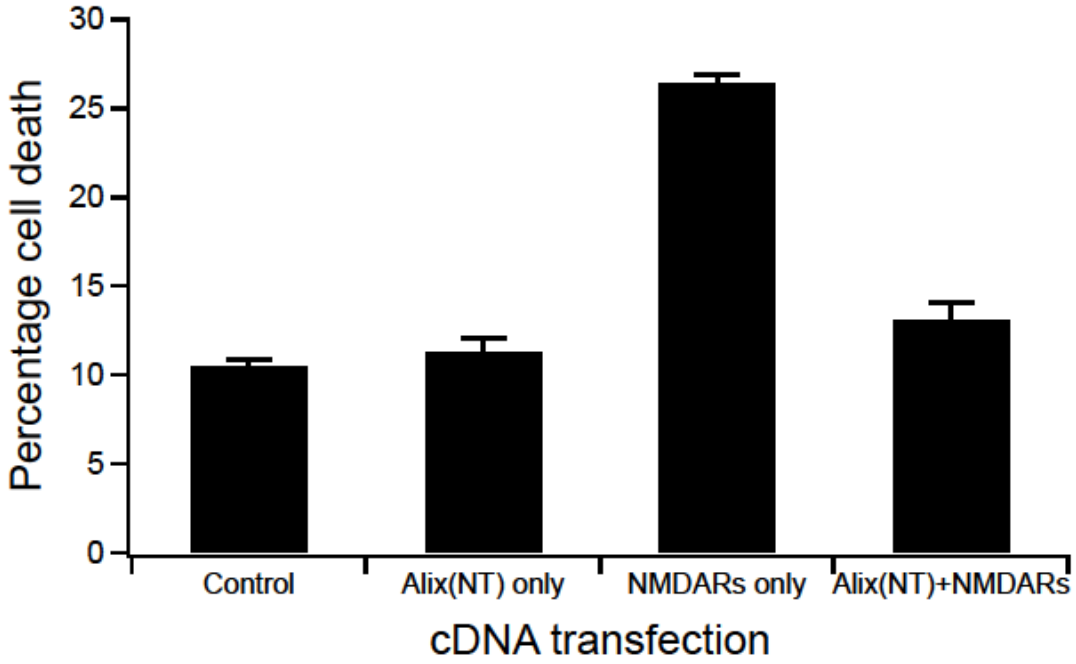

Figure 3.8 a: Modulation of NMDA cell death by mouse Alix NT. The cells were activated with physiological salt solution (PSS) with 1 mM NMDA and 50 µM Glycine. All data points correspond to the mean ± SE of values and statistical comparisons of cell death between groups were performed using a paired *t*-test to determine which groups were statistically different from each other.

Table 3.8 a: Percentage cell death after 6 hours following treatment with 1 mM NMDA/ 50 µM Glycine.

Column	Transfection	Percentage cell death ± SEM (%)	Sample size (n)
1	**Lipofectamine only**	**10.6 ± 0.3**	**3**
2	**Alix NT/EGFP**	**11.4 ± 0.7**	**3**
3	**GluN1/GluN2A/EGFP**	**26.4 ± 0.5**	**3**
4	**GluN1/GluN2A/Alix NT**	**13.2 ± 0.9**	**3**

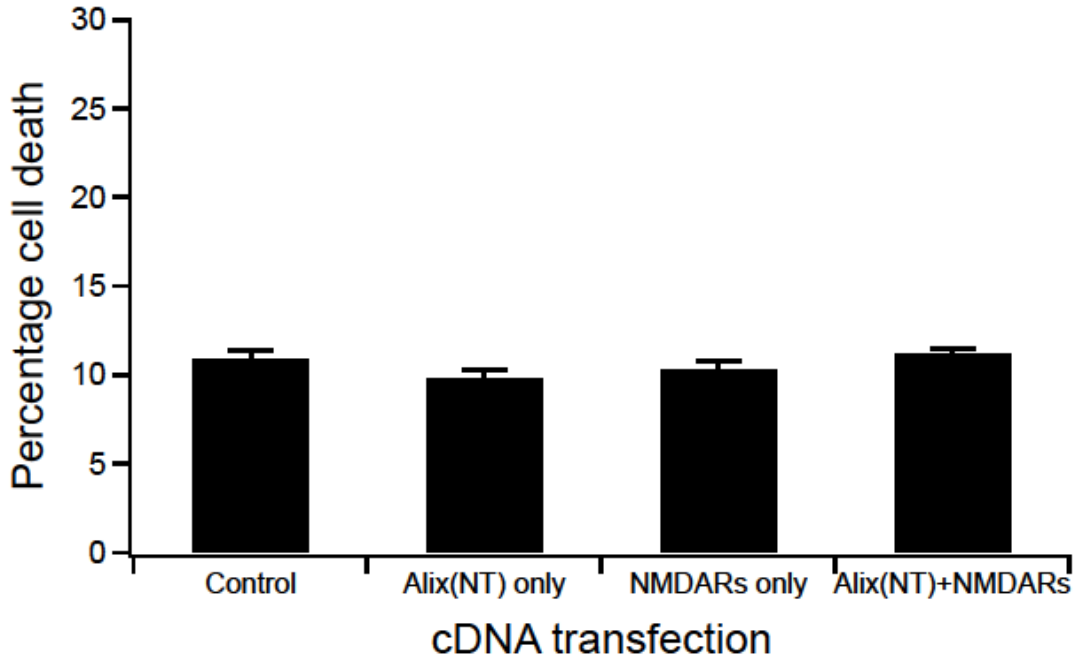

Figure 3.8 b: Modulation of NMDA cell death by Alix NT. The cells were treated with physiological salt solution (PSS) only. All data points correspond to the mean ± SE of values and statistical comparisons of cell death between groups were performed using a paired *t*-test to determine which groups were statistically different from each other.

Table 3.8 b: Percentage cell death after 6 hours following treatment with physiological salt solution (PSS) only.

Column	Transfection	Percentage cell death ± SEM (%)	Sample size (n)
1	**Lipofectamine only**	**11.0 ± 0.4**	**3**
2	**Alix NT/EGFP**	**9.9 ± 0.5**	**3**
3	**GluN1/GluN2A/EGFP**	**10.3 ± 0.4**	**3**
4	**GluN1/GluN2A/Alix NT**	**11.3 ± 0.3**	**3**

Transfection comparison		Mean Difference	Significance
Control Activated	NMDAR only Activated	-15.84100%*	P<0.001
	NMDA+ Alix NT Activated	-2.60646%*	P = 0.041
Alix NT Activated	Positive Control Activated	-15.03170%*	P<0.001
NMDAR only Activated	Negative Control Activated	15.84100%*	P<0.001
	Alix NT Activated	15.03170%*	P<0.001
	NMDA+ Alix NT Activated	13.23454%*	P<0.001
	Control Not Activated	15.42169%*	P<0.001
	Alix NT Not Activated	16.53079%*	P<0.001
	NMDAR only Not Activated	16.06126%*	P<0.001
	NMDA+ Alix NT Not Activated	15.12686%*	P<0.001
NMDA+ Alix NT Activated	Control Activated	2.60646%*	P = 0.041
	NMDAR only Activated	-13.23454%*	P<0.001
	Alix NT Not Activated	3.29625%*	P = 0.007
	NMDAR only Not Activated	2.82672%*	P = 0.023
Control Not Activated	NMDAR only Activated	-15.42169%*	P<0.001
Alix NT Not Activated	NMDAR only Activated	-16.53079%*	P<0.001
	NMDA+ Alix NT Activated	-3.29625%*	P = 0.007
NMDAR only Not Activated	NMDAR only Activated	-16.06126%*	P<0.001
	NMDA+ Alix NT Activated	-2.82672%*	P = 0.023
NMDA+ Alix NT Not Activated	NMDAR only Activated	-15.12686%*	P<0.001

Table 3.8 c: Anova Analysis of table of statistically significant NMDA cell death by Alix NT. All data points correspond to the mean difference of values and statistical significance of cell death between groups. Anova analysis was performed using Tukey post-hoc analysis to determine which groups were statistically different

from each other. Only statistically significant pairwise comparison is displayed and the values marked with * denotes that it is statistically significant at the level 0.05.

The negative control culture transfected without any DNA and maintained in PSS only had a mean of 11.0 ± 0.4% cell death at 6 hours (Figure 3.8 b). The negative control without any DNA that was activated with PSS with NMDA (1 mM) and glycine (50 µM) had a mean of 10.6 ± 0.3% cell death at 6 hours (Figure 3.8 a). Paired t-test and ANOVA analysis shows that the difference between the activated and non activated negative control is considered to be not statistically significant.

In cultures that were transfected with Alix NT subunits alone and maintained in PSS, cell death at 6 hours was 9.9 ± 0.5% (Figure 3.8 b). In cultures that were transfected with Alix NT subunit alone activated in PSS with NMDA (1 mM) and glycine (50 µM) had a mean of 11.4 ± 0.7% cell death at 6 hours (Figure 3.8 a). Paired t-test and ANOVA analysis shows that the difference between Alix NT alone activated and not activated is considered to be not statistically significant. There was also no statistical significance in cell death between cells expressing Alix NT alone and the negative control (without DNA) regardless if they were activated or not.

The positive control culture transfected with GluN1/GluN2A subunits and maintained in PSS only had a mean of 10.3 ± 0.4% cell death at 6 hours (Figure 3.8 b). Whereas, the positive control of cells expressing GluN1/GluN2A subunits that was activated with PSS with NMDA (1 mM) and glycine (50 µM) had a mean of 26.4 ± 0.5% cell death at 6 hours (Figure 3.8 a). Treatment with NMDA and glycine significantly enhanced cell death. Paired t-test shows that the difference between the positive control activated and not activated is considered to be extremely statistically significant with a P

value of less than 0.0001 which correlates with the ANOVA analysis significance value of $P<0.001$ (Table 3.8c).

Transfecting Alix NT with GluN1/GluN2A significantly reduced the percentage of dead cells compared with positive control GluN1/GluN2A subunits. The culture transfected with Alix NT, GluN1/GluN2A subunits and activated with PSS and NMDA with glycine had a mean of 13.2 ± 0.9% cell death at 6 h (Figure 3.8 a).Paired t-test shows that the difference between the activated positive control and activated cells expressing Alix NT, GluN1, GluN2A is considered to be very statistically significant with a P value of 0.0056 which correlates with the ANOVA analysis significance value of $P<0.001$ (Table 3.7c).

Non-activated Alix NT transfected with GluN1/GluN2A subunits (PSS alone) resulted in a mean cell death of 11.3 ± 0.3% cell death at 6 h (Figure 3.8 b). It is a similar percent of cell death compared to GluN1/GluN2A subunits that were not activated. Paired t-test and ANOVA analysis shows that the difference between the non-activated positive control and non-activated cells containing AlixNT, GluN1, GluN2A was considered to be not statistically significant. Thus this suggests that the N-terminal region of Alix is not responsible for increasing NMDAR triggered cell death in the absence of NMDA/glycine (Figure 3.8 b). but surprisingly is able to reduce NMDAR triggered cell death to levels similar to negative controls (Figure 3.8 a).

3.2.8 Modulation of NMDA cell death by mouse Alix DPRD

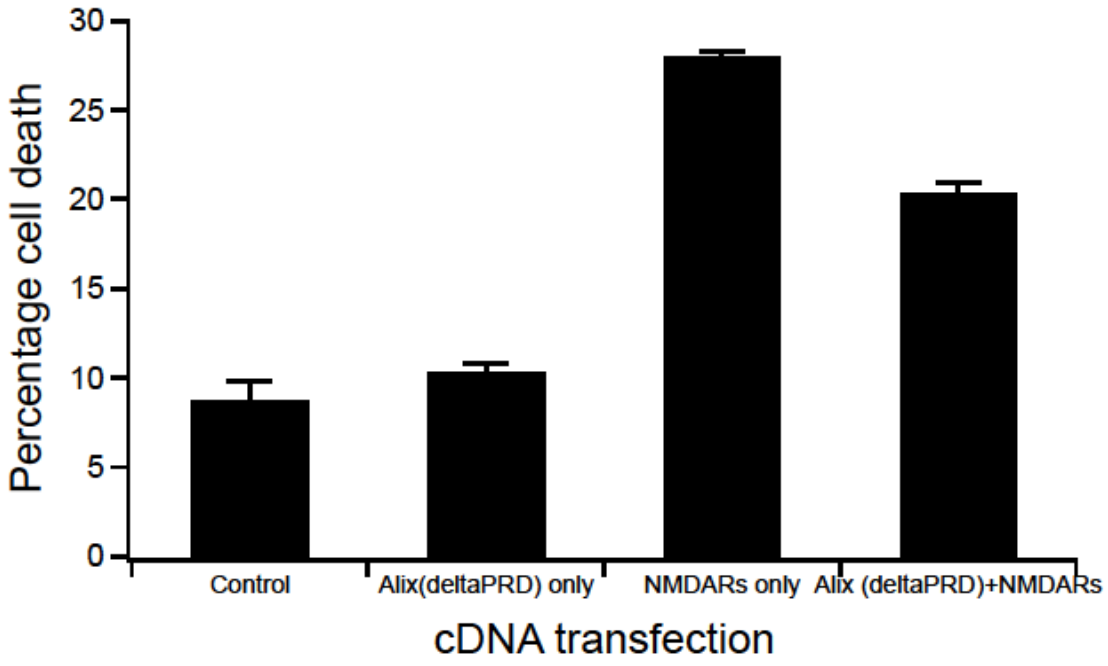

Figure 3.9 a: Modulation of NMDA cell death by mouse Alix DPRD. The cells were activated with physiological salt solution (PSS) with 1 mM NMDA and 50 µM Glycine. All data points correspond to the mean ±SE of values and statistical comparisons of cell death between groups were performed using a paired *t*-test to determine which groups were statistically different from each other.

Table 3.9 a: Percentage cell death after 6 hours following treatment with 1 mM NMDA/ 50 µM Glycine.

Column	Transfection	Percentage cell death ± SEM (%)	Sample size (n)
1	**Lipofectamine only**	**8.8 ± 1.0**	**3**
2	**Alix DPRD/EGFP**	**10.3 ± 0.5**	**3**
3	**GluN1/GluN2A/EGFP**	**28.0 ± 0.3**	**3**
4	**GluN1/GluN2A/Alix DPRD**	**20.4 ± 0.6**	**3**

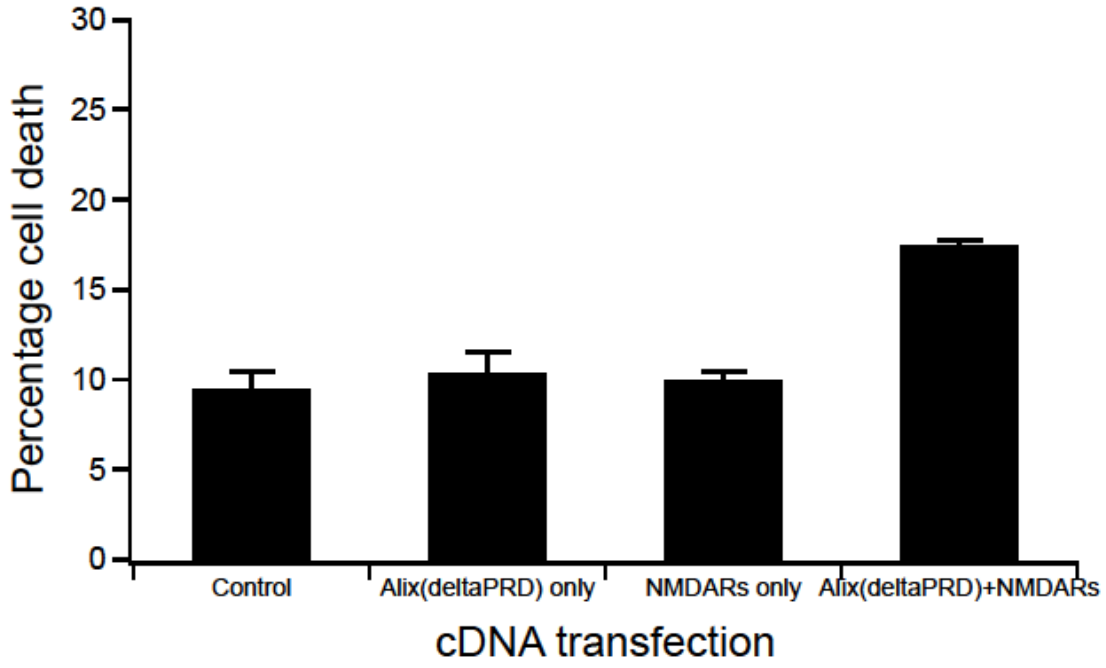

Figure 3.9 b: Modulation of NMDA cell death by Alix DPRD. The cells were treated with physiological salt solution (PSS) only. All data points correspond to the mean ± SE of values and statistical comparisons of cell death between groups were performed using a paired *t*-test to determine which groups were statistically different from each other.

Table 3.9 b: Percentage cell death after 6 hours following treatment with physiological salt solution (PSS) only.

Column	Transfection	Percentage cell death ± SEM (%)	Sample size (n)
1	**Lipofectamine only**	**9.5 ± 1.0**	**3**
2	**Alix DPRD/EGFP**	**10.4 ± 1.2**	**3**
3	**GluN1/GluN2A/EGFP**	**10.0 ± 0.5**	**3**
4	**GluN1/GluN2A/Alix DPRD**	**17.5 ± 0.2**	**3**

Transfection comparison		Mean Difference	Significance
Control Activated	NMDAR only Activated	-19.24538%*	P<0.001
	NMDA+ Alix DPRD Activated	-11.58024%*	P<0.001
	NMDA+ Alix DPRD Not Activated	-8.75617%*	P<0.001
Alix DPRD Activated	NMDAR only Activated	-17.70330%*	P<0.001
	NMDA+ Alix DPRD Activated	-10.03816%*	P<0.001
	NMDA+ Alix DPRD Not Activated	-7.21409%*	P<0.001
NMDAR only Activated	Control Activated	19.24538%*	P<0.001
	Alix DPRD Activated	17.70330%*	P<0.001
	NMDA+ Alix DPRD Activated	7.66514%*	P<0.001
	Control Not Activated	18.52615%*	P<0.001
	Alix DPRD Not Activated	17.66938%*	P<0.001
	NMDAR only Not Activated	18.02639%*	P<0.001
	NMDA+ Alix DPRD Not Activated	10.48921%*	P<0.001
NMDA+ Alix DPRD Activated	Control Activated	11.58024%*	P<0.001
	Alix DPRD Activated	10.03816%*	P<0.001
	NMDAR only Activated	-7.66514%*	P<0.001
	Control Not Activated	10.86101%*	P<0.001
	Alix DPRD Not Activated	10.00424%*	P<0.001
	NMDAR only Not Activated	10.36125%*	P<0.001
Control Not Activated	NMDAR only Activated	-18.52615%*	P<0.001
	NMDA+ Alix DPRD Activated	-10.86101%*	P<0.001
	NMDA+ Alix DPRD Not	-8.03694%*	P<0.001

	Activated		
Alix DPRD Not Activated	NMDAR only Activated	-17.66938%*	P<0.001
	NMDA+ Alix DPRD Activated	-10.00424%*	P<0.001
	NMDA+ Alix DPRD Not Activated	-7.18017%*	P<0.001
NMDAR only Not Activated	NMDAR only Activated	-18.02639%*	P<0.001
	NMDA+ Alix DPRD Activated	-10.36125%*	P<0.001
	NMDA+ Alix DPRD Not Activated	-7.53718%*	P<0.001
NMDA+ Alix DPRD Not Activated	Control Activated	8.75617%*	P<0.001
	Alix DPRD Activated	7.21409%*	P<0.001
	NMDAR only Activated	-10.48921%*	P<0.001
	Control Not Activated	8.03694%*	P<0.001
	Alix DPRD Not Activated	7.18017%*	P<0.001
	NMDAR only Not Activated	7.53718%*	P<0.001

Table 3.9 c: Anova Analysis of table of statistically significant NMDA cell death by Alix DPRD. All data points correspond to the mean difference of values and statistical significance of cell death between groups. Anova analysis was performed using Tukey post-hoc analysis to determine which groups were statistically different from each other. Only statistically significant pairwise comparison is displayed and the values marked with * denotes that it is statistically significant at the level 0.05.

The negative control culture transfected without any DNA and maintained in PSS only had a mean of 9.5 ± 1.0% cell death at 6 hours (Figure 3.9 b). The negative control without any DNA that was activated with PSS with NMDA (1 mM) and glycine (50 μM) had a mean of 8.8 ± 1.0% cell death at 6 hours (Figure 3.9 a). Paired t-test and ANOVA analysis shows

that the difference between the negative control activated and not activated is considered to be not statistically significant.

In cultures that were transfected with mouse Alix DPRD subunits alone and maintained in PSS, cell death at 6 hours was 10.4 ± 1.2% (Figure 3.9 b). In cultures that were transfected with Alix DPRD subunit alone activated in PSS with NMDA (1 mM) and glycine (50 µM) had a mean of 10.3 ± 0.5% cell death at 6 hours (Figure 3.9 a). Paired t-test and ANOVA analysis shows that the difference between cells expressing mouse Alix DPRD alone activated and not activated is considered to be not statistically significant. There was also no statistical significance between the cell death observed in cells expressing Alix DPRD alone and negative control (without DNA) regardless if it was activated or not.

The positive control culture transfected with GluN1/GluN2A subunits and maintained in PSS only had a mean of 10.0 ± 0.5% cell death at 6 hours (Figure 3.9 b). Whereas, the positive control GluN1/GluN2A subunits that was activated with PSS with NMDA (1 mM) and glycine (50 µM) had a mean of 28.0 ± 0.3% cell death at 6 hours (Figure 3.9 a). Treatment with NMDA and glycine significantly enhanced cell death. Paired t-test shows that the difference between the positive control activated and not activated is considered to be extremely statistically significant with a P value of less than 0.0001 which correlates with the ANOVA analysis significance value of $P<0.001$ (Table 3.9c).

The cultures transfected with mouse Alix DPRD, GluN1/GluN2A subunits and activated with PSS and NMDA with glycine had a mean of 20.4 ± 0.6% cell death at 6 hours (Figure 3.9 a). The paired t-test shows that the difference between the positive control activated and cells expressing Alix DPRD, GluN1 and GluN2A activated is considered to be very statistically significant with a P value of 0.0092 which correlates with the ANOVA analysis significance value of $P<0.001$ (Table 3.9c).

Cells expressing mouse Alix DPRD transfected with GluN1/GluN2A subunits and not activated (PSS alone) also yielded a mean of 17.5 ± 0.2% cell death at 6 hours (Figure 3.9 b). It is a higher percent of cell death compared to GluN1/GluN2A subunits that were not activated. Paired t-test shows that the difference between the positive control not activated and cells expressing mouse Alix DPRD, GluN1, GluN2A not activated is considered to be very statistically significant with a P value of 0.0073 which also correlates with the ANOVA analysis significance value of $P<0.001$ (Table 3.9c).There is also a T-test statistical significance in cell death between activated and non-activated cells expressing mouse Alix DPRD, GluN1 and GluN2A (P value of 0.0260) but no significance in the ANOVA analysis. Therefore these findings are similar to those seen with the full length human and mouse Alix.

3.2.9 Modulation of NMDA cell death by mouse Alix NT + CT coexpression

Since the Alix-CT mutant replicates some of the observations seen with full length human and mouse Alix, we wondered whether the coexpression of both mouse Alix NT and Alix CT mutants would fully replicate the observations seen with full length Alix. Experiments were performed in the presence of both Alix NT and Alix CT cotransfected together.

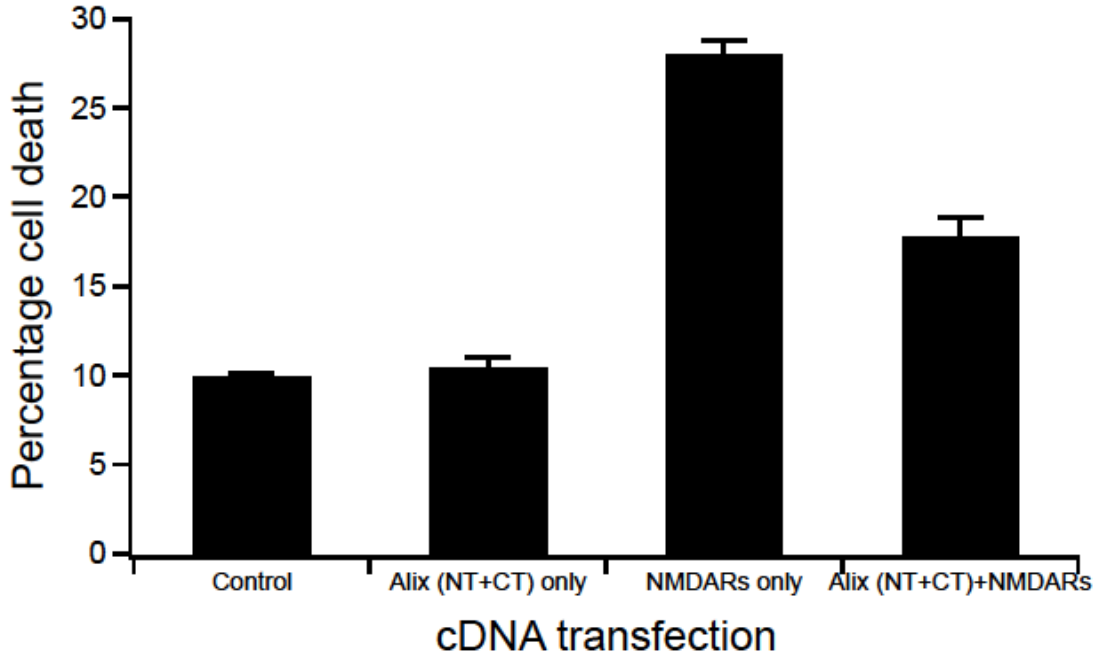

Figure 3.10 a: Modulation of NMDA cell death by mouse Alix NT + CT. The cells were activated with physiological salt solution (PSS) with 1 mM NMDA and 50 µM Glycine. All data points correspond to the mean ±SE of values and statistical comparisons of cell death between groups were performed using a paired *t*-test to determine which groups were statistically different from each other.

Table 3.10 a: Percentage cell death after 6 hours following treatment with 1 mM NMDA/ 50 µM Glycine.

Column	Transfection	Percentage cell death ± SEM (%)	Sample size (n)
1	**Lipofectamine only**	**10.0 ± 0.1**	**3**
2	**Alix NT+ CT /EGFP**	**10.4 ± 0.6**	**3**
3	**GluN1/GluN2A/EGFP**	**28.1 ± 0.7**	**3**
4	**GluN1/GluN2A/Alix NT+ CT**	**17.8 ± 1.1**	**3**

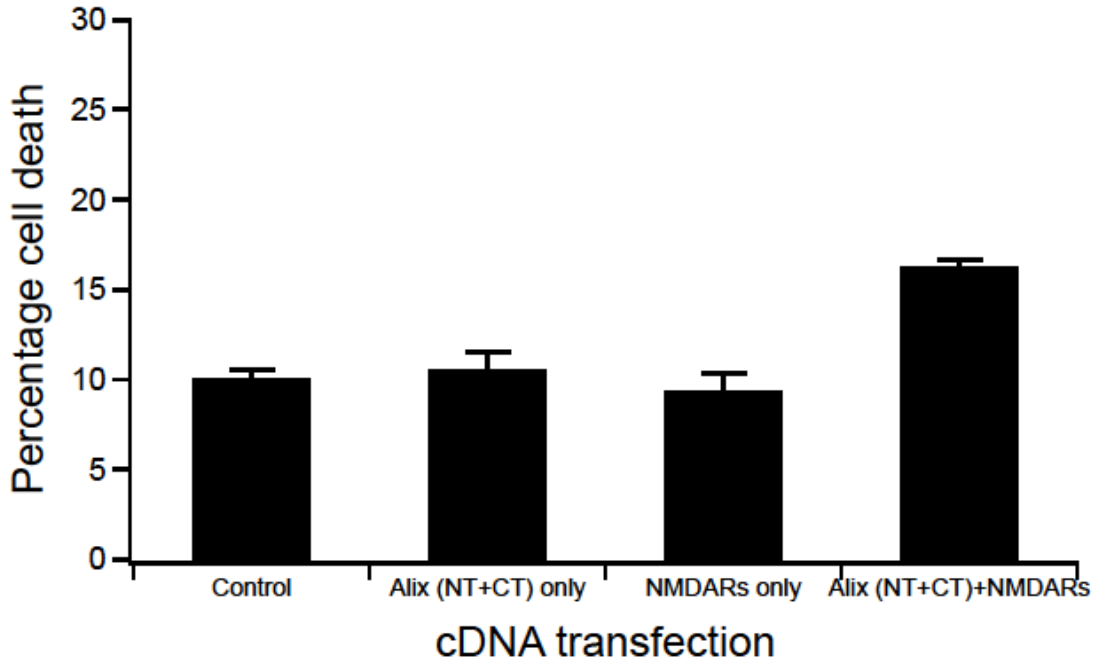

Figure 3.10 b: Modulation of NMDA cell death by mouse Alix NT + CT. The cells were treated with physiological salt solution (PSS) only. All data points correspond to the mean ± SE of values and statistical comparisons of cell death between groups were performed using a paired *t*-test to determine which groups were statistically different from each other.

Table 3.10 b: Percentage cell death after 6 hours following treatment with physiological salt solution (PSS) only.

Column	Transfection	Percentage cell death ± SEM (%)	Sample size (n)
1	**Lipofectamine only**	**10.1 ± 0.4**	**3**
2	**Alix NT+ CT /EGFP**	**10.6 ± 0.9**	**3**
3	**GluN1/GluN2A/EGFP**	**9.4 ± 0.9**	**3**
4	**GluN1/GluN2A/Alix NT+ CT**	**16.3 ± 0.4**	**3**

Transfection comparison		Mean Difference	Significance
Control Activated	NMDAR only Activated	-18.07109%*	P<0.001
	NMDA+ Alix CTNT Activated	-7.81250%*	P<0.001
	NMDA+ Alix CTNT Not Activated	-6.27950%*	P<0.001
Alix CTNT Activated	NMDAR only Activated	-17.65998%*	P<0.001
	NMDA+ Alix CTNT Activated	-7.40139%*	P<0.001
	NMDA+ Alix CTNT Not Activated	-5.86838%*	P<0.001
NMDAR only Activated	Control Activated	18.07109%*	P<0.001
	Alix CTNT Activated	17.65998%*	P<0.001
	NMDA+ Alix CTNT Activated	10.25859%*	P<0.001
	Control Not Activated	17.98095%*	P<0.001
	Alix CTNT Not Activated	17.47326%*	P<0.001
	NMDAR only Not Activated	18.71470%*	P<0.001
	NMDA+ Alix CTNT Not Activated	11.79159%*	P<0.001
NMDA+ Alix CTNT Activated	Control Activated	7.81250%*	P<0.001
	Alix CTNT Activated	7.40139%*	P<0.001
	NMDAR only Activated	-10.25859%*	P<0.001
	Control Not Activated	7.72236%*	P<0.001
	Alix CTNT Not Activated	7.21467%*	P<0.001
	NMDAR only Not Activated	8.45611%*	P<0.001
Control Not Activated	NMDAR only Activated	-17.98095%*	P<0.001
	NMDA+ Alix CTNT Activated	-7.72236%*	P<0.001
	NMDA+ Alix CTNT Not	-6.18935%*	P<0.001

	Activated		
Alix CTNT Not Activated	NMDAR only Activated	-17.47326%*	P<0.001
	NMDA+ Alix CTNT Activated	-7.21467%*	P<0.001
	NMDA+ Alix CTNT Not Activated	-5.68166%*	P = 0.001
NMDAR only Not Activated	NMDAR only Activated	-18.71470%*	P<0.001
	NMDA+ Alix CTNT Activated	-8.45611%*	P<0.001
	NMDA+ Alix CTNT Not Activated	-6.92311%*	P<0.001
NMDA+ Alix CTNT Not Activated	Control Activated	6.27950%*	P<0.001
	Alix CTNT Activated	5.86838%*	P<0.001
	NMDAR only Activated	-11.79159%*	P<0.001
	Control Not Activated	6.18935%*	P<0.001
	Alix CTNT Not Activated	5.68166%*	P = 0.001
	NMDAR only Not Activated	6.92311%*	P<0.001

Table 3.10 c: Anova Analysis of table of statistically significant NMDA cell death by Alix CTNT. All data points correspond to the mean difference of values and statistical significance of cell death between groups. Anova analysis was performed using Tukey post-hoc analysis to determine which groups were statistically different from each other. The values marked with * denotes that it is statistically significant at the level 0.05.

The negative control culture transfected without any DNA and maintained in PSS only had a mean of 10.1 ± 0.4% cell death at 6 hours (Figure 3.10 b). The negative control without any DNA that was activated with PSS with NMDA (1 mM) and glycine (50 µM) had a mean of 10.0 ± 0.1% cell death at 6 hours (Figure 3.10 a). Paired t-test and ANOVA

analysis shows that the difference between the negative control activated and not activated is considered to be not statistically significant.

In cultures that were transfected with mouse Alix NT + CT subunits alone and maintained in PSS, cell death at 6 hours was 10.6 ± 0.9% (Figure 3.10 b). In cultures that were transfected with mouse Alix NT + CT subunit alone activated in PSS with NMDA (1 mM) and glycine (50 µM) had a mean of 10.4 ± 0.6% cell death at 6 hours (Figure 3.10 a). Paired t-test and ANOVA analysis shows that the difference between mouse Alix NT + CT alone activated and not activated is considered to be not statistically significant. There was also no statistical significance between cell death observed in cells expressing mouse Alix NT + CT and the negative control (without DNA) regardless if they were activated or not.

The positive control culture transfected with GluN1/GluN2A subunits and maintained in PSS only had a mean of 9.4 ± 0.9% cell death at 6 hours (Figure 3.10 b). Whereas, the positive control GluN1/GluN2A subunits that was activated with PSS with NMDA (1 mM) and glycine (50 µM) had a mean of 28.1 ± 0.7% cell death at 6 hours (Figure 3.10 a). Treatment with NMDA and glycine significantly enhanced cell death. Paired t-test shows that the difference between the positive control activated and not activated is considered to be extremely statistically significant with a P value of less than 0.0001 which correlates with the ANOVA analysis significance value of $P<0.001$ (Table 3.10c).

The culture transfected with mouse Alix NT + CT, GluN1/GluN2A subunits and activated with PSS and NMDA with glycine had a mean of 17.8 ± 1.1% cell death at 6 hours (Figure 3.10 a). Paired t-test shows that the difference between the positive control activated and mouse Alix NT + CT, GluN1, GluN2A activated is considered to be

statistically significant with a P value of 0.0163 which correlates with the ANOVA analysis significance value of P<0.001 (Table 3.10c).

Cells expressing mouse Alix NT + CT transfected with GluN1/GluN2A subunits and not activated (PSS alone) also yielded a mean cell death of 16.3 ± 0.4% cell death at 6 hours (Figure 3.10 b). It is a higher percentage of cell death compared to GluN1/GluN2A subunits that were not activated. Paired t-test shows that the difference between the positive control not activated and cells expressing AlixNT + CT, GluN1, GluN2A not activated is considered to be very statistically significant with a P value of 0.0079 which also correlates with the ANOVA analysis significance value of P<0.001 (Table 3.10c). There was however no statistical significance in cell death between activated and non-activated cells expressing mouse Alix NT + CT, GluN1, GluN2A (P value of 0.3681) in both the T-test and ANOVA analysis. Therefore the results of the Alix NT +Alix CT coexpressed show similar results to the effects seen with Alix CT transfected alone.

3.3 Summary

We speculate that Alix may affect NMDAR triggered cell, where transfecting Alix with GluN1/GluN2A and activation with NMDA/glycine significantly reduces the percentage of dead cells compared with the activated positive control (Figure 3.1). However in the absence of NMDAR activation, Alix + NMDAR expressing cells displayed a significantly higher level of cell death compared to other non activated (PSS only) controls. We tried to validate our findings by doing a number of control experiments such as repeating the cell death assay with Alix and GluN1 or Alix with GluN2A alone. Here we found that there was no significant cell death compared to the negative control (Figure 3.2). This also acted as a control for any cell death specific effects which may be caused by different cDNA plasmid vectors. We also repeated the NMDA cell death assay with AP5 to block NMDA triggered calcium influx to see if Alix increased cell death requires NMDAR activation (Figure 3.3) and found that we abolish the high percentage of cell death caused by Alix and NMDAR. We then tried to modulate the concentration of NMDA (10 µM, 100 µM, 300 µM and 700 µM) in the PSS buffer in activated assay to see if this affected the cell death caused by Alix (Figure 3.4). We observed that by gradually increasing the NMDA concentration, we also increased cell death caused by activation of NMDARs. However, the addition of Alix in cells expressing NMDARs seems to cause a high amount of cell death even at a low concentration of NMDA (10 µM) (Figure 3.4grey circles) compared to the cell death seen with NMDAR alone at 10 µM NMDA(Figure 3.4 black squares). This suggests that low concentrations of glutamate and glycine in the cell media could cause a high level of cell death when we express Alix with NMDAR and be responsible for the higher levels of cell death seen in the non activated (PSS only) cell death assay. The NMDA EC50s calculated from the partial dose-response curves also supported this observation. We found that all of the Alix mouse variants used (Figure 3.6,

3.7, 3.8 and 3.9), generally showed a similar pattern of cell death, where Alix with NMDAR transfection significantly reduces the toxicity associated with NMDA receptor stimulation when activated, but seems to enhance cell death when not activated, as seen by the human Alix variant (Figure 3.1) except the Alix NT variant (Figure 3.8). This finding is quite interesting as it pinpoints the cause of the increased cell death in the absence of activation when Alix is expressed with NMDAR to the C terminal region of the protein.

4. Investigating the protein expression of recombinant Alix and GluN1 in cotransfected HEK293 cells and brain lysates/neuronal fractions:

4.1 Introduction:

In the previous chapter our data indicated that recombinant human Alix transfected together with GluN1/GluN2A NMDAR subunits influences NMDAR cell death. From Figure 3.1 a, transfecting Alix with GluN1/GluN2A significantly reduced the percentage of dead cells compared with cells expressing GluN1/GluN2A subunits and activated with NMDA. These data indicate that recombinant Alix, GluN1/GluN2A transfection significantly reduced the toxicity associated with NMDA receptor activation compared to GluN1/GluN2A only cells but enhanced the basal level of cell death when not activated by NMDA. However, the level of cell death in the presence of Alix was similar in activated (NMDA+glycine) or non activated (PSS only) conditions.

In this chapter we examined the specificity of antibodies raised against Alix and GluN1 on recombinant protein expressed in HEK293 cells and once we confirmed their specificity examined the protein expression of endogenous Alix and GluN1 in rat brain lysates and neuronal fractions. We also observed if there was any correlation between the modulation of NMDAR activity by Alix in the cell death assay and protein expression levels of Alix and GluN1 subunits. The protein expression of Alix and GluN1 was evaluated by transient transfection of HEK 293 cells with Alix and GluN1/ GluN2A subunit cDNAs in different combinations following Table 3.1 a, b and then lysed for protein extraction and western blotting.

We also substantiated the presence of Alix expression in the brain which we alluded to in the introduction. This was done by detection of Alix in whole rat adult and embryo brain lysates and subcellular neuronal fractions such as synaptosomes, light membrane and mitochondria.

4.2 Western Blotting Analysis Alix Modification of NMDA

Full length expression of Alix (96kDa) was confirmed using a mouse anti-Alix antibody in both the Alix alone and Alix and GluN1/GluN2A subunit cotransfections in both activated and non activated HEK293 cells (Figure 4.1a and b). The protein bands showed little degradation and no signal was detected in cell lysates from the lipofectamine only negative control. Both lipofectamine only controls maintained in PSS only or activated with NMDA (1 mM) and glycine (50 µM) had a mean protein expression of 0.08 ± 0.05 or 0.09 ± 0.03 respectively. In cultures that were transfected with Alix cDNA and EGFP only and maintained in PSS, Alix protein expression was significantly higher (2.39 ± 0.88)(Figure 4.1b). In cultures that were transfected with EGFP-Alix cDNA only and activated in PSS with NMDA (1 mM) and glycine (50 µM) had a mean protein expression of 3.77 ± 0.55 (Figure 4.1a). Paired T test showed that the difference between activated and not activated Alix only was statistically insignificant with a P value of 0.40.

The cultures transfected with Alix, GluN1/GluN2A subunits and activated with PSS and NMDA with glycine had a mean protein expression of 0.99 ± 0.23 (Figure 4.1a). Non activated cells transfected with Alix and GluN1/GluN2A subunits yielded a mean protein expression of 0.84 ± 0.18 (Figure 4.1b). The results indicate that there is little difference between the protein expression of Alix in activated and non-activated cells expressing Alix, GluN1, GluN2A. Paired T test was found to be not statistically significant with a P value of 0.61.

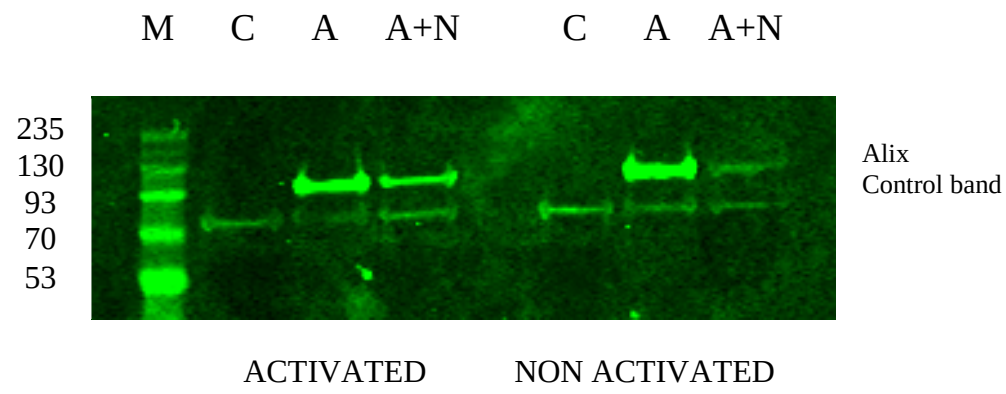

Figure 4.1: Protein expression of Alix protein in Alix/NMDAR cotransfected cells. BLUE wide range prestained protein ladder was used and an additional nonspecific band was detected by the Alix antibody at approximately 80 kD. This was used as an internal loading control and used to normalise expression levels within each lane. Additional controls include HEK293 cells transfected without cDNA, Alix only cells were transfected with 1 µg Alix and 2 µg EGFP and Alix +NMDARs cells were transfected with 1 µg Alix, 1 µg GluN1 and 1 µg GluN2A subunits (as Chapter 3.2.1). Lanes: M, protein marker lane (kD), C, control, A, Alix only, A+N, Alix + NMDARs,.

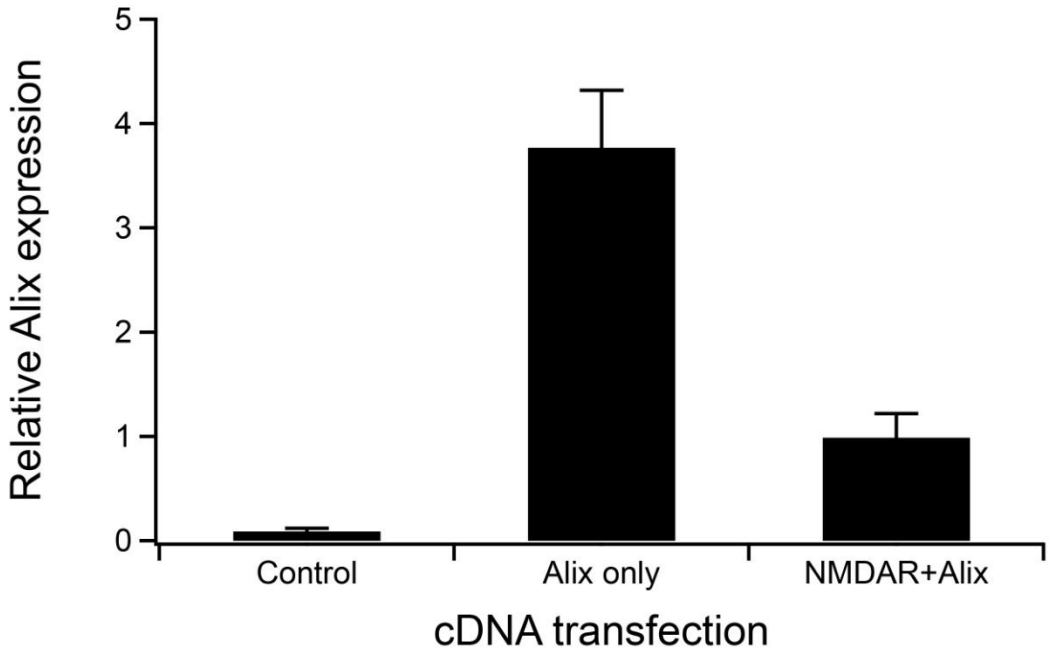

Figure 4.1a: Normalised activated Alix protein expression following transient transfection, protein extraction and western blotting (n = 4). Protein expression was normalised to the levels of the control protein band detected by the Alix antibody.

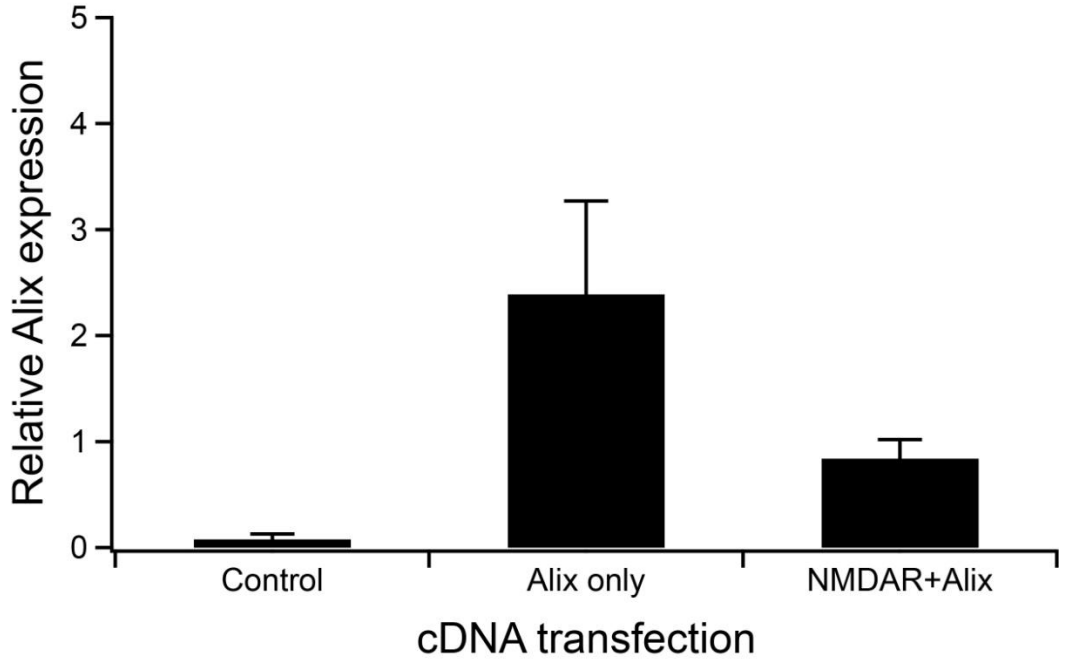

Figure 4.1b: Normalised not activated Alix protein expression following transient transfection, protein extraction and western blotting (n = 4). Protein expression was normalised to the levels of the control protein band detected by the Alix antibody.

Figure 4.1 a	**Transfection**	**Normalised expression ± SEM**
Lane 1	**Lipofectamine only**	**0.09 ± 0.03**
Lane 2	**Alix/EGFP only**	**3.77 ± 0.55**
Lane 3	**GluN1/GluN2A/Alix**	**0.99 ± 0.23**
Figure 4.1 b	**Transfection**	**Normalised expression ± SEM**
Lane 1	**Lipofectamine only**	**0.08 ± 0.05**
Lane 2	**Alix/EGFP only**	**2.39 ± 0.88**
Lane 3	**GluN1/GluN2A/Alix**	**0.84 ± 0.18**

Table 4.1: Normalised Alix expression levels from Figures 4.1 a and b with all data points corresponding to the mean normalised expression ± SEM.

4.3 Western Blotting Analysis of GluN1 subunit expression in Alix cotransfected cells

Full length expression of GluN1 (108kDa) was confirmed using a mouse anti-NMDAR1 antibody in both the NMDAR only and Alix and GluN1/GluN2A subunit in both activated and non activated HEK293 cells (Figures 4.2a and b). The bands showed little degradation and no GluN1 signal was detected in the negative control that was transfected with only lipofectamine.

Both lipofectamine only controls in the presence of PSS or NMDA (1 mM) and glycine (50 μM) had mean expression of 0.06 ± 0.05 or 0.15 ± 0.08 respectively (Figure 4.2 b and a respectively). In cultures that were transfected with GluN1/GluN2A only and maintained in PSS, GluN1 protein expression was 1.46 ± 0.64 (Figure 4.2 b). In cultures that were transfected with GluN1/GluN2A only and activated in PSS with NMDA (1 mM) and glycine (50 μM) had a mean protein expression of 1.33 ± 0.75 (Figure 4.2 a). This indicates that treatment with NMDA and glycine does not affect GluN1 expression levels and this was supported by a paired T test with a P value of 0.90 for both activated and non activated GluN1/GluN2A only cultures.

In cultures transfected with Alix, GluN1/GluN2A subunits and activated with PSS and NMDA with glycine had a mean GluN1 protein expression of 1.74 ± 0.42 (Figure 4.2 a). Non activated cells transfected with Alix and GluN1/GluN2A subunits yielded a mean expression of 0.87 ± 0.38 (Figure 4.2 b). We found that the difference between activated and not activated protein expression was not considered statistically significant with a P value of 0.38 from the paired T-test.

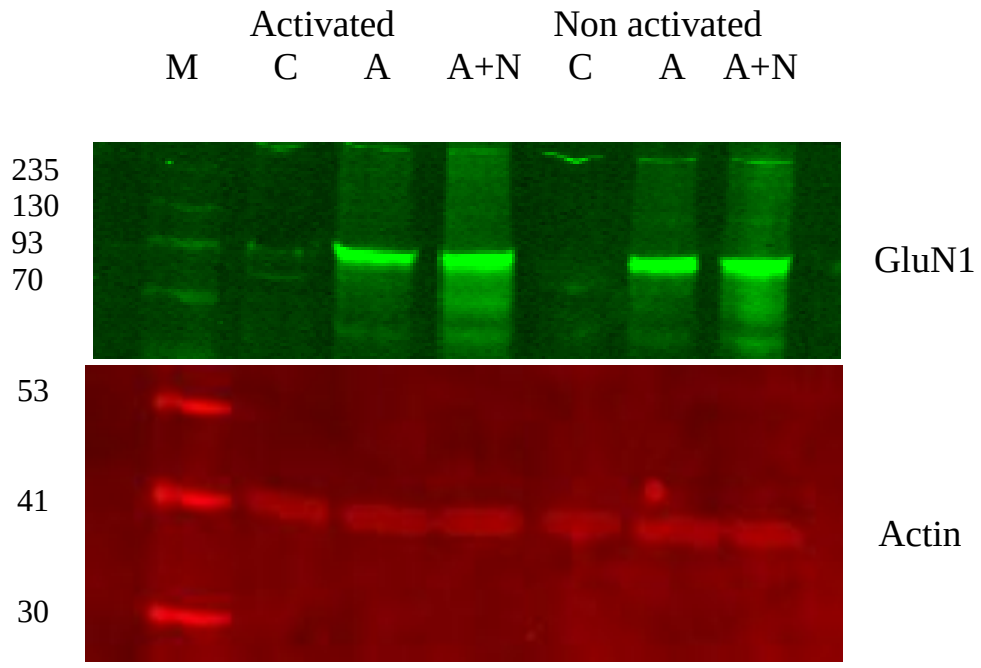

Figure 4.2: Western Analysis of GluN1 expression when cotransfected with Alix. BLUE wide range prestained protein ladder was used and actin was used as the loading control. Controls are HEK293 culture transfected without any DNA, NMDAR only are HEK293 culture transfected with 1 µg GluN1, 1 µg GluN2A and 1 µg EGFP subunits and Alix +NMDARs are HEK293 culture transfected with 1 µg Alix, 1 µg GluN1 and 1 µg GluN2A subunits (as Chapter 3.2.1). Lanes: M, protein marker lane (kD), C, control, A, Alix only, A+N, Alix + NMDARs.

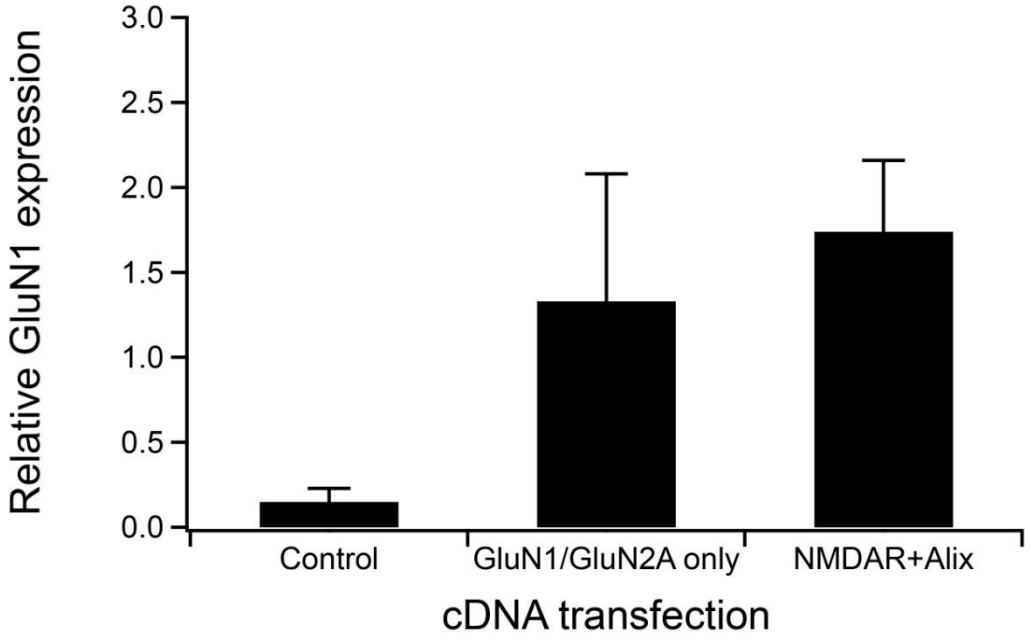

Figure 4.2a: Normalised protein expression of activated GluN1 following transient transfection, protein extraction and western blotting (n = 3). GluN1 expressed was normalised to the actin loading control.

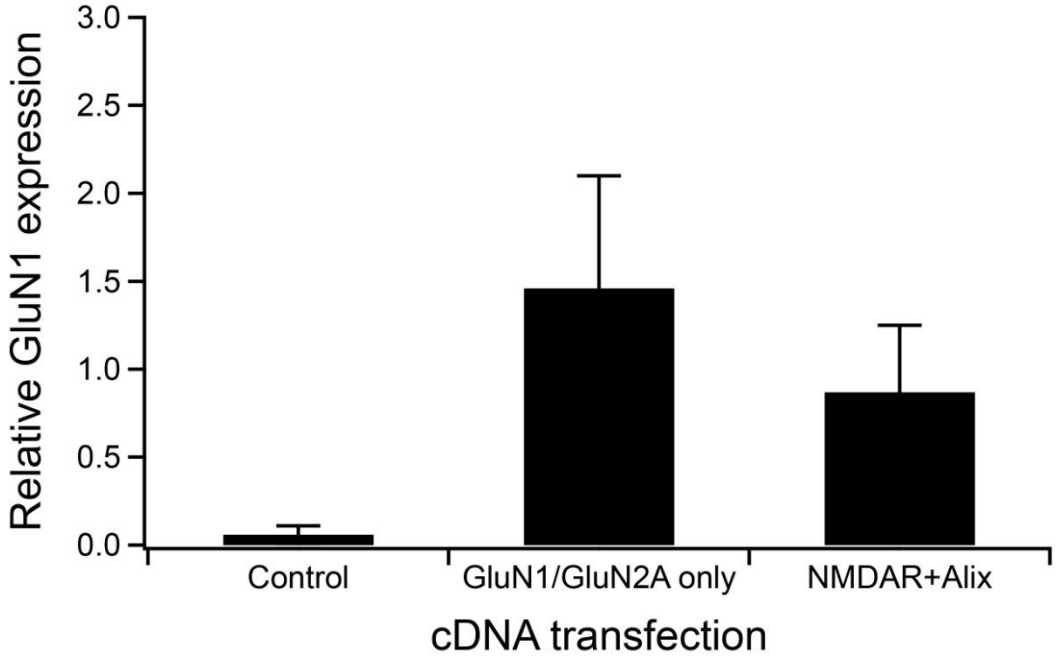

Figure 4.2b: Normalised protein expression of non activated GluN1 following transient transfection, protein extraction and western blotting (n = 3). GluN1 expressed was normalised to the actin loading control.

Graph 4.2 a	Transfection	Normalised expression ±SEM
Lane 1	Lipofectamine only	0.15 ± 0.08
Lane 2	GluN1/GluN2A only	1.33 ± 0.75
Lane 3	GluN1/GluN2A/Alix	1.74 ± 0.42
Graph 4.2 b	**Transfection**	**Normalised expression ±SEM**
Lane 1	Lipofectamine only	0.06 ± 0.05
Lane 2	GluN1/GluN2A only	1.46 ± 0.64
Lane 3	GluN1/GluN2A/Alix	0.87 ± 0.38

Table 4.2: Normalised protein levels of GluN1 from Figures 4.2a and b with all data points corresponding to the mean ± SEM.

4.4 Western Blotting Analysis of Alix in Neuronal Fraction

After checking the specificity of our Alix and GluN1 antibodies, we examined the expression of Alix in whole adult and embryo brain as well as neuronal fractions including synaptosomes, light membrane, myelin and mitochondria fractions. Unfortunately the myelin fraction which contains the insulating sheath that forms a layer around the axon of the neuron was too smeary to be able to detect a specific band. Full length expression of Alix (96kDa) was detected using a mouse anti-Alix antibody and the bands showed little degradation (Figure 4.3).

The whole brain from embryo had a mean protein expression of 0.15 ± 0.04. The expression of Alix in whole embryo brain seems comparatively quite low compared to the neuronal fractions. Whereas the whole adult brain had a slightly higher mean protein density of 0.29 ± 0.04. Synaptosome fractions showed the highest mean protein expression

of 1.52 ± 0.03. The mitochondria had a mean protein expression of 0.61 ± 0.11. The light membrane had a mean protein expression of 0.62 ± 0.13.

Paired T test was not statistically significant for embryo compared with whole adult, mitochondria and light membrane fractions with a P value of 0.22, 0.096 and 0.11 respectively. However, paired T test was very statistically significant for differences between whole adult brain extract and the synaptosome fraction with a P value of 0.0022 as well as between embryo extract and synaptosome fraction with a P value of 0.0019. These results indicate that although Alix is expressed at relatively low levels throughout the brain. Alix can be found at high levels within the synaptosome fraction and suggest that they are predominately localised to synaptic sites within the neuron. Why this is the case we are not sure, but it is possible for microvesicles released into the intercellular space with some protein markers of exosomes such as Alix that are transferred between cells (Guescini et al, 2010)

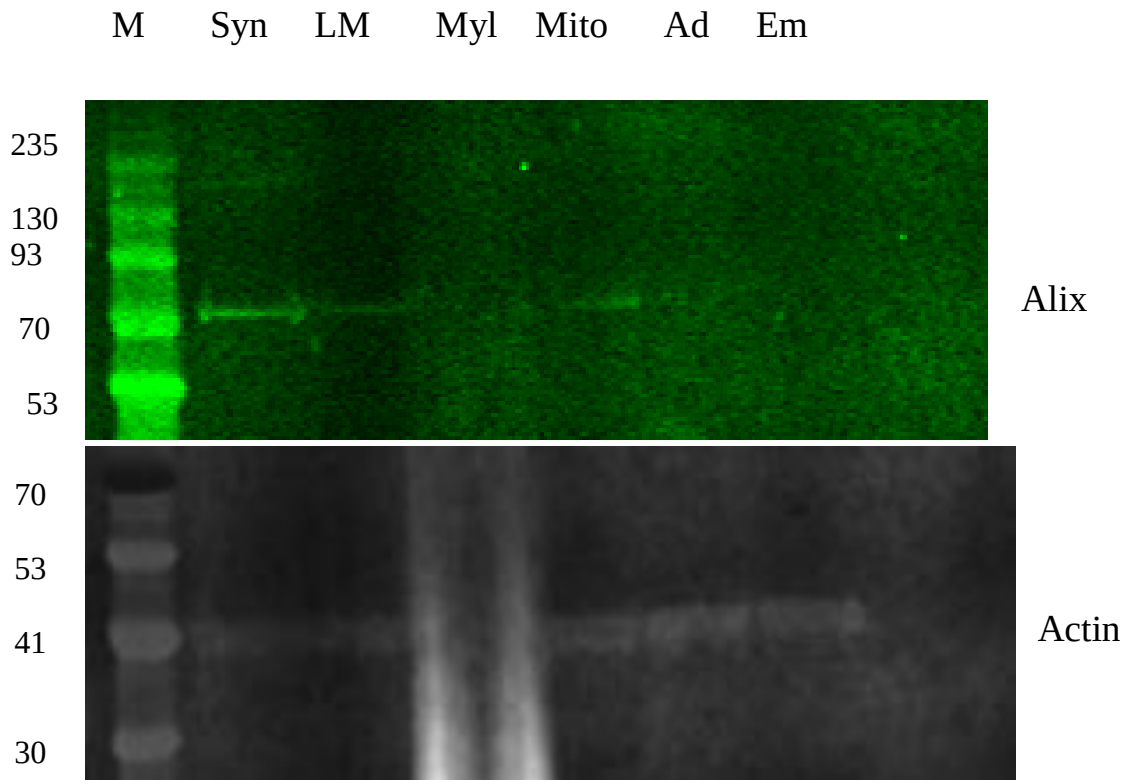

Figure 4.3: Protein expression of Alix detected in whole rat adult and embryo brain lysates and neuronal fractions such as synaptosome, light membrane and mitochondria. BLUE wide range prestained protein ladder was used and actin was used as the loading control. Lanes: M, Protein marker (kD), Syn, synaptosome extract, LM, Light membrane, Myl, myelin, Mito, mitochondria, Ad, adult whole brain, Em, embryo whole brain.

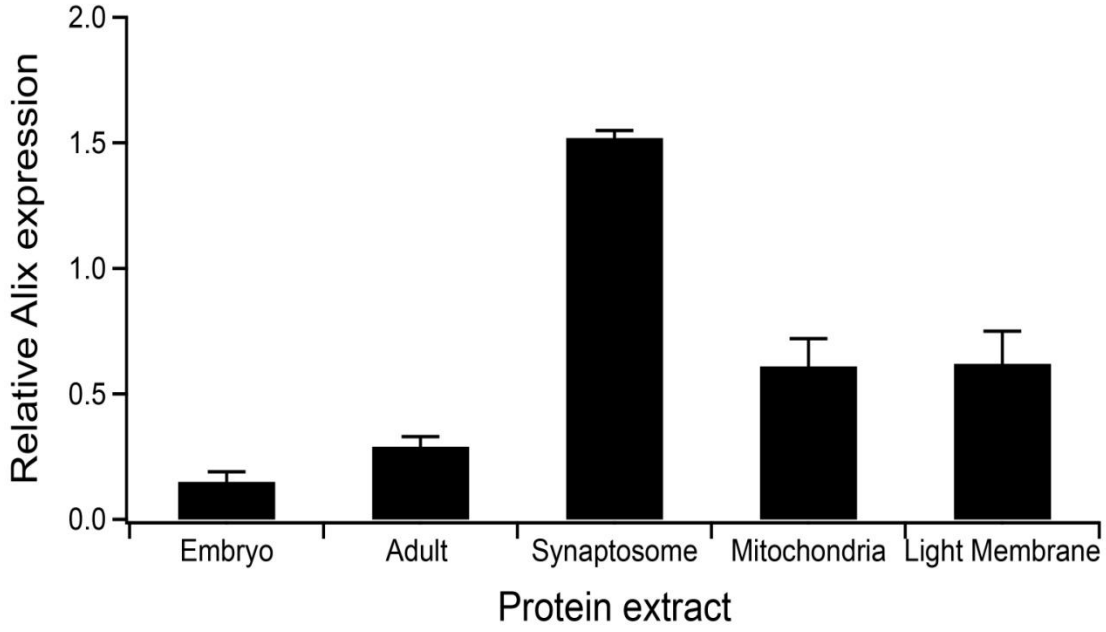

Figure 4.3a: Protein expression from n of 1 that was repeated 3 times against Alix from whole adult rat, embryo, synaptosome, light membrane and mitochondria. Protein levels were normalised using actin as a loading control.

Column	Protein sample	Normalised expression ± SEM
1	**Embryo**	**0.15 ± 0.04**
2	**Adult**	**0.29 ± 0.04**
3	**Synaptosome**	**1.52 ± 0.03**
4	**Mitochondria**	**0.61 ± 0.11**
5	**Light Membrane**	**0.62 ± 0.13**

Table 4.3: Protein expression of Alix from brain lysates and neuronal fractions in Figure 4.3a with all data points corresponding to the mean ± SEM.

4.5 Western Blotting Analysis of GluN1 in Neuronal Fraction

We also detected GluN1 protein expression in whole adult and embryo brain as well as synaptosome, light membrane, myelin and mitochondria fractions. Unfortunately like the Alix blot the Myelin fraction in the GluN1 blot was also too smeary to detect a distinct protein signal. Full length expression of GluN1 (108kDa) was detected using mouse anti-NMDAR1 antibody and the bands showed little degradation and actin was used as the loading control (Figure 4.4).

The whole brain from embryo had a mean protein expression of 0.53 ± 0.46. The whole adult brain had a slightly higher mean protein expression of 0.71 ± 0.62. Synaptosome fractions showed a mean protein expression of 1.38 ± 0.22. The mitochondria fraction showed the highest expression with a mean protein expression of 1.97 ± 0.28. The light membrane had a mean protein expression of 0.40 ± 0.15 (Figure 4.4). Paired T test was not statistically significant for embryo compared with whole adult, synaptosome and light membrane fractions with a P value of 0.22, 0.12 and 0.72 respectively. However, paired T test was statistically significant for differences between embryo extract and mitochondria fraction with a P value of 0.018. Conversely, paired T test was not statistically significant for whole adult compared with all the protein extract including embryo, synaptosome, mitochondria and light membrane fractions with a P value of 0.22, 0.29, 0.07 and 0.58 respectively. These results suggest that GluN1 is expressed at a higher level within the mitochondria fraction in the embryo.

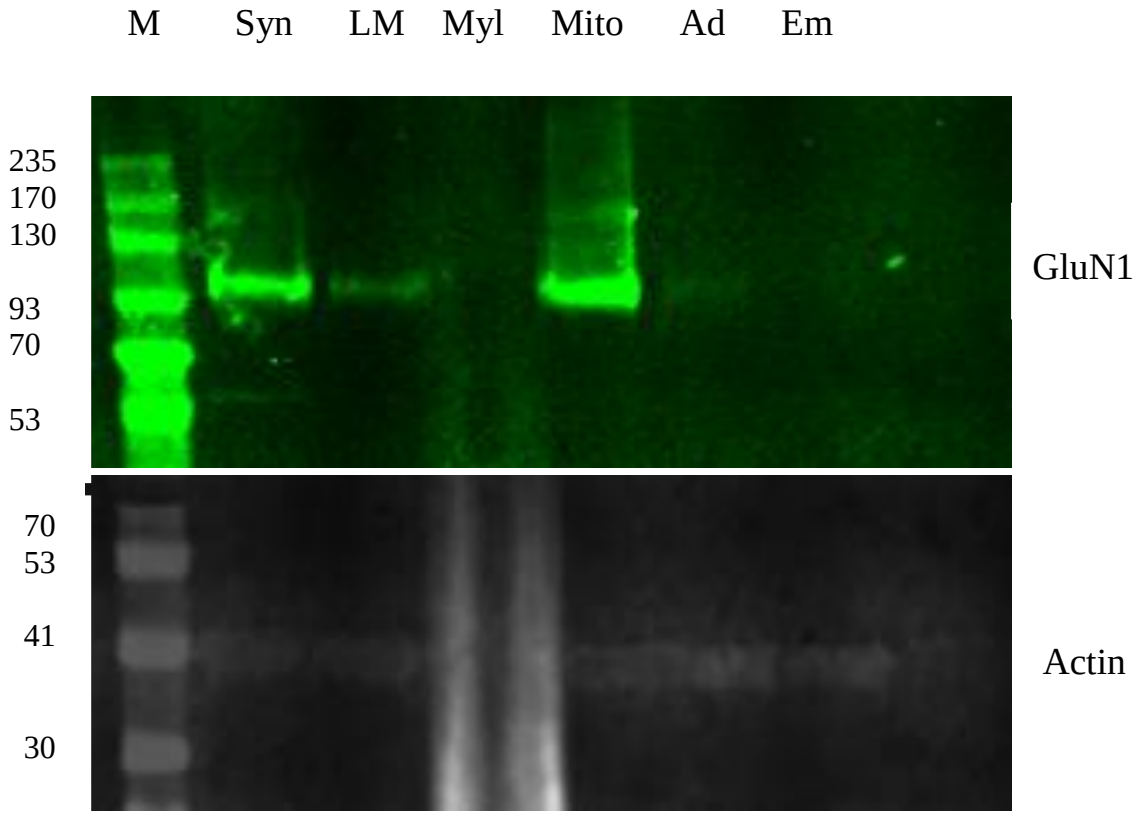

Figure 4.4: Protein expression of GluN1 in whole rat adult and embryo brain lysates and some of the neuronal fractions such as synaptosome, light membrane and mitochondria. BLUE wide range prestained protein ladder was used and Actin was used as the loading control. Lanes: Protein marker (kD), Syn, synaptosome extract, LM, Light membrane, Myl, myelin, Mito, mitochondria, Ad, adult whole brain, Em, embryo whole brain.

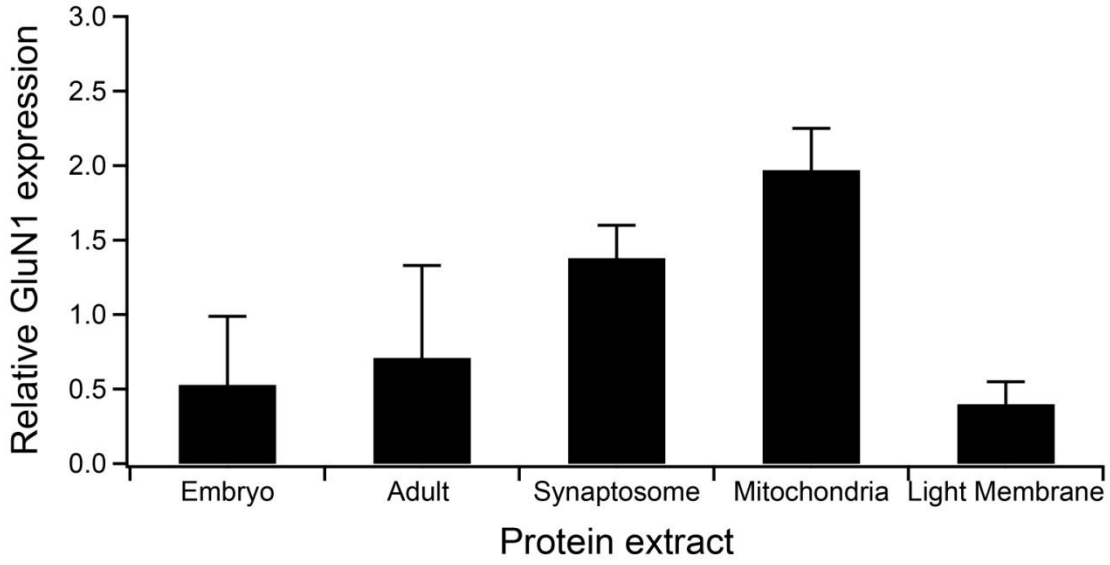

Figure 4.4a: Protein expression from n of 1 that was repeated 3 times against GluN1 from rat adult brain, embryo, synaptosome, light membrane and mitochondria. Protein levels were normalised to actin.

Column	Protein sample	Normalised expression ± SEM
1	**Embryo**	**0.53 ± 0.46**
2	**Adult**	**0.71 ± 0.62**
3	**Synaptosome**	**1.38 ± 0.22**
4	**Mitochondria**	**1.97 ± 0.28**
5	**Light Membrane**	**0.40 ± 0.15**

Table 4.4: Protein expression levels from Figure 4.4a with all data points corresponding to the mean ± SEM.

4.6 Summary

The analysis of Alix protein expression in NMDAR modification was performed and we established that both lipofectamine only controls maintained in PSS only or activated with NMDA (1 mM) and glycine (50 µM) had a mean protein expression of 0.08 ± 0.05 or 0.09 ± 0.03 respectively. Alix protein expression in Alix cDNA only and maintained in PSS was 2.39 ± 0.88 (Figure 4.1b) whereas Alix cDNA only and activated had a mean protein expression of 3.77 ± 0.55 (Figure 4.1a). Paired T test showed that the difference between activated and not activated for Alix only was statistically insignificant with a P value of 0.40. Alix and GluN1/GluN2A that was activated had a mean protein expression of 0.99 ± 0.23 (Figure 4.1a) while non activated of Alix and GluN1/GluN2A yielded a mean protein expression of 0.84 ± 0.18 (Figure 4.1b). Paired T test was found to be not statistically significant with a P value of 0.61 which indicate that there is little difference between both conditions.

We also analysed GluN1 subunit expression in Alix cotransfected cells. We established that lipofectamine only controls in the presence of PSS or NMDA (1 mM) and glycine (50 µM) had mean expression of 0.06 ± 0.05 or 0.15 ± 0.08 respectively (Figure 4.2 b and a respectively). Protein expression of GluN1/GluN2A only and maintained in PSS was 1.46 ± 0.64 (Figure 4.2 b) while protein expression of GluN1/GluN2A only and activated was 1.33 ± 0.75 (Figure 4.2 a). Paired T test was found to be not statistically significant with a P value of 0.90 for both activated and non activated GluN1/GluN2A only cultures. Protein expression of Alix, GluN1/GluN2A subunits and activated was 1.74 ± 0.42 (Figure 4.2 a) while protein expression of Alix and GluN1/GluN2A and maintained in PSS was 0.87 ± 0.38 (Figure 4.2 b). The difference was not considered statistically significant with a P value of 0.38 from the paired T-test.

We then examined the expression of Alix in whole adult and embryo brain as well as neuronal fractions including synaptosomes, light membrane, myelin and mitochondria fractions. We ascertained that the mean protein expression of whole embryo, whole adult, synaptosome, mitochondria and light membrane was each 0.15 ± 0.04, 0.29 ± 0.04, 1.52 ± 0.03, 0.61 ± 0.11 and 0.62 ± 0.13 respectively. Paired T test was not statistically significant for embryo compared with whole adult, mitochondria and light membrane fractions with a P value of 0.22, 0.096 and 0.11 respectively. However, paired T test was very statistically significant for differences between whole adult brain extract and the synaptosome fraction with a P value of 0.0022 as well as between embryo extract and synaptosome fraction with a P value of 0.0019. The results points to the fact that Alix might be expressed at higher level within the synaptosome fraction.

We also detected GluN1 protein expression in embryo brain, whole adult, synaptosome, mitochondria and light membrane fractions. Each had a mean protein expression of 0.53 ± 0.46, 0.71 ± 0.62, 1.38 ± 0.22, 1.97 ± 0.28 and 0.40 ± 0.15 respectively (Figure 4.4). Paired T test was not statistically significant for embryo compared with whole adult, synaptosome and light membrane fractions with a P value of 0.22, 0.12 and 0.72 respectively, however, paired T test was statistically significant for differences between embryo extract and mitochondria fraction with a P value of 0.018. Conversely, paired T test was not statistically significant for whole adult compared with all the protein extract including embryo, synaptosome, mitochodria and light membrane fractions with a P value of 0.22, 0.29, 0.07 and 0.58 respectively. These results suggest that GluN1 is expressed at relatively low levels throughout the whole brain extracts but is expressed at a higher level within the mitochondria fraction in the embryo. Relatively high levels of GluN1 (compared to whole brain extracts) where detected but the differences were not shown to be statistically significant.

5. Investigating Alix localization in cotransfected HEK293 cells:

5.1 Introduction:

Fluorescence microscopy is a powerful tool because in its simplest application, fluorescence can be used to mark the presence or location of proteins (Giepmans et al., 2006). For instance, a fluorescently-labelled protein can be localized to sub-cellular compartments, such as the dendrites or axons of neurons, or intracellular compartments, such as the endoplasmic reticulum or nucleus (Taraska and Zagotta, 2010). If two proteins interact in a complex, they both should be localized to the same region of a cell for example when two differently labelled proteins overlap, then the proteins are likely in the same subcellular neighbourhood (Patel et al., 2007).

In the previous chapter, Western blot analysis displayed the presence of Alix protein in both transiently transfected HEK293 cells as well as in crude protein extracts from rat embryo and adult brain. Our Western blot analysis indicated that lower concentrations of protein were detected when recombinant human Alix was transfected in HEK293 cells together with GluN1/GluN2A NMDAR subunits than in cells expressing Alix alone in both activated and non activated cells (Figure 4.1). Whereas, these changes were not observed for GluN1 expression under similar conditions (Figure 4.2).

In this chapter, we investigated firstly the cellular localisation of fluorescently labelled Alix in transfected HEK293 cells using fluorescent microscopy and immunocytochemistry.

5.2 Localisation of Alix in HEK293 cells

To determine the localisation of Alix in the HEK293 cells we transfected the cells following the protocol previously described in chapter 2.2.5, fixed and stained the cells with the appropriate antibodies or markers (chapter 3.2.1) before visualization under fluorescent microscopy. This will allow us to identify the presence of fluorescently labelled Alix and examine its cellular distribution and whether NMDAR activation induces any change in Alix cellular localisation.

5.2.1 Expression of Alix within the cytoplasm

Alix expression was examined in the presence of Hoechst dye, which is known to specifically stain for the nucleus by binding to DNA in live or fixed cells (Bonde et al., 2002). Alix expression was detected by GFP fluorescence was detected as a blue signal from the Hoechst dye (Figures 5.1 and 5.3).

Fluorescence images of Alix in HEK293 cells (Figures 5.1 and 5.3) revealed overall heterogeneous fluorescence within the cytoplasm and as expected Hoechst stained mainly in the nuclei. From the images there was little overlap between Alix and Hoechst signals. However, to confirm this we performed a Colocalization Scatter Plot (Figures 5.2 and 5.4). In the Scatter plot, pure blue and pure green pixels are coloured as such to correspond to Hoechst and Alix respectively. The degree of colocalization is determined by dispersion of the pixels in the plot, where the pixels tend to cluster more towards the axes of the plot in poorly colocalized staining. Whereas, if colocalized pixels are present, they appear as purple pixels and cluster towards the middle of the plot depending on the degree of colocalization (Sedarat et al., 2004). Colour scatter plots of Alix and Hoechst in HEK293 cells revealed a mostly uncorrelated plot that is more clustered towards the x and y-axes and further proven by a low Pearson's correlation value below 0.100 (n=3).

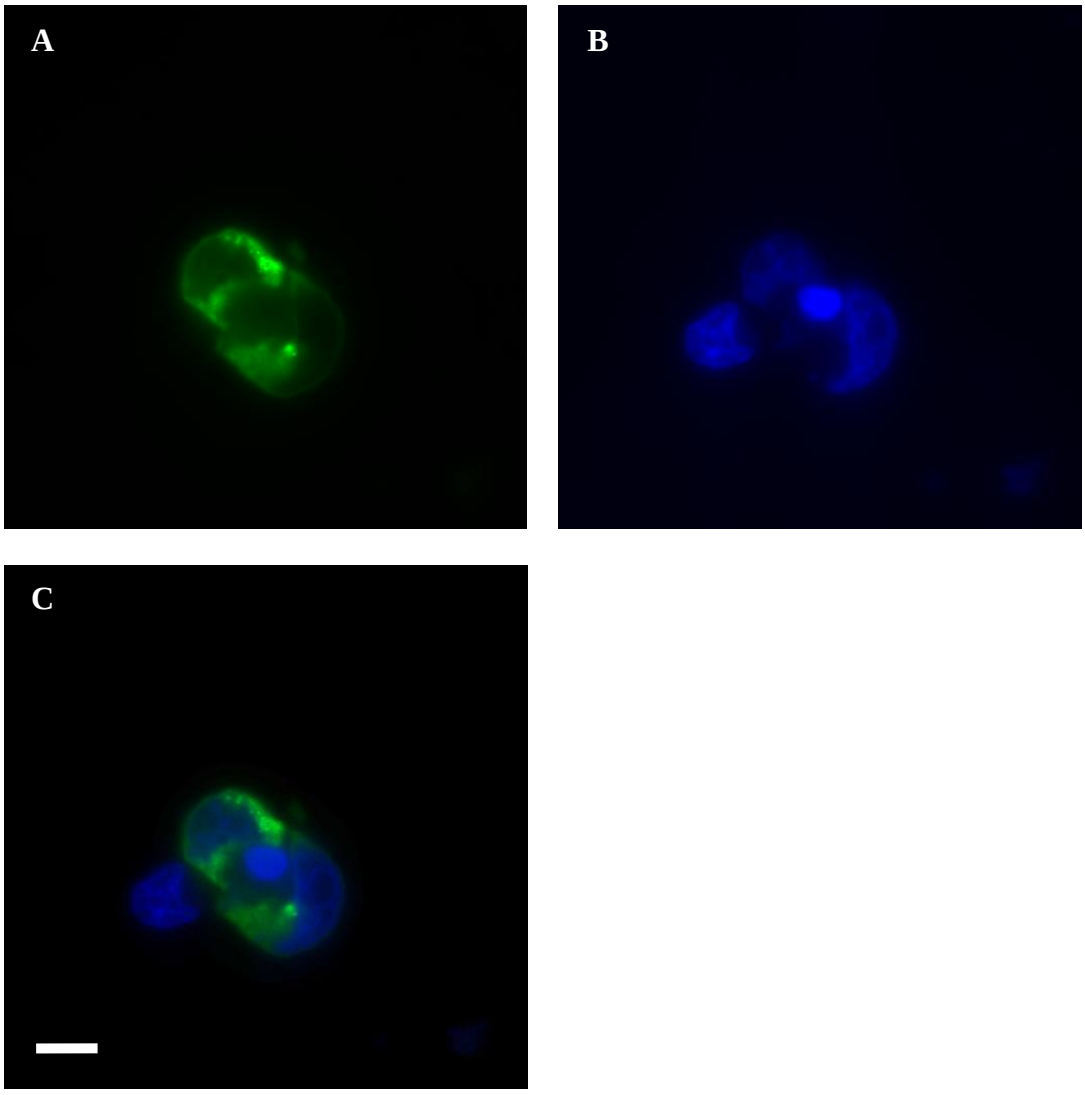

Figure 5.1 Intracellular distribution of Alix in three HEK293 cells transiently transfected with EGFP tagged Alix, following fixation and permeabilisation and treatment with Hoechst. Green fluorescence denotes Alix expression while blue corresponds to Hoechst stained nuclei. Fluorescence images of Alix transfected HEK293 cells (Panel A) reveal fluorescence within the cytoplasm of the cells but little expression within the nucleus. Panel B shows nuclear labelling with Hoescht and Panel C shows the merged image of Panel A and B. Scale Bar: 10 μm.

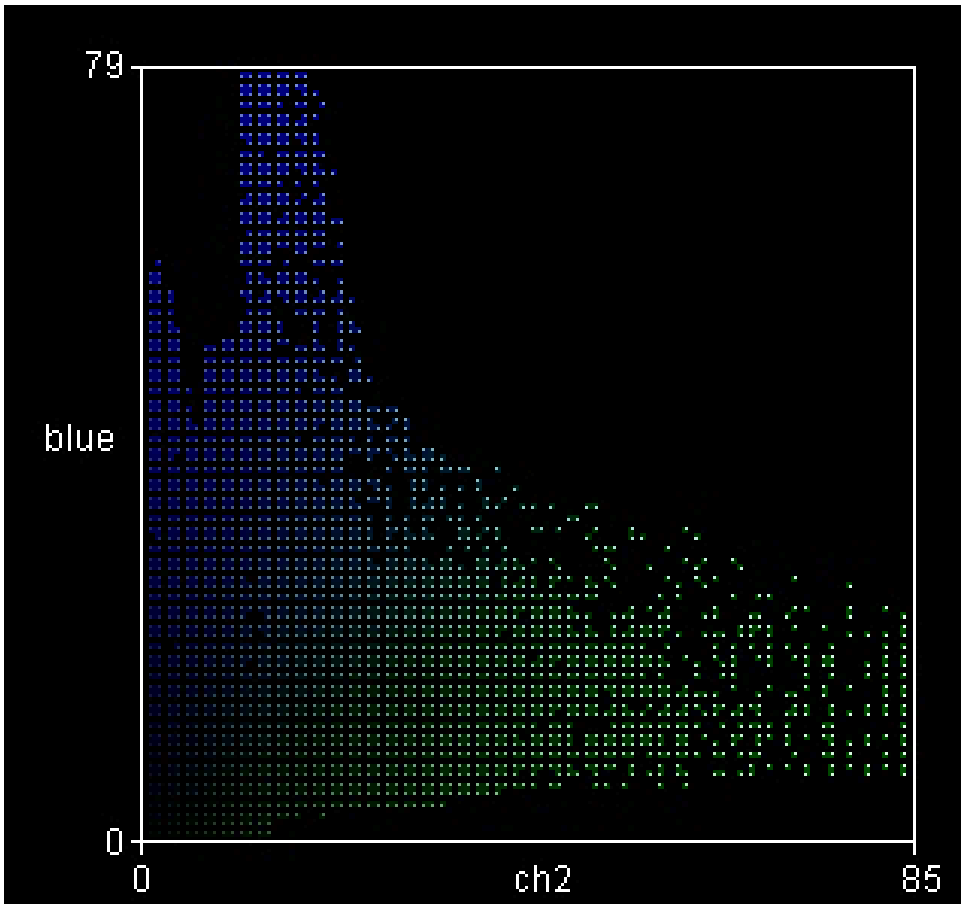

Figure 5.2 Colocalisation analysis from images shown in Figure 5.1. Green pixels denotes Alix expression while blue pixels corresponds to Hoechst. The Pearson's Correlation value that denotes the degree of overlap between the pixels within this image pair, calculated a minimal overlap of 0.097.

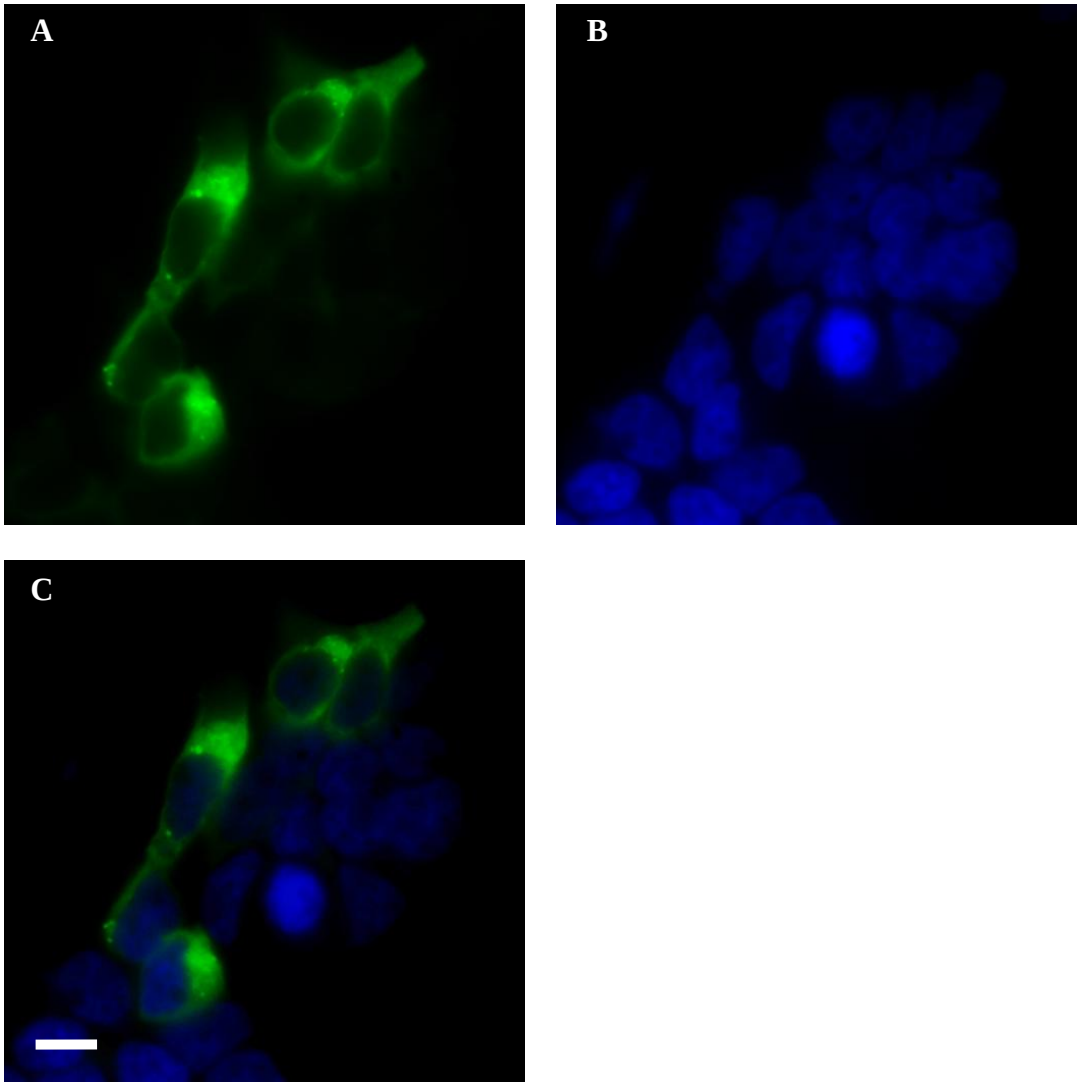

Figure 5.3 Intracellular distribution of Alix in a larger cluster of HEK293 cells transiently transfected with EGFP tagged Alix, following fixation and permeabilisation and treatment with Hoechst. Green fluorescence denotes Alix expression while blue corresponds to Hoechst stained nuclei. Fluorescence images of Alix transfected HEK293 cells (Panel A) reveal fluorescence within the cytoplasm of the cells but little expression within the nucleus. Panel B shows nuclear labelling with Hoescht and Panel C shows the merged image of Panel A and B. Scale Bar: 10 μm.

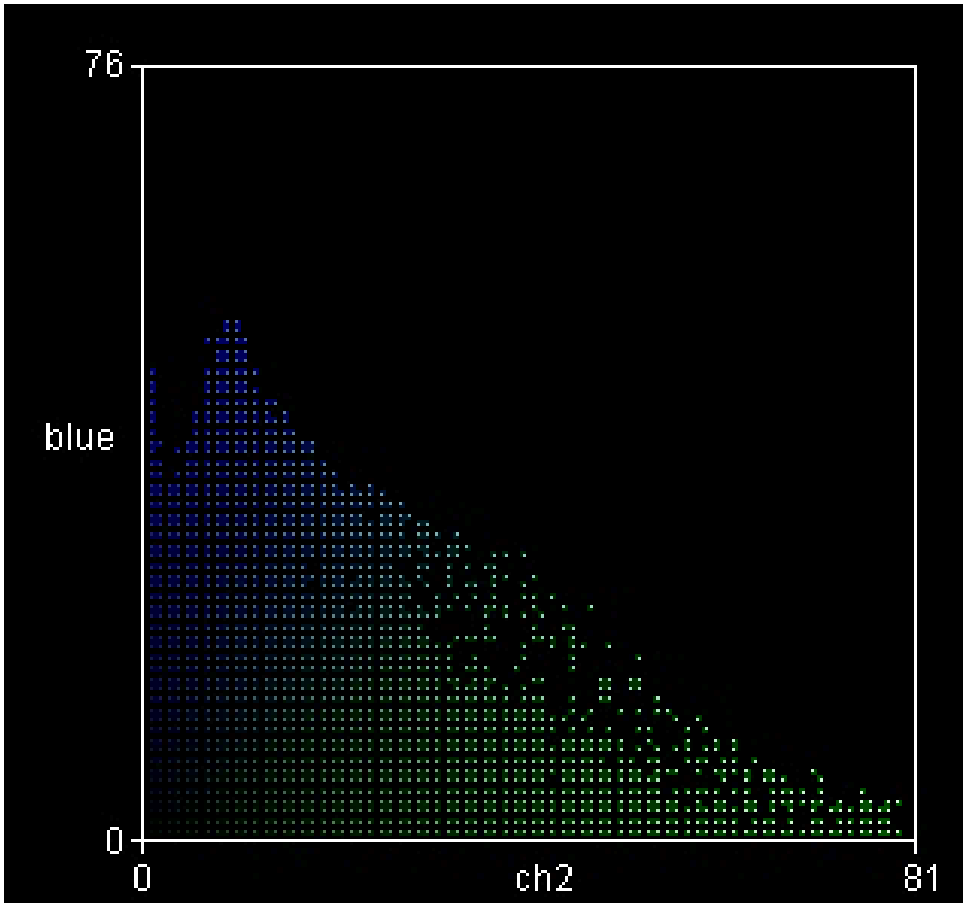

Figure 5.4 Colocalisation analysis from images shown in Figure 5.3. Green pixels denotes Alix expression while blue pixels corresponds to Hoechst signals. The Pearson's Correlation value that denotes the degree of overlap between pixels within this image pair, calculated a minimal overlap of -0.217.

5.2.2 Alix distribution and cellular endosome marker localisation

There is evidence that Alix has plays some involvement in ESCRT (endosomal sorting complex required for transport) (Trioulier et al., 2004; Ohkouchi et al., 2004) and given the Alix staining observed in Figure 5.1 and 5.3, we wanted to observe if there was any correlation between Alix expression and the endosome marker EEA1. We transiently transfected Alix, fixed and permeabilised the transfected cells and treated with primary antibodies against EEA1 and stained with Hoechst (Figure 5.5 and 5.7).

As before, fluorescence images of Alix revealed green fluorescence within the cytoplasm of the cells and as expected Hoechst stained mainly the nuclei. Staining with EEA1 revealed a punctate pattern consistent with cytoplasmic distribution within endosomes (Wilson et al., 2000). From the images there was little overlap between Alix and EEA1 signals. However, to confirm this we performed a Colocalization Scatter Plot (Figures 5.6 and 5.8). In the Scatter plot, pure red and pure green are coloured as such to correspond to EEA1 and Alix respectively. The degree of colocalization is determined by dispersion of the pixels in the plot. The colour Scatter plot of Alix and EEA1 in HEK293 cells revealed more variable correlation plots (Figures 5.6 and 5.8) with varying degrees of scatter pattern spread all over within the correlation plots. The mean Pearson's Correlation value of 0.252 (n =3) indicates that the correlation between both Alix and EEA1 expression patterns is weak.

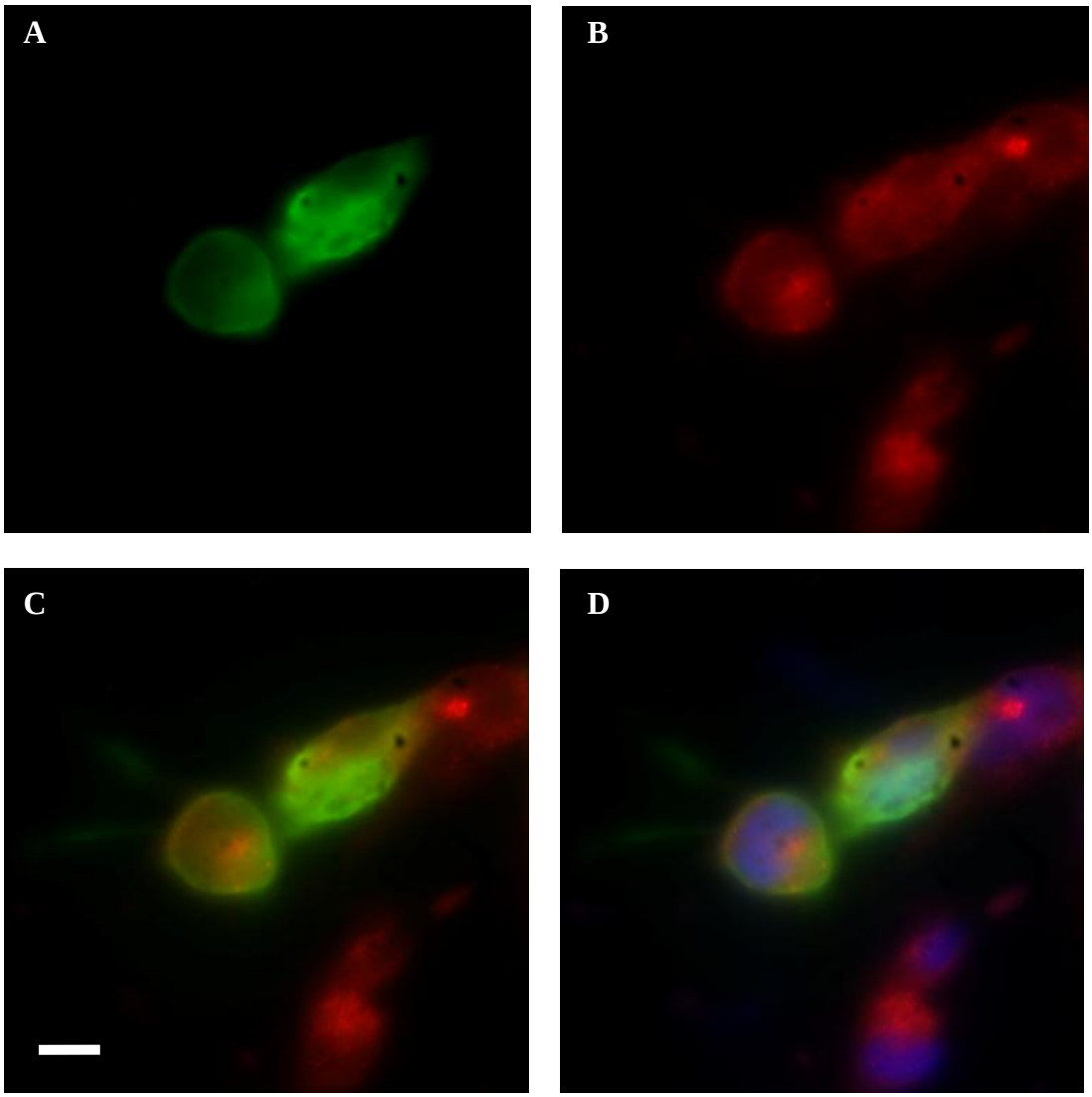

Figure 5.5 Intracellular distribution of Alix in a group of isolated HEK293 cells transiently transfected with EGFP tagged Alix, following fixation and permeabilisation, exposure to primary antibodies against EEA1 and treatment with Hoechst. Green fluorescence images of Alix transfected HEK293 cells (Panel A) reveal expression within the cell cytoplasm. Expression of EEA1 (Panel B) reveals a punctuate staining pattern consistent with cytoplasmic distribution of endosomes. Panel C shows nuclear labelling with Hoescht and Panel D shows the merged image of Panel A, B and C. Green expression denotes Alix fluorescence, red as EEA1 and blue corresponds to Hoechst stained nuclei. Scale Bar: 10 μM.

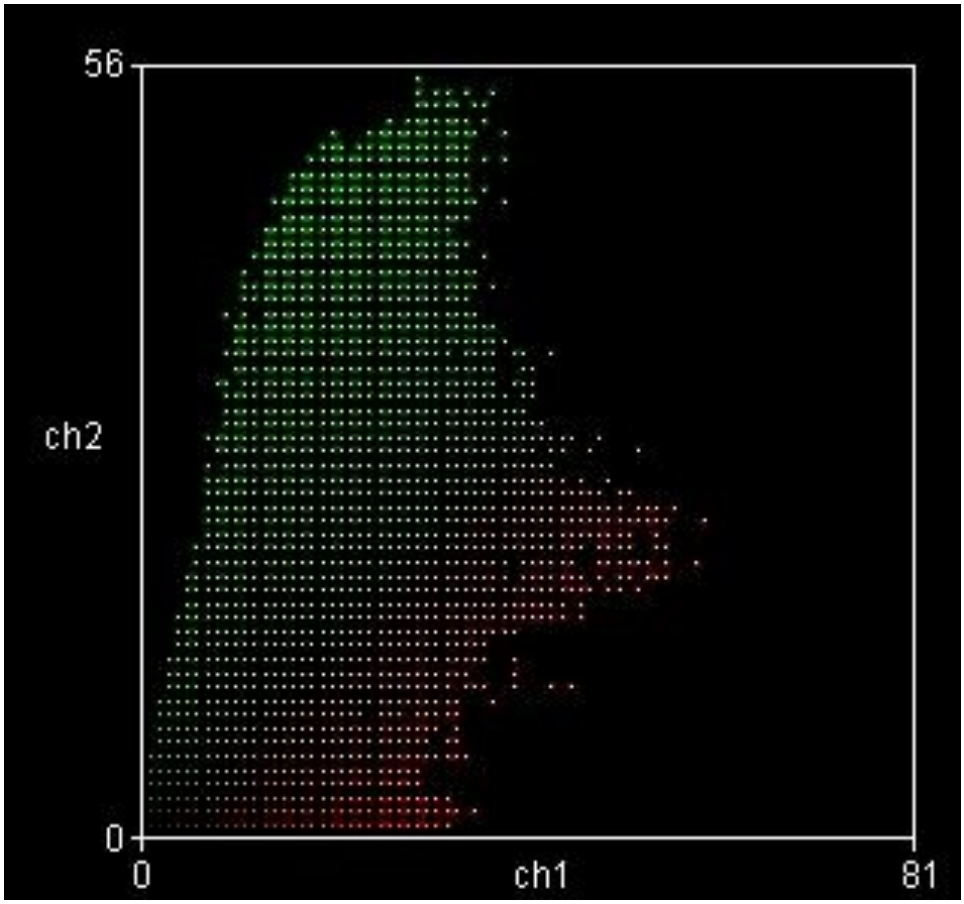

Figure 5.6 Colocalisation analysis from images shown in Figure 5.5. Green pixels denotes Alix, while red pixels corresponds to EEA1. The Pearson's Correlation value that denotes the degree of overlap between the pixels within this image pair, calculated a minimal overlap of 0.487.

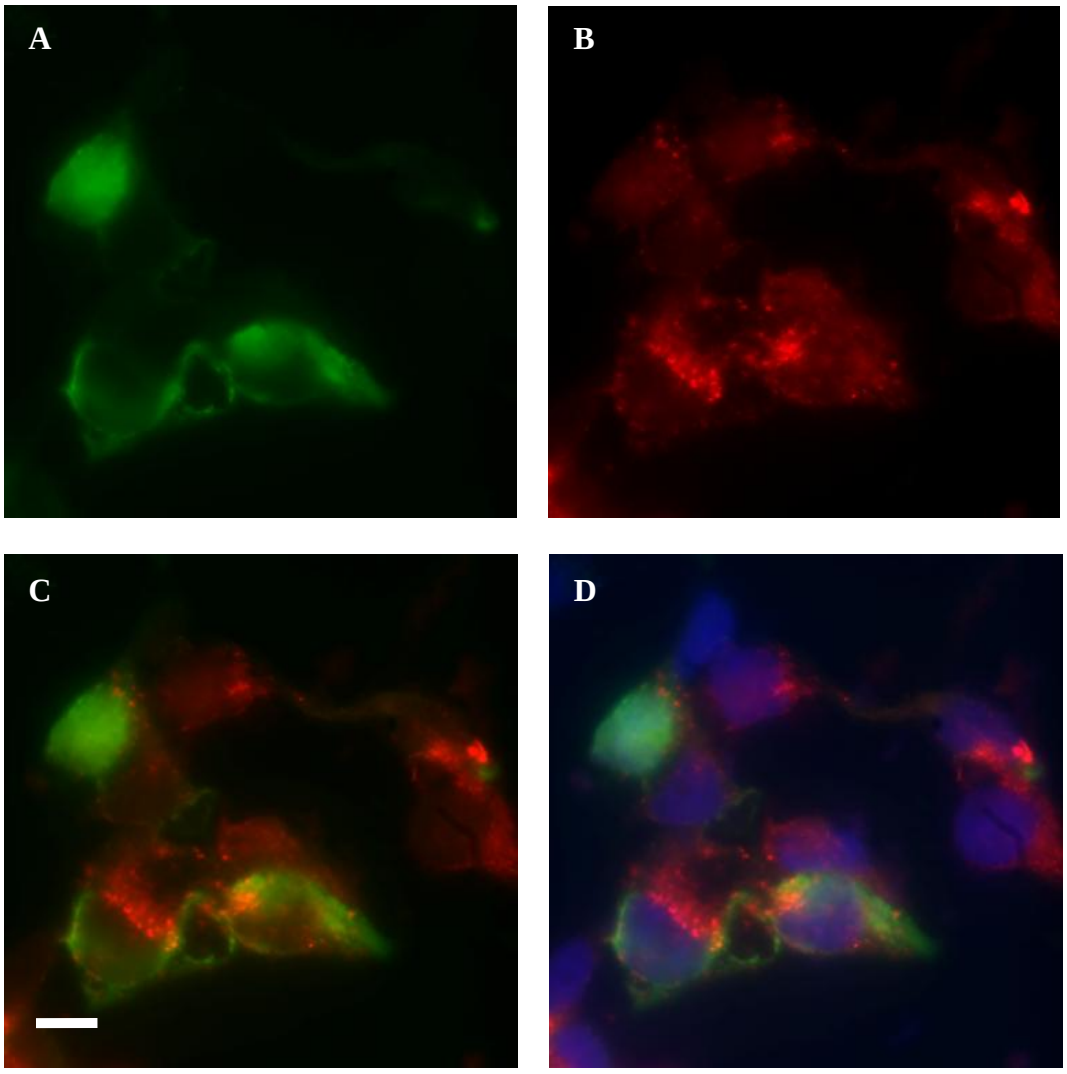

Figure 5.7 Intracellular distribution of Alix in a cluster of HEK293 cells transiently transfected with EGFP tagged Alix, following fixation and permeabilisation, exposure to primary antibodies against EEA1 and treatment with Hoechst. Green fluorescence images of Alix transfected HEK293 cells (Panel A) reveal expression within the cell cytoplasm. Expression of EEA1 (Panel B) reveals a punctuate staining pattern consistent with cytoplasmic distribution of endosomes. Panel C shows nuclear labelling with Hoescht and Panel D shows the merged image of Panel A, B and C. Green expression denotes Alix fluorescence, red as EEA1 and blue corresponds to Hoechst stained nuclei. Scale Bar: 10 μm.

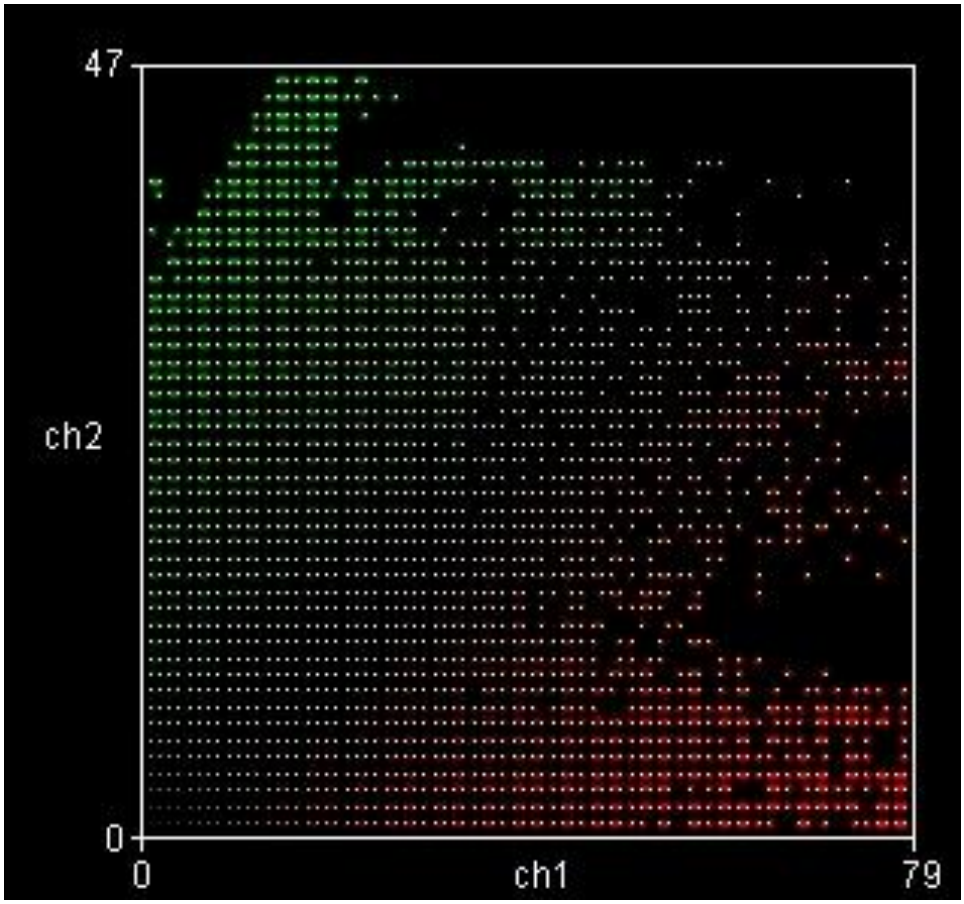

Figure 5.8 Colocalisation analysis from images shown in Figure 5.7. Green pixels denotes Alix, while red pixels corresponds to EEA1. The Pearson's Correlation value that denotes the degree of overlap between the pixels within this image pair, calculated a minimal overlap of 0.163.

5.2.3 Alix distribution and the cytoskeleton

In view of our finding of Alix's cytoplasmic localization within HEK293 cells (Figure 5.1 and 5.3), we examined if Alix is associated with the cytoskeleton. In order to investigate this we transiently transfected EGFP tagged Alix and stained the cells with phalloidin and Hoechst. Phalloidin staining is known display a cytoskeletal staining pattern consistent with F actin distribution (Pu et al., 2011).

Staining with phalloidin revealed a cytoskeletal staining pattern (Figures 5.9 and 5.11). From visual inspection of the images, there was no clear overlap btween Alix and phalloidin signals. However, to confirm this we did a Colocalization Scatter Plot (Figures 5.10 and 5.12). In the scatter plot, pure red and pure green are coloured as such to correspond to phalloidin and Alix respectively. Degree of colocalization is determined by dispersion of the pixels in the plot. The Colour Scatter plot of Alix and Phalloidin in HEK293 cells revealed varying degrees of scatter pattern spread all over the plot similar to that seen with EEA1 (Figures 5.6 and 5.8). The mean Pearson's Correlation value of 0.251 (n=3) indicates that the correlation is weak.

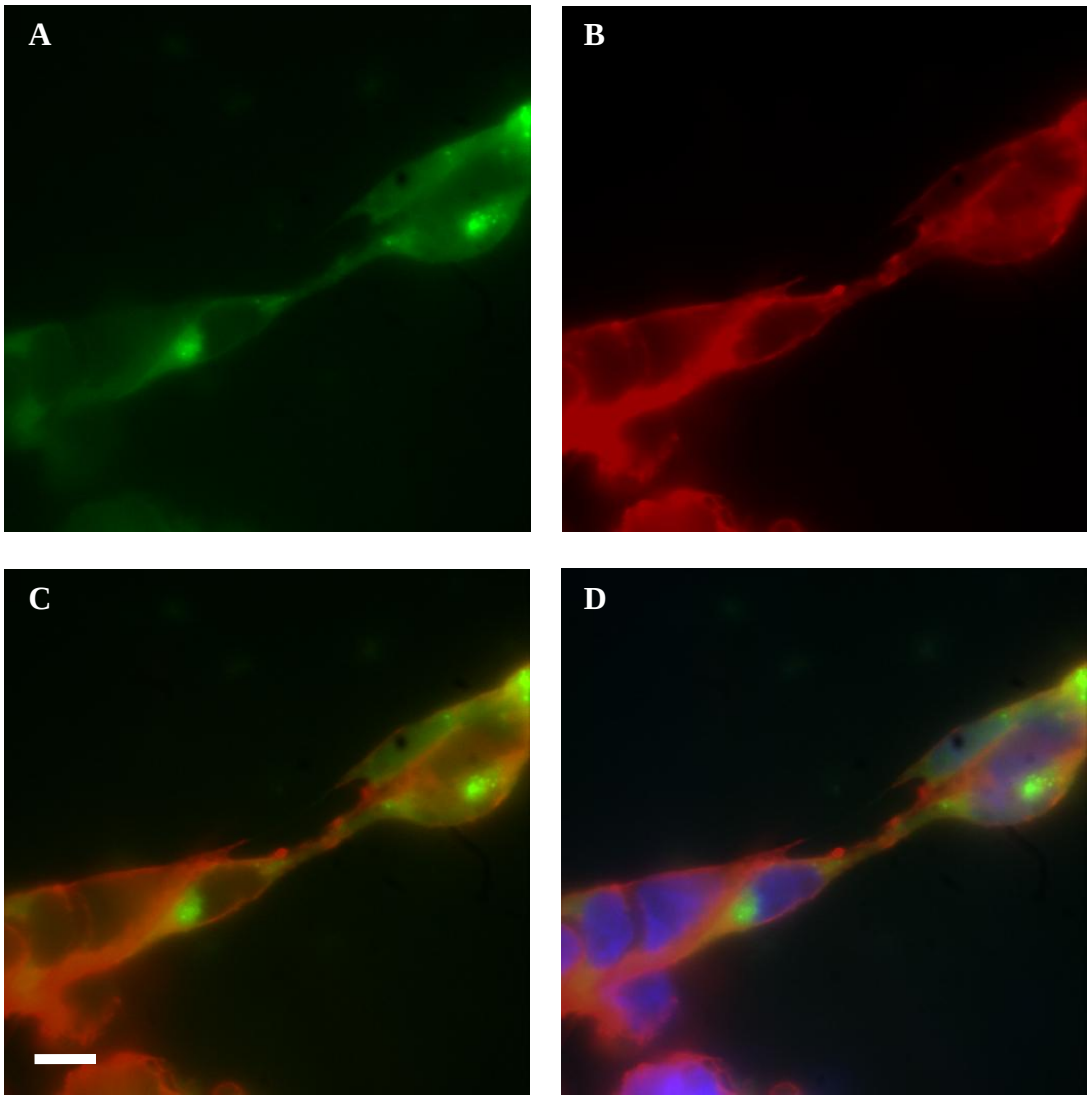

Figure 5.9 Intracellular distribution of Alix in a group of isolated HEK293 cells transiently transfected with EGFP tagged Alix, following fixation and permeabilisation, exposure to fluorescently conjugated peptides against phalloidin and treatment with Hoechst. Green fluorescence images of Alix transfected HEK293 cells (Panel A) reveal expression within the cell cytoplasm. Staining with Phalloidin (Panel B) revealed a cytoskeletal staining pattern consistent with F actin distribution. Panel C shows nuclear labelling with Hoescht and Panel D shows the merged image of Panel A, B and C. Green denotes Alix fluorescence, red as Phalloidin and blue corresponds to Hoechst stained nuclei. Scale Bar: 10 μM.

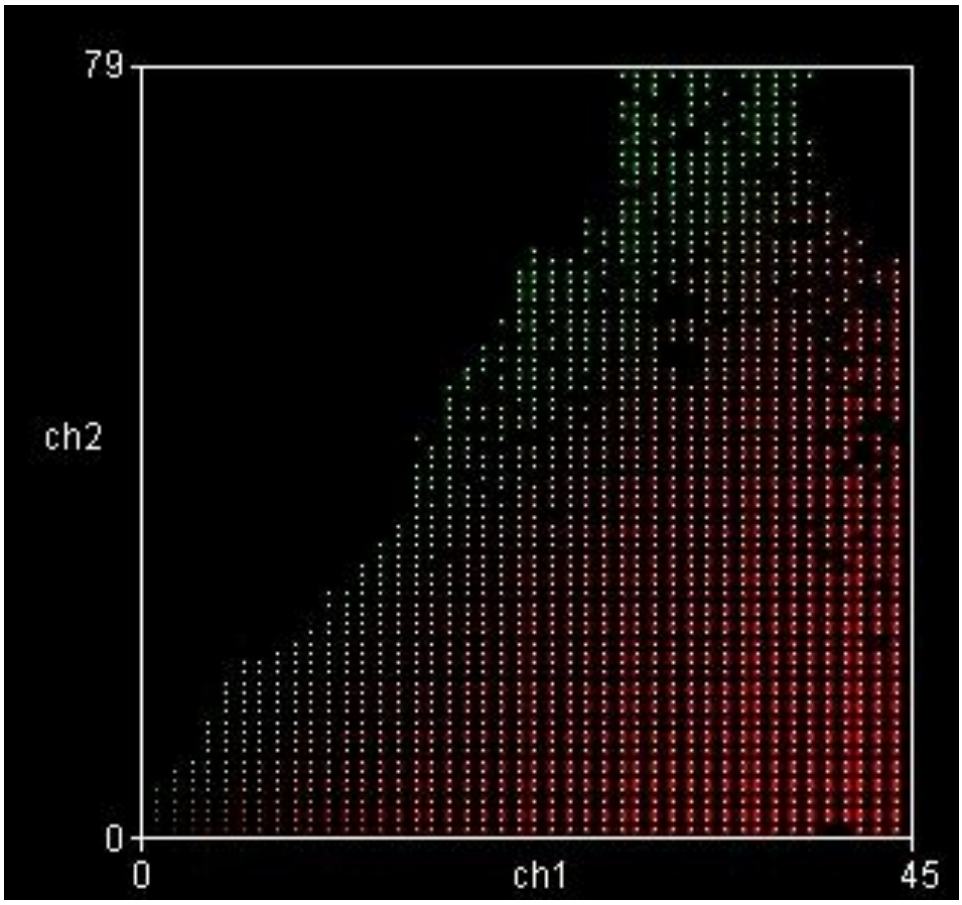

Figure 5.10 Colocalisation analysis from images shown in Figure 5.9. Green pixels denotes Alix, while red pixels corresponds to phalloidin. The Pearson's Correlation value that denotes the degree of overlap between the pixels within this image pair, calculated a minimal overlap of 0.335.

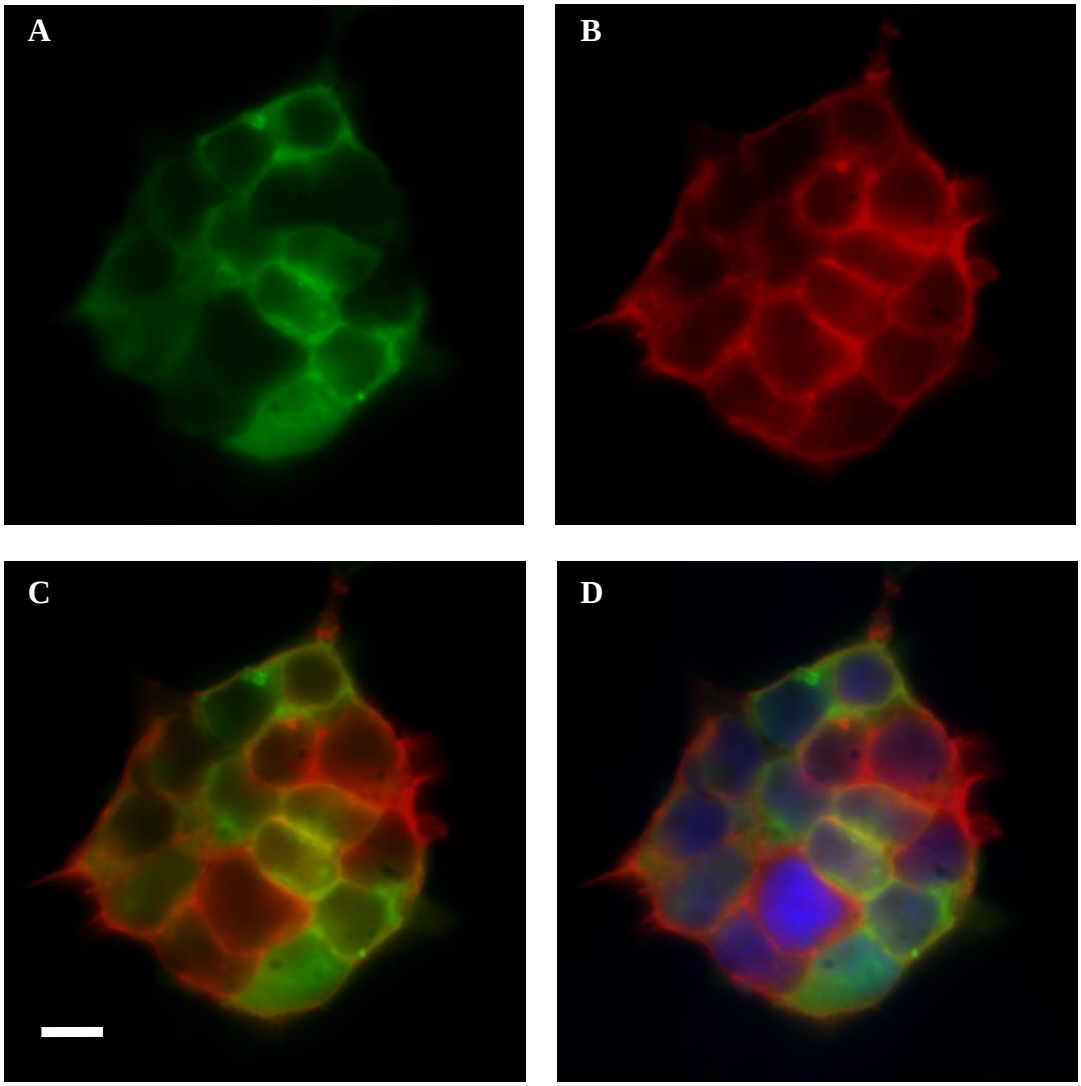

Figure 5.11 Intracellular distribution of Alix in a cluster of HEK293 cells transiently transfected with EGFP tagged Alix, following fixation and permeabilisation, exposure to fluorescently conjugated peptides against phalloidin and treatment with Hoechst. Green fluorescence images of Alix transfected HEK293 cells (Panel A) reveal expression within the cell cytoplasm. Staining with Phalloidin (Panel B) revealed a cytoskeletal staining pattern consistent with F actin distribution. Panel C shows nuclear labelling with Hoescht and Panel D shows the merged image of Panel A, B and C. Green denotes Alix fluorescence, red as phalloidin and blue corresponds to Hoechst stained nuclei. Scale Bar: 10 μM.

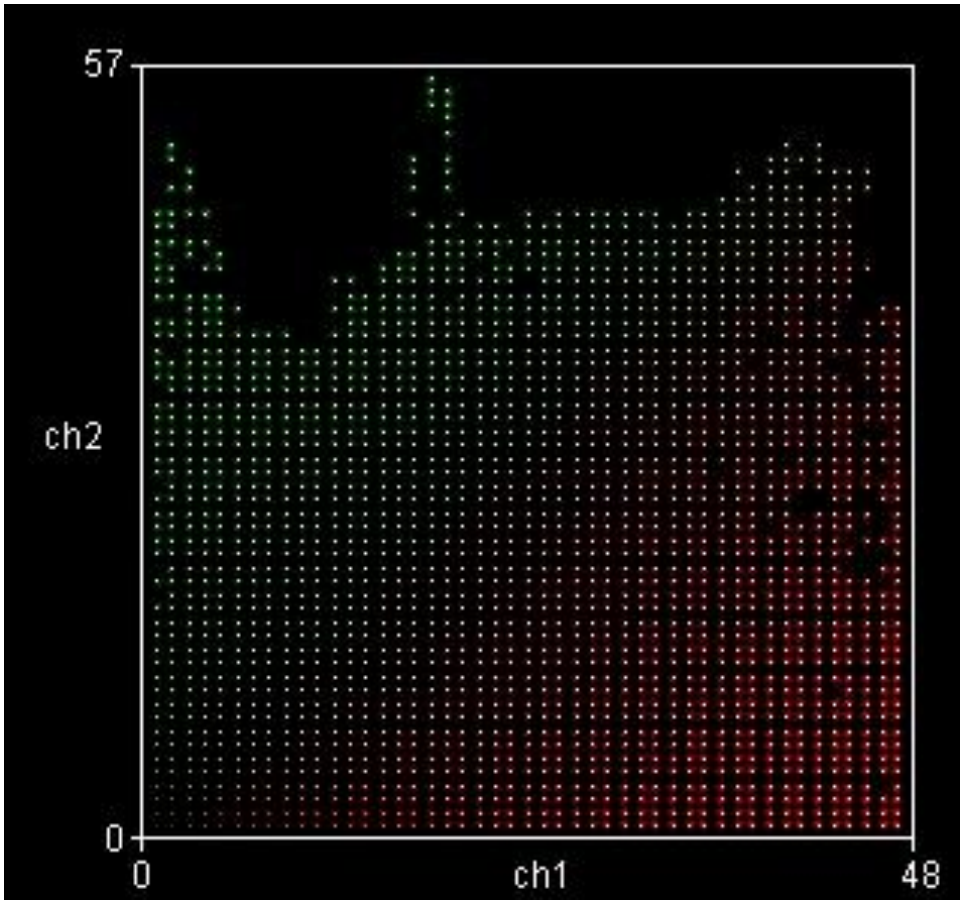

Figure 5.12 Colocalisation analysis from images shown in Figure 5.11. Green pixels denotes Alix, while red pixels corresponds to phalloidin. The Pearson's Correlation value that denotes the degree of overlap between the pixels within this image pair, calculated a minimal overlap of 0.172.

5.3 Localisation of Alix in NMDAR activated HEK293 cells

To assess if there is any association of two proteins in a cellular environment, co-localization microscopy of fluorescently tagged proteins is a widely used method to support a molecular interaction (Taraska and Zagotta, 2010). Here we wanted to see if there is any difference between the association level seen between Alix and NMDAR when the cells are activated or not following the similar conditions used in the NMDAR cell death assay described in section 3.2.1. Earlier sections (5.1 and 5.2) have determined the localisation and correlation of Alix in HEK293 cells relative to subcellular (Hoescht and phalloidin) and endosomal markers (EEA1). Using immunocytochemistry we determined Alix localisation when it is cotransfected with NMDAR subunits and if there is any change in expression when NMDARs are activated with 1 mM NMDA or only exposed to PSS.

5.3.1 Activated NMDARs and Alix localization

Fluorescence images of EGFP tagged Alix revealed a green fluorescence within the cytoplasm of the cells and GluN1 restricted to the cytoplasm as well as the cell membrane (5.13 and 5.15). Visual inspection of the images reveals a partial overlap between Alix and GluN1 expression. However, to confirm this we did a Colocalization Scatter Plot. In the scatter plot, pure red and pure green are coloured as such to correspond to GluN1 and Alix respectively. The degree of colocalization is determined by dispersion of the pixels within the plot. The Colour Scatter plot of Alix and GluN1 in HEK293 cells (Figures 5.14 and 5.16) revealed a varied correlation plot demonstrated by varying degrees of scatter pattern spread all over the plot. However, the analysis suggests some degree of correlation between Alix and GluN1 expression and with a mean Pearson's Correlation value of 0.5 (n=20) there is a statistically moderate correlation.

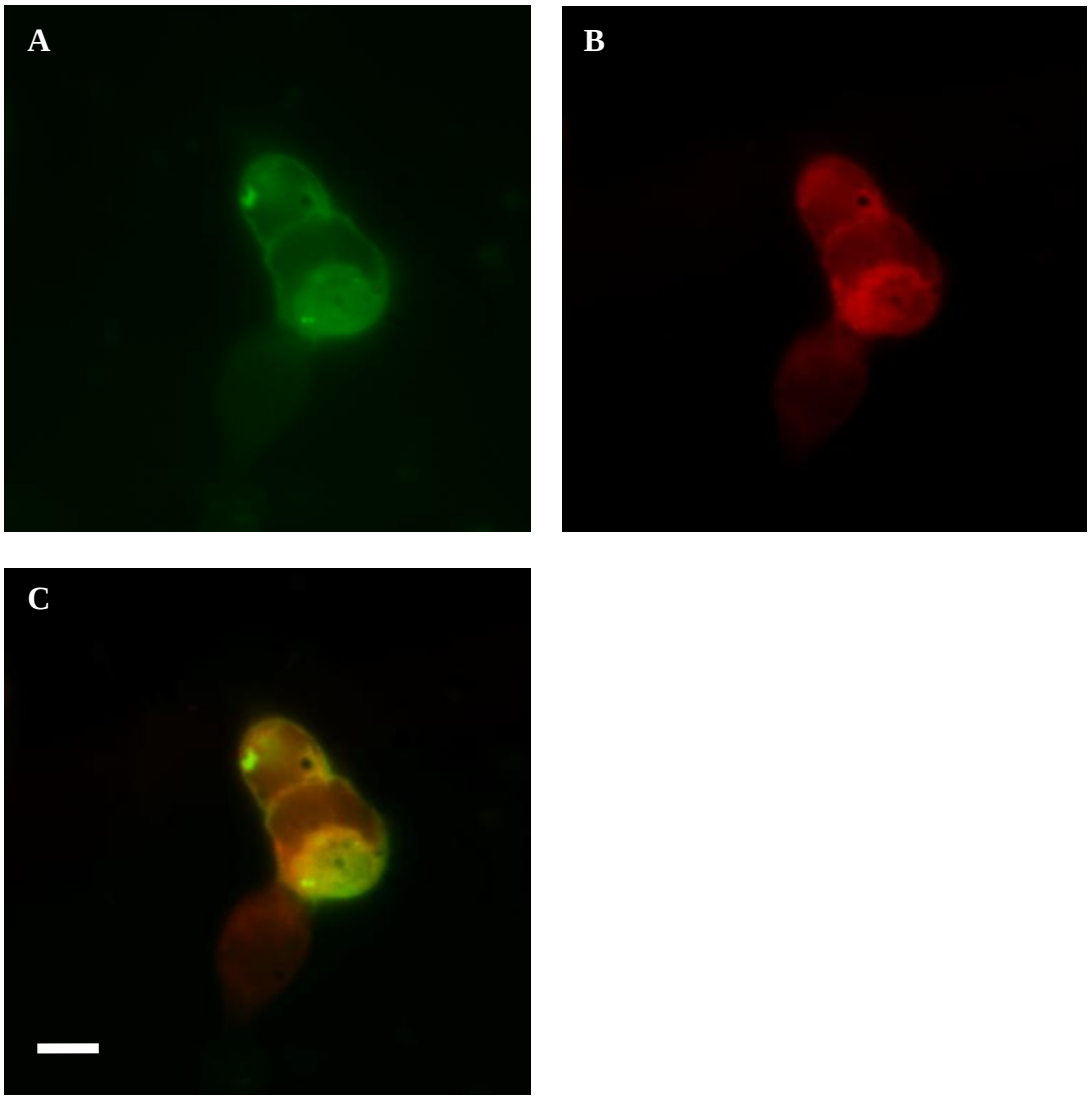

Figure 5.13 Intracellular distribution of Alix in a group of isolated HEK293 cells transiently transfected with EGFP tagged Alix and GluN1+GluN2A, following fixation and permeabilisation and exposure to primary antibodies against GluN1. Green denotes Alix fluorescence, while red is GluN1. Green fluorescence images of Alix transfected HEK293 cells (Panel A) reveal expression within the cell cytoplasm. Staining with GluN1 (Panel B) revealed a distribution of strong fluorescence in the plasma membrane. Panel C shows the merged image of Panel A and B. Scale Bar: 10 μm.

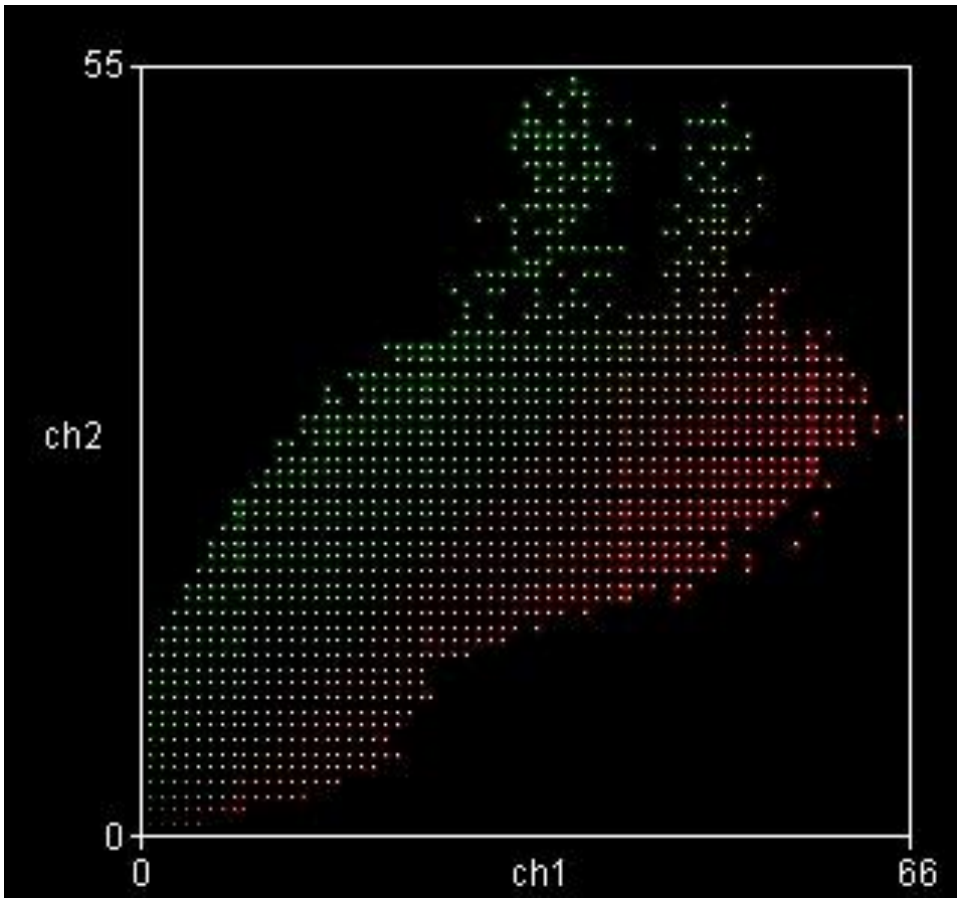

Figure 5.14 Colocalisation analysis from images shown in Figure 5.13. Green pixels denotes Alix, while red pixels corresponds to GluN1. The Pearson's Correlation value that denotes the degree of overlap between the pixels within this image pair, calculated a minimal overlap of 0.852.

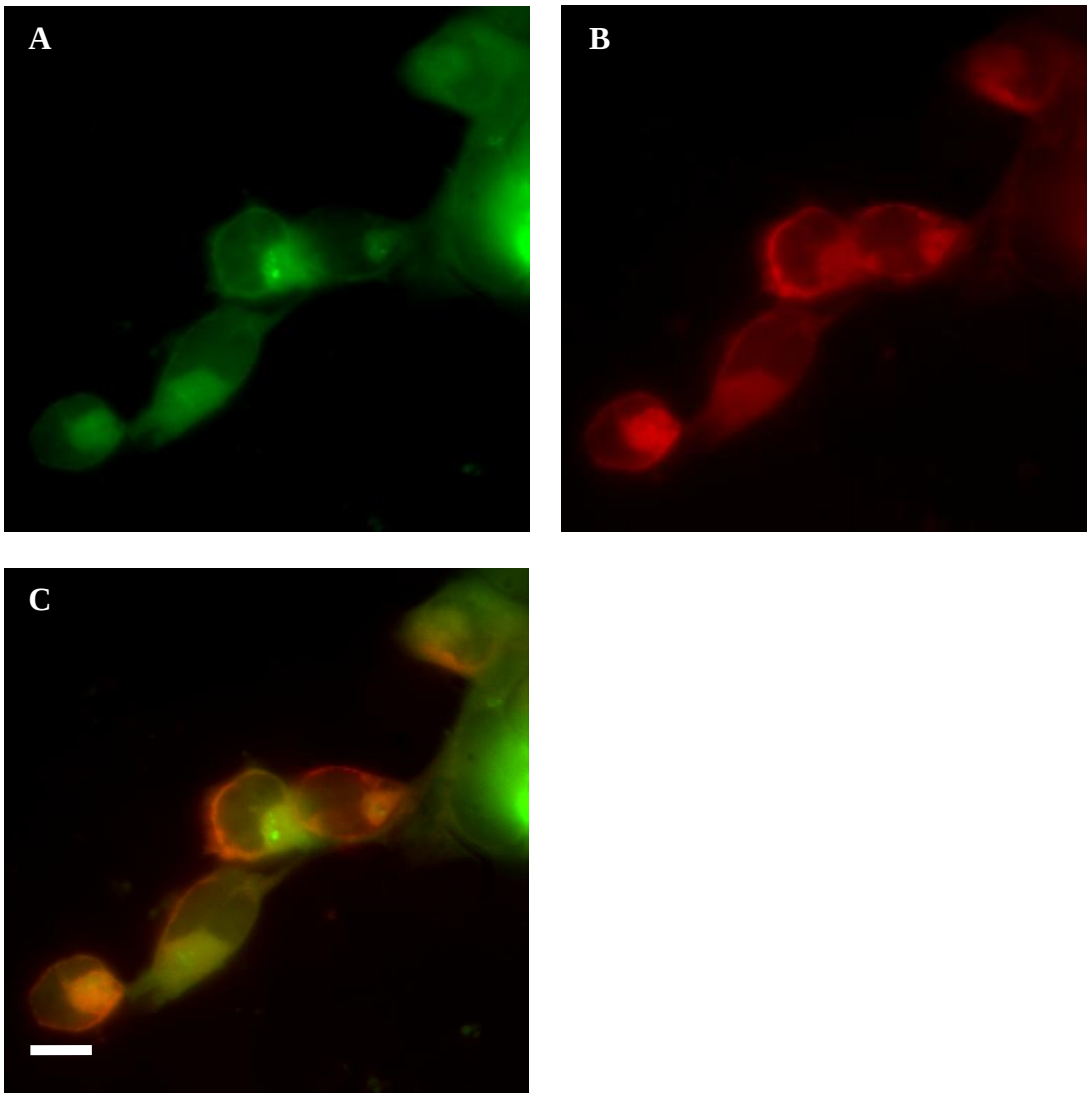

Figure 5.15 Intracellular distribution of Alix in a group of clustered HEK293 cells transiently transfected with EGFP tagged Alix and GluN1+ GluN2A, following fixation and permeabilisation and exposure to primary antibodies against GluN1. Green denotes Alix fluorescence, while red is GluN1. Green fluorescence images of Alix transfected HEK293 cells (Panel A) reveal expression within the cell cytoplasm. Staining with GluN1 (Panel B) revealed a distribution of strong fluorescence in the plasma membrane. Panel C shows the merged image of Panel A and B. Scale Bar: 10 μm.

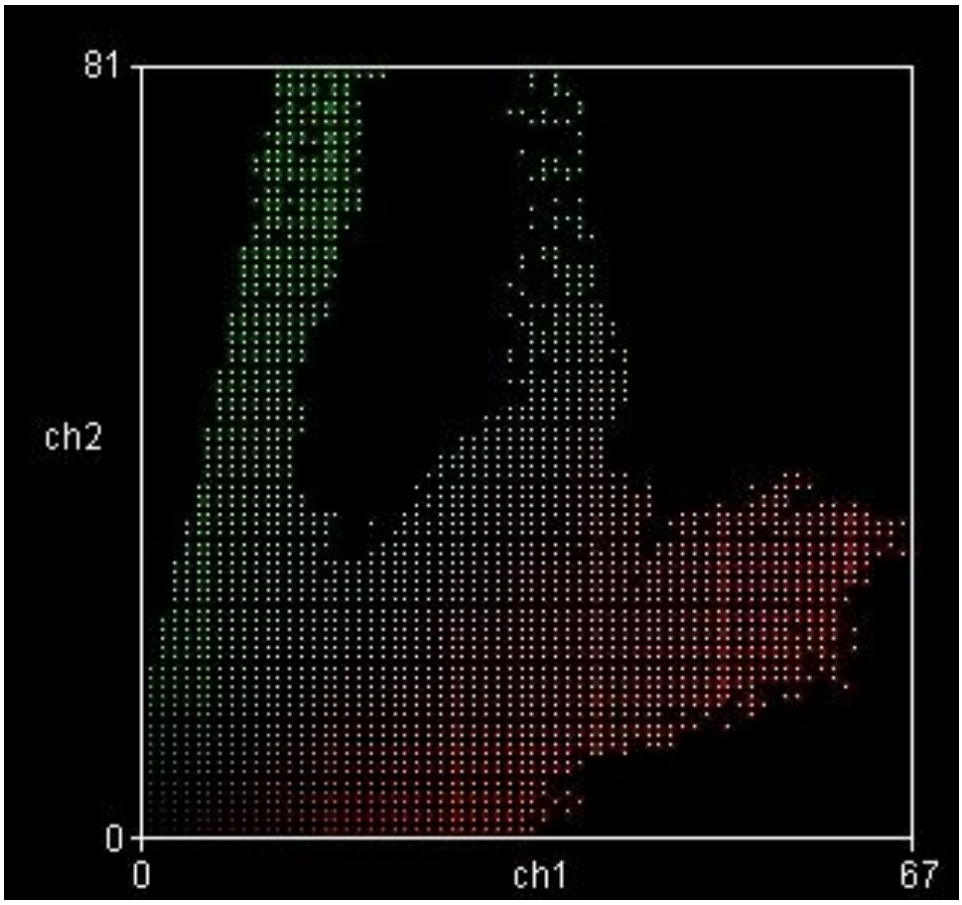

Figure 5.16 Colocalisation analysis from images shown in Figure 5.15. Green pixels denotes Alix, while red pixels corresponds to GluN1. The Pearson's Correlation value that denotes the degree of overlap between the pixels within this image pair, calculated a minimal overlap of 0.249.

5.3.2 Nonactivated NMDAR and Alix localization

Fluorescence images of Alix and GluN1 expression in non activated cells were similar to the activated cells in section 5.3.1. In the Colocalization Scatter Plot, pure red and pure green are coloured as such to correspond to GluN1 and Alix respectively. The Colour Scatter plot of Alix and GluN1 in HEK293 cells showed a variable scatter pattern but some degree of colocalisation. This was demonstrated by a mean Pearson's Correlation value of 0.44 (n=20) which suggests a statistically a moderate correlation and close to the value obtained for activated cells (section 5.3.1). Paired t-test shows that the difference between the activated and non activated correlation plot is considered to be not statistically significant with a P value of 0.499. These observations suggest there is little change in Alix localization following NMDAR coexpression or NMDAR activation.

The reason for the relatively high correlation rate observed here compared to earlier comparisons (sections 5.1 and 5.2) could be due to the fact that both Alix and GluN1 protein are overexpressed (via plasmid cDNA expression) in the transiently transfected HEK293 cells and this may not fully replicate endogenous expression.

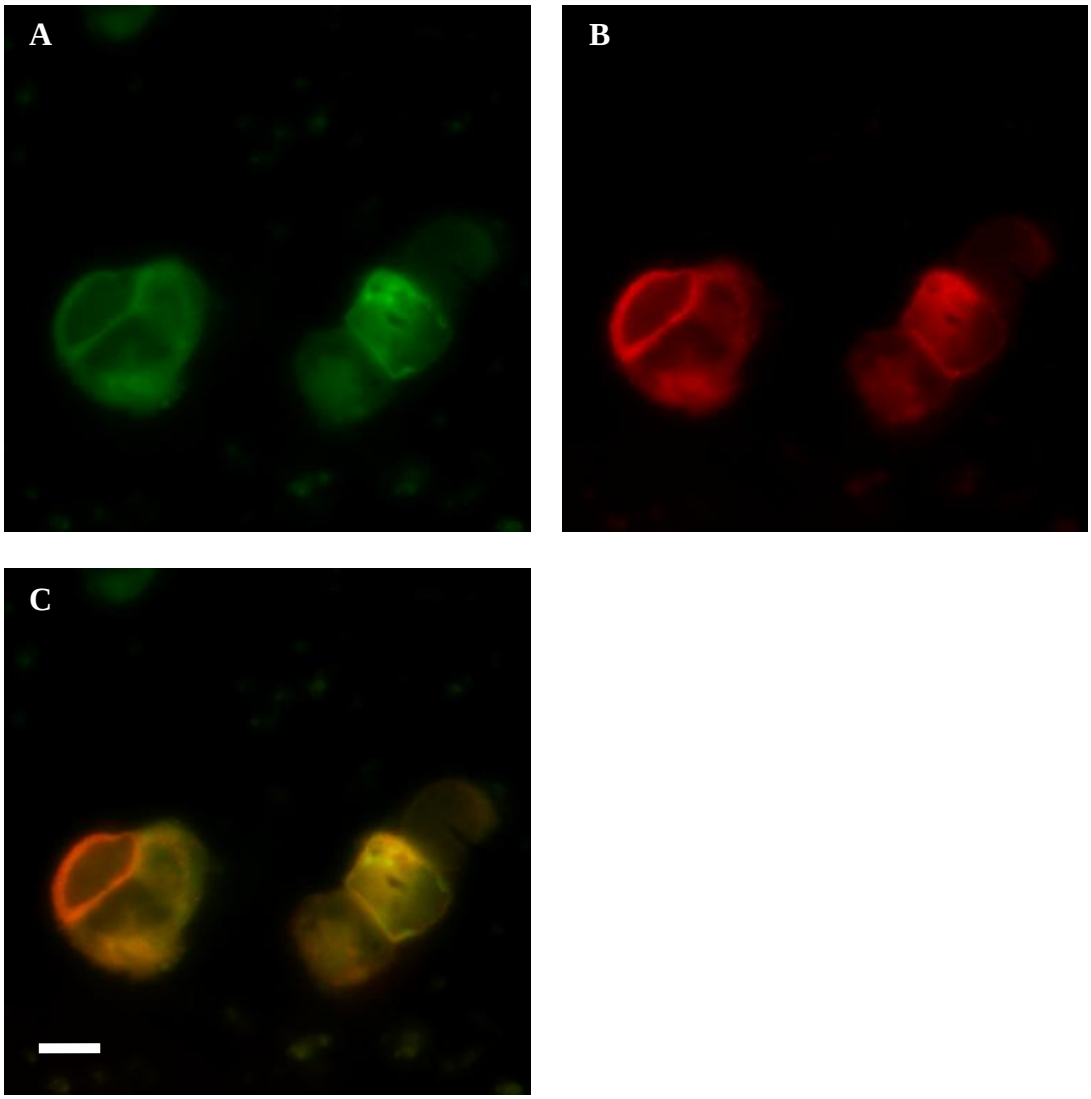

Figure 5.17 Intracellular distribution of Alix in a group of non activated HEK293 cells transiently transfected with EGFP tagged Alix and GluN1+ GluN2A, following fixation and permeabilisation and exposure to primary antibodies against GluN1. Green denotes Alix fluorescence, while red is GluN1. Green fluorescence images of Alix transfected HEK293 cells (Panel A) reveal expression within the cell cytoplasm. Staining with GluN1 (Panel B) revealed a distribution of strong fluorescence in the plasma membrane. Panel C shows the merged image of Panel A and B. Scale Bar: 10 μm.

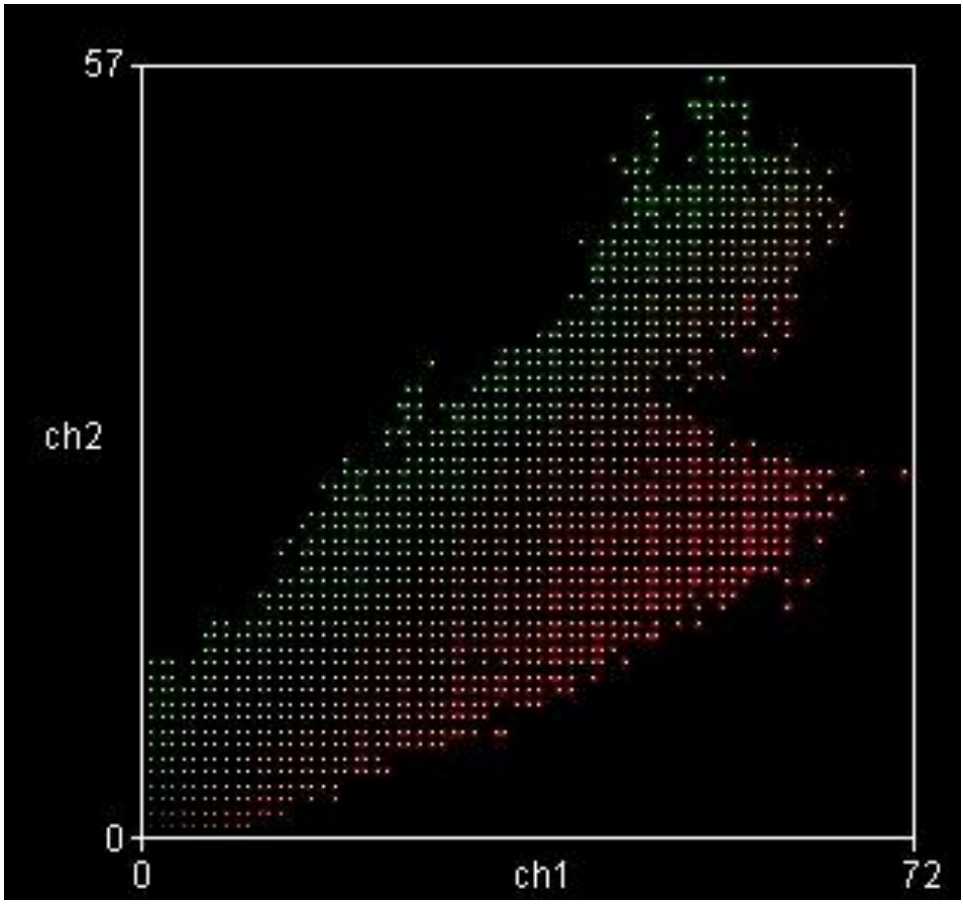

Figure 5.18 Colocalisation analysis from images shown in Figure 5.17. Green pixels denotes Alix, while red pixels corresponds to GluN1. The Pearson's Correlation value that denotes the degree of overlap between the pixels within this image pair, calculated a minimal overlap of 0.894.

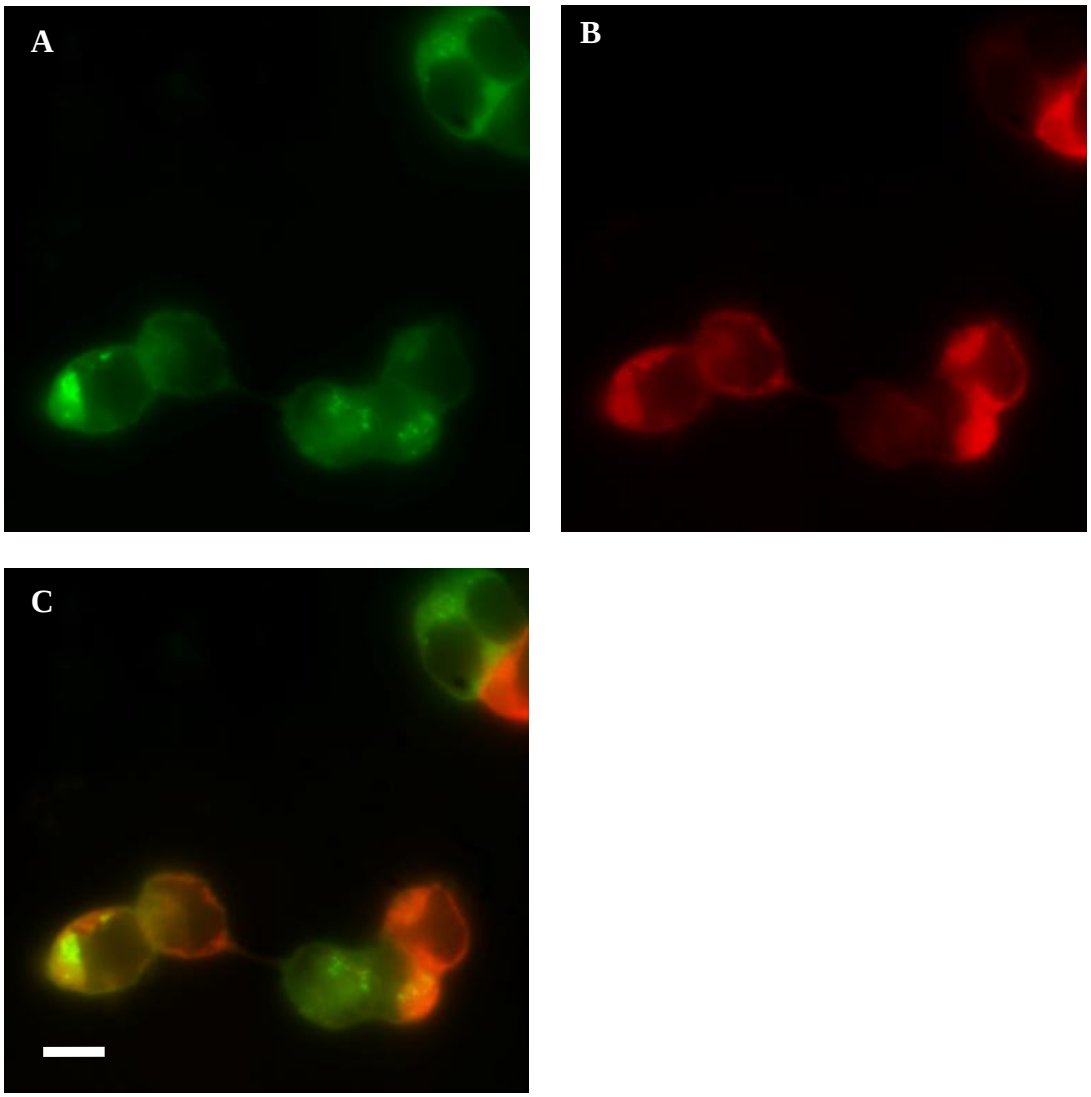

Figure 5.19 Intracellular distribution of Alix in a group of non activated HEK293 cells transiently transfected with EGFP tagged Alix and GluN1+GluN2A, following fixation and permeabilisation and exposure to primary antibodies against GluN1. Green denotes Alix fluorescence, while red is GluN1. Green fluorescence images of Alix transfected HEK293 cells (Panel A) reveal expression within the cell cytoplasm. Staining with GluN1 (Panel B) revealed a distribution of strong fluorescence in the plasma membrane. Panel C shows the merged image of Panel A and B. Scale Bar: 10 μm.

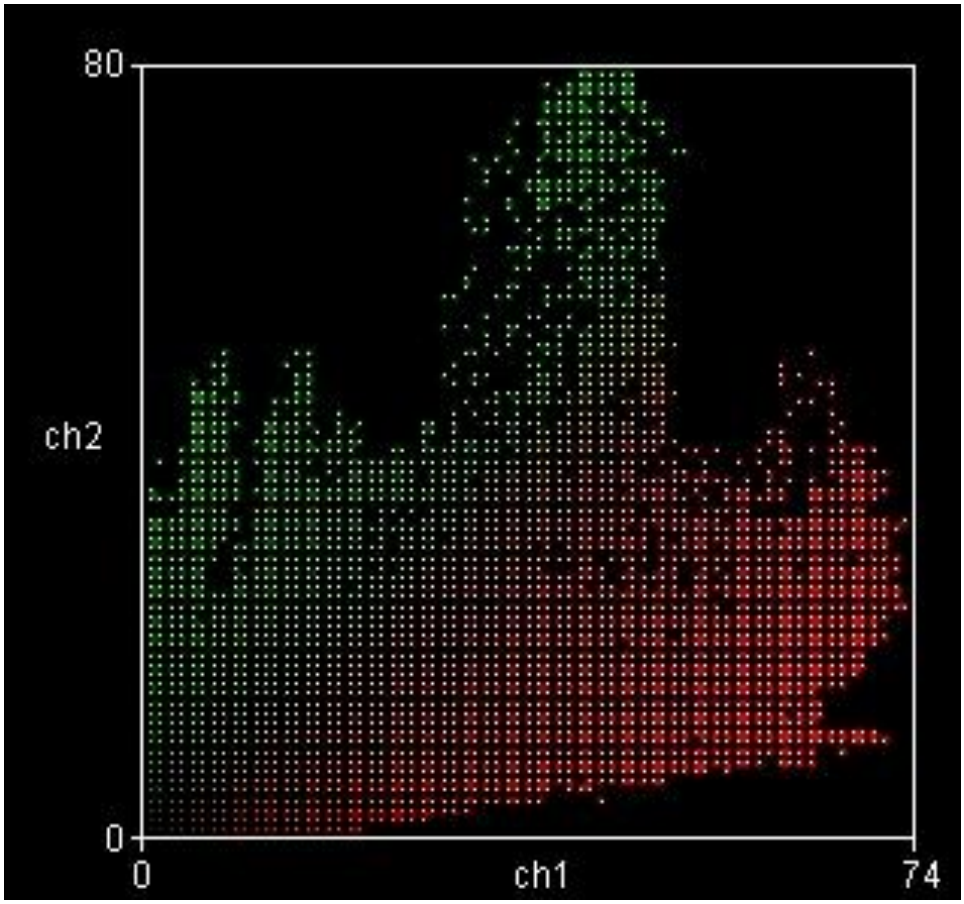

Figure 5.20 Colocalisation analysis from images shown in Figure 5.19. Green pixels denotes Alix, while red pixels corresponds to GluN1. The Pearson's Correlation value that denotes the degree of overlap between the pixels within this image pair, calculated a minimal overlap of 0.383.

5.4 Summary

From the images that we analysed, there was little overlap between Alix and Hoechst (Figures 5.1 and 5.3), Alix and EEA1 (Figures 5.5 and 5.7) and Alix and phalloidin (Figures 5.9 and 5.11). This was further proven by a low Pearson's correlation value of 0.100 (n=3) for Alix and Hoechst, 0.252 (n =3) for Alix and EEA1 and 0.251 (n=3) for Alix and phalloidin. Therefore there is little expression of Alix within the nucleus and little association with cytoskeletal proteins or the endosomal protein EEA1 in HEK293 cells.

However, our analysis suggests there is a moderate degree of correlation between Alix and GluN1 expression when activated with a mean Pearson's Correlation value of 0.5 (n=20) (Figure 5.13 and 5.15). There is a also a moderate degree of correlation between Alix and GluN1 expression when not activated with a mean Pearson's Correlation value of 0.44 (n=20)(Figure 5.17 and 5.19). A paired t-test showed no statistically significant difference between the activated and non activated correlation plots with a P value of 0.499. These observations suggest there is little change in Alix localization with GluN1 following NMDAR activation or non activation. However, as these recombinant proteins are expressed in a heterologous expression system, using plasmid vectors optimized for protein overexpression. The relatively high correlation detected between Alix and GluN1 expression in HEK293 cells could be due to excessive expression within the cell. In addition the HEK293 cells may not fully replicate the endogenous neuronal environment necessary for correct Alix localisation and thus may not be the ideal model system to examine Alix localization in this manner. Thus in order to investigate this further we decided to ascertain the correlation and expression of endogenous Alix in cultured primary neurons from rat hippocampus and cortex in the next chapters.

6.1 Localisation of Alix in primary cortical and hippocampal neurons

There is little information in the literature describing native Alix expression within neurons and we decided to ascertain the correlation and expression of basal Alix in cultured hippocampal and cortical primary neurons. We decided to use cultures that are 14 days old as neurons are reported with mature synapse from day 10 onwards in cultures (Grabrucker, A. 2009). We followed the immunocytochemistry protocols used for HEK293 cells previously described in chapter 5.

6.1.1 Expression of Alix within the cytoplasm of cortical neurons and hippocampal neurons

Fluorescence images of endogenous Alix expression revealed a punctate fluorescence within the cytoplasm of the cells with Hoechst staining the cell nuclei (Figures 6.1 and 6.3). There does not seem to be any overlap between Alix and Hoechst signals and to confirm with this we performed a Colocalization Scatter Plot. In the scatter plot, pure blue and pure red are coloured as such to correspond to Hoechst and Alix respectively. Colour scatter plot of Alix and Hoechst in the cortical neurons revealed a mostly uncorrelated plot seen by a scatter plot that is more clustered towards the x and y-axes and further proven by a low mean Pearson's correlation value of -0.133 (n=3) (Figures 6.2). The Colour scatter plot of Alix and Hoechst in the hippocampal neurons also revealed a mostly uncorrelated plot seen by a scatter plot that is more clustered towards the x and y-axes and further proven by a low mean Pearson's correlation value of -0.004 (n = 3) (Figure 6.4).

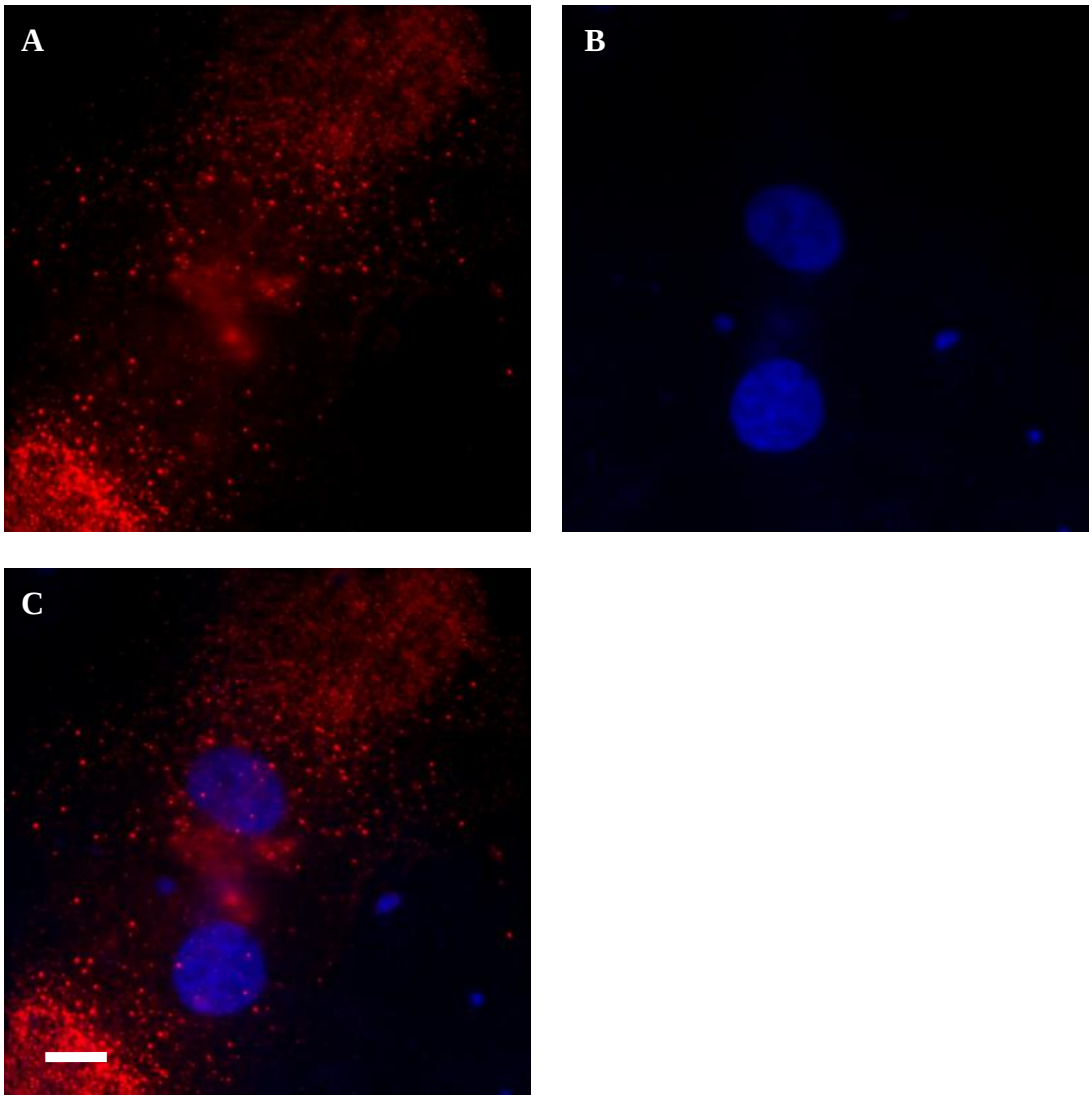

Figure 6.1 Intracellular distribution of endogenous Alix in primary cortical neuronal cultures stained with Hoechst. Fluorescence images of Alix reveal mostly a punctate fluorescence pattern within the cell cytoplasm. Red denotes Alix fluorescence while blue corresponds to Hoechst stained nuclei. Scale Bar: 10 μm.

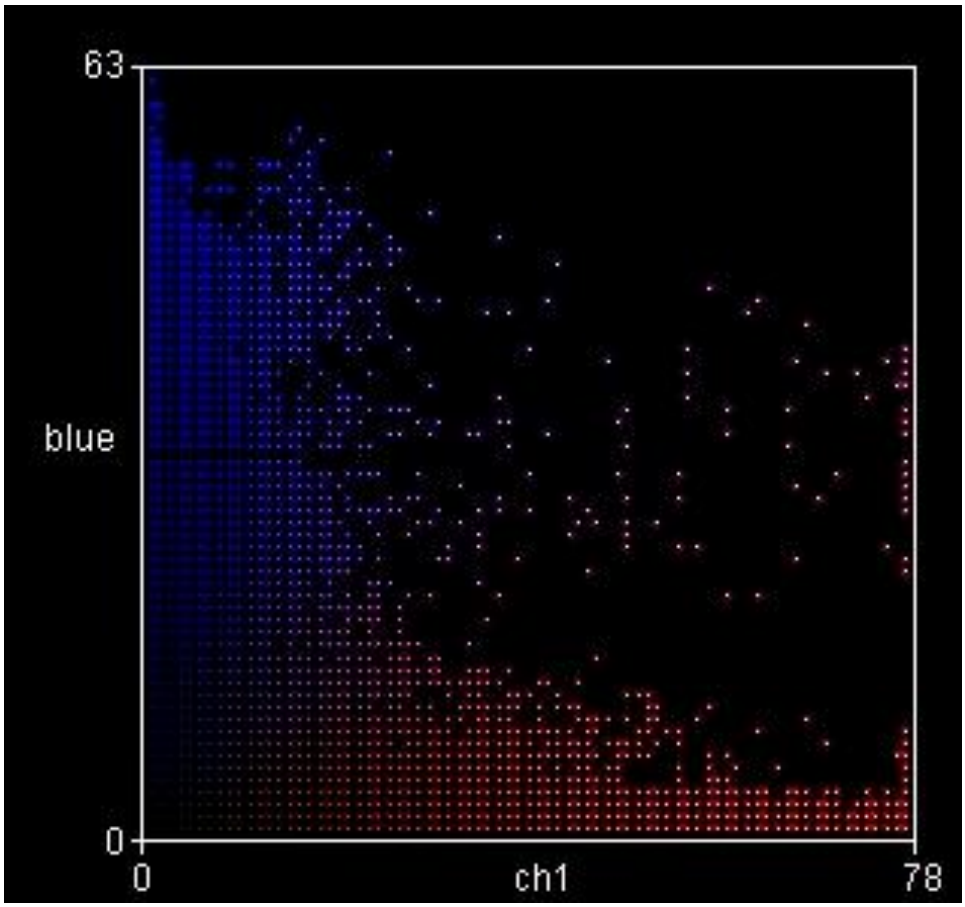

Figure 6.2 Colocalisation analysis from images shown in Figure 6.1. Red pixels denotes Alix while blue pixels corresponds to Hoechst. The Pearson's Correlation value that denotes the degree of overlap between the image pair calculated a minimal overlap of -0.354.

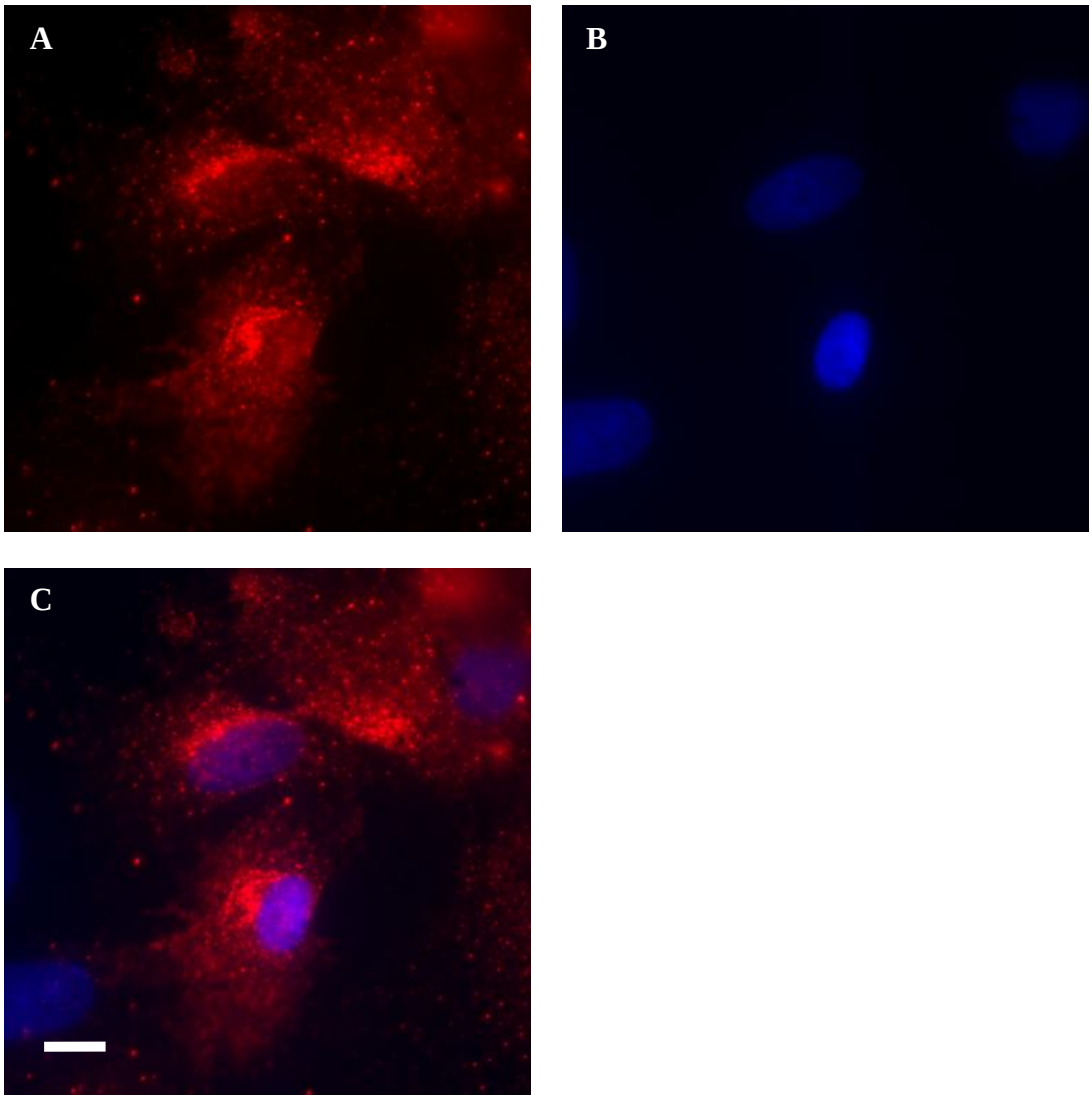

Figure 6.3 Intracellular distribution of endogenous Alix in primary hippocampal neuronal cultures stained with Hoechst. Fluorescence images of Alix reveal mostly a punctate fluorescence pattern within the cell cytoplasm. Red denotes Alix fluorescence while blue corresponds to Hoechst stained nuclei. Scale Bar: 10 μm.

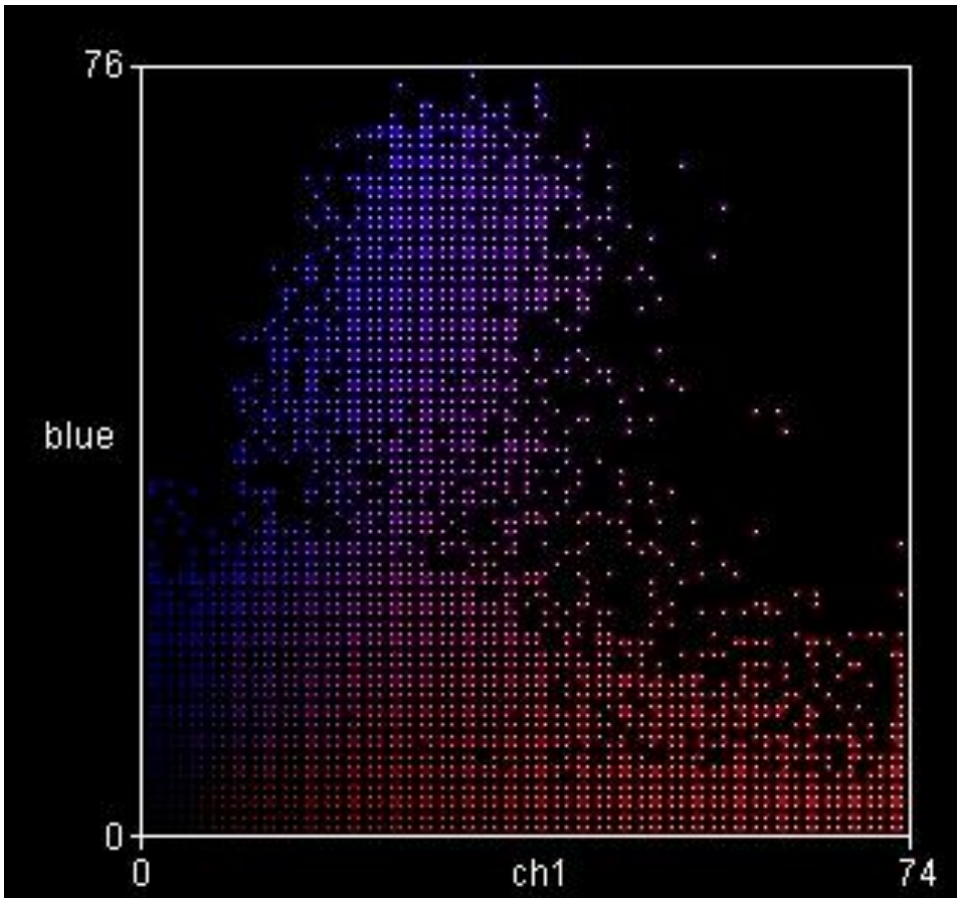

Figure 6.4 Colocalisation analysis from images shown in Figure 6.3. Red pixels denotes Alix while blue pixels corresponds to Hoechst. The Pearson's Correlation value that denotes the degree of overlap between the image pair calculated a minimal overlap of 0.185.

6.2.1 Endogenous Alix distribution in cortical and hippocampal neurons and the localization of the cellular endosome marker, EEA1

Previously we observed a weak correlation between Alix and EEA1 expression in HEK293 cells (Figure 5.5 and 5.7). We further investigated this by examining if there was any correlation between endogenous expression of Alix and the endosome marker EEA1 in primary cortical and hippocampal neurons. As before we fixed, permeabilised and treated the cells with primary and secondary antibodies against Alix and EEA1 and stained for nuclei with Hoechst.

The fluorescence images of endogenous Alix expression (Figures 6.5 and 6.7) revealed a sparse punctate fluorescence within the cell cytoplasm with Hoechst clearly showing the cell nuclei. Endogenous EEA1 expression revealed also a punctate staining pattern but was more evenly distributed throughout the cytoplasm compared to Alix. From the merged images it was difficult to clearly identify colocalisation between Alix and EEA1 expression. However, to confirm this we performed a Colocalization Scatter Plot. In the Scatter plot, pure red and pure green pixels correspond to Alix and EEA1 respectively. Colour scatter plot of Alix and EEA1 revealed a more varied correlation plot seen by varying degrees of scatter pattern spread all over the plot (Figures 6.6 and 6.8). We found a mean Pearson's Correlation value of 0.406 (n=3) for the cortical neurons which shows that there is a moderate correlation. On the other hand, with a mean Pearson's Correlation value of 0.307 (n = 3) we found that there is a weak correlation for the hippocampal neurons. However paired t-test shows that the difference between cortical and hippocampal neurons is considered to be not statistically significant with a P value of 0.676.

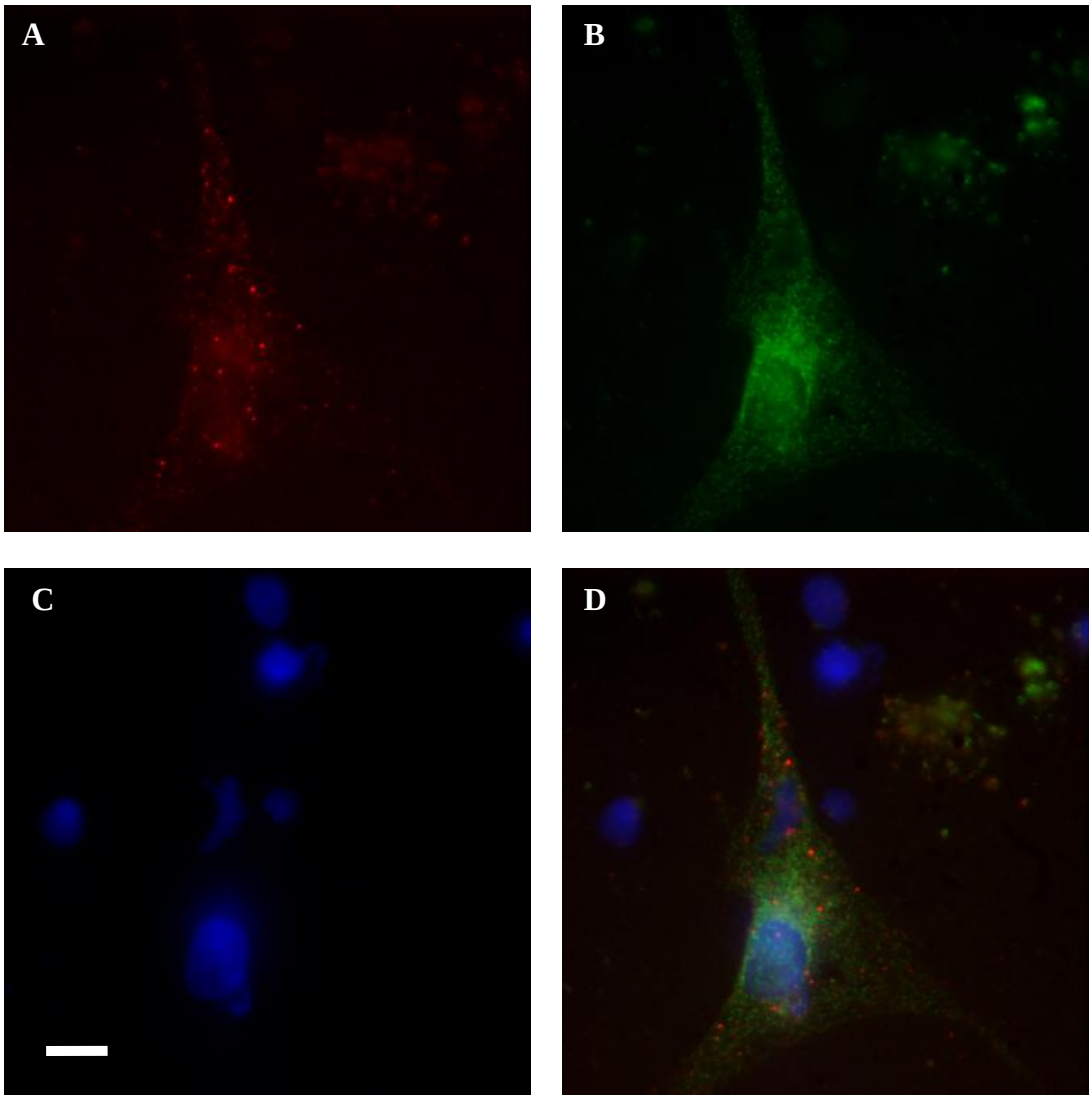

Figure 6.5 Intracellular distribution of endogenous Alix in cortical neurons, following fixation and permeabilisation, exposure to primary antibodies against Alix and EEA1 and treatment with Hoechst. Red fluorescence images of endogenous Alix (Panel A) reveal a punctate expression pattern within the cell cytoplasm. Expression of EEA1 (Panel B) also reveals a punctate staining pattern consistent with cytoplasmic distribution of endosomes. Panel C shows nuclear labelling with Hoescht and Panel D shows the merged image of Panel A, B and C. Red denotes Alix fluorescence, green as EEA1 and blue corresponds to Hoechst stained nuclei. Scale Bar: 10 μm.

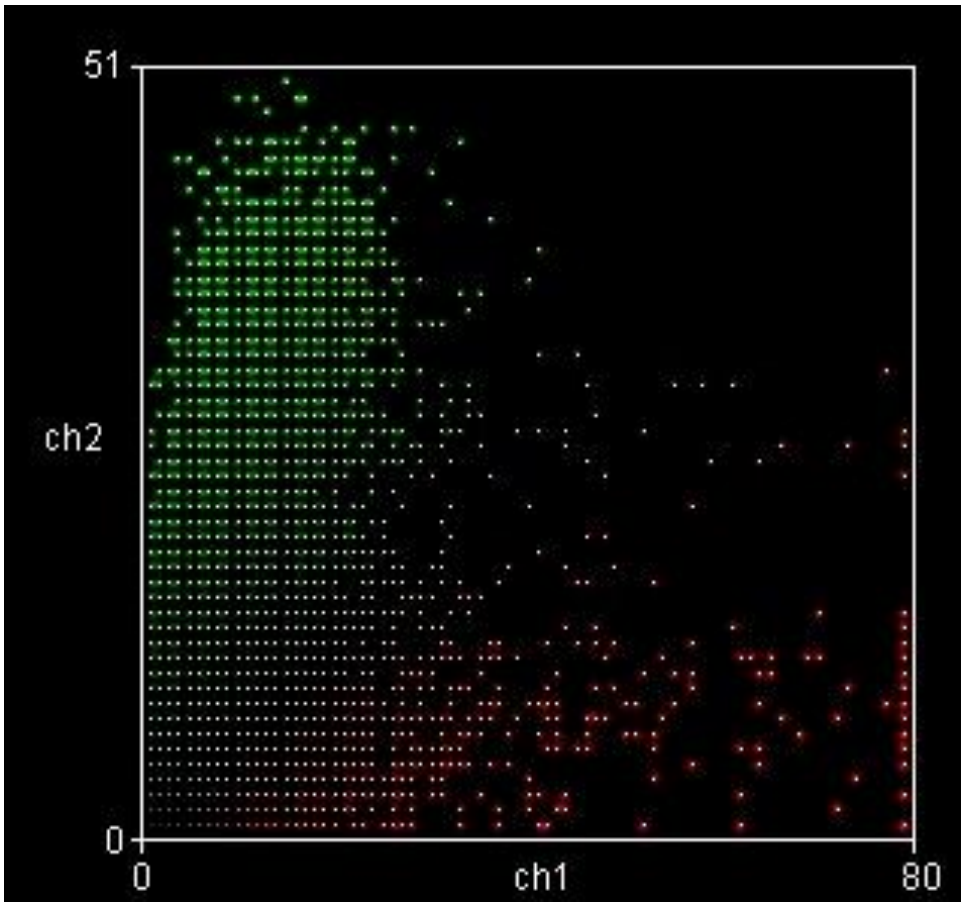

Figure 6.6 Colocalisation analysis from cortical images shown in Figure 6.5. Red pixels denotes Alix, while green pixels corresponds to EEA1. The Pearson's Correlation value that denotes the degree of overlap between the pixels within this image pair, calculated a moderate correlation of 0.532.

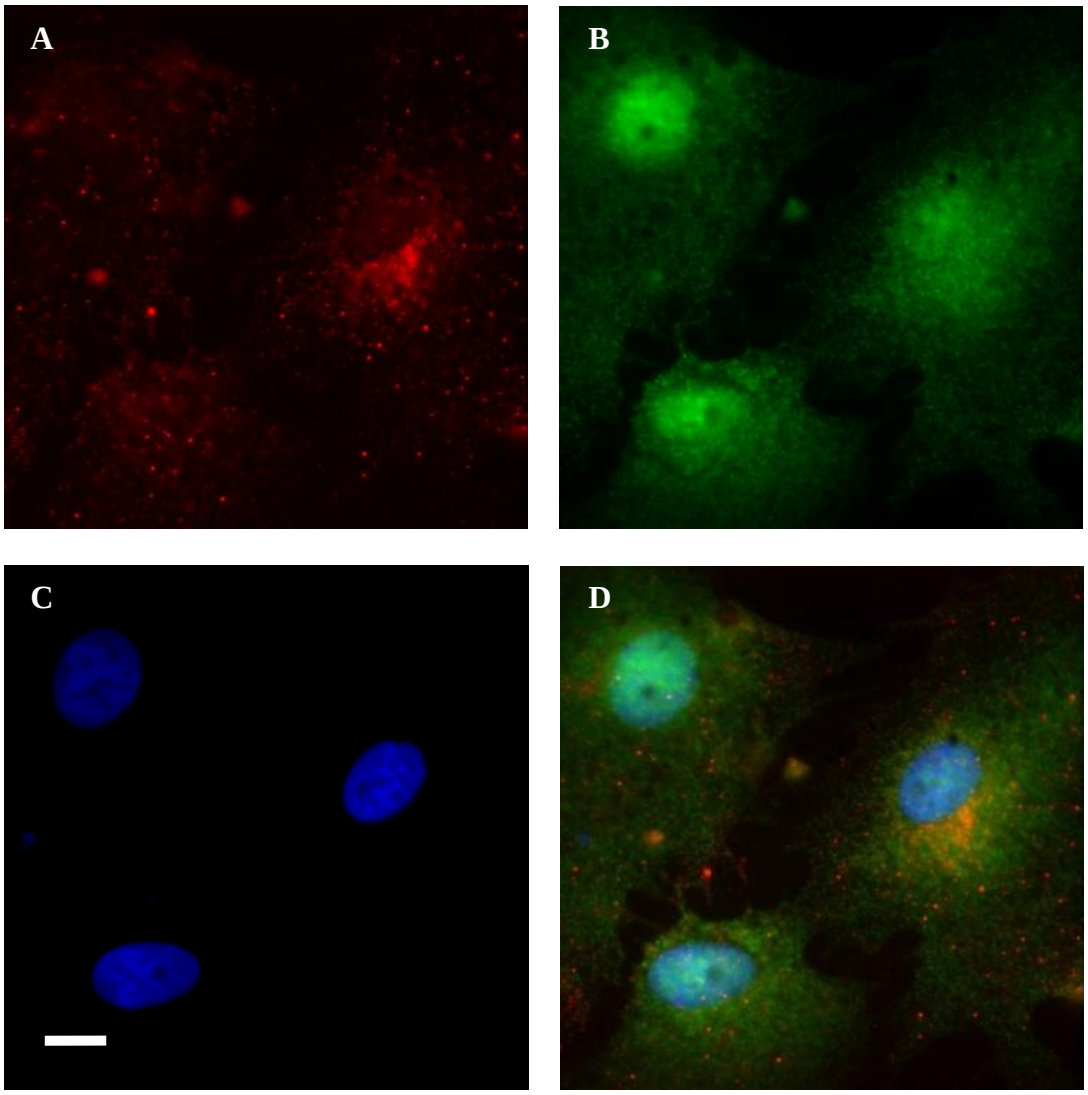

Figure 6.7 Intracellular distribution of endogenous Alix in hippocampal neurons, following fixation and permeabilisation, exposure to primary antibodies against Alix and EEA1 and treatment with Hoechst. Red fluorescence images of endogenous Alix (Panel A) reveal a punctate expression pattern within the cell cytoplasm. Expression of EEA1 (Panel B) also reveals a punctate staining pattern consistent with cytoplasmic distribution of endosomes. Panel C shows nuclear labelling with Hoescht and Panel D shows the merged image of Panel A, B and C. Red denotes Alix fluorescence, green as EEA1 and blue corresponds to Hoechst stained nuclei. Scale Bar: 10 μm.

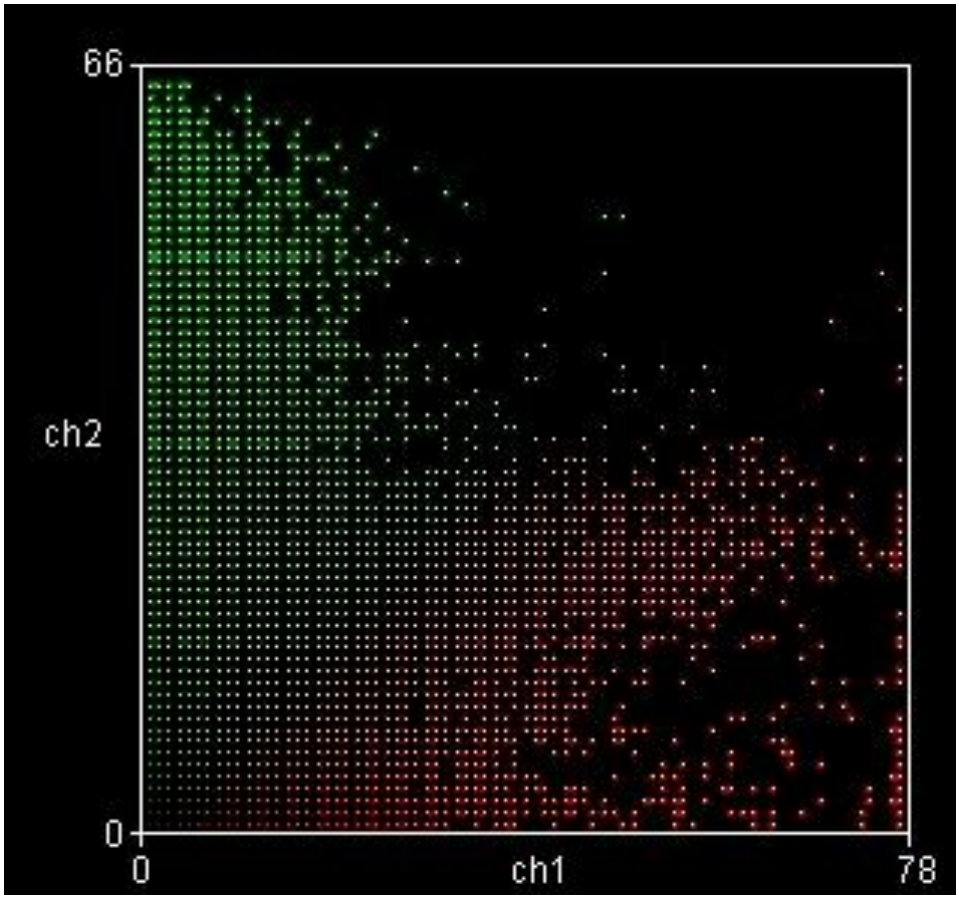

Figure 6.8 Colocalisation analysis from hippocampal images shown in Figure 6.7. Red pixels denotes Alix, while green pixels corresponds to EEA1. The Pearson's Correlation value that denotes the degree of overlap between the pixels within this image pair, calculated a very weak correlation of 0.181.

6.2.2 Endogenous Alix distribution and the cytoskeleton within cortical neurons

In view of our finding of Alix's weak correlation with Phalloidin in HEK293 cells (Figures 5.9 and 5.11), we investigated the distribution of endogenous Alix localization with the cytoskeleton in cortical and hippocampal neurons. Cortical and hippocampal neurons were stained with primary antibodies for Alix and costained with phalloidin.

Fluorescence images of endogenous Alix expression revealed punctate cytoplasmic expression but also a green background signal throughout the cytoplasm (Figures 6.9 and 6.11). Staining with Phalloidin revealed an expected cytoskeletal staining pattern. A Colocalization Scatter Plot was performed to assess colocalisation between endogenous Alix and phalloidin signals (Figures 6.10 and 6.12). In the scatter plot, pure red and pure green are coloured as such to correspond to Phalloidin and Alix respectively. The Colour Scatter plot of Alix and Phalloidin revealed a more varied correlation plot seen by varying degrees of scatter pattern spread all over the plot. However, with a mean Pearson's Correlation value of 0.538 (n= 3) we found that there is a moderate correlation in the cortical neurons. There was also a moderate correlation in the hippocampal neurons with a mean Pearson's Correlation value of 0.415 (n = 3).

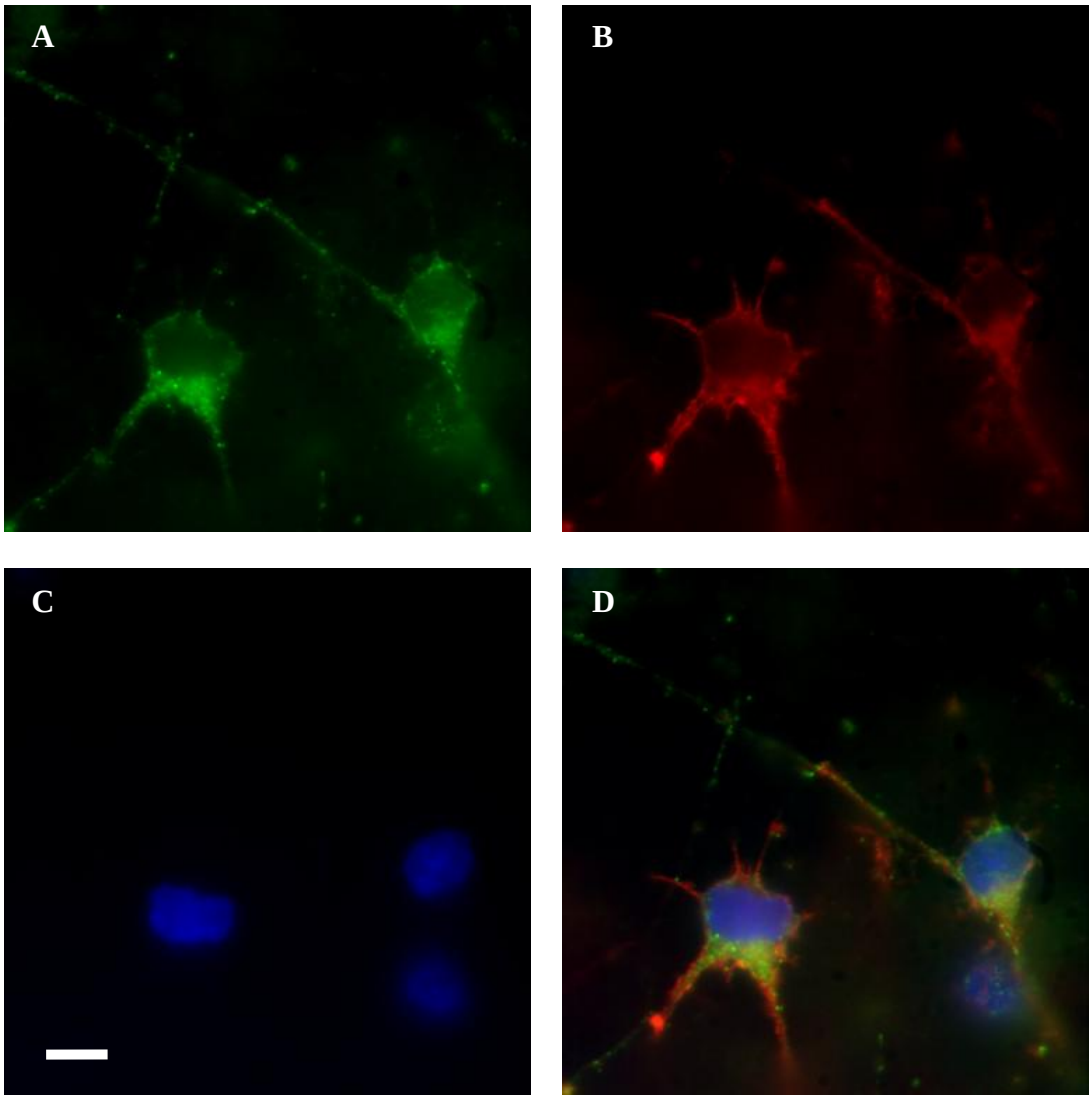

Figure 6.9 Intracellular distribution of endogenous Alix in cortical neurons, following fixation and permeabilisation, exposure to primary antibodies against Alix and treatment with phalloidin and Hoechst. Green fluorescence images of endogenous Alix (Panel A) reveal a punctate expression pattern within the cell cytoplasm. Phalloidin staining (Panel B) shows the cytoskeleton and is consistent with intracellular F actin distribution. Panel C shows nuclear labelling with Hoescht and Panel D shows the merged image of Panel A, B and C. Green denotes Alix fluorescence, red as phalloidin and blue corresponds to Hoechst stained nuclei. Scale Bar: 10 μm.

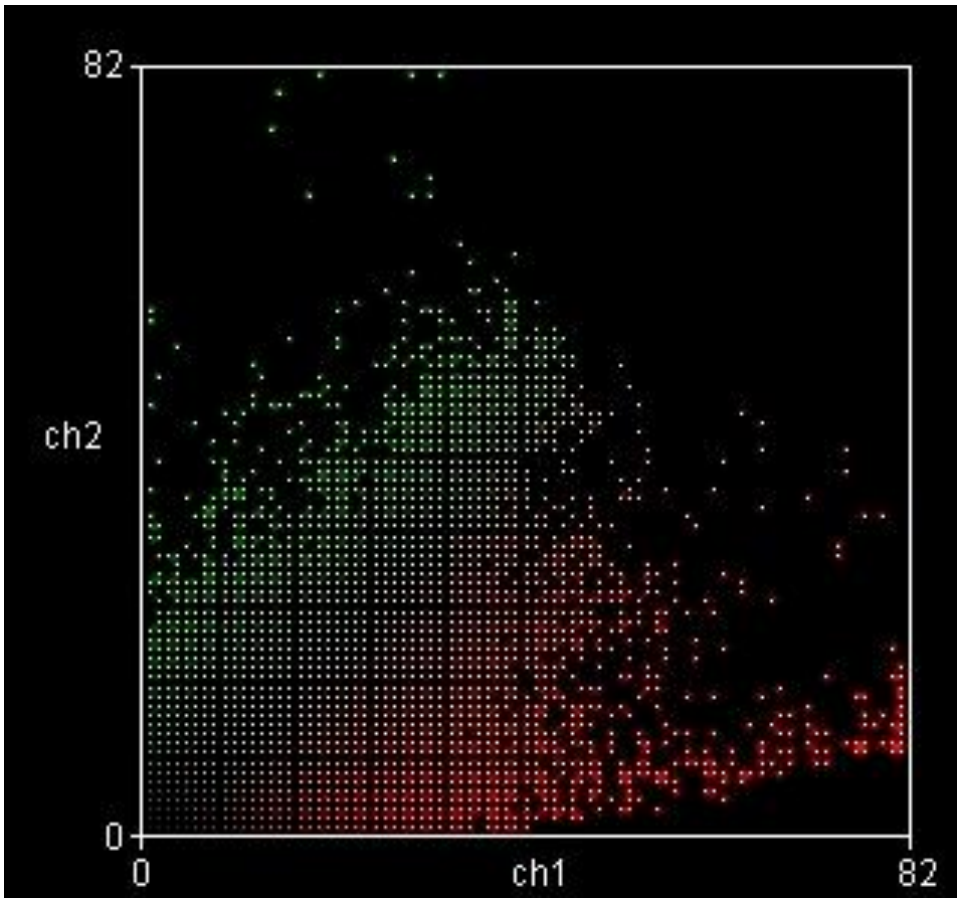

Figure 6.10 Colocalisation analysis of cortical neurons from images shown in Figure 6.9. Green pixels denotes Alix, while red pixels corresponds to phalloidin. The Pearson's Correlation value that denotes the degree of overlap between the pixels within this image pair, calculated a correlation of 0.699.

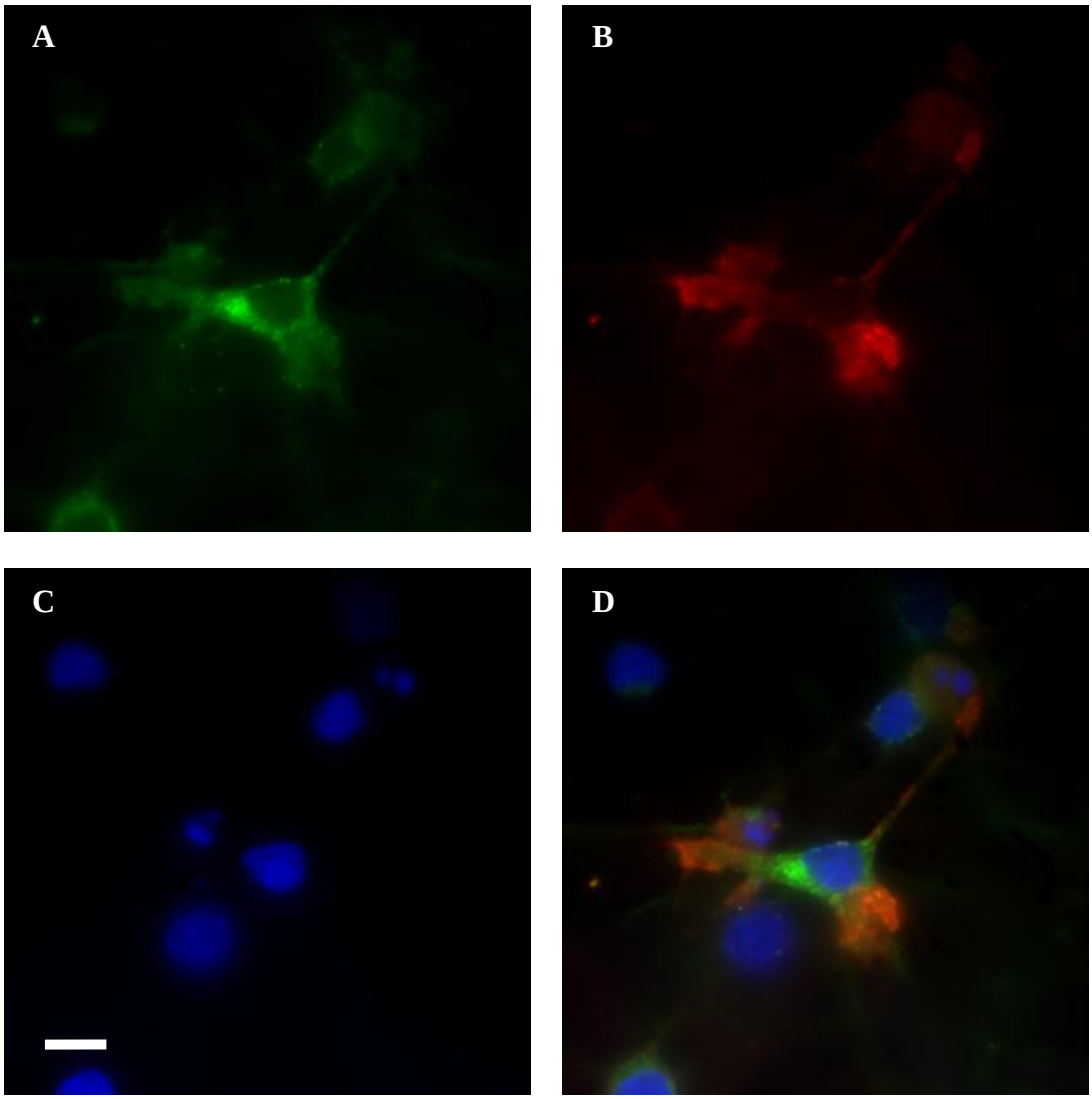

Figure 6.11 Intracellular distribution of endogenous Alix in hippocampal neurons, following fixation and permeabilisation, exposure to primary antibodies against Alix and treatment with phalloidin and Hoechst. Green fluorescence images of endogenous Alix (Panel A) reveal a punctate expression pattern within the cell cytoplasm. Phalloidin staining (Panel B) shows the cytoskeleton and is consistent with intracellular F actin distribution. Panel C shows nuclear labelling with Hoescht and Panel D shows the merged image of Panel A, B and C. Green denotes Alix fluorescence, red as phalloidin and blue corresponds to Hoechst stained nuclei. Scale Bar: 10 μm.

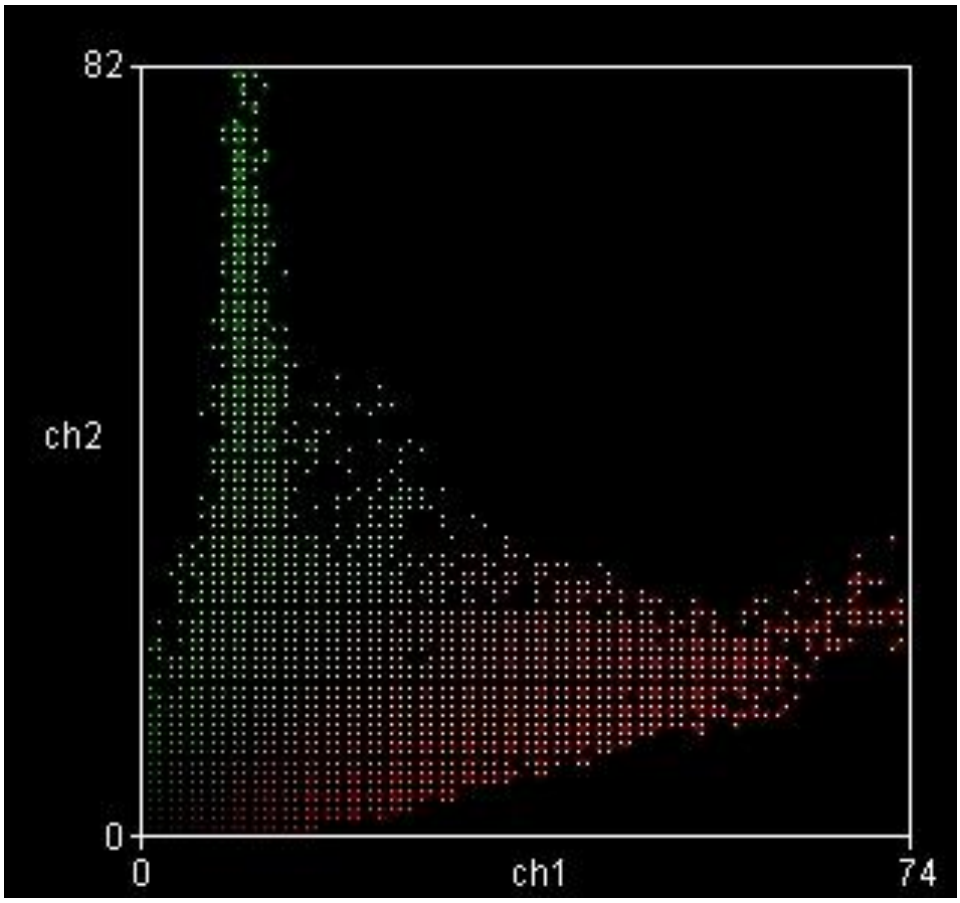

Figure 6.12 Colocalisation analysis of hippocampal neurons from images shown in Figure 6.11. Green pixels denotes Alix, while red pixels corresponds to phalloidin. The Pearson's Correlation value that denotes the degree of overlap between the pixels within this image pair, calculated a correlation of 0.480.

6.2.3 Endogenous Alix expression with NMDA receptors in cortical and hippocampal neurons

In chapter 5, we observed a moderate correlation of Alix and GluN1 expression in HEK293 cells (Figures 5.13 and 5.15), however given this was examined in a heterologous cell expression system, it is important to evaluate the endogenous expression pattern of these proteins within cortical and hippocampal neurons. Cortical and hippocampal neurons were treated with primary antibodies for Alix and GluN2A/B and respective fluorescent signals were visualized after exposure to fluorescently conjugated secondary antibodies.

Fluorescence images of Alix revealed a punctate fluorescence within the cytoplasm of the cortical and hippocampal neurons and GluN2A/2B shows cytoplasmic expression, but visually it was difficult to clearly distinguish whether the signals overlapped (Figures 6.13 and 6.15). A Colocalization Scatter Plot was constructed using pure red and pure green to correspond to Alix and GluN2A/2B respectively. The Colour Scatter plot of Alix and GluN2A/2B revealed a more varied correlation plot seen by varying degrees of scatter pattern spread all over the plot (Figures 6.14 and 6.16). The mean Pearson's Correlation value of 0.761 (n=3) suggested a strong correlation rate for the cortical neurons. However, with a mean Pearson's Correlation value of 0.275 (n = 3) we found that there is a weak correlation rate for the hippocampal neurons. On the other hand, paired t-test shows that the difference between cortical and hippocampal neurons is considered to be not statistically significant with a P value of 0.183. Therefore, the difference in Alix and GluN2A/B correlation between the two cell types is not statistically different.

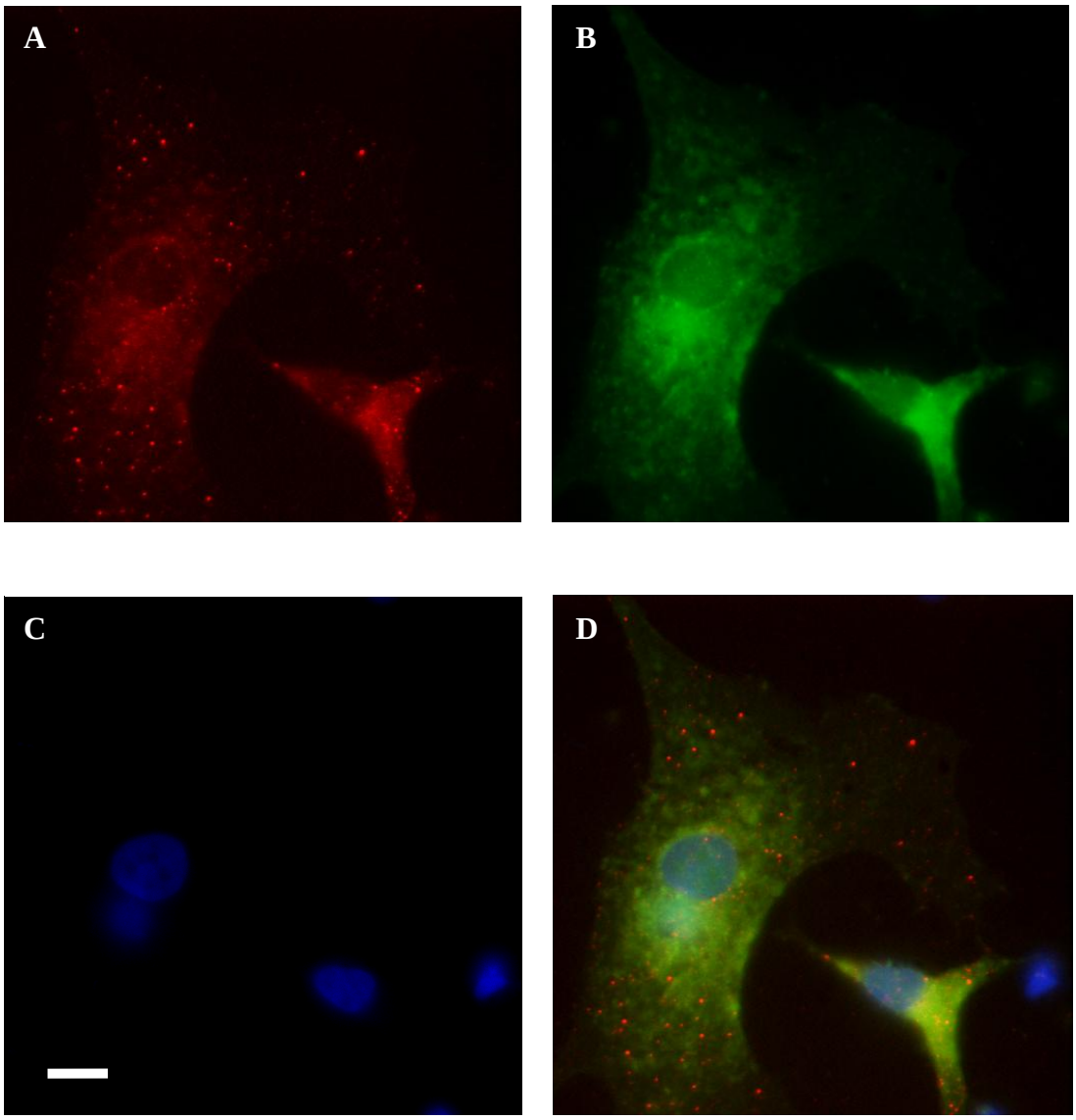

Figure 6.13 Intracellular distribution of Alix and GluN2A/2B in primary cortical neurons. Fluorescence images of Alix (Panel A) reveal a punctate fluorescence within the cytoplasm of the cells. Staining with GluN2A/2B (Panel B) reveals cytoplasmic staining pattern. Panel C shows nuclear labelling with Hoescht and Panel D shows the merged image of Panel A, B and C. Green denotes GluN2A/2B fluorescence, red as Alix and blue corresponds to Hoechst stained nuclei. Scale Bar: 10 μm.

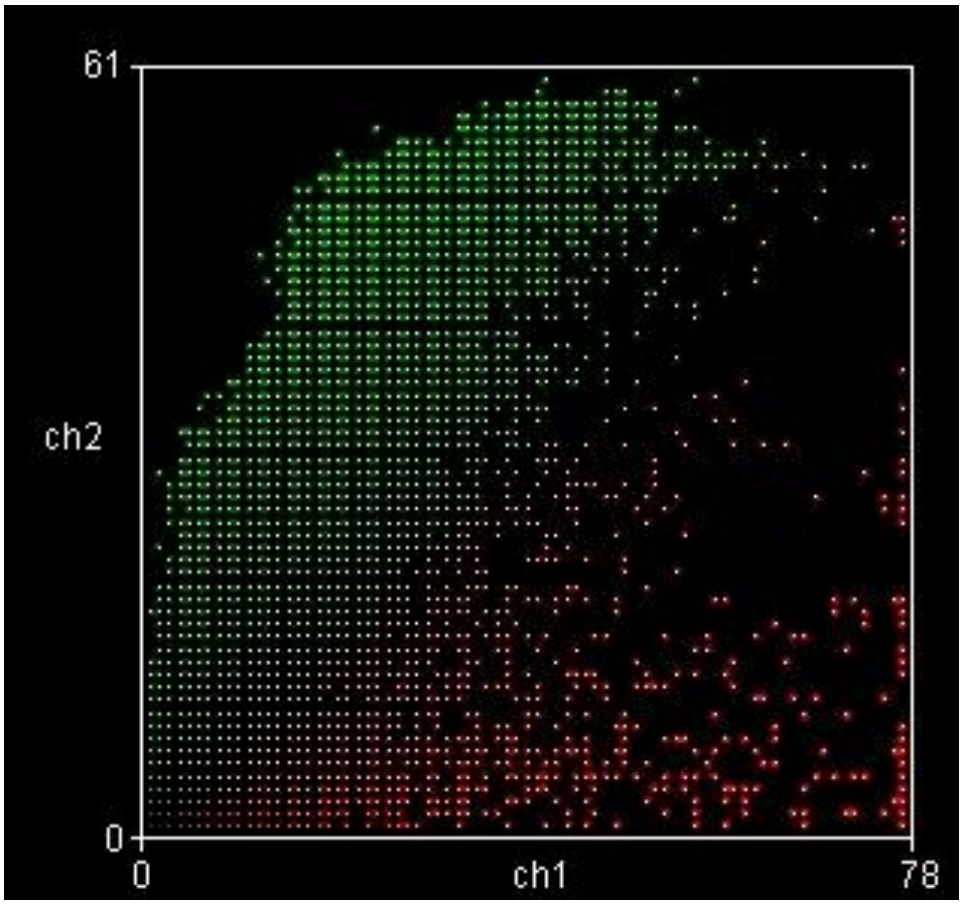

Figure 6.14 Colocalisation analysis of cortical neurons images shown in Figure 6.13. Red pixels denotes Alix while green pixel corresponds to GluN2A/2B. The Pearson's Correlation value denotes the degree of overlap between the pixels within the image pair calculated a very strong correlation rate of 0.770.

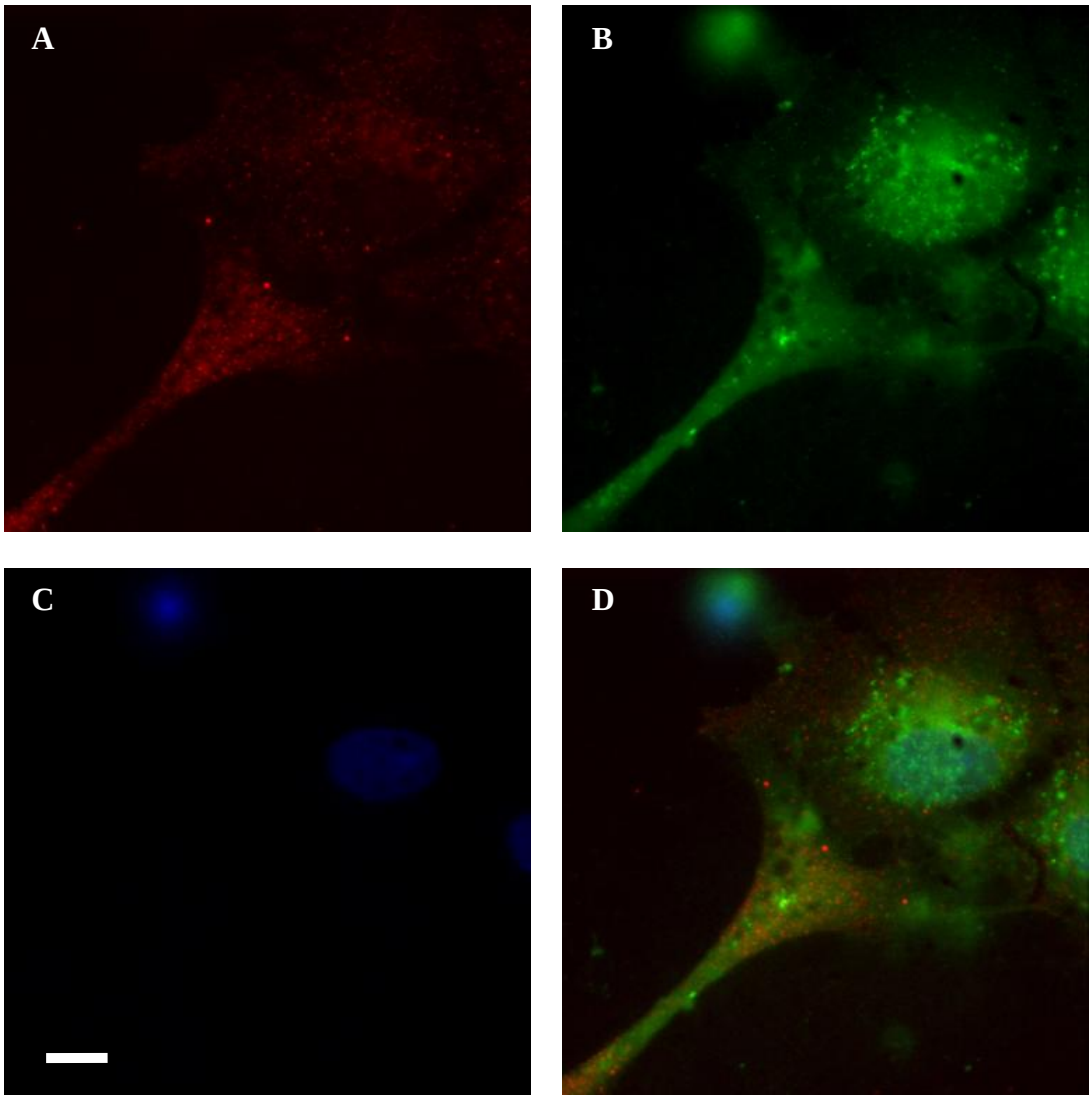

Figure 6.15 Intracellular distribution of Alix and GluN2A/2B in primary hippocampal neurons. Fluorescence images of Alix (Panel A) reveal a punctate fluorescence within the cytoplasm of the cells. Staining with GluN2A/2B (Panel B) reveals cytoplasmic staining pattern. Panel C shows nuclear labelling with Hoescht and Panel D shows the merged image of Panel A, B and C. Green denotes GluN2A/2B fluorescence, red as Alix and blue corresponds to Hoechst stained nuclei. Scale Bar: 10 μm.

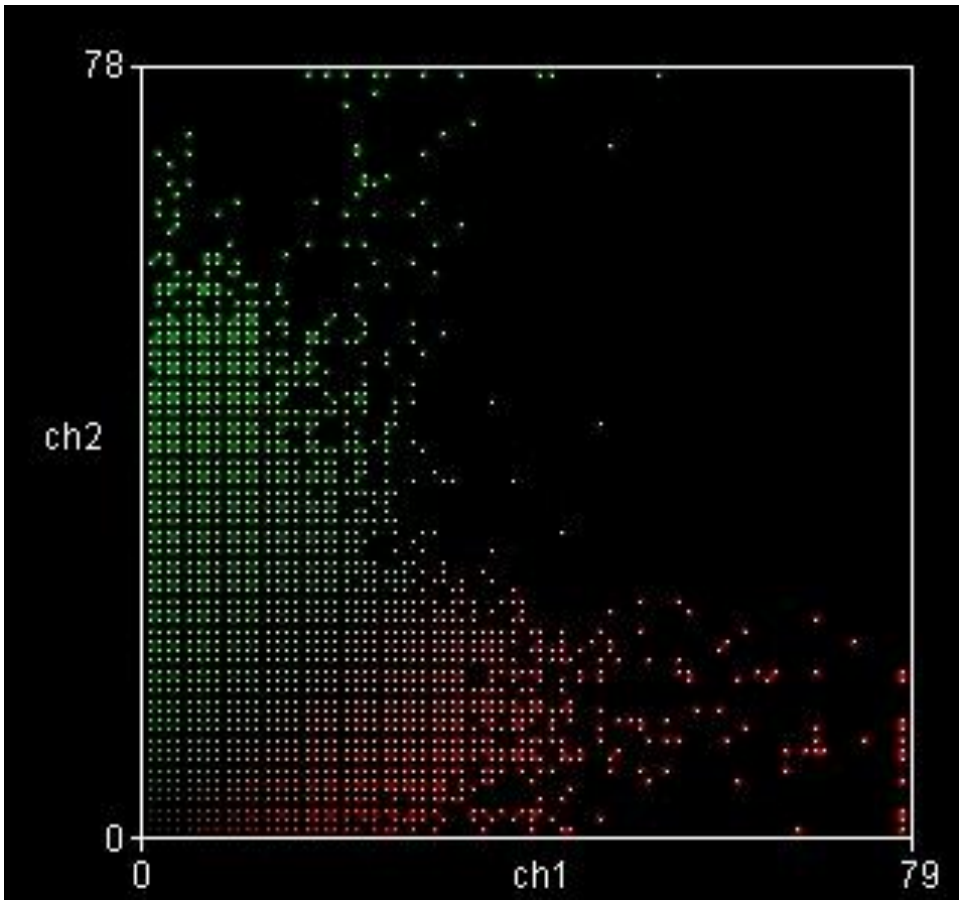

Figure 6.16 Colocalisation analysis of hippocampal neurons images shown in Figure 6.15. Red pixels denotes Alix while green pixel corresponds to GluN2A/2B. The Pearson's Correlation value denotes the degree of overlap between the pixels within the image pair calculated a very week correlation rate of 0.146.

6.2.4 Endogenous Alix with PSD 95 in cortical neurons

Another well-characterized intracellular protein known to associate with NMDARs is PSD95 (Sheng, 2001) and we examined whether Alix could correlate with PSD95 expression in cortical and hippocampal neurons. Cortical and hippocampal neurons were treated with primary antibodies for Alix and PSD95 and respective fluorescent signals were visualized after exposure to fluorescently conjugated secondary antibodies.

Fluorescence images of Alix also revealed a dispersed punctate fluorescence pattern within the cytoplasm of the cells and the PSD95 signal revealed a punctate pattern that was spread across the cytoplasm (Figures 6.17 and 6.19). A Colocalization Scatter Plot was performed where pure red and pure green pixels correspond to Alix and PSD95 respectively. The Colour Scatter plot of Alix and PSD95 revealed a more varied correlation plot seen by varying degrees of scatter pattern spread all over the plot (Figures 6.18 and 6.20). The mean Pearson's Correlation value of 0.496 (n = 3) indicated a moderate correlation rate for the cortical neurons. However, there was a weaker correlation in hippocampal neurons with a mean Pearson's Correlation value of 0.264 (n = 3). The paired t-test shows that the difference between cortical and hippocampal neurons is considered statistically significant with a P value of 0.018.

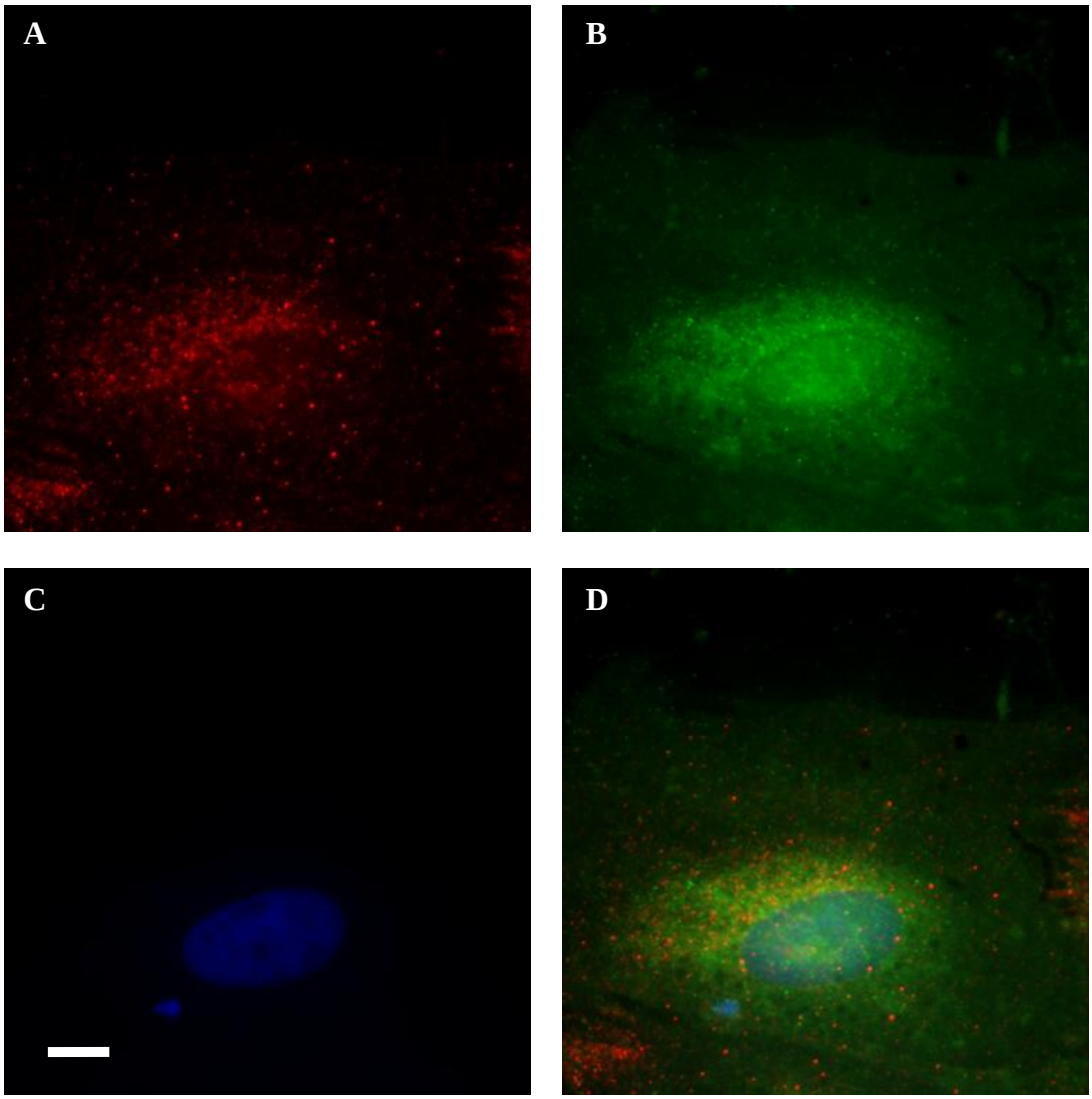

Figure 6.17 Intracellular distribution of Alix and PSD95 in primary cortical neurons. Fluorescence images of Alix (Panel A) reveal a dispersed punctate fluorescence within the cytoplasm of the cells. Staining with PSD95 (Panel B) reveals a punctate cytoplasmic staining pattern. Panel C shows nuclear labelling with Hoescht and Panel D shows the merged image of Panel A, B and C. Green denotes PSD95 fluorescence, red as Alix and blue corresponds to Hoechst stained nuclei. Scale Bar: 10 μm.

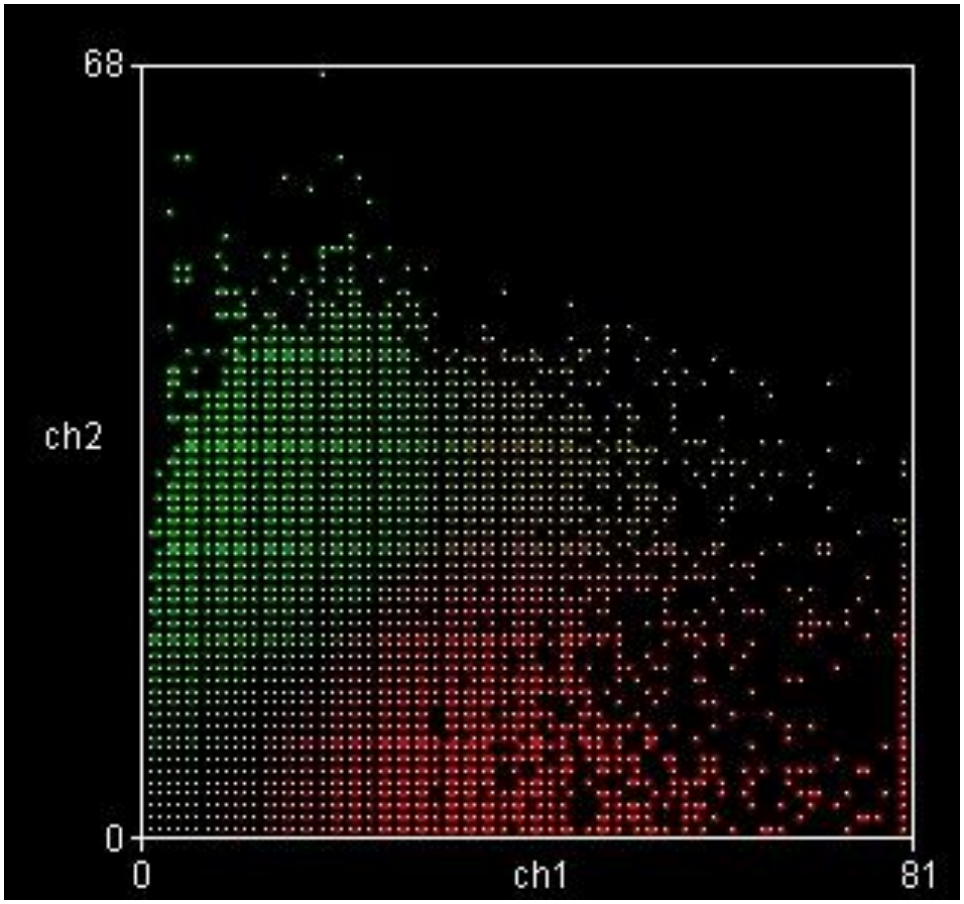

Figure 6.18 Colocalisation analysis of cortical neurons images shown in Figure 6.17. Red pixels denotes Alix while green pixel corresponds to PSD95. The Pearson's Correlation value denotes the degree of overlap between the pixels within the image pair calculated a moderate correlation rate of 0.503.

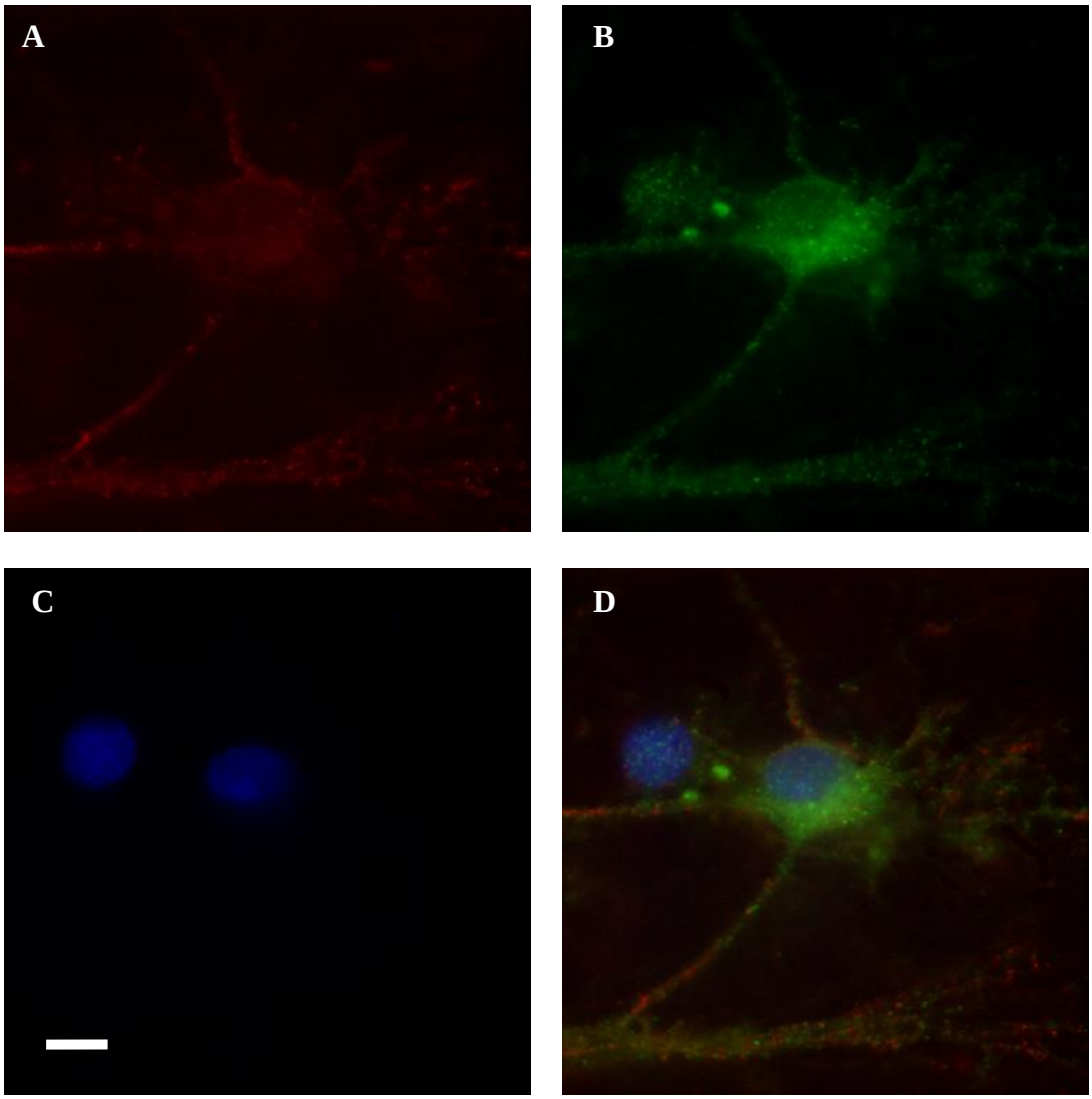

Figure 6.19 Intracellular distribution of Alix and PSD95 in primary hippocampal neurons. Fluorescence images of Alix (Panel A) reveal a dispersed punctate fluorescence within the cytoplasm of the cells. Staining with PSD95 (Panel B) reveals a punctate cytoplasmic staining pattern. Panel C shows nuclear labelling with Hoescht and Panel D shows the merged image of Panel A, B and C. Green denotes PSD95 fluorescence, red as Alix and blue corresponds to Hoechst stained nuclei. Scale Bar: 10 μm.

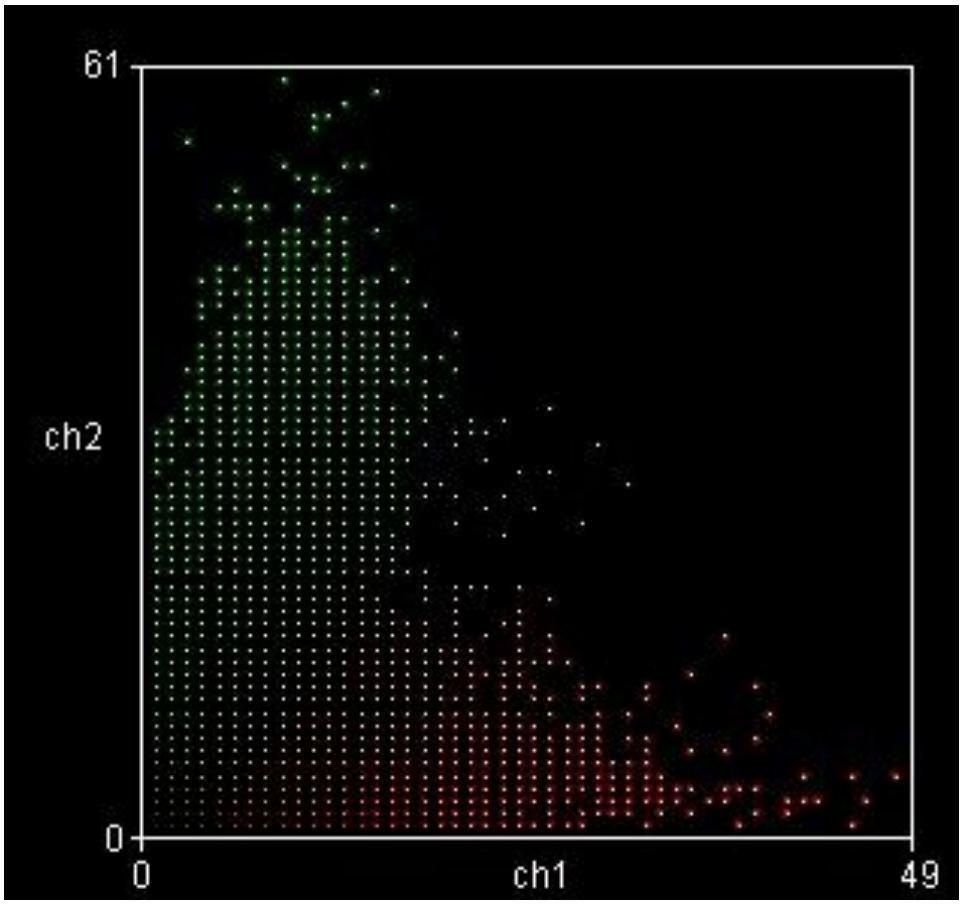

Figure 6.20 Colocalisation analysis of cortical neurons images shown in Figure 6.19. Red pixels denotes Alix while green pixel corresponds to PSD95. The Pearson's Correlation value denotes the degree of overlap between the pixels within the image pair calculated a weak correlation rate of 0.353.

6.2.5 Endogenous Alix localisation with synaptophysin in cortical neurons

Synaptophysin is a binding partner for the SNARE protein (SNAP (Soluble NSF Attachment Protein) Receptor), synaptobrevin and is often used as marker for synaptic localization (Reisinger et al., 2004) and we examined the localization of Alix with synaptophysin in primary cortical and hippocampal neurons. Cortical and hippocampal neurons were treated with primary antibodies for Alix and synaptophysin and respective fluorescent signals were visualized after exposure to fluorescently conjugated secondary antibodies.

Fluorescence images of Alix and synaptophysin both showed a punctate pattern within the cell cytoplasm (Figures 6.21 and 6.23). A Colocalization Scatter Plot was performed using pure red and pure green pixels to correspond to Alix and synaptophysin. The Colour Scatter plot of Alix and synaptophysin revealed a more varied correlation plot seen by varying degrees of scatter pattern spread all over the plot (Figures 6.22 and 6.24). There was a weak correlation rate with a mean Pearson's Correlation value of 0.31 (n = 3) in the cortical cultures and 0.238 (n = 3) in the hippocampal cultures.

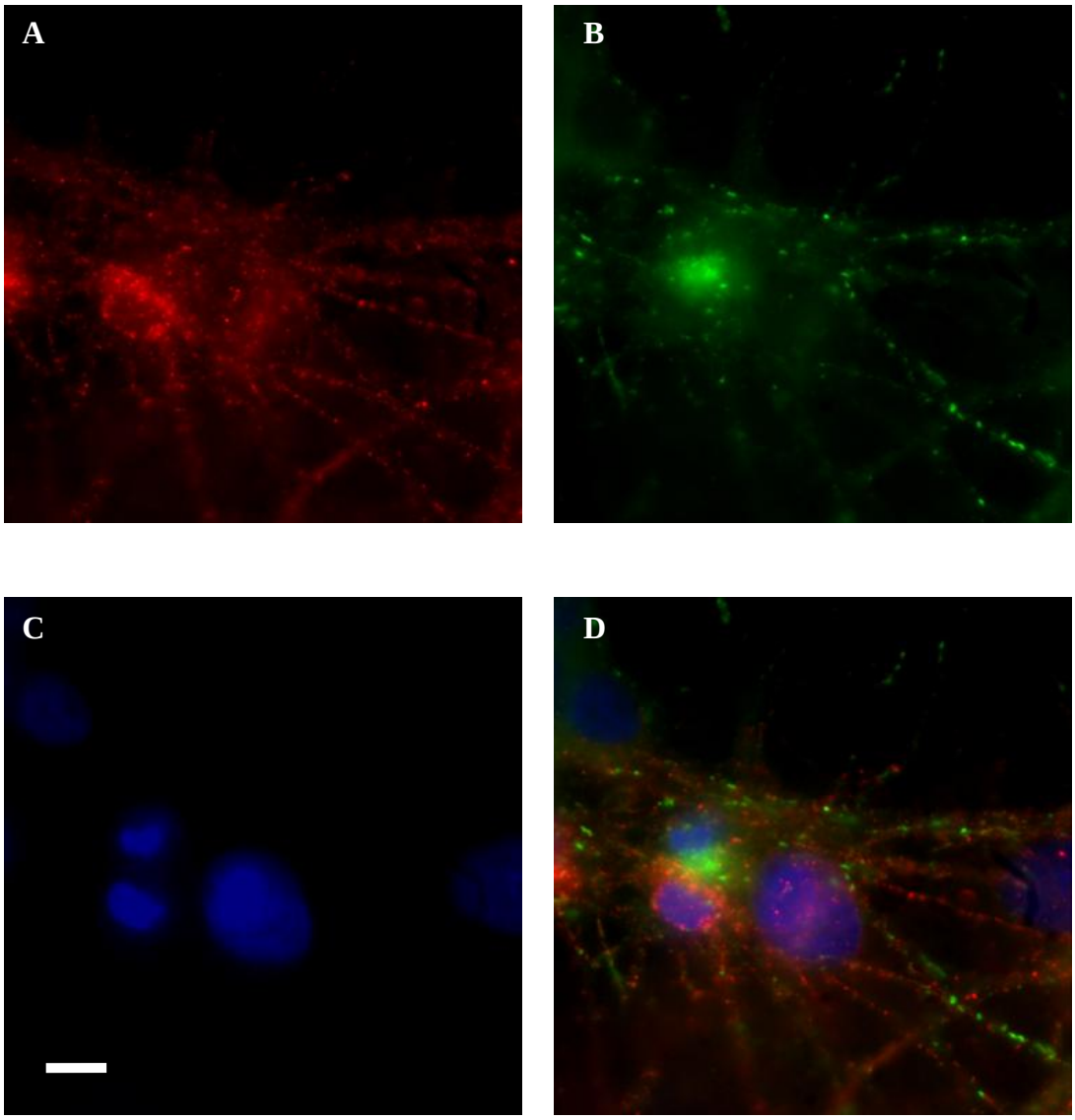

Figure 6.21 Intracellular distribution of Alix and synaptophysin in primary cortical neurons. Fluorescence images of Alix (Panel A) reveal a dispersed punctate fluorescence within the cytoplasm of the cells. Staining with synaptophysin (Panel B) reveals a punctate staining pattern restricted to certain regions of the neuron. Panel C shows nuclear labelling with Hoescht and Panel D shows the merged image of Panel A, B and C. Green denotes synaptophysin fluorescence, red as Alix and blue corresponds to Hoechst stained nuclei. Scale Bar: 10 μm.

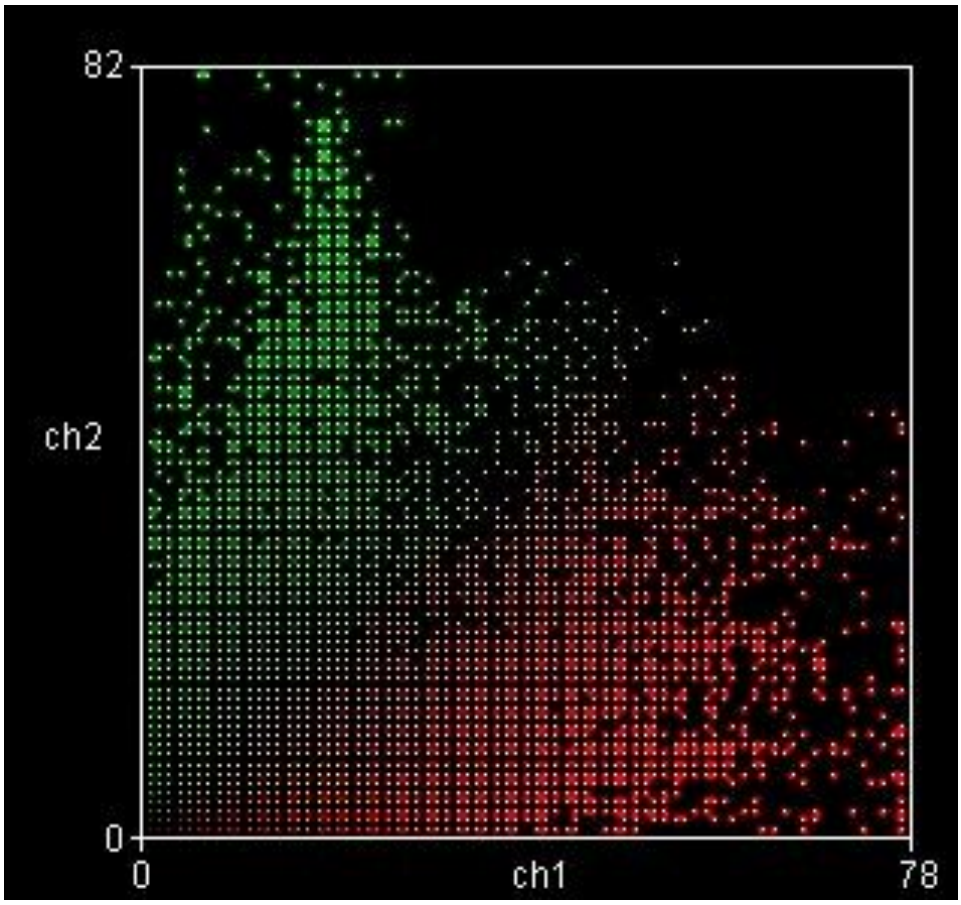

Figure 6.22 Colocalisation analysis images shown in Figure 6.21. Red pixels denotes Alix while green pixel corresponds to synaptophysin. The Pearson's Correlation value denotes the degree of overlap between the pixels within the image pair calculated a weak correlation rate of 0.383.

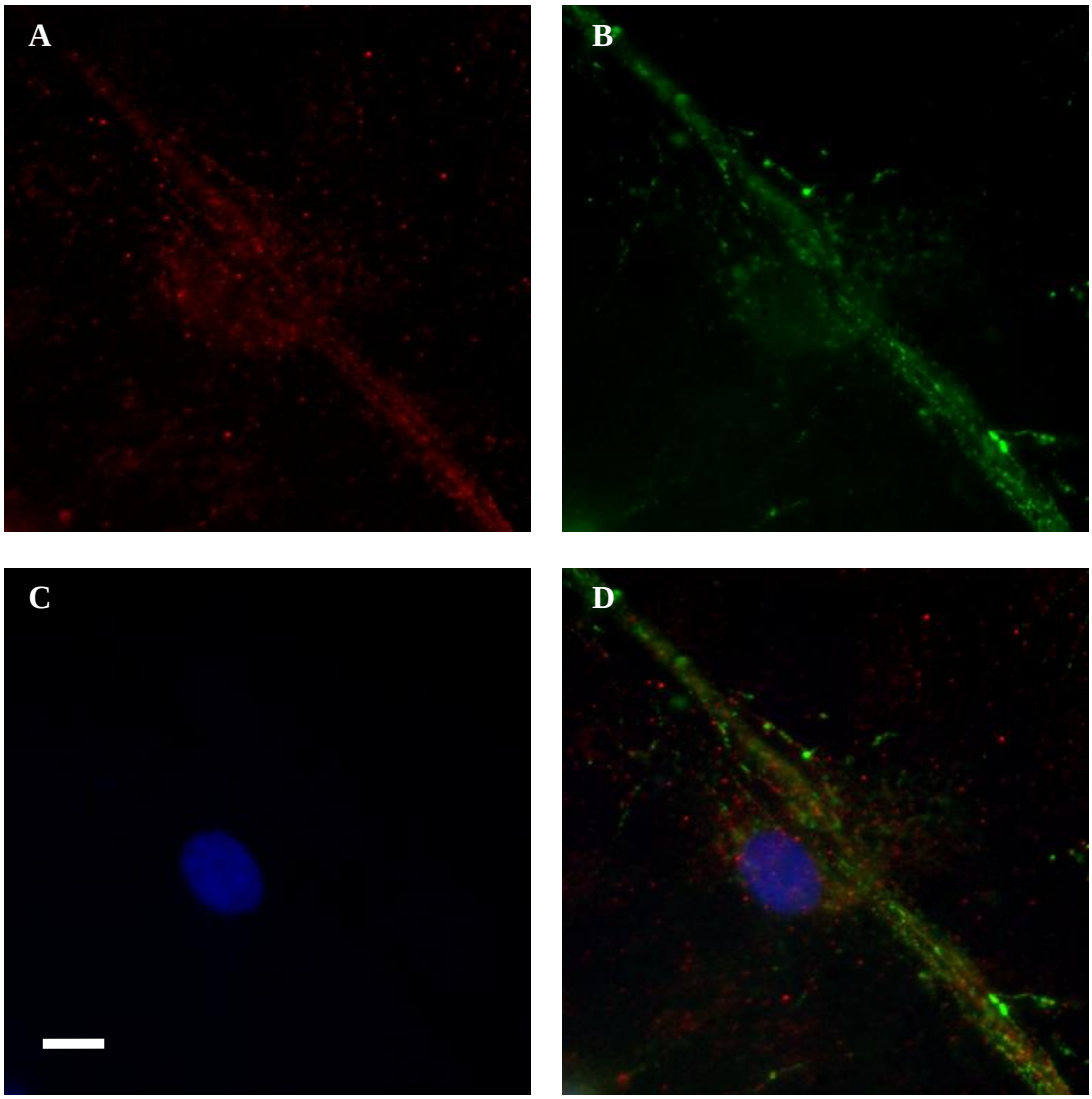

Figure 6.23 Intracellular distribution of Alix and synaptophysin in primary cortical neurons. Fluorescence images of Alix (Panel A) reveal a dispersed punctate fluorescence within the cytoplasm of the cells. Staining with synaptophysin (Panel B) reveals a punctate staining pattern restricted to certain regions of the neuron. Panel C shows nuclear labelling with Hoescht and Panel D shows the merged image of Panel A, B and C. Green denotes synaptophysin fluorescence, red as Alix and blue corresponds to Hoechst stained nuclei. Scale Bar: 10 μm.

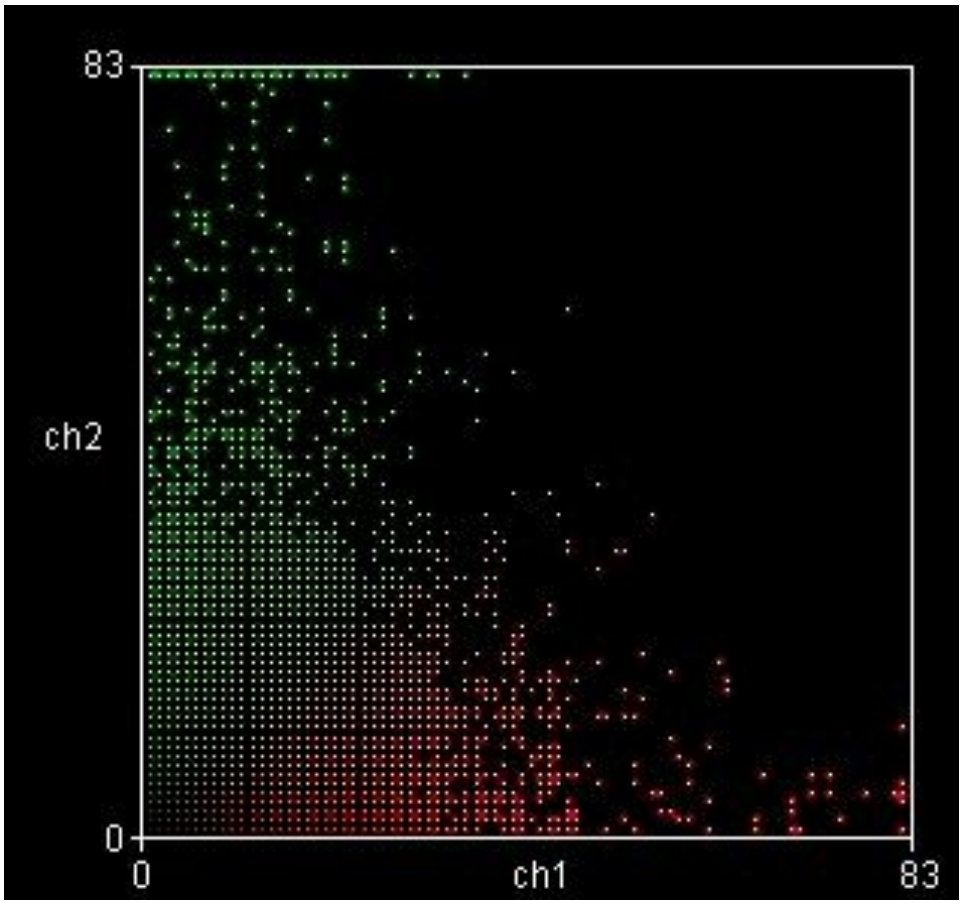

Figure 6.24 Colocalisation analysis images shown in Figure 6.23. Red pixels denotes Alix while green pixel corresponds to synaptophysin. The Pearson's Correlation value denotes the degree of overlap between the pixels within the image pair calculated a week correlation rate of 0.335.

6.3 Summary

Previously, we observed a weak correlation between Alix and EEA1 expression in HEK293 cells (Figure 5.5 and 5.7). Conversely, we observed a moderate correlation for the cortical neurons (0.406, n=3) but there was a weak correlation for the hippocampal neurons (0.307, n=3) (Figures 6.5 and 6.7). However, paired t-test shows that the difference between cortical and hippocampal neurons is considered to be not statistically significant with a P value of 0.676.

We found that previously Alix had a weak correlation with Phalloidin in HEK293 cells (Figures 5.9 and 5.11). However, with a mean Pearson's Correlation value of (0.538, n= 3) in the cortical neurons and (0.415, n=3) in the hippocampal neurons we found that there is a moderate correlation for both primary cultures (Figures 6.9 and 6.11).

In chapter 5, we observed a moderate correlation of Alix and GluN1 expression in HEK293 cells (Figures 5.13 and 5.15). There seems to be also a strong correlation rate for the cortical neurons with a mean Pearson's Correlation value of (0.761, n=3) but there was on the other hand, a weak correlation with an average Pearson's Correlation value of (0.275, n=3) in the hippocampal neurons (Figures 6.13 and 6.15). Then again, paired t-test shows that the difference between cortical and hippocampal neurons is considered to be not statistically significant with a P value of 0.183.

Next, we examined whether Alix expression could correlate with PSD95 expression in cortical and hippocampal neurons (Figures 6.17 and 6.19). We observed a moderate correlation for the cortical neurons with a mean Pearson's correlation value of (0.496, n = 3) but there was a weaker correlation in hippocampal neurons with a mean Pearson's Correlation value of (0.264, n = 3). Interestingly, we also observed a statistically significant P value of 0.018 from the paired t-test between the cortical and hippocampal primary cultures.

We then decided to examine the localization of Alix with synaptophysin in primary cortical and hippocampal neurons (Figures 6.21 and 6.23). We found that there was a weak correlation rate in both the cortical and hippocampal cultures with a mean Pearson's Correlation value of 0.31 (n = 3) in the cortical culture and 0.238 (n = 3) in the hippocampal cultures.

Overall, these results support previous observations from other work and indicate that Alix colocalises with the cytoskeletal protein, phalloidin and shows moderate colocalisation with postsynaptic proteins such as PSD95 but weak correlation with presynaptic proteins such as synaptophysin (Schmidt et al., 2003); Bayes et al., 2010). Although we found differing correlation rates between cortical and hippocampal cultures between Alix and EEA1, Alix and GluN2A/2B and Alix and PSD95, the only correlation difference that was statistically significant was the difference between Alix and PSD95 localisation (Figures 6.17 and 6.19). Although this might indicate important differences in Alix localization between both neuronal cell types, it would need to be verified by further analysis of a larger sample size (for example the differences between Alix and EEA1 and Alix and GluN2A/B). Furthermore, we are not sure why Alix would display such cell type specific localisation. There is evidence that Alix containing exosomes can display cell type specific interactions. (Chivet et al., 2014) found that exosomes from neuroblastoma cells bind randomly to neurons and glial cells and could be endocytosed preferentially by glial cells but exosomes secreted from stimulated cortical neurons were endocytosed and bound to only neurons. They hypothesise that exosomes that are released by synaptic activation do not bind to glial cells but specifically to other neurons suggesting a novel aspect of interneuronal communication. Although, this would indicate specific differences in exosome interaction between neuronal and glial cell types, the role of Alix and the molecular processes underlying these specific interactions remain unclear.

7. Discussion:

7.1 Discussion of modulation of NMDA receptor function by Alix in Cell Death Assay

In order to examine whether Alix had any effect on NMDAR function, we measured NMDAR triggered cell death in HEK293 cells expressing human, mouse Alix or Alix mouse mutants with NMDARs. We used two statistical tests to analyse our results, a paired t-test for individual pairwise comparisons but also performed multiple comparisons across all eight variables within an experiment using ANOVA analysis and performed Tukey's post-hoc tests to identify which pairs of data displayed statistically significant differences. In all cases the results from the t-test comparisons correlated with those identified following ANOVA and Tukey's post-hoc test.

Our results in this chapter show that Alix and all deletion mutants (except the Alix NT mutant) have an effect on NMDAR triggered cell death when assessed using either paired t-test comparisons and when the data from the activated and non-activated cells have been compared together using ANOVA and post-hoc analysis.

Wagey et al. found that a proportion of HEK cells transfected with NMDAR subunits die following exposure to NMDAR agonists, depending on the NMDAR subunit composition. To establish if the activation of Alix could influence NMDA induced cell death we evaluated the cell death percentage in HEK293 cells transfected with NMDAR subunits. Activation of NMDARs was performed by incubating the cells in PSS containing NMDA and glycine. The cell death percentage was later calculated by trypan blue exclusion six hours following activation.

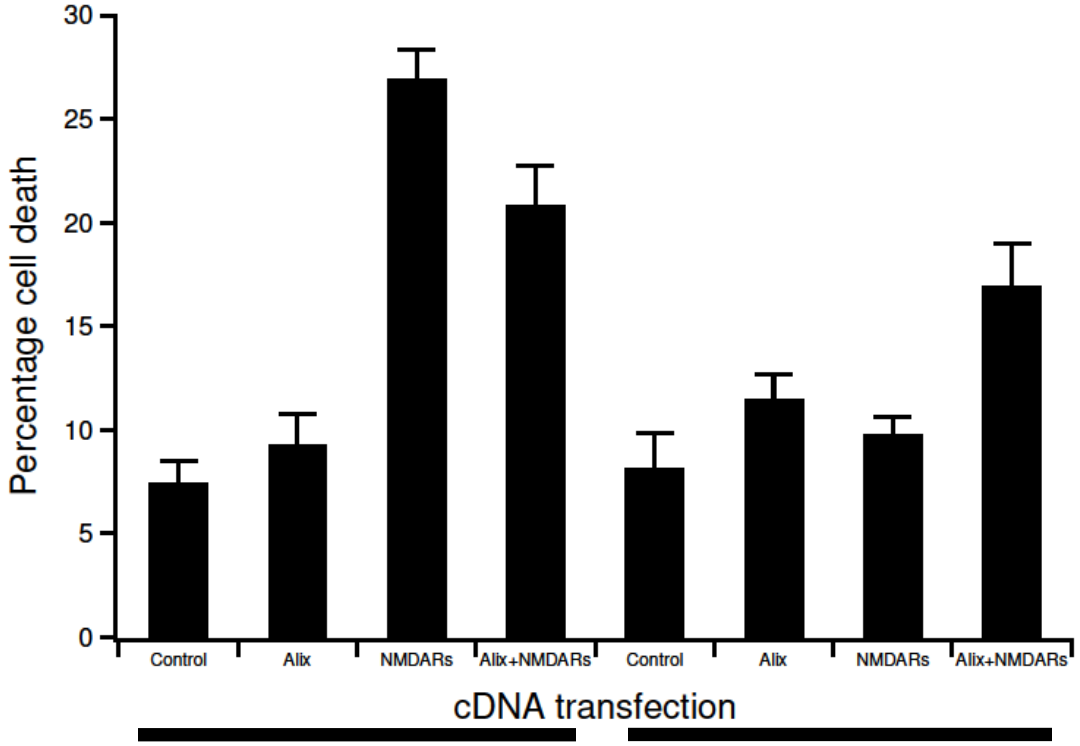

Figure 7.1: Modulation of NMDA cell death by Alix in activated and non activated cells. All data points correspond to the mean ±SE of values and statistical comparisons of cell death between groups were performed using a paired *t*-test and ANOVA analysis to determine which groups were statistically different from each other.

We over expressed GFP tagged human Alix via lipofectamine in a HEK293 mammalian cell line and examined its effect on NMDA receptor triggered cell death (Figure 3.1 ab and Figure 7.1). The result that we achieved for the positive control was in line with the findings of R. Wagey and C. Krieger, 2001. They reported that over activation of NMDA receptors leads to cell death in HEK293 cells, which have been transfected with recombinant NMDA receptors. Under their experimental conditions the positive control where cells transfected with GluN1/GluN2A subunits are activated with PSS containing NMDA (1 mM) and glycine (50 µM) enhanced cell death to 27.4 ± 0.7% (p =0.005) compared to a non activated positive control that had a basal mean cell death of 13.8 ±

1.4%. They attributed the level of basal cell death to low levels of glutamate present within the cultures media which could stimulate functional NMDA receptors expressed in GluN1/GluN2A transfected cells. To alleviate the effect of this background level of glutamate we added the NMDAR antagonist, AP5 to block any background NMDA activation before the PSS treatment.

Our own findings revealed similar results, where we found that cells expressing GluN1/GluN2A subunits that were not activated (PSS only) had a mean cell death of 11.6 ± 0.7% (Table 3.1 b). Whereas, cells expressing GluN1/GluN2A subunits that were activated had a mean cell death of 27.4 ± 1.4% (Table 3.1 a). Treatment with NMDA and glycine significantly enhanced cell death as previously reported. In agreement with the observations by Wagey et al., 2001, the Paired t-test and ANOVA analysis showed that the difference between the activated and non activated positive controls (expressing NMDARs) is considered to be statistically significant with a $P<0.001$.

We also found that the levels of cell death observed following transfection of Alix alone whether it was activated or not, were not statistically different compared to the negative control cell lines (without DNA transfection) or to non activated positive control (GluN1/GluN2A transfected cells)(Table 3.1 a and 3.1 b).

Transfecting Alix with GluN1/GluN2A and activating them with NMDA significantly reduced the percentage of dead cells compared with the activated positive control (cells only expressing GluN1/GluN2A). The culture transfected with Alix, GluN1/GluN2A subunits and activated NMDA with glycine had a mean cell death of 21.6 ± 1.9% (Table 3.1 a). The paired t-test and ANOVA analysis showed that the difference between the activated positive control (GluN1/GluN2A only) and activated Alix, GluN1, GluN2A combination is statistically different with a $P<0.001$ (marked with ** in Figure 3.1 a).

An interesting finding was also seen in non activated cells transfected with Alix and GluN1/GluN2A subunits which yielded a mean cell death of 17.3 ± 1.0% (Table 3.1 b). This was a higher percentage of cell death compared to non activated GluN1/GluN2A transfected cells. A paired t-test and the ANOVA analysis showed that the difference between these two conditions is considered to be statistically different with a $P<0.001$ (also marked with ** on the right hand side of Figure 3.1 b). There was however no statistical significance in cell death (P value of 0.0511) between activated or non-activated cells if they both expressed Alix, GluN1, and GluN2A together.

These data indicate that recombinant Alix, GluN1/GluN2A transfection significantly reduced the toxicity associated with NMDA receptor activation compared to GluN1/GluN2A only cells but enhanced the basal level of cell death when not activated by NMDA. Moreover the overall level of cell death in the presence of Alix coexpressed with NMDARs is similar in both activated or non activated cells. Why this is the case is still not understood, but it suggests that Alix is exerting an influence on NMDA receptor triggered cell death measured in these cells.

Therefore to investigate this observation further, we then confirmed that Alix transfected on its own was not causing high levels of cell death in the absence of NMDAR expression since GluN2 subunits are not transported to the cell surface unless they associate with GluN1 subunits (McIlhinney et al., 2003) by doing a control experiment where we repeated the cell death assay with cotransfections of Alix and GluN1 or Alix with GluN2A and found that there was no significant change in cell death compared to the negative control (Table 3.2 a and 3.2 b). We then tried to modulate the concentration of NMDA (10 µM, 100 µM, 300 µM and 700 µM) in the PSS buffer to see if this affected the cell death caused by Alix (Figure 3.4). In both cases, increasing the concentration of NMDA increased the level of cell death. However, the levels of cell death were higher in the

presence of Alix at low concentrations of NMDA (10-100 μM) compared to cells expressing only GluN1/GluN2A subunits. This further supported the view that the presence of Alix is reducing the NMDA concentration required to trigger maximal levels of cell death in our assay (>20 %) and suggests that the increased cell death in the presence of Alix seen in non activated cells is probably caused by low levels of glutamate and thus NMDAR activation within the culture media.

Furthermore, this is supported by curve fitting the partial dose-response curves with the Hill equation. This revealed that the coexpression of Alix decreased the NMDA EC50 for inducing cell death by 7 fold compared to NMDARs expressed alone. Another issue to consider are the NMDA EC50 values measured in the cell death assay. These differ quite considerably compared to those measured in other systems where recombinant NMDA receptor function has been recorded by oocyte electrophysiology (NMDA EC50 = 47 μM) (Chen et al., 2005). There are a number of reasons for this discrepancy and this has probably been influenced by the transfection efficiency of both GluN1 and GluN2A subunits within the same cell, the ability to detect changes in cell death over prolonged periods of time and the influence of multiple second messenger pathways needed before cell death is detected. Nevertheless there is common agreement that EC50 values cannot be easily compared across different tissue systems/assay measurements and their interpretation has to be used appropriately (Colquhoun,1998). Unfortunately, we have been unable to compare our EC50 values with other published work as most studies on NMDAR cell death only use a maximal agonist concentration to activate NMDARs (Wagey and Krieger, 2001). We have only been able to measure partial dose-response curves during cell death measurements and further work is required to investigate this issue further using a wider range of NMDA concentrations and also other NMDAR agonists.We next repeated the NMDA cell death assay in the presence of AP5 to specifically block NMDA receptor

activity and the subsequent calcium influx to see if the high cell death levels induced by Alix in the absence of NMDA activation were directly caused by stimulation of the NMDA receptor (Figure 3.3 a and 3.3 b). We found that by adding AP5 to the medium before, during and after NMDA treatment (activated or without activation) that we abolished the high percentage of cell death caused by Alix and NMDAR as previously seen in Figure 3.1 a and 3.1 b. Therefore, this suggests that our observations with Alix are specific to NMDA receptor function and that Alix is able to simulate a pathway downstream from the NMDA receptor, which triggers the cell death process in our assay.

We know that the interaction between Alix and ALG-2 occurs through its C-terminal proline-rich region and is known to be Ca^{2+} dependent, where Ca^{2+} binding to ALG-2 induces a conformational change which allows it to interact with Alix (Katoh et al., 2003; Strappazzon et al., 2010). Although we did not use ALG-2 in our experiments, our results suggest that Alix alone and NMDARs may also play a part in this process as the vessel that permits excessive Ca^{2+}influx which then triggers a variety of processes that leads to apoptosis. This is also consistent with the high level of cell death caused by recombinant Alix, GluN1/GluN2A transfection in non activated (PSS only) cells as our low NMDA concentration assay suggests that in the presence of Alix the levels of cell death are higher than in the absence of Alix.

The mechanism of how Alix is able to enhance receptor triggered cell death is unclear, but another theory can be taken from the work by (Schneider-Brachert et al., 2004) that reported the activation of caspase 8 by TNFR1 (tumour necrosis factor α receptor 1) in lymphocytes can only occur when the receptor has been endocytosed and passed on to MVBs. This finding started the notion of death inducing signalling endosomes. It is possible that the process requires NMDARs to be endocytosed and passed on to MVB which then starts the apoptosis process. Furthermore, there is evidence that the ESCRT

complex is involved in lysosomal degradation of neurotransmitter receptors and it has been speculated that impairment of this process may lead to neurodegeneration (Isaacs et al. 2011).

Deletion variants of the Alix mouse mutants were used to determine what effect these variants had on the cell death assay. We know that the N-terminal of Bro1 domain mediates localization to endosomes, and is an important functional site for Alix (Odorizzi, 2006). The C-terminal region interacts with the majority of proteins that connect Alix to cellular processes. The Bro1 domain and C-terminal region are linked by a relatively uncharacterized sequence containing two coiled-coil domains and the whole sequence ends with a proline rich domain (Odorizzi, 2006).

We found that all of the Alix mouse variants used (Figure 3.6 or Figure 7.2, Figure 3.7 or Figure 7.3 and 3.9 or Figure 7.4), produced a similar pattern of cell death, where Alix coexpressed with NMDAR significantly reduced the toxicity associated with NMDA receptor stimulation when activated, but seems to enhance cell death when not activated, as seen by the human Alix variant (Figure 7.1). The only exception to this result was the Alix NT variant (Figure 3.8 or Figure 7.5). This finding is quite interesting as it pinpoints the Alix region responsible for the enhanced NMDA cell death to the C terminal domain of the Alix protein. The C terminal of Alix is known to interact with ALG-2 in a Ca^{2+}-dependent manner (Ohkouchi et al., 2004) and has been linked with cytoplasmic vacuolization (Chatellard-Causse et al. 2002) but how this could increase cell death triggered by NMDAR activation is less straightforward. It is possible that this region of Alix is able to influence processes downstream of NMDARs (presumably in a Ca^{2+}-dependent manner). It is not known if this is a direct interaction or via downstream signalling processes but the implication of these results seem to suggest a possible function linkage between these two proteins.

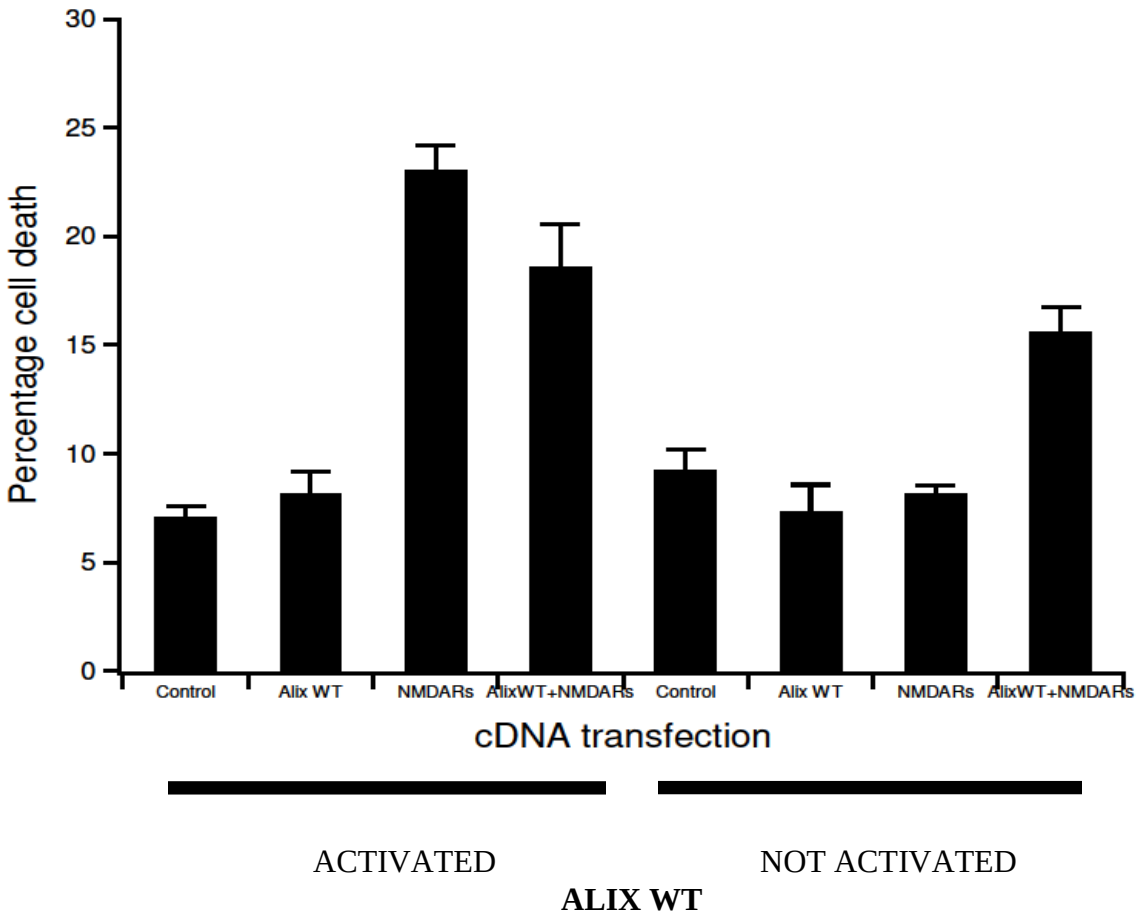

Figure 7.2: Modulation of NMDA cell death by Alix WT in activated and non activated cells. All data points correspond to the mean ± SE of values and statistical comparisons of cell death between groups were performed using a paired *t*-test and ANOVA analysis to determine which groups were statistically different from each other.

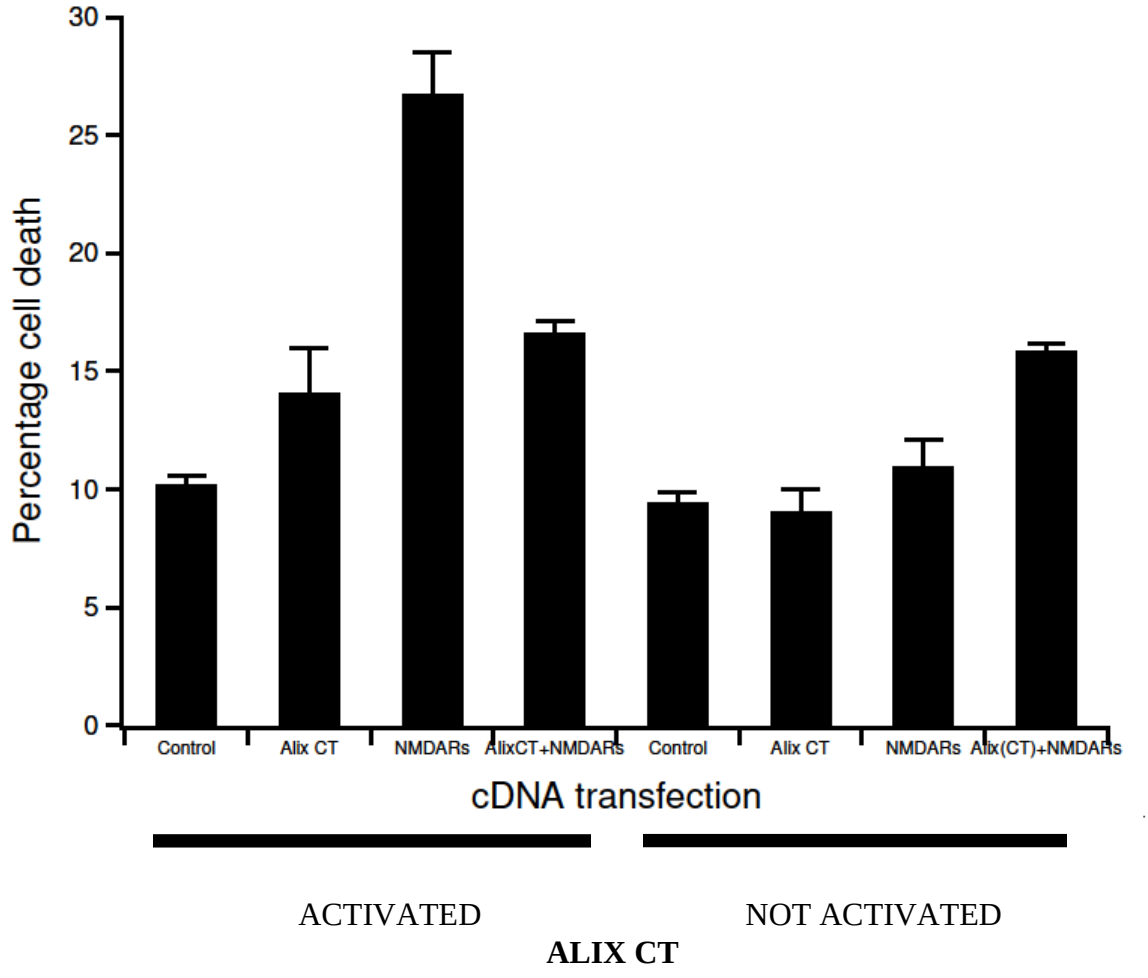

Figure 7.3: Modulation of NMDA cell death by Alix CT in activated and non activated cells. All data points correspond to the mean ± SE of values and statistical comparisons of cell death between groups were performed using a paired *t*-test and ANOVA analysis to determine which groups were statistically different from each other.

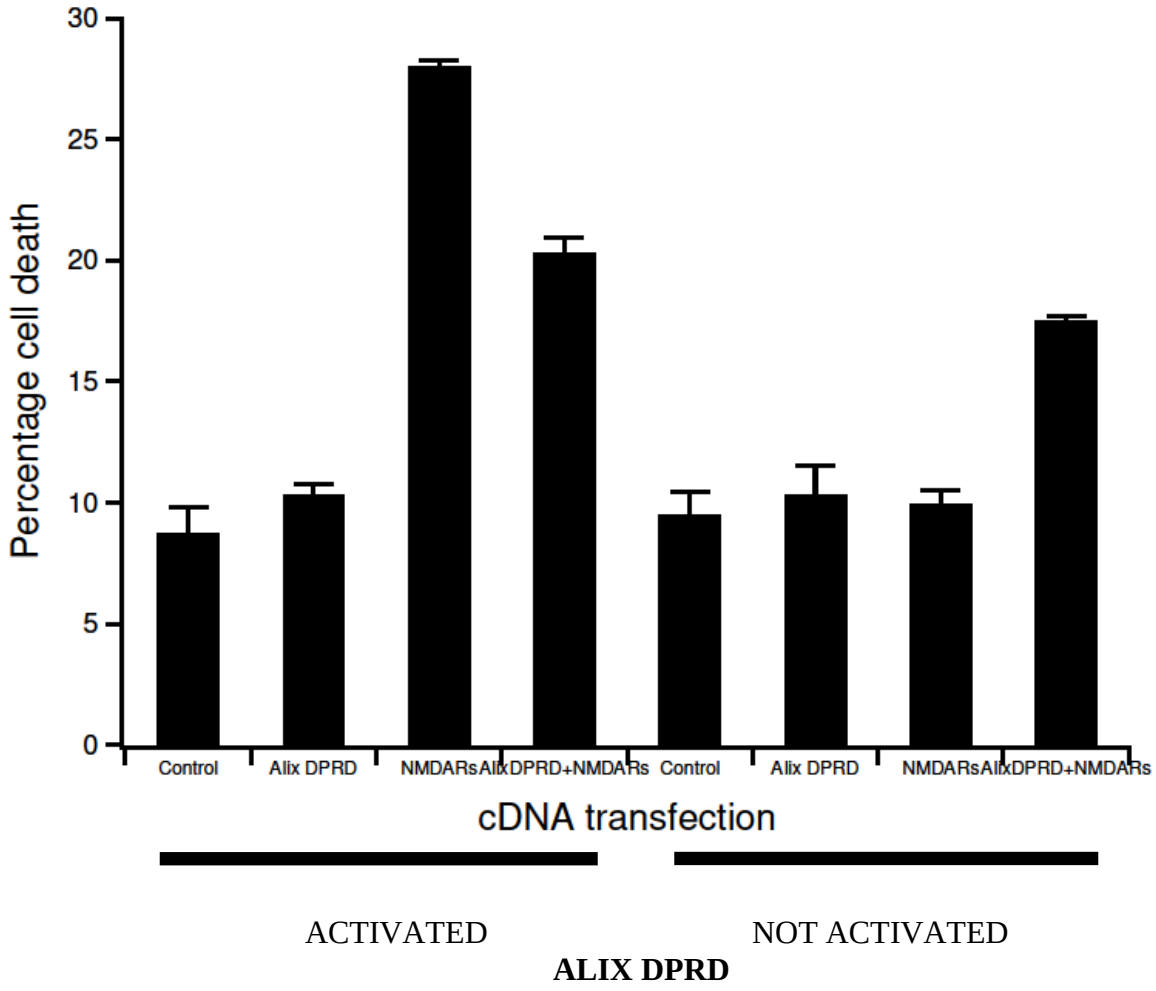

Figure 7.4: Modulation of NMDA cell death by Alix DPRD in activated and non activated cells. All data points correspond to the mean ± SE of values and statistical comparisons of cell death between groups were performed using a paired *t*-test and ANOVA analysis to determine which groups were statistically different from each other.

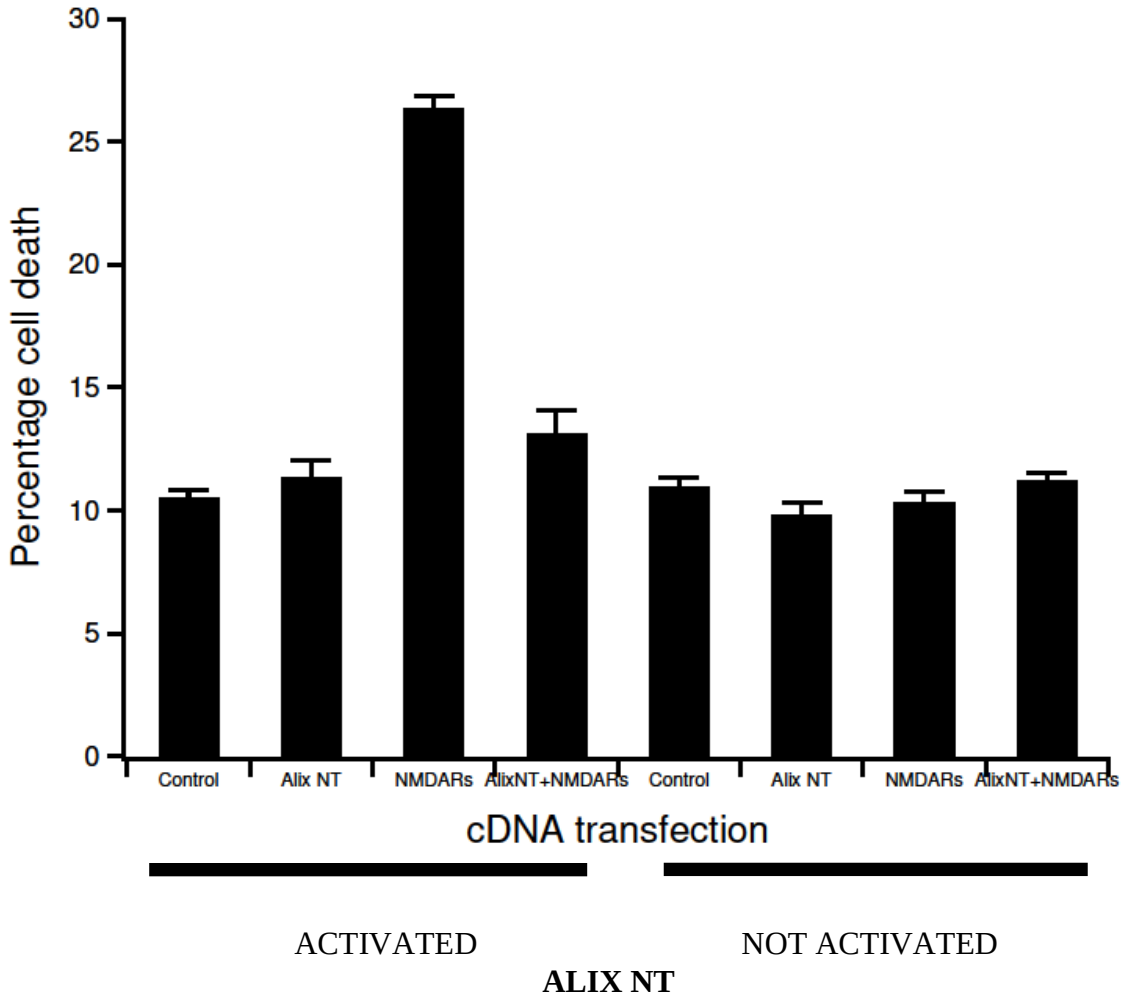

Figure 7.5: Modulation of NMDA cell death by Alix NT in activated and non activated cells. All data points correspond to the mean ± SE of values and statistical comparisons of cell death between groups were performed using a paired *t*-test and ANOVA analysis to determine which groups were statistically different from each other.

7.2 Discussion of western blot analysis of NMDA/Alix coexpression within HEK293 cells

We then examined the protein expression of Alix in our transfected HEK293 cells to investigate whether Alix was exerting its effect on NMDAR cell death by influencing protein expression. Full length expression of Alix (96kDa) was confirmed using a full length mouse anti-Alix antibody in both the Alix alone and Alix and GluN1/GluN2A subunit in both activated and non activated HEK293 cells (Figure 4.1). The bands showed little degradation and the negative control did not show a clear protein signal when transfected with only lipofectamine.

In cultures that were transfected with only Alix cDNA and EGFP and maintained in PSS, mean relative Alix protein expression was 2.39 ± 0.88 (Figure 4.1b). In cultures that were transfected with EGFP-Alix cDNA only and activated in PSS with NMDA (1 mM) and glycine (50 µM) had a mean relative protein expression of 3.77 ± 0.55 (Figure 4.1a). Therefore it seems that NMDA/glycine treatment elevates Alix expression. But a paired T test showed that this difference was statistically insignificant with a P value of 0.40.

In cells transfected with Alix, GluN1/GluN2A subunits and activated with PSS and NMDA with glycine had a mean relative Alix protein expression of 0.99 ± 0.23 (Figure 4.1a). Non activated cells transfected with Alix and GluN1/GluN2A subunits yielded a relative mean protein expression of 0.84 ± 0.18 (Figure 4.1b). The difference here was also found to be not statistically significant with a P value of 0.61.

We observed a higher protein expression of Alix in Alix only transfected cells compared to Alix, GluN1/GluN2A cotransfected cells when activated with NMDA. In the activated cells, the paired T test suggests that the differences are statistically significant with a P value of 0.019. However, there was a smaller (non statistically significant) change in Alix expression between Alix only transfected cells compared to non activated Alix,

GluN1/GluN2A cotransfected cells with a P value of 0.22. It is unclear why Alix expression levels differ here but it could be induced by general changes in protein expression within cells when they are activated by NMDA during the cell death assay rather than a specific effect on Alix expression.

We then examined NMDA receptor expression by examining protein expression of GluN1 subunit (108kDa) and this was confirmed using a mouse anti-NMDAR1 antibody in both the NMDAR only and Alix and GluN1/GluN2A expressing cells in both activated and non activated HEK293 cells (Figure 4.2).

In cultures that were transfected with GluN1/GluN2A only and maintained in PSS, GluN1 mean relative protein expression was 1.46 ± 0.64 (Figure 4.2b). In cultures that were transfected with GluN1/GluN2A only and activated in PSS with NMDA (1 mM) and glycine (50 μM) had a mean relative protein expression of 1.33 ± 0.75 (Figure 4.2a). Therefore, activation with NMDA and glycine has little effect on GluN1 protein levels and this was supported by a paired T test with a P value of 0.90 for both activated and non activated GluN1/GluN2A only cultures.

In cells transfected with Alix, GluN1/GluN2A subunits and activated with PSS and NMDA with glycine had a mean relative expression of 1.74 ± 0.42 (Figure 4.2a). Non activated cells transfected with Alix and GluN1/GluN2A subunits yielded a mean relative expression of 0.87 ± 0.38 (Figure 4.2b). Thus, the protein expression levels of GluN1 seem to differ between activated and non-activated cells expressing Alix. However, this difference was not considered statistically significant with a P value of 0.38 (paired T-test). Therefore our overall conclusion is that the levels of GluN1 are not altered when these proteins are coexpressed and the levels of both proteins are not changed significantly before or after NMDA receptor activation.

We previously discussed that Alix is found in the human PSD (Bayes et al., 2011) which would lead credence for us to examine whether there is a similar expression pattern in rat brain. Using the antibodies described earlier, we examined Alix in whole adult and embryo brain protein extracts as well as Synaptosome, Light Membrane, Myelin and Mitochondria fractions. Unfortunately the Myelin fraction which is comprised of the insulating sheath around the axon of the neuron was too smeary for us to detect a distinct protein signal. But full length Alix expression (96kDa) was detected using mouse anti-Alix in all other fractions (Figure 4.3).

We found that whole embryo brain sample had a mean relative protein expression of 0.15 ± 0.04 (Table 4.3). The expression of Alix in whole embryo brain seems comparatively quite low. Whereas the whole adult brain had a slightly higher mean relative protein expression of 0.29 ± 0.04 (Table 4.3). Synaptosome fractions showed the highest mean relative protein expression of 1.52 ± 0.03 (Table 4.3). Synaptosomes are isolated from the synaptic terminal of a neuron (Chicurel et al., 1993) and the high relative protein expression would be consistent with the findings from Bayes et al. 2011 that Alix is located within the human PSD. The mitochondria fraction had a mean protein expression of 0.61 ± 0.11 (Table 4.3) and represents the energy providing organelles that are also involved in signalling cellular differentiation, cell cycle, cell growth and cell death (Antico Arciuch et al., 2012). The light membrane had a mean protein expression of 0.62 ± 0.13 (Table 4.3) and are comprised of the gradient centrifugation of the cell membrane (Bermejo et al., 2014). Paired T test was not statistically significant for embryo compared with whole adult, mitochondria and light membrane fractions with a P value of 0.22, 0.096 and 0.11 respectively. Paired T test showed very statistically significant for differences between whole adult brain extract and the synaptosome fraction with a P value of 0.0022 as well as between embryo extract and synaptosome fraction with a P value of 0.0019. Therefore this

might suggest that Alix expression is stronger in the synaptosomal fractions and would be consistent with its association with the PSD. We have to also consider that there is a lower level of expression from both the embryo and whole adult brain extract, which makes a true comparison with all the other fractions difficult even though we loaded the similar levels of protein as seen from the actin control (Figure 4.3).

We also examined GluN1 expression in whole adult and embryo brain as well as Synaptosome, Light Membrane, Myelin and Mitochondria fractions. Unfortunately, like the Alix blot the Myelin fraction in the GluN1 blot was also too smeary for identifying a distinct protein signal. Full length expression of GluN1 (108kDa) was detected using a mouse anti-NMDAR1 antibody (Figure 4.4).

The whole embryo brain extract had a mean relative protein expression of 0.53 ± 0.46 (Table 4.4). The expression of GluN1 in whole embryo brain extract seemed comparatively quite low. Whereas the whole adult brain extract had a comparatively higher mean relative protein expression of 0.71 ± 0.62 (Table 4.4). Synaptosome fractions showed a mean relative protein expression of 1.38 ± 0.22 (Table 4.4). The mitochondria fraction showed the highest expression with a mean protein expression of 1.97 ± 0.28 (Table 4.4). The light membrane had a mean protein expression of 0.40 ± 0.15 (Table 4.4) and is the isolation of gradient centrifugation of the cell membrane (Figure 4.4). Paired T test was not statistically significant for embryo compared with whole adult, synaptosome and light membrane fractions with a P value of 0.22, 0.12 and 0.72 respectively, however, paired T test was statistically significant for differences between embryo extract and mitochondria fraction with a P value of 0.018. Conversely, paired T test was not statistically significant for whole adult compared with all other protein extracts including embryo, synaptosome, mitochondria and light membrane fractions with a P value of 0.22, 0.29, 0.07 and 0.58 respectively. These results suggest that GluN1 might be expressed at a higher level within

the mitochondria fraction compared to other fractions/brain extracts. Again, with the low level of expression seen from both the embryo and whole adult brain extract a true comparison with all the other fractions is difficult even though we loaded the similar levels of protein as seen from the actin control (Figure 4.4).

It is interesting that we see a very statistically significant difference when we compared Alix protein expression in whole adult brain as well as embryo brain against synaptosome fractions. Wang et al., 2011 theorised the possibility that synapsin is released from cells via exosomes and that the interior of exosomes contains cytoplasmic proteins, such as synapsin. They did a serial centrifugation from the cell culture supernatant of cultures enriched in cortical astrocytes to isolate a significant amount of exosomes that contain synapsin and the exosomal marker protein Alix. Therefore our findings that Alix expression is higher in synaptosomes compared to other cell preparations and is consistent with other reports that Alix is present in the PSD.

7.3 Discussion of Alix localization in cotransfected HEK293 cells, primary cortical and hippocampal cultures

Our immunoblotting revealed strong Alix expression in GFP-Alix transfected HEK293 cells and in rat brain fractions and we then investigated the cellular localisation of Alix in HEK293 cells and primary neuronal cultures. The presence of Alix was evaluated by transfecting HEK293 cultures with Alix and GluN1/ GluN2A subunit in different combination following Table 3.1 a, b and then stained with specific antibodies. Previous work has shown that Alix is mainly localised in the cytoplasm and cytosol and cytoskeleton (Pan et al., 2008; Vito et al., 1999). Fluorescence images of Alix in HEK293 cells revealed overall heterogeneous fluorescence within the cytoplasm of the cells with a few green circular structures but little expression in the nuclei (Figure 5.1 and 5.3). Visually there does not seem to be any overlap between Alix and nuclear Hoechst staining and this was confirmed by an uncorrelated scatter plot with Alix and Hoechst pixels more clustered towards the axes and further proven by a low Pearson's correlation value below 0.100 with a minimum n of 3.This cellular localisation is consistent with the cytoplasmic localization of transfected Alix in L66 fibroblasts observed in previous work (Vito et al. 1999).

Considering Alix is known to interact with ESCRT (endosomal sorting complex required for transport) (Trioulier et al., 2004; Ohkouchi et al., 2004) and the green structures that we observed in the previous Alix staining (figure 5.1 and 5.3) we wanted to observe if there was any correlation between Alix and the endosome marker EEA1 (Figure 5.5 and 5.7). Staining with EEA1 revealed an expected punctuate staining pattern consistent with cytoplasmic distribution of endosomes. The colour scatter plot and mean Pearson's correlation (0.252) suggested that the correlation between EEA1 and Alix staining is weak.

We also examined Alix colocalisation with the cytoskeleton using phalloidin staining (Schmit and Lambert 1990) (Figure 5.9 and 5.11). Again the colour scatter plot of

Alix and Phalloidin in HEK293 cells revealed a variable correlation plot and a mean Pearson's Correlation value of 0.251 (n = 3) which suggests that the correlation is weak. However there is evidence that siRNA knockdown of Alix expression can cause redistribution of the actin cytoskeleton (Cabezas et al., 2005) in HeLa cells and coimmunopreciptation studies in HEK293 cells have shown Flag tagged Alix protein interaction with structural elements of the cytoskeleton (Schmidt et al. 2003) in HEK293 cells. It is possible that the GFP tagged to the N-terminus of Alix protein (Zhan et al. 2008) used in this study may have affected or weakened the cytoskeletal interactions of Alix within the cell. Although this may suggest that the GFP tagged Alix used in this study could lead to spurious results, it should be noted that the Flag tagged mouse Alix construct used in the NMDAR cell death assay produced identical results with the GFP tagged human Alix construct (Figure 3.6 a and b, 3.7 a and b, 3.8 a and b and 3.9 a and b).

Once we determined the localisation and correlation of Alix expressed alone in the HEK293 cells, with EEA1 and with Phalloidin, we wanted to establish if there was any correlation between Alix and NMDAR expression following the same conditions as the NMDAR cell death assay we have established in Chapter 3.2.1. This allowed us to determine the intracellular distribution of Alix is when it is transfected with NMDARs and to examine if there is any change in expression or localisation when NMDARs are activated or not activated.

Our results suggested that there was a partial overlap between Alix and GluN1 expression in activated (Figure 5.13 and 5.15) and non activated HEK293 cells (Figure 5.17 and 5.19). In both cases the colour scatter plots and the mean Pearson's correlation suggested a moderate correlation (0.5, n=20 and 0.44, n=20). A paired t-test showed no statistically significant difference between the activated and non activated correlation plots with a P value of 0.499. Therefore the effects of NMDAR activation have little effect on the

colocalisation pattern of both Alix and GluN1 within the cell. One reason for the moderate correlation observed between Alix and GluN1 expression could be due to the fact that Alix and GluN1 cDNAs are both transfected into HEK293 cells and expressed under CMV promoters optimized for a higher cell expression than basal expression levels.

All models of experiments have limitations that must be considered and with mammalian cell lines we have the ability to examine cells in a more controlled enviroment, ease of experimental replication and shortened time scale. However primary cultures are more complex, genetically stable and are the actual cells partaking in endogenous neuronal processes which makes it more likely to replicate the neuronal environment. As it is not possible to observe endogenous expression of Alix in HEK293 cells, we decided to ascertain the correlation and expression of endogenous Alix in cultured neurons from the hippocampus and cortex. This will allow us to establish the localisation of endogenous Alix, where it is distributed and if there is any change in its expression in these neurons from different brain regions. The hippocampus is known to play an important role in short and long term memory and spatial navigation (King et al., 2004) and in the cortex which is known to play a key role in memory and cognitive processing (Rubenstein, 2011).

However there are limitations with in vitro dissociated neuronal cultures in terms of their ability to form appropriate synaptic structures and circuitary. Furthermore the normal brain tissue structure is absent in these primary cultures and this may have significant effects on the functions of these cells. More appropriate ex vivo systems could involve organotypic slice culture systems, however these systems are much harder to maintain and visualize protein expression using immunocytochemistry (Cho et al., 2007).

The main cell types in the CNS are neurons and glial cells, which can be identified by a variety of morphological and functional characteristics. We know that neurons have two processes with axon and dendrites and glial are star shaped cells with only one (Kriegstein,

1983). We did not inhibit the growth of glia in our cultures and it is possible that our immunocytochemistry contained a mixed population of neurons and glia. Alix is also expressed in exosomes released by glia (Chen et al., 2000; Guescini et al. 2010) and this is one of the reasons we used synaptophysin as a marker as we know that astrocytes do not express synaptic proteins (Sofroniew and Vinters 2010). Alternatively we could have detected and Alix immunofluorescence within astrocytes and their relative expression compared to neurons within our cultures by staining for specific glial protein markers such as GFAP.

Another important point to consider is whether the time point of synaptic marker visualisation in our cultured primary neurons truly represents the formation of excitatory synapses and the formation of a mature PSD. All neurons were examined after 14 days in vitro and studies suggest that at this time point synapses are beginning to mature and increase in number until 21 days (Graburcker et al. 2009). Furthermore, this study provided evidence supporting the ultrastructural maturity of synapses, localised expression of pre and postsynaptic proteins after 14 days in vitro and showed that the thickness of the PSD measured using electron microscopy remained unchanged after 14 days in vitro and suggests that these synapses are structurally mature at this point in culture. The endogenous levels of Alix in the cortical and hippocampal cultures (Figure 6.1 and 6.3) revealed a punctate fluorescence within the cell cytoplasm. As seen with the HEK293 cells, we found little colocalisation with Hoechst in the colocalisation scatter plot and a mean Pearson's correlation coefficient (-0.133, n=3) for the cortical neurons and (-0.004, n=3) for the hippocampal neurons.

Considering the weak correlation of Alix and EEA1 in the HEK293 cells we wanted to observe if there was any correlation between the basal level of Alix and the endosome marker EEA1 in the cortical and hippocampal cultures (Figure 6.5 and 6.7). Staining with

EEA1 revealed an expected punctuate staining pattern consistent with cytoplasmic distribution of endosomes. We found a moderate correlation of Alix and EEA1 in the cortex, with a Pearson's Correlation value of 0.406 (n = 3). However, we found a weak correlation of Alix and EEA1 in the hippocampal cultures with a mean Pearson's Correlation value of 0.307 (n = 3) However paired t-test shows that the difference between cortical and hippocampal neurons is considered to be not statistically significant with a P value of 0.676.

Given that we found Alix weakly correlated with Phalloidin in HEK293 cells, we wanted to observe endogenous Alix localization with Phalloidin in the cortical and hippocampal cultures (Figure 6.9 and 6.11). In both cases, we found that there was a moderate correlation in the cortical cultures and the hippocampal cultures with a mean Pearson's Correlation value of 0.538 (n = 3) and 0.415 (n = 3) respectively. This supports previous reports that Alix may associate with cytoskeletal proteins in HEK293 cells and cortical astrocytes (Schmidt et al. 2003; Cabezas et al. 2005). However, these studies have used indirect methods to base their conclusions (siRNA and immunoprecipation of cytoskeletal associated proteins) and evidence is still lacking for a direct association of Alix with microtubules or the cytoskeleton. It is possible that rather than forming a direct interaction, Alix may use similar transport or structural machinery and thus be able to influence cytoskeletal regulation.

Since we previously observed that Alix displayed a moderate correlation with NMDAR in HEK293 cells, it was important to examine endogenous Alix localization with NMDAR in the cortical and hippocampal cultures. The Colour scatter plot of Alix and GluN2A/2B showed that this colocalisation was strong in cortical cultures (Figure 6.13) with mean Pearson's Correlation value of 0.761 (n = 3). However, this correlation was much weaker in hippocampal neurons with a mean Pearson's Correlation value of 0.275 (n

= 3) (Figure 6.15). However, paired t-test shows that the difference between cortical and hippocampal neurons is considered to be not statistically significant with a P value of 0.183. Therefore, the difference in Alix and GluN2A/B correlation between the two cell types is not statistically different.

Next we wanted to observe if Alix might correlate with PSD95 in the cortical and hippocampal cultures as we know that PSD95 is a well-characterized intracellular protein known to associate with NMDARs (Sheng, 2001). We found a moderate correlation rate between Alix and PSD95 in the cortical cultures with a mean Pearson's Correlation value of 0.496 (n = 3)(Figure 6.17). However, there was a weaker correlation in hippocampal neurons with a mean Pearson's Correlation value of 0.264 (n = 3) (Figure 6.19). The paired t-test shows that the difference between cortical and hippocampal neurons is considered statistically significant with a P value of 0.018. This suggests a stronger colocalisation of PSD95 with Alix in cortical neurons compared to hippocampal neurons.

As Alix displays a correlation with PSD95 expression we wanted to examine if Alix might correlate with another synaptic protein, synaptophysin in the cortical and hippocampal cultures (Figure 6.21 and 6.23). Synaptophysin is a binding partner for the SNARE protein, synaptobrevin and is often used as marker for synaptic localization (Reisinger et al., 2004). However, we did not see any overlap between Alix and synaptophysin in both the cortical and hippocampal cultures. There was a weak correlation rate with a mean Pearson's Correlation value of 0.31 (n = 3) in the cortical cultures and 0.238 (n = 3) in the hippocampal cultures. Considering that synaptophysin is mainly localized to presynaptic compartments of the synapse this observation would support the evidence of Alix association with the PSD (Bayes et al. 2011; Chassefeyre et al. 2015).

Alix correlation seems to follow the same pattern of displaying strong correlation with the expression of PSD95 in the cortical cultures but not in the hippocampal cultures. It

is unclear why this is the case and may suggest a neuronal specific localization of Alix that distinguishes between these cell types. There is little information in the literature reporting differences between cortical and hippocampal localization of specific proteins. But it has been reported that these cell types can produce differential changes in mGluR5 expression following exposure to certain pharmacological treatments (Yu et al 2001). Another factor that may contribute to this observation could be based on the variety of cell types within the cortices or hippocampi used in both cultures and the ratio of neurons to glia within both types of cultures and how this could influence the correlation analysis of PSD95 with Alix.

It is also possible that the correlation could be influenced by microvesicles released into the intercellular space as observed by Guescini et al., 2010 where glioblastoma and astrocytes released microvesicles with some protein markers of exosomes such as CD9 and Alix that are transferred between cells. However, as mentioned earlier this would be dependent on the level of Alix expression in astrocytes and the ratio of neurons to glia within our primary cultures.

Another possible explanation for the differences in colocalisation between cell types could be caused by the visualization of synaptic protein markers by detecting puncta following immunocytochemistry and measurement of colocalisation using Pearson's coefficient. The limitations of this method of protein detection include spatial resolution to subcellular compartments, sensitivity for low protein expression, appropriate comparison of pixel intensity distributions and the level of noise generated by background fluorescence (Bolte and Cordelieres, 2006). Although, there is a popular assumption that most proteins required for neuronal function are made in the cell body Sutton, 2006 found that dendritic protein synthesis is essential in the neurons. This highlights the limitation of colocalization analysis using synaptic markers in cell culture rather than visualizing the whole synaptic structure from sections of whole brain using electron microscopy.

However, there is strong evidence that Alix is highly expressed in neurons following neuronal insults. Hemming et al., 2004 found that Alix expression was increased in neuronal cell bodies very rapidly after kainate induced neurodegeneration and this occurred before/during neuronal eosinophilia and cell oedema. This increased Alix expression persisted 24 hours after kainate injection in the piriform cortex and it has been postulated that Alix may play an early role in the cell death mechanism. To support this, Blum et al., 2004 also found that Alix upregulation in the cerebellar granule cells may be instrumental in inducing cell death. It is not completely clear whether Alix is a trigger or an early marker for neurodegenerative processes and the role it plays within the ESCRT-III complex. Evidence suggests that Alix is important for endosomal trafficking and triggering caspase dependent and independent pathways (Trioulier et al. 2004), but loss of Alix has been shown to disrupt normal cytoskeletal organization within the cell (Cebezas et al. 2005) and thus may play an important role in supporting the structure of the PSD within dendritic spines (Chassefeyre et al. 2015). It is intriguingly to note that C-terminal truncations in one of the core components of the ESCRT-III complex, Chmp2b have been linked to familial frontotemporal dementia (Isaacs et al., 2011) but how this leads to neurodegeneration requires further investigation.

7.4 General summary

The investigations described in this thesis can be split into two parts; the effects of Alix on NMDAR triggered cell death and the protein expression and localisation of Alix in primary neurons. In the first part we have examined the influence of Alix from different species (human and mouse) on NMDAR triggered cell death during NMDA treatment and in the absence of NMDA treatment. The most interesting finding is the fact that Alix coexpression increased the proportion of cell death in the absence of NMDA treatment

compared to cells expressing only NMDARs. Further investigation of this observation has shown that this requires the formation of a complete NMDA receptor and requires NMDAR activation (no enhanced cell death seen with control experiments with Alix alone or incubation with the NMDAR antagonist, AP5) and can be partly explained by Alix increasing the glutamate/glycine sensitivity of NMDAR expressing cells in triggering cell death. We observed similar effects with the mouse variant of Alix and using deletion mutants and have identified the C-terminal of Alix as important for this process. The increased cell death in the presence of Alix does not affect GluN1 or Alix protein expression or cellular localisation in HEK293 cells.

For the second part of this study, our results have described the protein expression in synaptosomes and the cellular localisation of Alix in hippocampal and cortical primary neurons. Alix was detected in synaptosome preparations supporting the previous reports of Alix expression within the PSD. Furthemore, there is little information on the cellular localisation of Alix within neurons and we performed immunocytochemistry to examine Alix localisation in primary neuron cultures prepared from rodent hippocampus and cortex. Although there are limitations with the analysis we have used, our initial observations of the immunofluorescent images suggest that Alix exhibits a punctate expression throughout the cytoplasm of both types of neurons and may show colocalisation with the endosomal marker, EEA1, the cytoskeletal proteins and the well characterised postsynaptic density protein, PSD95.

7.5 Future studies

To give us an idea of how Alix may affect NMDAR triggered cell death and the NMDA receptor pathway, we could perform a protein complex immunoprecipitation (Co-IP) of Alix to analyse protein to protein interactions with NMDAR subunits or associated intracellular proteins such as PSD95. One of the limitations of our NMDAR cell death assay is whether this is replicated in neuronal environment and we could also repeat our NMDA cell death assay in the cortical and hippocampal cultures to assess if Alix would still cause a higher percentage of cell death when activated. Another avenue would be to manipulate expression levels of Alix with RNAi on primary neuronal cultures by knocking down Alix expression and determining the effect on glutamate receptor function in culture.

References:

Anson LC, Chen PE, Wyllie DJ, Colquhoun D, Schoepfer R (1998) Identification of amino acid residues of the NR2A subunit that control glutamate potency in recombinant NR1/NR2A NMDA receptors. J Neurosci (United States) 18(2):581-9.

Antico Arciuch VG, Elguero ME, Poderoso JJ, Carreras MC (2012) Mitochondrial regulation of cell cycle and proliferation. Antioxid Redox Signal (United States) 16:1150-1180.

Bayes A, van de Lagemaat LN, Collins MO, Croning MD, Whittle IR, Choudhary JS, Grant SG (2011) Characterization of the proteome, diseases and evolution of the human postsynaptic density. Nat Neurosci (United States) 14:19-21.

Bermejo MK, Milenkovic M, Salahpour A, Ramsey AJ (2014) Preparation of synaptic plasma membrane and postsynaptic density proteins using a discontinuous sucrose gradient. J Vis Exp (United States) (91):e51896. doi:e51896.

Blum D, Hemming FJ, Galas MC, Torch S, Cuvelier L, Schiffmann SN, Sadoul R (2004) Increased alix (apoptosis-linked gene-2 interacting protein X) immunoreactivity in the degenerating striatum of rats chronically treated by 3-nitropropionic acid. Neurosci Lett (Ireland) 368:309-313.

Bolte S, and Cordelieres FP (2006) A guided tour into subcellular colocalisation analysis in light microscopy J. Microscopy 224:213-232.

Bonde C, Noraberg J, Zimmer J (2002) Nuclear shrinkage and other markers of neuronal cell death after oxygen-glucose deprivation in rat hippocampal slice cultures. Neurosci Lett (Ireland) 327:49-52.

Breedlove, S. Marc., Watson, Neil. V. (2013) Biological psychology: An introduction to behavioral, cognitive and clinical neuroscience.

Budd SL, Tenneti L, Lishnak T, Lipton SA (2000) Mitochondrial and extramitochondrial apoptotic signaling pathways in cerebrocortical neurons. Proc Natl Acad Sci U S A (UNITED STATES) 97:6161-6166.

Cabezas A, Bache KG, Brech A, Stenmark H (2005) Alix regulates cortical actin and the spatial distribution of endosomes. 118:2625-2635.

Chassefeyre R, Martinez-Hernandez J, Bertaso F, Bouquier N, Blot B, Laporte M, Fraboulet S, Coute Y, Devoy A, Isaacs AM, Pernet-Gallay K, Sadoul R, Fagni L, Goldberg Y (2015) Regulation of postsynaptic function by the dementia-related ESCRT-III subunit CHMP2B. J Neurosci (United States) 35:3155-3173.

Chatellard-Causse C, Blot B, Cristina N, Torch S, Missotten M, Sadoul R (2002a) Alix (ALG-2-interacting protein X), a protein involved in apoptosis, binds to endophilins and induces cytoplasmic vacuolization. J Biol Chem (United States) 277:29108-29115.

Chatellard-Causse C, Blot B, Cristina N, Torch S, Missotten M, Sadoul R (2002b) Alix (ALG-2-interacting protein X), a protein involved in apoptosis, binds to endophilins and induces cytoplasmic vacuolization. J Biol Chem (United States) 277:29108-29115.

Chen B, Borinstein SC, Gillis J, Sykes VW, Bogler O. (2000) The gliona-associated protein SETA interacts with AIP/Alix and ALG-2 and modulates apoptosis in astrocytes. J. Biol. Chem. 275:19275-19281.

Chen PE, Geballe MT, Stanfeld PJ, Johnston AR, Yuan H, Jacob AL, Snyder JP, Traynelis SF, Wyllie DJ (2005) Structural features of glutamate binding site in recombinant NR1/NR2A N-methyl-D-aspartate receptors determined by site directed mutagenesis and molecular modeling. Mol Pharmacol 67(5):1470-84.

Cho s, Wood A and Bowlby M. (2007) Brain Slices as models for neurodegenerative disease and screening platforms to identify novel therapeutics. Current Neuropharmacology 5:19-33.

Chicurel ME, Terrian DM, Potter H (1993) mRNA at the synapse: Analysis of a synaptosomal preparation enriched in hippocampal dendritic spines. J Neurosci (UNITED STATES) 13:4054-4063.

Chivet M, Hemming F, Pernet-Gallay K, Fraboulet S, Sadoul R (2012) Emerging role of neuronal exosomes in the central nervous system. Front Physiol (Switzerland) 3:145.

Chivet M, Javalet C, Laulagnier K, Blot B, Hemming FJ, Sadoul R (2014) Exosomes secreted by cortical neurons upon glutamatergic synapse activation specifically interact with neurons. J Extracell Vesicles (Sweden) 3:24722.

Clarke PG (1990) Developmental cell death: Morphological diversity and multiple mechanisms. Anat Embryol (Berl) (GERMANY, WEST) 181:195-213.

Colquhoun, D (1998) Binding, gating, affinity and efficacy: The interpretation of structure-activity relationships for agonists and of the effects of mutating receptors. Br J Pharmacol 125:923-947.

Dawson VL, Dawson TM, London ED, Bredt DS, Snyder SH (1991) Nitric oxide mediates glutamate neurotoxicity in primary cortical cultures. Proc Natl Acad Sci U S A (UNITED STATES) 88:6368-6371.

Debanne D, Daoudal G, Sourdet V, Russier M (2003) Brain plasticity and ion channels. 97:403-414.

Endoh T (2004) Characterization of modulatory effects of postsynaptic metabotropic glutamate receptors on calcium currents in rat nucleus tractus solitarius. Brain Res (Netherlands) 1024:212-224.

Feng W, Zhang M (2009) Organization and dynamics of PDZ-domain-related supramodules in the postsynaptic density. Nat Rev Neurosci (England) 10:87-99.

Finch A (2013) *Receptor signalling lecture slides*. (UNSW) .

Giepmans BN, Adams SR, Ellisman MH, Tsien RY (2006) The fluorescent toolbox for assessing protein location and function. Science (United States) 312:217-224.

Guescini M, Genedani S, Stocchi V, Agnati LF (2010) Astrocytes and Glioblastoma cells release exosomes carrying mtDNA. J Neural Transm (Vienna) 117(1):1-4.

Girault JA, Greengard P (2004) The neurobiology of dopamine signaling. Arch Neurol (United States) 61:641-644.

Gould TD, Manji HK (2005) DARPP-32: A molecular switch at the nexus of reward pathway plasticity. Proc Natl Acad Sci U S A (United States) 102:253-254.

Greengard P (2001) The neurobiology of slow synaptic transmission. 294:1024-1030.

Grabrucker A, Vaida B, Bockman J, Boeckers TM (2009) Synaptogenesis of hippocampal neurons in primary cell culture. Cell Tissue Res 338(3):333-41.

Gruenberg J, Stenmark H (2004) The biogenesis of multivesicular endosomes. Nat Rev Mol Cell Biol (England) 5:317-323.

Hemming FJ, Fraboulet S, Blot B, Sadoul R (2004) Early increase of apoptosis-linked gene-2 interacting protein X in areas of kainate-induced neurodegeneration. Neuroscience (United States) 123:887-895.

Hirsch SR, Das I, Garey LJ, de Belleroche J (1997) A pivotal role for glutamate in the pathogenesis of schizophrenia, and its cognitive dysfunction. 56:797-802.

Hurley JH, Odorizzi G (2012) Get on the exosome bus with ALIX. Nat Cell Biol (England) 14:654-655.

Isaacs AM, Johannsen P, Holm I, Nielsen JE, FReJA consortium (2011) Frontotemporal dementia caused by CHMP2B mutations. Curr Alzheimer Res (United Arab Emirates) 8:246-251.

Johnson JW, Ascher P (1990) Voltage-dependent block by intracellular Mg2+ of N-methyl-D-aspartate-activated channels. Biophys J (UNITED STATES) 57:1085-1090.

Kantrowitz JT, Javitt DC (2010) N-methyl-d-aspartate (NMDA) receptor dysfunction or dysregulation: The final common pathway on the road to schizophrenia? 83:108-121.

Karakas E, Regan MC, Furukawa H (2015) Emerging structural insights into the function of ionotropic glutamate receptors. Trends Biochem Sci 40:328-337.

Katoh K, Shibata H, Suzuki H, Nara A, Ishidoh K, Kominami E, Yoshimori T, Maki M (2003) The ALG-2-interacting protein alix associates with CHMP4b, a human homologue of yeast Snf7 that is involved in multivesicular body sorting. J Biol Chem (United States) 278:39104-39113.

Kennedy MB (1997) The postsynaptic density at glutamatergic synapses. Trends Neurosci (ENGLAND) 20:264-268.

Kim E, Sheng M (2009) The postsynaptic density. Curr Biol (England) 19:R723-4.

King JA, Trinkler I, Hartley T, Vargha-Khadem F, Burgess N (2004) The hippocampal role in spatial memory and the familiarity--recollection distinction: A case study. Neuropsychology (United States) 18:405-417.

Krantic S, Mechawar N, Reix S, Quirion R (2005) Molecular basis of programmed cell death involved in neurodegeneration. Trends Neurosci (England) 28:670-676.

Kriegstein AR, Dichter MA (1983) Morphological classification of rat cortical neurons in cell culture. J Neurosci (8):1634-47.

Kristiansen LV, Huerta I, Beneyto M, Meador-Woodruff JH (2007) NMDA receptors and schizophrenia. 7:48-55.

LaHoste GJ, Henry BL, Marshall JF (2000) Dopamine D1 receptors synergize with D2, but not D3 or D4, receptors in the striatum without the involvement of action potentials. 20:6666-6671.

Lau CG, Takeuchi K, Rodenas-Ruano A, Takayasu Y, Murphy J, Bennett MV, Zukin RS (2009) Regulation of NMDA receptor Ca2+ signalling and synaptic plasticity. Biochem Soc Trans (England) 37:1369-1374.

Lee FJ, Xue S, Pei L, Vukusic B, Chery N, Wang Y, Wang YT, Niznik HB, Yu XM, Liu F (2002) Dual regulation of NMDA receptor functions by direct protein-protein interactions with the dopamine D1 receptor. 111:219-230.

Li M, Zhang DQ, Wang XZ, Xu TJ (2011) NR2B-containing NMDA receptors promote neural progenitor cell proliferation through CaMKIV/CREB pathway. Biochem Biophys Res Commun (United States) 411:667-672.

Lipton SA (2006) Paradigm shift in neuroprotection by NMDA receptor blockade: Memantine and beyond. Nat Rev Drug Discov (England) 5:160-170.

Lipton SA (2004) Failures and successes of NMDA receptor antagonists: Molecular basis for the use of open-channel blockers like memantine in the treatment of acute and chronic neurologic insults. NeuroRx (United States) 1:101-110.

Lipton SA, Nicotera P (1998) Calcium, free radicals and excitotoxins in neuronal apoptosis. Cell Calcium (SCOTLAND) 23:165-171.

Liu XY, Chu XP, Mao LM, Wang M, Lan HX, Li MH, Zhang GC, Parelkar NK, Fibuch EE, Haines M, Neve KA, Liu F, Xiong ZG, Wang JQ (2006) Modulation of D2R-NR2B interactions in response to cocaine. 52:897-909.

Mahul-Mellier AL, Strappazzon F, Chatellard-Causse C, Blot B, Beal D, Torch S, Hemming F, Petiot A, Verna JM, Fraboulet S, Sadoul R (2009) Alix and ALG-2 make a link between endosomes and neuronal death. Biochem Soc Trans (England) 37:200-203.

Mahul-Mellier AL, Strappazzon F, Petiot A, Chatellard-Causse C, Torch S, Blot B, Freeman K, Kuhn L, Garin J, Verna JM, Fraboulet S, Sadoul R (2008) Alix and ALG-2 are involved in tumor necrosis factor receptor 1-induced cell death. J Biol Chem (United States) 283:34954-34965.

McIlhinney RA, Philipps E, Le Bourdelles B, Grimwood S, Wafford K, Sandhu S, Whiting P (2003) Assembly of N-methyl-D-aspartate (NMDA) receptors. Biochem Soc Trans (England) 31:865-868.

Missale C, Nash SR, Robinson SW, Jaber M, Caron MG (1998) Dopamine receptors: From structure to function. 78:189-225.

Morita E, Colf LA, Karren MA, Sandrin V, Rodesch CK, Sundquist WI (2010) Human ESCRT-III and VPS4 proteins are required for centrosome and spindle maintenance. Proc Natl Acad Sci U S A (United States) 107:12889-12894.

Nicoll RA, Malenka RC (1999) Expression mechanisms underlying NMDA receptor-dependent long-term potentiation. Ann N Y Acad Sci (UNITED STATES) 868:515-525.

Odorizzi G (2006) The multiple personalities of alix. J Cell Sci (England) 119:3025-3032.

Ohkouchi S, El-Halawany MS, Aruga F, Shibata H, Hitomi K, Maki M (2004) DdAlix, an alix/AIP1 homolog in dictyostelium discoideum, is required for multicellular development under low Ca2+ conditions. Gene (Netherlands) 337:131-139.

Oscar Arias Carrion, Ernst Poppel (2007) Dopamine, learning and reward seeking behavior. 481.

Pan S, Wang R, Zhou X, Corvera J, Kloc M, Sifers R, Gallick GE, Lin SH, Kuang J (2008) Extracellular alix regulates integrin-mediated cell adhesions and extracellular matrix assembly. EMBO J (England) 27:2077-2090.

Paoletti P, Bellone C, Zhou Q (2013) NMDA receptor subunit diversity: Impact on receptor properties, synaptic plasticity and disease. Nat Rev Neurosci (England) 14:383-400.

Patel SS, Belmont BJ, Sante JM, Rexach MF (2007) Natively unfolded nucleoporins gate protein diffusion across the nuclear pore complex. Cell (United States) 129:83-96.

Pearlstein E, Gouty-Colomer LA, Michel FJ, Cloarec R, Hammond C (2015) Glutamatergic synaptic currents of nigral dopaminergic neurons follow a postnatal developmental sequence. Front Cell Neurosci (Switzerland) 9:210.

Pei L, Lee FJ, Moszczynska A, Vukusic B, Liu F (2004) Regulation of dopamine D1 receptor function by physical interaction with the NMDA receptors. J Neurosci (United States) 24:1149-1158.

Pu J, Li Y, Liu Z, Yan Y, Tian J, Chen S, Zhang B (2011) Expression and localization of FRMD7 in human fetal brain, and a role for F-actin. Mol Vis (United States) 17:591-597.

Reisinger C, Yelamanchili SV, Hinz B, Mitter D, Becher A, Bigalke H, Ahnert-Hilger G (2004) The synaptophysin/synaptobrevin complex dissociates independently of neuroexocytosis. J Neurochem (England) 90:1-8.

Rubenstein JL (2011) Annual research review: Development of the cerebral cortex: Implications for neurodevelopmental disorders. J Child Psychol Psychiatry (England) 52:339-355.

Sadoul R (2006) Do alix and ALG-2 really control endosomes for better or for worse? 98:69-77.

Salvesen GS, Dixit VM (1997) Caspases: Intracellular signaling by proteolysis. Cell (UNITED STATES) 91:443-446.

Schmidt MH, Chen B, Randazzo LM, Bogler O (2003) SETA/CIN85/ruk and its binding partner AIP1 associate with diverse cytoskeletal elements, including FAKs, and modulate cell adhesion. J Cell Sci (England) 116:2845-2855.

Schneider-Brachert W, Tchikov V, Neumeyer J, Jakob M, Winoto-Morbach S, Held-Feindt J, Heinrich M, Merkel O, Ehrenschwender M, Adam D, Mentlein R, Kabelitz D, Schutze S (2004) Compartmentalization of TNF receptor 1 signaling: Internalized TNF receptosomes as death signaling vesicles. Immunity (United States) 21:415-428.

Schorge S, Colquhoun D (2003) Studies of NMDA receptor function and stoichiometry with truncated and tandem subunits. J Neurosci (United States) 23:1151-1158.

Scott L, Aperia A (2009) Interaction between N-methyl-D-aspartic acid receptors and D1 dopamine receptors: An important mechanism for brain plasticity. 158:62-66.

Sedarat F, Lin E, Moore ED, Tibbits GF (2004) Deconvolution of confocal images of dihydropyridine and ryanodine receptors in developing cardiomyocytes. J Appl Physiol (1985) (United States) 97:1098-1103.

Sheng M (2001) Molecular organization of the postsynaptic specialization. Proc Natl Acad Sci U S A (United States) 98:7058-7061.

Siekevitz P (1985) The postsynaptic density: A possible role in long-lasting effects in the central nervous system. Proc Natl Acad Sci U S A (UNITED STATES) 82:3494-3498.

Sofroniew MV, Vinters HV (2010) Astrocytes: biology and pathology. Acta Neuropathol 119(1):7-35.

Sperandio S, Poksay K, de Belle I, Lafuente MJ, Liu B, Nasir J, Bredesen DE (2004) Paraptosis: Mediation by MAP kinases and inhibition by AIP-1/alix. Cell Death Differ (England) 11:1066-1075.

Strappazzon F, Torch S, Chatellard-Causse C, Petiot A, Thibert C, Blot B, Verna JM, Sadoul R (2010) Alix is involved in caspase 9 activation during calcium-induced apoptosis. Biochem Biophys Res Commun (United States) 397:64-69.

Subramanian L, Crabb JW, Cox J, Durussel I, Walker TM, van Ginkel PR, Bhattacharya S, Dellaria JM, Palczewski K, Polans AS (2004) Ca2+ binding to EF hands 1 and 3 is essential for the interaction of apoptosis-linked gene-2 with alix/AIP1 in ocular melanoma. Biochemistry (United States) 43:11175-11186.

Sutton MA, Ito HT, Cressy P, Kempf C, Woo JC, Schuman EM (2006) Miniature neurotransmission stabilizes synaptic function via tonic suppression of local dendritic protein synthesis. Cell 125(4):785-99.

Taraska JW, Zagotta WN (2010) Fluorescence applications in molecular neurobiology. Neuron (United States) 66:170-189.

Tenneti L, D'Emilia DM, Troy CM, Lipton SA (1998) Role of caspases in N-methyl-D-aspartate-induced apoptosis in cerebrocortical neurons. J Neurochem (UNITED STATES) 71:946-959.

Thornberry NA, Lazebnik Y (1998) Caspases: Enemies within. Science (UNITED STATES) 281:1312-1316.

Traynelis SF, Wollmuth LP, McBain CJ, Menniti FS, Vance KM, Ogden KK, Hansen KB, Yuan H, Myers SJ, Dingledine R (2010) Glutamate receptor ion channels: Structure, regulation, and function. Pharmacol Rev (United States) 62:405-496.

Trioulier Y, Torch S, Blot B, Cristina N, Chatellard-Causse C, Verna JM, Sadoul R (2004) Alix, a protein regulating endosomal trafficking, is involved in neuronal death. 279:2046-2052.

Vito P, Pellegrini L, Guiet C, D'Adamio L (1999) Cloning of AIP1, a novel protein that associates with the apoptosis-linked gene ALG-2 in a Ca2+-dependent reaction. J Biol Chem (UNITED STATES) 274:1533-1540.

Wagey R, Hu J, Pelech SL, Raymond LA, Krieger C (2001) Modulation of NMDA-mediated excitotoxicity by protein kinase C. J Neurochem (United States) 78:715-726.

Wilson JM, de Hoop M, Zorzi N, Toh BH, Dotti CG, Parton RG (2000) EEA1, a tethering protein of the early sorting endosome, shows a polarized distribution in hippocampal neurons, epithelial cells, and fibroblasts. Mol Biol Cell (UNITED STATES) 11:2657-2671.

Wollert T, Hurley JH (2010) Molecular mechanism of multivesicular body biogenesis by ESCRT complexes. Nature (England) 464:864-869.

Wu Y, Pan S, Luo W, Lin SH, Kuang J (2002) Hp95 promotes anoikis and inhibits tumorigenicity of HeLa cells. Oncogene (England) 21:6801-6808.

Yu MF, Lin TY, Ho WH and Yin HS (2001) Amphetamine induces differential changes in the gene expression of metabotropic glutamate receptor 5 in cultured cortical and hippocampal neurons J Mol Neurosci. 17:13-24

Yelo E, Bernardo MV, Gimeno L, Alcaraz-Garcia MJ, Majado MJ, Parrado A (2008) Dock10, a novel CZH protein selectively induced by interleukin-4 in human B lymphocytes. Mol Immunol (England) 45:3411-3418.

Zhan L, Liu B, Jose-Lafuente M, Chibalina MV, Grierson A, Maclean A, Nasir J (2008) ALG-2 interacting protein AIP1: A novel link between D1 and D3 signalling. 27:1626-1633.

Zhan L, Kerr JR, Lafuente MJ, Maclean A, Chibalina MV, Liu B, Burke B, Bevan S, Nasir J (2011) Altered expression and coregulation of dopamine signalling genes in schizophrenia and bipolar disorder. Neuropathol Appl Neurobiol (England) 37:206-219.